SMART IMPLANT: THE BIOMECHANICAL TESTING OF INSTRUMENTED INTRAMEDULLARY NAILS DURING SIMULATED CALLUS HEALING USING TELEMETRY FOR FRACTURE HEALING MONITORING

By

Jaya Luxshmi Nemchand

COMMERCIAL IN CONFIDENCE

Submitted in fulfilment of the requirements for the degree of

Doctor of Philosophy

Experimental Techniques Centre

Graduate School

Brunel University

London, UK

Abstract

The purpose of this study is to investigate the effect of loading during long bone fracture healing *in-vitro* and *in-vivo*. Fracture healing has until now only been monitored using radiographs and ultrasound. An intramedullary nail instrumented with strain gauges has the potential to monitor loading *in-vivo* during bone fracture healing. Strain has been previously monitored over time though external fixation devices however there has been no published data about monitoring through a nail. The load carried by a telemetric intramedullary nail during simulated fracture healing is monitored in-vitro with the aid of custom designed jigs, integrated in a biomechanical test frame. Clinically predetermined loading conditions are applied to the construct and synthetic bone composites are used developed to simulate mechanical strength of early to mature osteogenic bone, approximating natural healing processes. Four different synthetic bone composites have been designed and developed to mimic the mechanical properties of granulation tissue, fibrous tissue, cartilaginous tissue and immature bone. Three different generations (GEN I – IIIa) of intramedullary nails were developed and biomechanically tested *in-vitro*. GEN I and II were purely biomechanical nails that underwent compression, torsional and 4pt bend tests. Different fracture patterns and callus morphology were simulated and tested biomechanically. Circumferential and segmental application of the synthetic materials were applied on the artificial fractured bone instrumented with GEN I. Observations from live animal study provided x-rays from which callus growth patterns were extracted and repeated *in-vitro*. Cadaveric biomechanical tests and pre-clinical trial of GEN IIIa was conducted. The aim was to repeat the biomechanical tests while at the same time monitoring healing with an instrumented nail implanted in an induced fractured, ovine left hind limb. A loading rig was designed for the *in-vivo* test. The hypothesis proposed is that forces experienced by an intramedullary nail will progressively decrease as fracture heals. Results from GEN I have shown that strain measurement can be monitored during fracture healing *in-vitro*. The GEN IIIa nail is yet to be tested *in-vivo* for the same biomechanical tests for comparison. There is currently no published study on simulating fracture healing with accuracy.

Dedication

For Mum, Dad

& Anju!!

Acknowledgements

"Are you there yet?" has been the question I have been asked one too many times in the past few months but I would not be here without them. Doing a PhD has been exciting, challenging not to mention frustrating and depressing but also maybe the most indescribable process I have and will ever undertake. However, the path to completion would have been so arduous without the continuous guidance and support of numerous people.

First and foremost, I would like to thank both my supervisors, Professor Tony Anson and Dr Benjamin Jones. My words will never be enough to thank my supervisor Professor Tony Anson, who has continuously and extremely patiently guided and supported me throughout these past few years. His continuous encouragement and trust in me has been the one thing that kept me going even in situations that seem the most complicated and unfathomable to me.

I would like to thank those who have made it possible for me to do a PhD in the first place by funding the PhD, Smith & Nephew Plc (S&N) & the Technology Strategy Board (TSB). More specifically Dr Darren J Wilson from York Research Centre who has been very patient with my incessant questioning but who also gave me some unique opportunities to work alongside his team and gain some extremely insightful knowledge and experience in the field. I will definitely not forget the extremely crazy driving on the long winding roads that made me focus more on the questions than which side of the road we were on!! Thanks to the other people at S&N (UK & USA), Dr Si Janna, Bill and the IVB team attached to the York Research Centre. A lot of my experimental work has been conducted at Institute of Musculoskeletal Sciences (IOMS), University College London (UCL) based at the Royal National Orthopaedic Hospital in Stanmore. I would like to extend my thanks and gratitude to Dr Stephen J G Taylor, Dr Ian McCarthy, Dr Shiying Hao and Mark Harrison who took the time to guide me with their own expertise in the project and helping me complete my experiments successfully, using their facilities to do so.

Thanks to the staff at ETCBrunel, who have helped me in their own right either just encouraging me or teaching me how to use the instruments. Thanks to my colleague and friend Nico Nelson who agreed to be a modelling candidate for photography purposes. Thanks to School of Engineering and Design (SED) technical staff, Keith & Malcolm, who have been very helpful and taught me how to use the mechanical testing instruments and made time to allow me to use the machines even at busiest times. There also some other people who have listened, supported and advise me at Brunel University without whom the process would have seemed harder. Thanks to Dr Beverley Crooks who has been a great support in challenging time.

Last but not least, my family and my friends! Special thanks to my parents and my sister, thank you for all the support, encouragement and unconditional love that allowed me to successfully complete all the education I could have only dreamt of! Thanks to Elke and her family, without forgetting the loudest cat Feline, for being always very supportive and encouraging and listening to me. Special thanks to Hema, who encouraged and supported me until the very end but sadly passed away due to illness days after I completed.

Author's Declaration

I hereby declare that I am the sole author of this thesis.

Jaya Luxshmi Nemchand

"Healing is a matter of time, but it is sometimes also a matter of opportunity"

- Hippocrates (460 BC -375 BC)

Table of Contents

List of Figures

List of Tables

List of Symbols

ε	Strain
L	Unit of length
ΔL	Change in length
R	Resistance
ρ	Resistivity of material
A	Cross sectional area of material
l_c	Critical fibre length
d	Fibre diameter
σ_f	Ultimate tensile strength
τ_c	Fibre matrix bond strength
F_c	Total load sustained by composite
F_m	Total load carried by matrix
F_f	Fibre phase
σ	Stress
E_{ct}	Modulus of elasticity in transverse direction
V_m	Volume of matrix
V_f	Volume of fibre
ε_c	Strain in composite
ε_m	Strain in matrix
ε_f	Strain in fibre
E_{CD}	Modulus of composite in discontinuous and random orientation
E^f	Young's modulus of fibre
E^m	Young's modulus of matrix
k	Fibre efficiency parameter

Glossary of Terms

- 2D/3D – two/ three dimension
- Anastomosis – communication between two blood vessels without any intervening capillary network
- AE – Acoustic Emission
- AO – Arbeitsgemeinschaft für Osteosynthesefragen
- BSE – Back Scattered Electron
- BW – Bodyweight
- CAD – Computer Aided Design
- CT – Computer Tomography
- Callus – composite mass of tissue that forms between bone ends when a fracture is healing
- DCPD – Di-Calcium Phosphate Dehydrate
- DXA – Dual energy X-ray Absorptiometry
- EBSD – Electron Back Scattered Diffraction
- EDX – Energy Dispersive X-ray
- FE/ FEA – Finite Element/ Finite Element Analysis
- GEN I – First generation biomechanical nail
- GEN II – Second generation biomechanical nail
- GEN IIIa – Third generation pre-clinical nail version “a”
- GEN IIIc – Third generation pre-clinical nail version “c”
- GRP – Glass Reinforced Polymer
- GUI – Graphical User Interface
- HA – Hydroxyapatite or Hydroxyl apatite
- IM – Intramedullary
- IOMS – Institute of Orthopaedics and Musculoskeletal Science
- Luxated - dislocated
- Mechanobiology – biology relating to a mechanical source
- MRI –Magnetic Resonance Imaging
- MSDS – Material Safety Data Sheet
- Osteotomy – surgical operation to cut a bone into two parts, followed by realignment of the ends to allow healing
- OTA - Orthopaedic Trauma Association
- PCB – Printed Circuit Board
- S&N – Smith & Nephew

- SEM – Scanning Electron Microscope
- SMD – Strain Measurement Devices
- Symphysis – a joint in which the bones are separated by fibrocartilage
- Thrombose – affected by a local coagulation or clotting of the blood in a part of the circulatory system
- TEM – Transmission Electron Microscope
- TSB – Technology Strategy Board
- UCL – University College London
- XRD – X-ray Diffraction

1 Introduction

A bone fracture has been medically defined as a break in the continuity of the bone. When a patient is admitted with a bone fracture, clinicians at the hospital will have to act swiftly according to their initial management assessment. A secondary survey is conducted to assess any other injuries; radiographs are taken, splints are placed, vascularity and neurological status are checked and a skin examination is conducted for any indication of an open wound. If the radiographic examination shows a hairline fracture, an orthopaedic cast as a non-invasive wound management is used. The reported mean time for clinical union using a cast is 16 weeks. Fracture fixation devices are one of the operative management options and there are various orthopaedic devices available on the market.

Intramedullary (IM) nails are commonly used in long bone fracture fixation. IM nails have been around for many decades and have been performing successfully in most cases. Currently, there are various methods used to assess fracture healing but most of them are either invasive or use medical imaging. When does clinical union occurs is still an unanswered question within the clinical orthopaedic arena. However, there are cases whereby clinical union does not occur and it becomes imperative for the surgeon to reassess the fracture treatment by invasive methods.

This study proposes a novel way to assess bone fractures during the first critical weeks of healing. The study aims to innovate and develop the already existing intramedullary nail into a “smart” nail. It will be instrumented with strain gauges, energiser and a reader system to be able to wirelessly measure the load taken by the nail and better understand the healing process. It will be validated using a set of loading protocols that clinicians can use in order to assess, analyse and make a clinical judgement relating to effective bone healing as early as possible.

This study is funded by the Technology Strategy Board (TSB) through Smith & Nephew Ltd and is in partnership with the Institute of Orthopaedics and Musculoskeletal Science, University College London (UCL).

The study consists of an *in-vitro* and *in-vivo* phase as part of the development of the telemetry system of the nail. The *in-vitro* section consists of testing the nail in a series of artificial bone models (Sawbone®) with induced fractures under a set loading protocol with the strain data collected and analysed. The fractured Sawbone® are synthetically repaired simulating the various stages of fracture healing using a callus bone mimic and the loading protocol is repeated each time. The design and development of the bone callus mimic has been conducted at Brunel University and is an innovative method to simulate the healing stages *in-vitro*. The development of the telemetered intramedullary nail has been conducted over several generations of the systems. The telemetry system has been developed by the Institute of Orthopaedics and

Musculoskeletal Science (IOMS), University College London (UCL) and the biomechanical testing of the telemetered nail *in-vitro* has been conducted by Brunel University.

The *in-vivo* testing has been conducted by Smith & Nephew (S&N), with the collaboration of UCL and Brunel University. UCL provided the wireless telemetered nail and the data collection system while Brunel University designed the loading rigs for the *in-vivo* loading protocol in collaboration with both UCL and S&N. The *in-vivo* testing comprised of cadaveric and live animal models. The live animal study was strictly conducted by S&N as the project license holder in accordance to the 1986 Animal (Scientific Procedures) Act.

The thesis is divided in a number of sections to understand the use of intramedullary nails in the orthopaedic arena as well as the need and importance of a novel instrument. A detailed literature review has been conducted examining the background of bone biology, clinical techniques and the most recent ways of fracture healing monitoring. Statistical data of tibial fractures and related morbidity has been analysed to show trend and the need for a better way to diagnose and monitor fracture healing in figures.

The study focuses on intramedullary nails for long bones such as the tibia hence the review looks at the structure of the tibia, and normal loading conditions are analysed before focusing on the intramedullary nail and its role in the monitoring of fracture healing. Current and historical use of telemetry has been considered for the development of the wireless telemetric intramedullary nail.

The methodology, results and discussion have been integrated accordingly and the chapters are divided between *in-vitro* and *in-vivo* investigations with subsections of the detailed components of each chapter. The *in-vitro* section consists of the design and development of the synthetic bone callus material, the testing of two generations of instrumented IM nails in Sawbone® with induced fractures and the application of the synthetic bone callus material to simulate healing. Prior to *in-vivo* testing, the design of a loading rig has been conducted and validated to be utilised in the *in-vivo* study.

The *in-vivo* section looks at the pre-clinical trial of the instrumented nail along with setting a validated loading protocol to be used by clinicians in assessing healing. The loading protocol included the design of instrumentation for the application of the load described in the protocol. A cadaveric trial of the telemetered nail was conducted at UCL Centre for Biomedical Engineering on an excised left hind limb of a sheep to assess the ease of implantation without causing any damage to the electronic components on the nail as well as to assess the functionality of the nail under set and repetitive loading conditions.

The live phase animal study was conducted at a Smith & Nephew facility in compliance with the 1986 Animal (Scientific Procedures) Act. The live phase animal study was designed to assess the functionality of the smart nail in animals during a set period, according to the functional time of the nail. The thesis also covers the surgical implantation details of the telemetered nail with pre-operational and post-operational strain measurements. During the live phase study, radiographic imaging of the fractured leg of the animals, strain measurements and temperature were recorded to monitor and understand the biological healing environment of the fracture. The analysis and discussion of the results are presented accordingly leading onto the concluding chapter, scope for further work and recommendations.

1.1 Epidemiology of tibial fractures

This section will analyse the past statistical trends of bone fractures in the body focusing on tibial-fibular fractures. Epidemiological data have been derived from studies conducted between 1988 and 2010. The data compiled are from the UK, USA and Finland in relation to the country's population at the time of the study [1-6].

An epidemiological study published in 1995 by Court-Brown et al. [6] found that 77% of tibial fractures included the fibula. The study was conducted with data gathered over a two year period between 1988 and 1990. Their study aimed to analyse the main causes of tibial diaphyseal fractures using **A**rbeitsgemeinschaft für **O**steosynthesefragen or AO classification to show the distribution. The data analysed was calculated from a sample of 523 fractures treated at the Royal Infirmary of Edinburgh which looks after a population of 750,000. The population of the UK in 1990 according to the Office for National Statistics was 57.2 million [57]. Considering the population of the UK in 1990, the number of tibial fractures in the UK in 1990 was calculated to have been approximately 40,000. The study also showed that the highest incidence recorded at 37.5% was road traffic accidents with an average age of 39.8yrs. The lowest cause of fracture was due to fall at 2.5% with an average age of 48.5yrs. The victims of the road traffic accidents were further classified in three groups namely pedestrians, vehicle drivers or passengers and cyclist or motorcyclists. From this analysis, it was seen that the highest incidence occurred in pedestrians with an average age of 45.1 yrs. The lowest incidence was that of the car occupants with an average age of 37.5yrs.

A Finnish study conducted in 1999, showed a total of 1422 tibial fractures treated from a population of approximately 5.2 million with an incidence of 28 fractures in every 100 000 [4,5]. In the USA, each year approximately 580, 000 tibial fractures are registered according to a study published in 2008 [58] from a population of approximately 305 million inhabitants [2]. In 2007, an epidemiological study conducted by Donaldson *et al.* [1], showed that the true annual incidence and lifetime prevalence of bone fractures in England within the general population. The study showed that the calculated fracture incidence is estimated at 3.6% or approximately 2.2 million for the UK. The study conducted by Donaldson *et al.* [1] focused on all bone fractures rather than tibial fractures only. More recent data from Jenkins *et al.* showed 16,000 tibial fractures annually [3] which is about 0.03% of the population [57].

So far, epidemiological studies on their own do not lead to improved fracture treatment or monitoring of the healing. Studies seem to show a 60% decrease in the tibial fracture incidence over two decades within the UK. However, tibial fractures are only one type of fractures; there are still approximately 2.2 million bone fractures every year. Epidemiological data dating two

decades back is quite scarce however a study published in 2001 detailing data between 1988 and 1998 [59] shows an approximate calculated total of 605,000 fractures annually. Comparing annual bone fracture incidence from the two studies, a three-fold increase in the fracture incidence can be observed. The values correlate to the US study and shows that there is an increasing demand for efficient functional fixation devices.

Most medical device companies do their own market research and analysis of the supply and demand in the trauma fixation sector. However, according to Global Data's [7] new report on "Trauma Fixation Devices – Global Pipeline Analysis, Competitive Landscaped and Market Forecasts to 2017", the forecast for the trauma fixation device market is set to reach US $6.7 billion in 2017. In 2011, the US and European orthopaedic trauma device markets was valued at close to US $3.87 billion [8]. The US comprised of approximately 76% [8] of the total market making it the largest in the world. There are many orthopaedic medical device companies that have bone fracture fixation devices on the market but there are 7 major competitors namely; Stryker, DePuy, Zimmer, Smith & Nephew, Synthes, Biomet and Orthofix. In 2008, the US trauma market was at $2.529 billion, with a 9.9% increase from 2007 according to data compared by the Orthopedic Network News, 2009 [9]. Sales figures from Smith & Nephew, US in 2008 shows that the total number of Total Tibial nail sold was at 1521 and Total Retro Femoral nail at 705 [10].

The demand for trauma fixation devices has been rising steadily according to the above figures. Although more recent epidemiological data is not available as to the average age of the patients requiring fixation devices, the rapid change in lifestyle in the past decades also meant that people are more demanding with the products they are being offered by their health provider. Even though in the UK, unless a patient has private healthcare, the decision as to which fixation device will be used for the treatment rests with the surgical team. But in the US for example, patients are allowed and able to choose which company's device they want to use and hence the market is more competitive and demanding in the US. Most patients want a very short stay in the hospital and a shorter recovery time sliding back into normal routine activity. Currently surgeons monitor the mechanical integrity of the bone at 5-6 weeks postoperatively using radiographs and by manually palpating and assessing the mechanical condition of the bone while also monitoring the pain the patient incur during the assessment. With the current versions of fixation devices on the market, the clinicians cannot really assess the integrity of the bone mechanically until about 5-6 weeks post operatively at the earliest depending on patient case.

Despite the success of the standard intramedullary nail, clinicians have to be careful as to the prescribed loading regime with only radiographic imaging to use as influence in their clinical judgement. This emphasises on the need and requirement of a device which can help clinicians

diagnose when the fracture is not healing or how long it may take to heal. It will help to understand how to incorporate loading exercises to promote healing as well as to reassure patients how their treatment is going.

The next section will highlight a few of the different fixation devices available on the market with their benefits and as to why the intramedullary nail is such a popular method of fixation.

1.2 Fracture fixation

The previous statistical analysis shows that tibial fractures in the UK alone make up 0.03% of the population annually. Fracture management treatment is selected on a case by case basis; every single patient is different hence the treatment differs for open and closed fractures. Conservative methods of treatment such as cast are still very widely used for closed fractures. Open fractures treatment depends of the placement and nature of the fracture and the bone concerned.

The aim of non-conservative treatment ensure that bone fragments are held in the most favourable position and provide a suitable biomechanical setting to promote union, allowing early joint locomotion and preventing loss of position or stiffness. All techniques have their own set of advantages and disadvantages like any other product on the market. The following review will look at the types of orthopaedic fracture fixation techniques and the decision making and planning involved prior to choosing the right fracture fixation device for treatment.

The assessment, decision making and planning involved prior to choosing the right treatment has to be very patient focused. The ideal situation is to have a fracture which can be treated in isolation but in this case looking at fractures in the lower limb is not as straightforward. Musculoskeletal injuries often occur accompanied by injuries to other part of the body and/or to other soft tissue nearby. Assessments are carried out to accurately judge and diagnose the severity of the patient's condition. The main concern in surgical procedures is to save a life, followed by saving the limb, joints and re-establishing functions to bodily processes [11]. The different main types of fixation systems used are classified as follows; plate and screw systems, intramedullary nails and external fixators.

1.2.1 Plates and screws

Plates and screws are used as a system together or separately. A screw is a very efficient device for fracture fixation by interfragmentary compression. It is also used to fix plates, nails or fixators to the bone. There are two main types of bone screws: the cortex and the cancellous bone screws [11]. The different screws are designed for different applications to various fracture sites on the bone, type and quality of the soft tissue surrounding the fracture [11]. Screws have evolved over the years with clinical excellence in order to provide improved anchorage. The success and failure

of screws are dependent on axial pull out, bending forces or both. According to Perren *et al.* [11], screws should not be tightened to the limits of strength or ductility but to about ⅔ of these limits, to allow resistance to any additional functional loading.

1.2.2 Plates

Plates have a very fixed position in the fracture fixation market. There are two types of plates, namely locking plates and non-locking plates. Plates provide rigid internal fixation in cases where intramedullary nailing is not the preferred method. Locking plates are thought to increase the stability of the plate-screw system but they are not recommended for use in all fractures [9]. The most recent plates system on the market has been the Less Invasive Stabilisation System (LISS) extramedullary, internal fixation system. The main attribute of this system is the minimal bone contact, the locked, fixed angle construct and the atraumatic insertion.

1.2.3 External fixator

An external fixator is a device placed outside the body percutaneously stabilising the bone fragments through wires or pins connected to one or more longitudinal bars or tubes. They are used in a wide range of open fractures until soft tissues are stable. They are used mainly on long bones but are also often used on pelvic fractures. External fixation device kits consist of many components and they vary per cases. Individual components consist of screws, wires, rings, clamps and rods. The main advantages of external fixation are that there is less damage to the blood supply with reduced interference to the soft tissue. It is very useful for stabilising open fractures and the rigidity of the fixation can be adjusted non-invasively. Its main disadvantages are that the pins and wires penetrate the soft tissue and there is restricted joint motion and increased risk of infection.

1.2.4 Intramedullary (IM) nailing

Intramedullary (IM) nailing technique is the third largest trauma segment which accounted for 14.8% of the sales of trauma product in 2008 according to the Orthopaedic Network News [9]. IM nailing is one of the most common methods of treatment for long bone fractures. Conventional Küntscher nails with longitudinal slots have been around since the 1940's. The Küntscher nail is a tight fit, unlocked nail. The latter is restricted to simple midshaft diaphyseal fractures as the stabilisation is dependent on the contact between the implant and stiff bone. Reaming the intramedullary canal can increase the area of contact but reaming can also introduce biological disadvantages such as an increase in intramedullary pressure, temperature rise, disruption to the blood supply and bone necrosis [9, 11]. The Grosse and Kempf universal nail was introduced as a tight fitting locked nail. It had not only interlocking screws but it also improved the mechanical

properties of the intramedullary implant and widened the range of indications to more proximal and distal fractures.

Nailing can be done with or without reaming. The physiological effect of reaming and no reaming during intramedullary nailing is explained here in order to stress its importance for treatment. According to Krettek [11], reaming the medullary cavity causes damage to the internal cortical blood supply. Other changes that arise during reaming include potential pulmonary embolisation, temperature related changes of the coagulation system and the humoral, neural and inflammatory reactions amongst others. In nailing without reaming, smaller diameter nails are used. The benefits are fewer disturbances to the blood supply and less heat production. It also reduces postoperative infection.

1.3 Market analysis of the medical device and diagnostic

The Medical Device and Diagnostic (MD&D) sector is a rapidly evolving one. It has been steadily growing over the past decade and there are steep rises in sales of devices due to the change in lifestyle as well as the aging population. The 2008 US trauma market was valued at $2.529 billion with a 9.9% increase from 2007 according to the market analysis conducted by the Orthopaedic Network News [9]. The methodology used to analyse the size of the market for trauma fixation devices for the purpose of this study is to take the numbers and definitions of trauma found in the publicly traded companies' annual reports and compiled to derive an understanding. According to the Smith & Nephew Plc. 2010 annual report [12], the company boasts about $3,962 million revenue with an increase by 4% in sales compared to 2009. From their financial performance section, their orthopaedics business unit registered $2,195 million with their trauma segment getting revenue of $435 million with a 3% increase. They also give an overview on the global orthopaedic market and the competition they face.

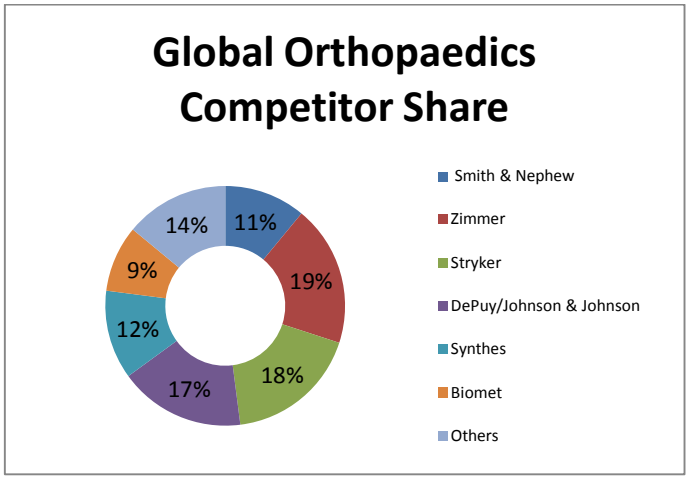

Figure 1: Pie chart illustrating the global orthopaedic market

Figure 1 shows a pie chart illustrating data that has been extracted from the Smith & Nephew 2010 Annual Report. The data shows the global orthopaedics market served by the Group consisting of orthopaedic reconstruction and orthopaedic trauma. The competitor shares are based on estimates for selected segments and competitors and may not be comprehensive. From the above market distribution, J&J and Synthes were two separate businesses. As of 2011, Synthes are now trading under the J&J, family of companies. J&J on its own is valued at $61.1 billion [13]. The sales figures by segment from their 2010 annual report showed their MD&D segment valued at $24.6 billion and form about 40% of J&J. Figure 2 shows the different divisions of J&J and their percentage value extracted from J&J 2010 annual report.

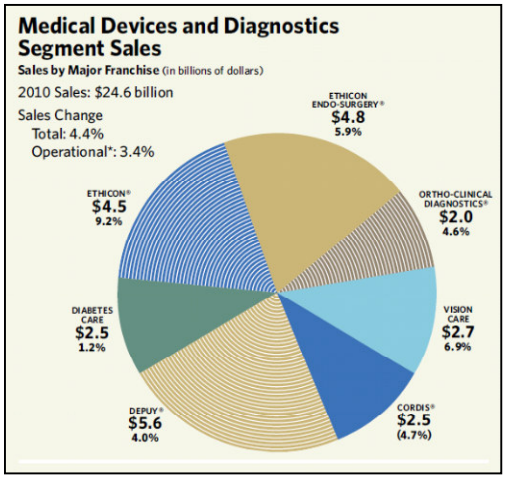

Figure 2: Extracted from J&J 2010 annual report [13]

In terms of trauma fixation devices, DePuy is the main manufacturer to compete with players like Smith & Nephew, Stryker, Biomet and Zimmer. The Zimmer market share in trauma is about 5% as stated in their 2010 annual report with a market size of $5 billion and an annual growth of 6% [14]. Stryker on the other hand has two distinct segment in their business; Orthopaedic implants (59%) and Medical surgical equipment (41%) [15].The 2010 figures show the company's revenue was at $4,308 million with an increase of 5%. There was no further description as to what the market segment for trauma devices is and its annual revenue. Biomet which is another major orthopaedic device company states that their US musculoskeletal products market is $426.3 million with their sports extremities and trauma fixation at $85.4 million with a 12% increase in net sales by the end of Quarter 2 of 2012 [16]. The above overview of the trauma fixation device market gives a sense of direction the trend is taking and what can be expected in the next decade in the trauma fixation device market.

1.3.1 Overview of intramedullary nail currently on the market

There are many types of intramedullary nails commercially available on the market but they can be divided into two main categories, slotted and non-slotted nails. The nail's function is to stabilise the fracture fragments, allowing load transfer across the fracture site while maintaining anatomic alignment of the bone. There have been numerous *in-vivo* and *in-vitro* studies that have documented the performance of the nails. Biomechanical studies have shown that in torsion, slotted nails have a considerably lower rigidity than non-slotted nails, but in bending [17]. Küntscher nails were popular in the 1940's and were slotted nails. The majority of nails provide holes at their proximal and distal extremes for interlocking to prevent shortening and rotation of the fracture fragments in unstable fractures.

Table 1 (page 29) shows three different intramedullary nails from DePuy, B Braun and Smith & Nephew which are currently on the market. All three of them have are interlocking nailing systems that are currently used. The ideal market analysis in terms of the usage of these nails would be a realistic statistic as to the cases these nails have been used for and compared for the same types of fractures in terms of clinical union. Unfortunately, currently there is no such statistical data that are available for comparison. This shortage in statistical data about the nails used as per the types of fractures is an area which needs to be investigated. This would allow a better understanding of the usage of the types of nails and the healing monitored accordingly for a more in depth analysis of the bone fracture healing. Thus emphasizing on the clinical need for a monitoring device, this can be used to collect the data as per patient. This leads to the literature review of the current practice of fracture healing monitoring, what has been tried and tested and where those practices are leading to.

DePuy Versanail Tibial Nailing System [18]	Aesculap Orthopaedics Targon® F/T Interlocking Nail system for Femur and Tibia [19]	Smith & Nephew Trigen META Nail – Tibial nailing system [20]
		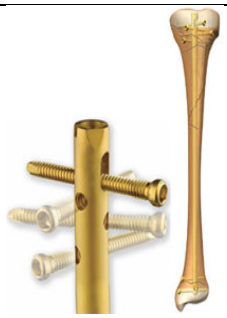
Specification • Enhanced locking options treat a range of fracture patterns • Oblique orientation of the proximal locking screws provides maximum stability • Large core diameter of the proximal 5.5mm screws decreases risk for screw breakage • Expanded working length treats a greater range of proximal and distal fractures • Bullet-style tip and 2°bend increase ease of insertion	**Specification** • Implants are anatomically adapted • Implants have been developed that can be used in either left or right leg • Proven quality and modern manufacturing processes ensure excellent load bearing capacity in all relevant dimensions. • The drilled implantation technique is supplemented by the drill-free technique for situations with a high degree of soft-parts damage, high blood loss or severe thoracic trauma	**Specification** • Indicated for fractures of the proximal and distal third of the tibia including the shaft, stable and unstable fractures, non-unions, mal-unions and for the prophylactic nailing of impending pathological fractures

Table 1: Data extracted from company websites [18, 19, and 20]

1.4 Current fracture healing monitoring methods

Fracture healing monitoring has been an on-going challenge for orthopaedic surgeons for many years. The healing process is progressive and it is not always feasible to indicate a time when the fracture is said to be healed. In the recent years, several different methods have been developed to assess and monitor fracture healing. The following is a review of the different methods of fracture healing monitoring developed, used during the past decades and how beneficial they

were. There are three instances where union is said not to have occurred, delayed union, mal-union and non-union. Delayed union relates to the prolonged time taken for fracture union to occur. Mal-union refers to fracture union occurring with poor anatomical clinical alignment. Non-union refers to cases where the fracture has not healed and is not likely to do so without intervention.

Figure 3 below shows a radiograph of a typical development of fracture callus at week 8 in an ovine model. The fracture line is still visible as well as the callus geometry which should eventually lead to clinical union.

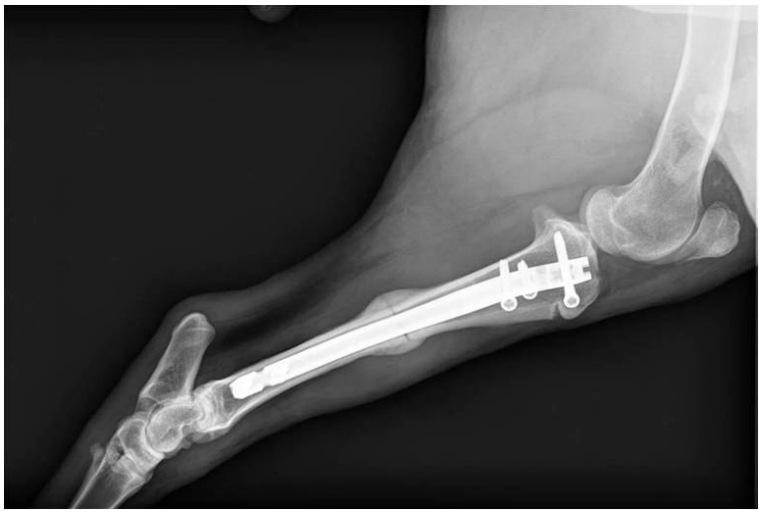

Figure 3: Lateral view of fractured left hind limb in an ovine model, treated with an intramedullary nail. Fracture line and fracture callus are visible around the midshaft area at week 8 post-operatively.

Wanatabe *et al.* developed a non-destructive method for monitoring fracture healing with acoustic emission (AE) [21]. It was suggested by Nicholls and Berg [22] that AE can be a potential method for evaluating fracture healing. AE is a technique that is facilitated by an acoustic pulse that occurs when energy is released in conjunction with the destruction and transformation of a material. An AE is a stress wave that travels through a material as a result of a sudden release of strain energy. The study was conducted on rat femurs tested in tension and torsion at various points during healing after fracture. This resulted in some indication that some mechanical properties of healing fractures could be estimated by monitoring changes in AE signals [21, 22].

Njeh *et al.* showed that the use of quantitative ultrasound using phantoms to monitor fracture healing warranted further investigation *in-vivo* [23]. Ultrasound was first used across a fracture site in 1958 by Siegel *et al.* [24]. Since then few others have conducted similar experiments but it was not until the introduction of the SoundScan 2000, which was primarily designed for osteoporosis assessment, that ultrasound propagation was used for monitoring fracture healing

[23]. The study revealed that if the SoundScan 2000 was to be trialled on a real fracture, it was likely that healing could be monitored quantitatively over a phase. It would have been an opportunity to forecast healing time for more complex fracture patterns in the study [23]. But the study had its limitations when it came to clinically complicated long bone fractures; the phantom simulated in the experiment was through constant soft tissue and in clinical situations this will vary with time [23].

In 1996, Oduncu *et al.* described a new approach to measure the strain in internal fixation plate using magnetoelastic properties of positive magnetostrictive amorphous magnetic ribbons [25]. The theory hypothesised in this study is the inverse effect of magnetorestriction; the magnetisation change caused by the application of mechanical stress. The coupling of magnetic moments to the mechanical structure leads to magnetoelastic effects, including the stress sensitivity of magnetisation and changes in elastic constants resulting from the rotation of magnetic moments [25]. The experiment consisted of applying known stress values and expecting strains which are usually observed during the healing process. The study showed that magnetic detection is a possible tool for monitoring stress and strain during fracture healing. However, the small diameter of excitation and the search coils used for experimental purposes is not a realistic scenario. In clinical situation, in order to accommodate a whole leg inside the coil, improved search coils will be required with accurate air flux compensation [25].

Nikiforidis *et al.* presented a study for monitoring fracture healing based on bone vibrational response [26]. The study was validated in clinics showing that the natural frequency shift and the phase angle shift are related to mechanical properties of simulated fracture callus further relating to fracture healing progress. However, the experiment was conducted only on transverse fracture. The author does suggest that there is still more work to be conducted to look at more severe fractures as well as the problem in the soft tissue variation [26].

Wippermann *et al.* [27] used micro bone densitometry to predict the mechanical properties of external fracture callus by correlating the mineral density and morphological characteristics of the callus. A high resolution single photon absorptiometry was custom-made for the analysis of small bone specimen [28]. The experiment was used to simulate *in-vivo* application of quantitative computed tomography (CT) imaging which can be adapted for use in absorptiometry scanners but the latter are conventionally 2-D images of 3-D structures, which may be difficult to be applied *in-vivo* [27].

Cattermole *et al.* [29] used dual energy x-ray absorptiometry (DXA) in order to quantify measurement of fracture healing with internal fixation over plain conventional radiographs. Conventional radiographs do not allow for valuable established information and dual energy x-ray

absorptiometry improved radiography by giving a quantified measure of mineralisation at the fracture site. However, the author concluded that even though small changes were observed with DXA, it still does not offer any significant diagnostic benefit over plain radiography.

Indentation testing [30] was designed to verify the association between the structural properties of bone healing and the bone's torsional strength. The latter was performed in canines with secondary gap healing under stable external fixation. It was found to be in agreement with other previous studies [31, 32]. However, the indentation stiffness test is not enough to be used alone. A combination of the mineral bone density within the bone volume together with the distance of the region from the bone's torsional axis may be an alternative method of describing the torsional properties of fracture healing according to Markel *et al.* [30].

The various methods of monitoring fractures described above have all been developed with the aim to further understand the healing mechanics of the skeletal system but so far none has progressed to be used on humans as a base method within the health care sector. Currently the methods of monitoring the fracture healing have been non-invasive techniques such as X-rays, computed tomography (CT) and magnetic resonance imaging (MRI). However, it has been observed that these techniques are costly and inadequate for accurate diagnosis as only the geometry of the callus is seen and there is no way of quantifying the load sharing between the implant and the bone during fracture healing. It is also detrimental to the health of the patients by exposing them to repeat imaging techniques which uses radiation. Medical imaging only gives the surgeon an indication of the fracture gap bridging but it does not allow them to tell if the bone is mechanically ready to take full load again. This is usually when fractures go undetected until the trauma implant fails. In other cases, the surgeon, using the imaging techniques to monitor the healing, might remove the implant prior to clinical healing and mal union can occur.

According to Moulder *et al.*, the tibia is more susceptible to a failure in the biological healing process because of the large subcutaneous edge with soft tissue cover and an unstable vascular supply [33]. The latter also states as the tibia is a weight bearing bone hence the level of morbidity of a non-union is high [33]. Intramedullary nailing is one of many fracture fixation devices currently used as described in the previous section. The use of strain gauges on an implant to monitor fracture healing has been investigated over the years by several research groups [34-36]. Fracture treatment by means of intramedullary nail [35, 36] is an established and widely used method of treating transverse and short oblique, axially stable fractures of the femoral diaphysis. The purpose of the intramedullary nail is to aid healing, secured by its stiffness, which is usually expressed according to load directions as bending or torsional stiffness [34].

Strain gauges have been used in monitoring fracture healing in femoral fractures by Schneider *et al.* [34]. He stated that there was no study to measure the load supported by an intramedullary nail during fracture healing. The study proved that an implant equipped with a multi-channel telemetry system is a very powerful tool for investigating the implant loading *in-vivo* [34]. Moreover, it was observed that even after fracture consolidation, approximately 50% of the load was transmitted through the nail and that muscular activity plays an important role in the fracture healing [34].

Intramedullary nails can be subjected to three types of loading and combinations of loading; bending, torsion and compression. These loads may be measured indirectly by measuring sensor output of a series of strain gauges mounted on the nail. The instrumented nail will have the capacity to provide an accurate measurement of the applied mechanical load across the implant. The telemetric implant will consist of a control unit and an orthopaedic implant that includes sensors and associated electronic components for measurement of loads and transmission of the sensor data to an external data logger [37].

The literature results reported by Schneider *et al.* [34] were *in-vivo* measurements that are unique and cannot be compared. Manley *et al.* measured the *in-vivo* tensile and compression loads in a canine femur but could not measure the complete set of load components. Furthermore the loading condition in a quadruped is not comparable to human [38]. Obara *et al.* measured the *in-vivo* strains of an intramedullary nail during fracture healing in goats, a decrease in implant strains were noted but again the comparison to human was questionable [39]. This leads to the next section which examines the definition and use of telemetry in the past, present and possible near future.

1.5 What is telemetry?

The term telemetry is defined by the Oxford Dictionaries Online [40] as “an apparatus used for transmitting and recording the readings of an instrument to a distant receiving set or station” or the “science of transmission of inaccessible data to accessible locations.” The Greek root “*tele”* means remote and “*metron”* means to measure, is where the word was derived from. Telemetry dates back to the early 17th century, where an Italian astronomer named Porro, used a technique called tachymetry (quick measurement) to determine distances [41, 42]. The earliest documented use of telemetry was in 1885, where a US patent was granted for a telemetry system as a result of the invention of the telegraph [41, 42]. This led to the invention of the telephone later on. The systems were used to monitor the use and distribution of electricity in the early years [42]. The 20th century saw telemetry system being used to transmit data using the power lines. The latter were either voltage or current-type systems, which later led onto the development of the pulse-

type wired telemetry in the 1920s [41, 42]. However, the use of telemetry system was limited to aircrafts and it was not until after World War II that those telemetry systems were applied in other areas such as agriculture, retail businesses, medicine, space and wildlife amongst others.

Biomedical telemetry is the monitoring of biological functions in humans or animals by means of a miniaturised transmitter implanted and read by electronic instruments from a distant point [43]. It has been used for real time monitoring in the early 1960s to monitor physiological responses of human subjects with the advent of the space program. In the last four decades, biomedical telemetry have allowed actual or encoded parameters to be transmitted via acoustic or radio waves in various conditions without the hindrance and restriction of wires to connect the transmitter and the receiver [44]. The type of measurement required by the system typically dictates its requirement. One of the most important considerations is the number of data channels required and the frequency of each channel. Other factors are transmission range and the environment the system is likely to be subjected to [44]. Most telemetry system uses some form of transducer to convert physical quantities into electrical signals such as strain gauges, accelerometers, gyros and thermocouples.

Once established there was a widespread use of biomedical telemetry in biological, environmental and medical research. Real time physiological monitoring has been extensively used in hospitals since 1970s [44]. More recent years have seen the design and development of implanted miniaturised multichannel radio bio-telemetric systems. Major achievements and technological advances have led to the design of small, reliable and low power consuming implant devices that can communicate data from the inside of the human body in real time. This leads to the review of the historical use of biomedical telemetry in the field of orthopaedics; understanding the challenges and learning from its benefit and how it can be further adapted to suit to purposes such as enabling fracture healing monitoring.

1.6 History of telemetry in orthopaedics

The year 1966 saw the advent of telemetry in the area of orthopaedics by Rydell *et al.* [45]. The latter measured the load, in 2 adults aged 51 and 56 years old, by replacing the head and neck of the femoral bone with a modified hip prosthesis. Rydell successfully recorded the peak loads in those two subjects for normal walking and running [46]. Carlson *et al.* [46] developed a miniature sized radio telemetry device to monitor the magnitude of the cartilage surface pressures in the human hip. Carlson *et al.* believed that measuring cartilage surface pressure *in-vivo* will enable researchers to have a better insight on the functioning of normal cartilage and further understand diseases such as osteoarthritis. The system performance was satisfactory when loaded in contact with hip sockets from cadavers [46]; however the system did not fit into common hip implants.

Crownshield *et al.* [47] conducted a study to examine the human hip during specific levels of activity. The experiment was consistent with Rydell's measurement as the latter was one of the rare *in-vivo,* direct experimental readings taken for abnormal joints.

English and Kilvington [48] reported the results of measurements taken from a dynamic human hip loaded *in-vivo* using a femoral prosthesis instrumented with strain gauges at its neck. The readings were fed from the transducers to a locally implanted transmitter, which was picked by a receiver on the outside of the body. Within 10 minutes after implantation, the transmitter signal strength stabilised and the records show an increase in load between the dislocated and complete reduction. Readings after 24hr with the patient resting in supine position was 0.72 times the total body weight (BW). Muscle relaxant drug was assumed to have worn off at that point in time. Supine readings 48hr later increased to 0.84 times BW and again on day three to 0.96 BW. They selected a heavy patient (80kg) as it was considered to be helpful in increasing stresses and variations in the signal strength of the system. English and Kilvington [48] showed that the system is an efficient method with predictable factors without the need for intricate calculation of results.

Bergmann *et al.* [49] study examined the problems involved in the force measurements and telemetric strain. The study encompassed various other studies where telemetry has been previously used and gave a survey on the problem of telemetrised implants. Brown *et al.* [60] reported on the telemetry system they developed to investigate forces in bone plates. The system was functional but was nevertheless relatively large. Barlow *et al.* [61-62] developed a telemetry system for artificial hip joints powered inductively, but due to the size it had to be implanted separately. Most of the systems studied by Bergmann *et al.* [49] had serious shortcomings such as toxic batteries, too bulky in size and had restricted operating time. Polymeric materials were used to seal the wires however they were not creep resistant or moisture proof.

The research group at the Charité Institute in Berlin, led by Bergmann et al. [63-69] has been the front of many telemetered devices over the past few decades. From shoulder prostheses, to knee tibial plateaus via the spinal and hip joint, the group has developed several systems and many of which have been tested in patients over many years successfully. Their aim has always been to develop a system that will function mechanically with the added benefit of a system sending data back in order to further understand the physiology *in-vivo*. They developed a hip joint prosthesis for *in-vivo* measurement of forces and moments in the joints. A modified hip implant with strain gauges in the implant neck to measure deformation along with a small coil for inductive power supply was used. The cavity in the neck of the implant was hermetically sealed using electron beam welding. The system has a sampling rate of 120Hz, with pulses transmitting through the

antenna inside the ceramic head. Data was telemetered from real time loads from the measured deformations with a maximum error of 2% including crosstalk. Kutxner et al. from the same group also used telemetry to measure the direct effect of footwear on the tibiofemoral contact loads during walking.6 subjects were tested clinically in four different shoes and the data was compared to barefoot loading during walking. The footwear was shown to have a slight increase knee joint loading. Forces measured were very low and it was hence questionable whether it does contribute to gonarthrosis. Rohlmaan et al. has recently published with Bergmann on instrumented vertebral body replacements. These were implanted in 5 patients with severe compression fracture of the lumber vertebral body. Using a clinically approved product and instrumenting it with 6 strain gauges, a telemetry unit and an inductive coil for power supply, the aim was to measure the spinal loads during various positions. The study showed that there may be high forces acting on the spine when changing positions. These can be reduced by supporting the upper body with arms and following closely the instructions provided by the physiotherapists. Kutzner et al. has also previously used telemetered knee prostheses in 3 subjects in order to measure the medial compartment load when wearing valgus braces. The loads were measured during various activities using two different braces. The study shows that the load reduction depends on brace stiffness and the valgus adjustment and vary from one individual to the next. Spinal fixation devices were instrumented and sealed to monitor loads acting on these devices in a study conducted by Graichen et al. The devices were implanted in two patients. The device measured the load acting on the two devices however, the loads shared between the implant and the spine is unknown. Heller et al. conducted a study on measuring the loading of the proximal femur in 4 patients during walking and stair climbing using instrumented hip prosthesis. The system proved to be a useful means to determine valid conditions for the analysis of prosthesis loading, bone modelling or remodelling processes around implants and fracture stability following internal fixation. Bergmann et al. instrumented shoulder implants to measure contact forces and moments. The contact forces for the first 7 months were noted to be below 100% bodyweight however, more clinical data is needed for longer period of time. The Charité Institute in Berlin has been very much at the forefront of the technological advancement in using telemetry in biomedical engineering [63-69].

Mid 1990s saw improvement in the development of telemetric systems for the *in-vivo* force measurements as described by Taylor *et al.* [50] following Bergmann et al. [63-69]. Taylor et al. [50] instrumented four hip prostheses which were implanted and data recorded successfully over 7 years. The implant was hermetically sealed and various elements of the system design have been proven *in-vivo* over a number of years. The implant failure was associated to the malfunctioning of the coil leads or breakdown of the encapsulation. Taylor *et al.* [51]

instrumented and implanted two femoral replacements to measure axial forces at two different sites within the prosthesis. Their goal was to measure the changes in force distribution over time. Progressive transfer of the axial load was observed from the proximal to the distal part of the stem. The measurements were recorded via telemetry as well as radiographically, which showed bone remodelling had taken around the proximal part of the stem [51]. Tung-Wu *et al.* [52] instrumented massive proximal femoral prostheses, which were custom-made, to be implanted in patients after a tumour resection. Axial forces were telemetrically recorded during single and double leg stances and isometric exercises of the hip muscles.

Taylor *et al.* [53] reported on the forces produced in the distal femur and the knee during various activities measured by telemetry. Their study examined the sensitivity to each applied load which was determined by applying the loads separately and measuring the sensitivity of every strain gauge output to the applied load. A cross sensitivity matrix was produced during the processing of the data recorded, which on inversion yielded the coefficients to void the mechanical cross talk between channels. In order to take measurements, the subject wore a small battery powered energiser connected to the external coil which was positioned around the leg in the plane of the implant coil. The data was telemetered wirelessly without the requiring leads to be connected to the subject for power supply or telemetry. Taylor *et al*. [53] acknowledged that despite the limitations of their study, the *in-vivo* data of the forces of a midshaft femur in various activities and that at the knee during walking was still valuable. Biomechanical forces and moments from the shaft of two distal femoral implants and the data were reported for up to 2.5 years by Taylor *et al*. [54]. The study used a matrix method to account for cross sensitivities of all channels to the applied loads. A measurement matrix was derived in the data acquisition software, for both prostheses. Over the 2.5years when the measurements were taken, the history charts show a trend of slight increase in peak forces. Forces recorded during jogging at 3.1-3.6BW were the highest observed. After 2.5yrs no further measurements were taken. The implants were explanted for various reasons [70].

D'Lima *et al.* [55] developed an implantable telemetry system to measure tibio-femoral compressive forces and the system was successfully dynamically tested on a cadaveric knee. D'Lima *et al.* [55] recognised the fact that telemetry has been shown to successfully measure *in-vivo* data from implanted transducers in the hip, spine and femur. The technology has been proven to be a safe and accurate means of obtaining data *in-vivo* [55]. An instrumented tibial prosthesis was deemed to have the potential to measure forces during activities of daily living.

The above review emphasises on the developmental design telemetry in medicine has undergone. Intramedullary nails implanted tend to be for life unless there are specific causes as to why their

removal is required. This could be due to pain, infection or to comply with patient request. It proves the beneficial potential for a telemetered intramedullary nail in today's orthopaedic trauma management arena. The introduction of a wireless telemetry system will enhance the patient's experience during treatment allowing clinicians to accurately assess and diagnose the mechanical integrity of the bone as healing progresses. It will allow surgeons to tackle non-union and mal-union as early as required and as efficiently as possible. It is very likely that with the advent of the wireless telemetered nail to monitor fracture healing, clinical healing can be measured quantitatively hence allowing clinicians to make an informed diagnostic as to the when it is safe to remove the nail if required.

1.7 Overview of the project plan with Gantt chart

The purpose of this study is to review and investigate the effect of loading on intramedullary nails during simulated fracture healing *in-vitro* using custom designed jigs and different fractured artificial bone, which will be integrated in a biomechanical test frame. Figure 4 (page 44) shows the outline of the design progression of TriGEN META Nail from a biomechanical test nail to a commercial nail.

The design and development of the instrumentation for the telemetrised nail were all conducted in by UCL and Smith & Nephew. For each nail, more details would be outlined, in the respective sections, about the instrumentation, encapsulation and wire-bonding processes. All through the project 4th Generation Sawbone® was used. The Sawbone® was partly prepared by Smith & Nephew Ltd, Memphis, USA but the major drilling and sectioning to simulate fractures was undertaken at UCL and Brunel University facilities. The custom designed frame for the biomechanical test was designed and manufactured at UCL facilities as well as the data acquisition system for the entire set of telemetrised nails.

Callus composite was initially developed during an MSc Dissertation project output [56]. However, the majority of the design and development were conducted using different materials to simulate low and high stiffness of early to mature osteogenic bone as part of this doctoral degree. This allowed for a more realistic view on the mechanical strength of the callus material and the effect it has on the load shift as healing progresses.

GEN I & II were *in-vitro* biomechanical nails and had a wired system. The aim each generation nails are further described in Figure 4 on page 40.

320 x 10 mm	340 x 10 mm	180 x 10 mm	340 x 10 mm	Multiple sizes
Spiral configuration	1 extended pocket	1 short pocket	1 extended pocket	1 short pocket
Wired energizer/reader	Wired energizer/reader	Wireless energizer/reader	Wireless energizer/reader	Wireless energizer/reader
9/8 slave stations	5 slave stations	2 slave stations	3 slave stations	1 slave stations
24-27 gauges	20 gauges	6 gauges	12 gauges	1-2 gauges
3 gauges per slave site aligned at +45°, 0° and -45° to nail axis	4 gauges per slave site aligned at 0° (x3), and 45° (x1) to nail axis	3 gauges per slave site aligned at 0° (2), and 45° (1) to nail axis	4 gauges per slave site aligned at 0° (3), and 45° (1) to nail axis	1-2 gauges per slave site aligned at 0° and/or +45° to nail axis
Establishing loading protocols, validating fracture models, & understanding gauge sensitivity to fracture location	User experience on software and hardware components prior to GEN III nail. Soft encapsulant & biocompatibility testing	User experience on software and hardware components in animals prior to GEN III nail. 8 patients in vivo study of strain changes during fracture healing	User experience on software & hardware components in patients prior to commercial GEN IV; 5 patients in vivo study of strain changes during fracture healing	Verification & Validation of GEN III nail. Pocket will be shorter than 70 mm (GEN IIIa).

Figure 4: Design progression of TriGEN META IM nail from biomechanical test nail to commercial nail

GEN IIIa was the pre-clinical nail that was designed specifically to be implanted in Blue Faced Suffolk Sheep in order to conduct a live-phase pre-clinical trial of the wireless telemetric intramedullary nail at the IVB Test House with Smith & Nephew leading the experiments. Loading protocols were designed for the pre-clinical trial along with a loading kit. The loading kit consists of several custom-made rigs designed for the load application on the sheep during pre-clinical trial. Another loading rig has been designed that could be potentially be used for human clinical trial in the future by Brunel University. A copy of the Gantt chart can be found in Appendix A along with the edited versions produced as the project changed. The next chapter examine more in depth the skeletal system and the mechanobiology of the bone.

1.8 References

[1]. LJ Donaldson, IP Reckless, S Scholes, JS Mindell, NJ Shelton. The epidemiology of fractures in England. Journal of Epidemiology & Community Health,2008, 62,174-180 .

[2]. 2008 World Population Data Sheet, Population Reference Bureau. Available at: http://www.prb.org/Publications/Datasheets/2008/2008wpds.aspx (last accessed: 15/05/2011 22:42)

[3]. PJ Jenkins, JF Keating, AH Simpson. Fractures of the tibial shaft. Surgery, 2010, 28,10

[4]. J.A.K.Toivanen. The management of closed tibial shaft fractures. Current Orthopaedics, 2003, 17, 167-175.

[5]. Encyclopedia of the Nations. Available at:http://www.nationsencyclopedia.com/economies/Europe/Finland.html (last accessed: 15/05/2011 22:42)

[6]. C.M.Court-Brown, J.McBirnie. The epidemiology of tibial fractures. Journal of Bone and Joint Surgery [Br], 1995, 77-B, 417-21.

[7]. http://www.businesswire.com/news/home/20110318005685/en/Research-Markets-Trauma-Fixation-Devices---Global (last accessed: 29/09/2011 18:04)

[8]. http://www.prweb.com/releases/2011/12/prweb9064431.htm (last accessed: 03/10/2012 18:27)

[9]. Orthopaedic News Network, Vol 20, No.2, April 2009; Mendenhall Associates Inc.

[10]. Smith & Nephew Tibial Nail US sales report, Smith & Nephew Plc, 2010-11

[11]. T.P. Rüedi, W.M. Murphy. AO principles of fracture management. Thieme Publishing. 2000

[12]. 2010 Summary Annual review, Smith & Nephew Plc. (last accessed 30/09/2011, 17:22)

[13]. J&J 2010 Annual Report, Johnson & Johnson Inc. (last accessed 30/092011, 18:39)

[14]. Zimmer Holdings, Inc. 2011 Fact Sheet. Zimmer Holdings Inc. (last accessed 30/09/2011, 17:59)

[15]. 2010-2011 Fact book, Stryker Corporation.(last accessed 30/09/2011, 17:52)

[16]. http://www.biomet.com/corporate/investors/presentations/corporatePresentation.cfm (last accessed: 02/04/2012 21:18)

[17]. R.J.Eveleigh. A review of biomechanical studies of intramedullary nails. Medical Engineering & Physics, 1995, 17**,** 5, 323-331.

[18]. http://www.depuy.com/healthcare-professionals/product-details/versanail-tibial-system (last accessed: 02/04/2012 21:37)

[19]. http://www.bbraun.com/cps/rde/xchg/bbraun-com/hs.xsl/products.html?prid=PRID00002322 (last accessed: 02/04/2012 21:35)

[20]. http://global.smith-nephew.com/us/TRIGEN_TIBIAL_NAIL_SYS_15436.htm (last accessed: 02/04/2012 21:36)

[21]. Yoshinobu Watanabe, Shinro Takail, Yoshiyuki Arai, Nobuyuki Yoshino, Yasusuke Hirasawa. Prediction of mechanical propertied of healing fractures using acoustic emission. Journal of Orthopaedic Research, 2001, 19, 548- 553.

[22]. Niclolls PJ, Berg E. Acoustic emission properties of callus. Medical and Biological Engineering and Computing, 1981, 19, 416-8.

[23]. C.F.Njeh, J.R.Kearton, D.Hans, C.M.Boivin. The use of quantitative ultrasound to monitor fracture healing: a feasibility study using phantoms. Medical Engineering & Physics, 1998, 20, 781-786.

[24]. Siegel IM, Anast GT, Fields T. The determination of fracture healing by measurement of sound velocity across the fracture site. Surgery Gynaecology and Obstetrics, 1958, 107, 327–332.

[25]. H.Oduncu & T.Meydan. A novel method of monitoring biomechanical movements using the magnetoelastic effect. Journal of Magnetism and Magnetic Materials, 1996, 160, 233-236.

[26]. G.Nikiforidis, A.Bezerianos, A.Dimarogonas and C.Sutherland. Monitoring of fracture healing by lateral and axial vibrational analysis. Journal of Biomechanics, 1990, 23, 7, 323-330.

[27]. Wippermann BW, Aro HT, Hodgson SF, Wahner HW, Lewallen DG, Chao EY. Prediction of properties of fracture callus by measurement of mineral density using micro-bone densitometry. Journal of Bone & Joint Surgery [Am], 1989, 71, 1020-30.

[28]. HT Aro, BW Wippermann, SF Hodgson, HW Wahner, DG Lewallen and EYS Chao. Prediction of properties of fracture callus by measurement of mineral density using micro-bone densitometry. The Journal of Bone and Joint Surgery, 1989, 71-A, 7, 1020-1030.

[29]. Cattermole HC, Fordham JN, Muckle DS, Cunningham JL. Dual energy x-ray absorptiometry as a measure of healing in fractures treated by intramedullary nailing. Journal of Orthopaedic Trauma, 1996, 10, 563-8.

[30]. Markel MD, Wikenheiser MA, Chao EY. A study of fracture callus material properties: relationship to the torsional strength of bone. Journal of Orthopaedic Research, 1990, 8, 843-50.

[31]. Aro H, Kelly PJ, Lewallen DG, Chao EYS. Comparison of the effects of dynamisation and constant rigid fixation on rate and the quality of bone osteotomy union in external fixation. Transactions of the Orthopaedic Research Society, 1988, 13, 303.

[32]. Aro HT, Wahner HW, Kelly PJ, Chao EYS. Comparison of stable transverse and unstable oblique osteotomy healing in the canine tibia under external fixation. Transactions of the Orthopaedic Research Society, 1989, 14, 121.

[33]. Elizabeth Moulder, Hemant K Sharma. Tibial non-union: a review of current practice. Current Orthopaedics, 2008, 22, 434-441.

[34]. Erich Schneider, Markus C.Michel, Martin Genge, Kurt Zuber, Reinhold Ganz & Stephan M.Perren. Loads acting in an intramedullary nail during fracture healing in the human femur. Journal of Biomechanics, 2001, 34, 849-857.

[35]. Allen W.C, Piotrowsky G., Burstein A.H, Frankel V.H. Biomechanical principles of intramedullary fixation. Clinical Orthopaedics, 1968, 60, 13-20.

[36]. Kuentscher G.B.G.; Die Marknagelung von Knochenbruechen. Archiv fuer klinische Chirurgie, 1940, 200-243

[37]. http://www.wipo.int/pctdb/en/wo.jsp?WO=2007025191&IA=US2006033326&DISPLAY=DESC (last accessed: 16/05/201114:11)

[38]. Manley P.A, Schatzker J, Sumner-Smith G. Evaluation of tension and compression forces in the canine femur *in-vivo*. Archives of Orthopaedic and Trauma Surgery, 1982, 99**,** 213-216.

[39]. Obara T., Nippon Seikeigeka Gakkai Zasshi. A biomechanical study on the fracture treatment – intravital measurement of the strain on an intramedullary nail in the healing process of the femoral fracture in goats, 1979, 53, 2, 199-212.

[40]. http://oxforddictionaries.com/definition/telemeter?q=telemetry#telemeter__5 (last accessed: 20/04/2012 15:18)

[41]. Harry L.Stiltz. Aerospace telemetry, Volume 1. Prentice Hall Space Technology Series. 1961

[42]. Bassam Shaer and Jay M.Lalik Sr. Aerospace Telemetry. Department of Electrical and Computer Engineering; University of West Florida, Pensacola, Florida, USA. Available at: http://nguyendangbinh.org/Proceedings/IPCV08/Papers/CIC4206.pdf (last accessed: 20/04/2012 15:30)

[43]. http://www.thefreedictionary.com/biotelemetry (last accessed: 20/04/ 15:46)

[44]. Robert S.H.Istepanian & Milica Stojanovic. Underwater Acoustic Digital Signal Processing and Communication Systems. Kluwer Academic Publishers. 2002

[45]. N. W. Rydell. Forces Acting on the Femoral Head-Prothesis. A study on strain gauge supplied prostheses in living persons. Acta Orthopaedica Scandinavica, 1966, 37, 88, 1-132.

[46]. Charles E.Carlson, Robert W.Mann, William H.Harris. A radio telemetry device for monitoring cartilage surface pressures in the human hip. IEEE Transactions on Biomedical Engineering, 1974, 21, 4.

[47]. R.D. Crownshield, R.C.Johnston, J.G.Andrews and R.A.Brand.A biomechanical investigation of the human hip. Journal of Biomechanics, 1978, 11, 75-85.

[48]. T.A.English and M.Kilvington. *In-vivo* records of hip loads using a femoral implant with telemetric output (A preliminary report). Journal of Biomedical Engineering, 1979, 1, 2.

[49]. G.Bergmann, F.Graichen, J.Siraky, H.Jendrzynski, A.Rohlmann. Multichannel strain gauge telemetry for orthopaedic implants. Journal of Biomechanics, 1988, 21, 2, 169-176.

[50]. SJG Taylor. A telemetry system for measurement of forces in massive orthopaedic implants *in-vivo*. 18th Annual International Conference of the IEEE Engineering in Medicine and Biology Society, Amsterdam, 1996.

[51]. S.J.G Taylor, J.S. Perry, J.M. Meswania, N.Donaldson, P.S.Walker and S.R Cannon. Telemetry of forces from proximal femoral replacements and relevance to fixation. Journal of Biomechanics, 1997, 30, 3, 225-234.

[52]. Tung-Wu Lu, Stephen J.G Taylor, John J. O'Connor and Peter S. Walker.Influence of muscle activity on the forces in the femur: an *in-vivo* study. Journal of Biomechanics, 1997, 30, 11/12, 1101-1106.

[53]. S.J.G Taylor, P.S. Walker, J.S.Perry, S.R.Cannon, R.Woledge; The forces in the distal femur and the knee during walking and other activities measured by telemetry. The Journal of Arthroplasty, 1998, 13, 4.

[54]. S.J.G. Taylor, P.S Walker; Forces and moments telemetered from two distal femoral replacements during various activities. Journal of Biomechanics, 2001, 34, 839-848.

[55]. Darryl D. D'Lima, Christopher P.Townsend, Steven W.Arms, Beverley A.Morris, Clifford W.Colwell Jr. An implantable telemetry device to measure intra-articular tibial forces. Journal of Biomechanics, 2005, 38, 299-304.

[56]. Jaya L Nemchand; Smart implants multi-channel strain gauge telemetry for monitoring fracture healing *in-vitro*, MSc Biomedical Engineering dissertation 2007/2008.

[57]. http://www.neighbourhood.statistics.gov.uk/HTMLDocs/dvc1/UKPyramid.html (last accessed: 03/10/2012 16:33)

[58]. Friedlaender Gary E., Perry Clayton R., Cole J. Dean, Cook Stephen D., Cierny George, Muschler George F., Zych Gregory A., Calhoun Jason H., Laforte Amy J., Yin Samuel. Osteogenic Protein-1 (Bone Morphogenetic Protein-7) in the treatment of tibial nonunions. Journal of Bone and Joint Surgery Am., 2001, 83-A, Suppl 1, Pt 2, S151-S158.

[59]. T.P van Staa, E.M Dennison, H.G.M Leufkens, C Cooper. Epidemiology of fractures in England and Wales. Bone, 2001, 29, 6, 517-522.

[60]. Brown RH, Burstein AH & Frankel VH, J . Telemetering *in-vivo* loads from nail plate implants. Biomechanics, 1982, 15, 815-823.

[61]. Barlow, J.W., Goldie, I.F., Horwood, J.M.K., Lee, A.J.C. and Ramson, R.P. *In-vivo* records of strain in a total hip joint. Institution of Mechanical Engineer. 1984, C216/84, 55–61.

[62]. Barlow, J.W., Horwood, J.M.K., Lee, A.J.C. and Ramson, R.P. A thick film implantable data acquisition module In: *Proc. INTERNEPCON,* 1984, 367–374.

[63]. P Damm, F Graichen, A Rohlmann, A Bender, G Bergmann. Total hip joint prosthesis for *in-vivo* measurement of forces and moments. Medical Engineering & Physics, 2010, 32, 95-100.

[64]. I Kutzner, D Stephan, J Dymke, A Bender, F Graichen, G Bergmann. The influence of footwear on knee joint loading during walking *in-vivo* load measurements with instrumented knee implants. Journal of Biomechanics 2012, Available at: http://dx.doi.org/10.1016/j.jbiomech.2012.11.020

[65]. A Rohlmann, R Petersen, V Schwachmeyer, F Graichen, G Bergmann. Spinal loads during position changes. Clinical Biomechanics, 2012, 27, 754-758.

[66]. I Kutzner, S Küther, B Heinlein, J Dymke, A Bender, A Halder, G Bergmann. The effect of valgus braces on medial compartment load of the knee joint – *in-vivo* load measurements in three subjects. Journal of Biomechanics, 2011, 44, 1354-1360.

[67]. F Graichen, G Bergmann, A Rohlmann. Patient monitoring system for load measurement with spinal fixation devices. Medical Engineering and Physics, 1996, 18, 2, 167-174.

[68]. M O Heller, G Bergmann, G Deuretzbacher, L Dürselen, M Pohl, L Claes, N P Haas, G N Duda . Musculo-skeletal loading conditions at the hip walking and stair climbing. Journal of Biomechanics, 2001, 34, 883-893.

[69]. G Bergmann, F Graichen, A Bender, M Kääb, A Rohlmann, P Westerhoff. *In-vivo* glenohumeral contact forces – measurements in the first patient 7 months postoperatively. Journal of Biomechanics, 2007, 40, 2139-2149.

[70]. Verbal confirmation with SJG Taylor, 13/02/2012

2 The skeletal system

The human body is divided into three different planes (sagittal, coronal, transverse) and four anatomical positions (medial, lateral, proximal and distal) to describe position reference points accurately (see figure 5 below). The human body is made up of several biological systems and the skeletal system is one of the systems comprising of bones, joints, ligaments and cartilage. The skeletal system like any other system in the body does not work independently; it works alongside the muscular system to achieve its functions. The main functions of the skeletal system is to support the whole body, provide protection to internal organs, allow movement of the body from one point in space to another, acts as a mineral storage and for red blood cell formation.

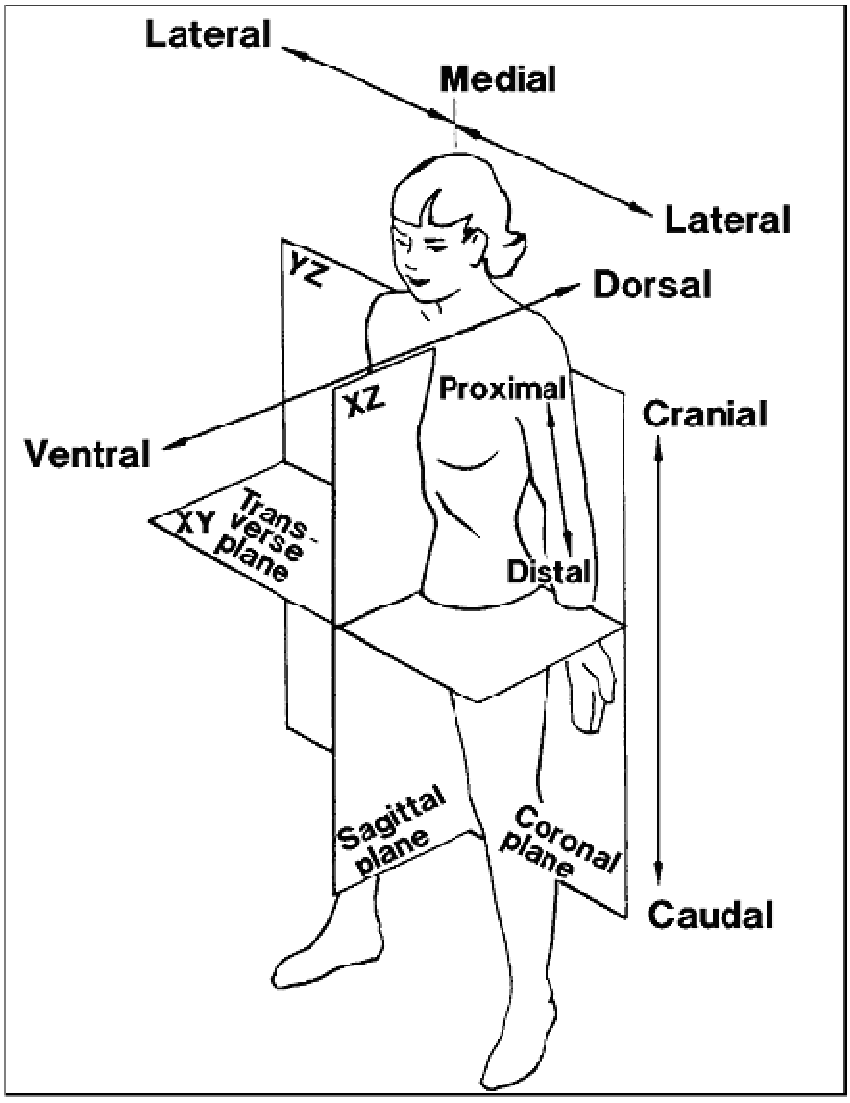

Figure 5: Anatomical position and body planes [52]

There are over 200 bones in the skeleton which is divided between the axial and appendicular skeletons. The axial skeleton consist of bones found along the axis of the body whereas the

appendicular skeleton consist of appendages such as the legs, arms and the girdles such as shoulder, pelvic which connect with the axial skeleton. Bones, joints, ligaments and cartilage make a framework which together with the muscular system allows locomotion in the body. The general structure of the skeletal system is made of joints, articular cartilage, synovial joints, and articular capsules, synovial fluid and reinforced ligaments.

2.1 The structure of the bone

Ossification is the process by which bone tissue starts to form *in-utero*. Ossification centres develop in positions determining the basic skeletal blueprint of the adult. The foetus is normally born with ossified precursors of adult bones in place. After birth, the bones elongate and change shape to assume the adult form [1]. Bones are made up of different tissues; osseous tissue dominates bones but they also contain nerves, blood vessels, connective tissues, cartilages and associated muscles. This section will look at the bone structure at three structural levels: the overall structure, the microscopic level and a brief overview of the cellular level. The overall structure of a long bone is discussed more in details in this section. Figure 6 below is the illustration of the cross section of a tibial bone.

1	Proximal epiphysis	End of the bone closest to the torso
1	Distal epiphysis	End of the bone closest to the knee
2	Metaphysis	The flaring portion near the bone end
3	Diaphysis	The shaft section
4	Spongy or trabecular bone	Porous are of the internal bone
5	Compact or cortical bone	Dense area of the outer bone
6	Medullary cavity	Hollow section of the bone where the blood is produced
7	Epiphyseal line	A fusion of the bone where it is denser
8	Periosteum	The outer most layer around the bone where the nerves are

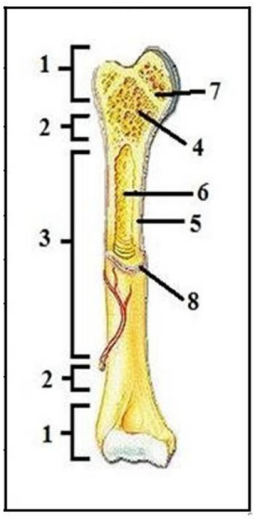

[2]

Figure 6: Illustration of a long bone

2.2 Cortical and cancellous bone

Long bones are divided into the epiphysis, metaphysis and the diaphysis as shown in Figure 6 (page 53). The diaphysis is mainly composed of cortical bone whereas the metaphysis and the diaphysis consist of cancellous bone. Cortical bone is dense and has a solid mass with minuscule channels. The cortical bone makes up about 80% of the skeletal mass in the adult human skeletal

system [1, 4]. Cortical bone is the outer wall of all bones and is the part responsible for support and protective function of the skeleton. The volume of cortical bone is in the shaft of long bones of the appendicular skeleton. The remaining 20% is cancellous bone and trabecula bone. The distribution of cancellous and cortical bone varies from bone to bone [1, 4, 5].

Cortical bones are made up of units called osteons or the Haversian systems, which run along the length. Each osteons consist of layers called the lamellae that surround the Haversian canal [5, 6]. The canal surrounds the bone's nerve and blood supplies. The interface between osteons is filled with interstitial lamellae. Osteons connects to each other and the periosteum (the outer bone sheath), through the Volkmann's canal [5, 6]. The Volkmann's canal usually run obliquely to the Haversian canals and contain blood vessels, lymphatics, nerves and loose connective tissue that continue through the bone marrow and the periosteum. Figure 7 below shows an illustration of the cortical and cancellous part of the bone with the Haversian system and the Volkmann's canal.

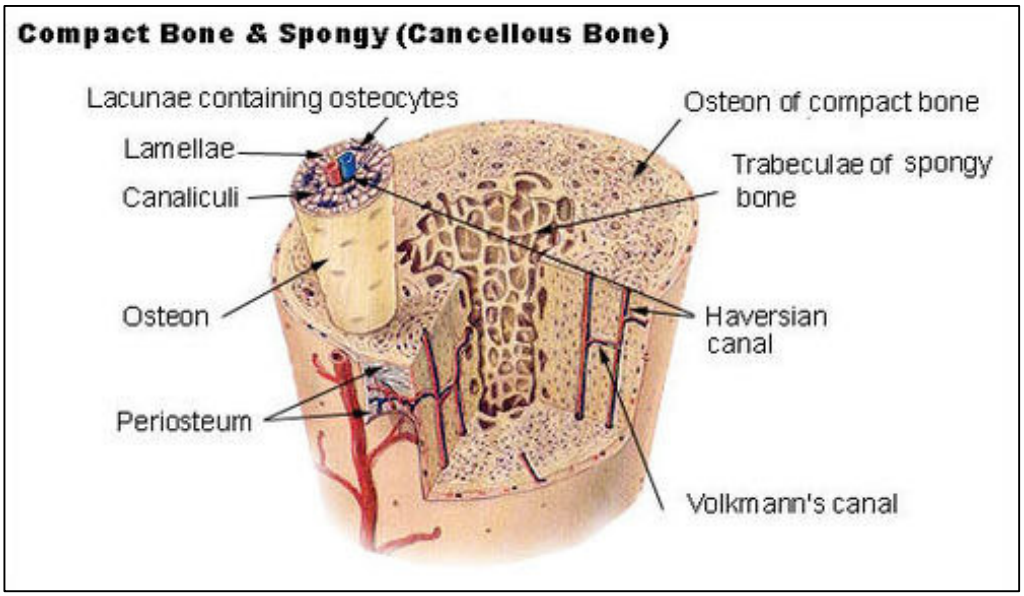

Figure 7: Cross Section of a bone illustrating cortical and cancellous part [7]

2.3 Bone cells and matrix

There are several major cells that form the elements of the bone. These consist of osteoclasts, osteoblasts, osteocytes, bone-lining cells, cells of the marrow compartment, and an immune regulatory system that supplies the precursor cells and regulates bone growth and maintenance. The following is a brief overview of the osteocytes, osteoclasts, osteoblasts and the bone lining cells.

2.3.1 Osteocytes

Osteocytes comprise nearly 95% of all adult bone cells. They derive from osteoblasts that have become rooted in the bone matrix. Osteocytes are the cells that sense the magnitude and distribution of strains. They are purposefully placed to respond to changes in mechanical strain and stimulate local osteoblastic bone formation. They respond to adaptive modelling and remodelling behaviour through cell to cell interaction. Osteocytes play a key role in homeostatic, morphogenetic, restructuring processes of bone that constitutes regulation of the mineral hydroxyapatite ($Ca_{10}(PO_4)_6(OH)_2$) and architecture. Mechanical stresses and localized microdamage may induce osteocyte apoptosis. [5, 8]

2.3.2 Osteoclast

Osteoclasts are multinucleated bone resorbing cells. Bone remodelling normally starts with resorption which osteoclasts coordinate. They are larger cells whose function is to dissolve bone by acting on the mineral matrix involving hydrolysis of collagen. The cells are multinucleated with cytoplasm full of mitochondria, free ribosome, Golgi apparatus and lysosome. Monocytes from the bone marrow serve as precursor of osteoclasts. Bone is a dynamic living tissue, which is continuously being remodelled in response to influences such as structural change and the body requirement. Osteoclasts are found in the Howship lacunae, small depressions formed from the digestion of underlying bone. The osteoclasts bind to the bone surface by numerous cytoplasmic extensions. Microscopically, osteoclasts have ruffled borders which play a very crucial part in the resorption process [5, 8]. They are also polarized cells containing the sealing zone, a ruffled border, a functional secretory domain and a basolateral membrane. It attaches to the matrix through the sealing zone and forms the ruffled border. The ruffled border is a resorbing organelle formed by intracellular acidic vesicles fusion with the region of plasma membrane facing the bone. The vesicle transported to the ruffled border delivering hydrochloric acid and protease through the ruffled border into the Howship lacunae. The Howship lacuna is the extracellular space between the ruffled border membrane and the bone matrix and is sealed form the extracellular fluid by the sealing zone [53]

2.3.3 Osteoblast

Osteoblasts are bone forming cells that are derived from mesenchymal stem cells. Osteoblast maturation is a process comprising precursor cell commitment to the osteoblast lineage, cell proliferation, bone matrix deposition, matrix maturation and bone mineralization [5, 8]. Following the process of bone formation, osteoblasts may eventually form bone lining cells, become embedded within matrix as osteocytes or undergo apoptosis [9].

2.3.4 Bone lining cells

Bone lining cells are believed to be derived from inactive osteoblast. They are found on the exterior surface of the bone. They are capable of bone formation without prior bone resorption. Bone lining cells, like osteocytes, may be influenced by mechanical strain within bone tissue. Little is known of the bone lining cell history [5]. Studies have shown that they may be involved in homeostatic, morphogenetic and restructuring processes that constitute regulation of bone mineral, mass, architecture and hematopoietic process [8].

Bones within the skeletal system do not work independently; they are as much dependent on the other systems in the body to function. The muscular, vascular and the nervous system are three main systems that work in partnership with the skeletal to function correctly. The next section examines how these different systems interact with each other to form the balance required in the body.

2.4 Vascular, muscular and nerve supply to the bone

Studies conducted by Clopton Havers in 1691 described how a large nutrient artery pierces the shaft of long bones and enters in bone marrow [10]. The study also examined groups of arteries which entered the extremities of long bone. According to Havers [10], they formed a vascular mesh in the cortex which gave rise to 'vast numbers of veins' leaving the bone at its periosteal surface. These earliest observations on the vascularisation of bones comprise of centrifugal nutrition of bone cortex from the marrow outwards, through the compact bone of the shaft, into the veins of the periosteum.

The beginning of the nineteenth century [10] saw the general acceptance that internal structures of bone were as full of blood and soft tissues with healing properties and is subjected to growth. Moreover bone as a tissue is normally formed and broken down in relation to blood vessels, because these are the route by which diffusible ions and molecules pass to bone cells and into the organic matrix and mineral component of bone substance [4, 10]. The vascular anatomy of bones has a significant bearing on their shape and microscopic structure; they greatly influence these characters in both health and disease. The study of microcirculation and vascular reactivity of bone tissue has allowed studies to move forward on understanding the physiology of the osseous circulation and its relationship to the control of bone growth.

The cardiovascular system contains within itself several specialized circulations. Each is made up of three main vascular groupings namely afferent arteries, a functional vascular network and efferent veins. Only the vascular network is the site of ionic exchange between blood and it's surrounding. In the case of the osseous circulation, the afferent vessels are the extra-osseous nutrient arteries and their intra-osseous medullary branches [10]. The vascular network is a

sinusoid system. Unusually long and wide sinusoids make up the functional vascular network in compact bone. The efferent vessels encompass veins in the periosteum, attached muscles and large medullary venous sinuses and nutrient veins. Through these numerous vessels, the osseous circulation is drained into the systemic veins of the cardiovascular system shown in Figure 8 below.

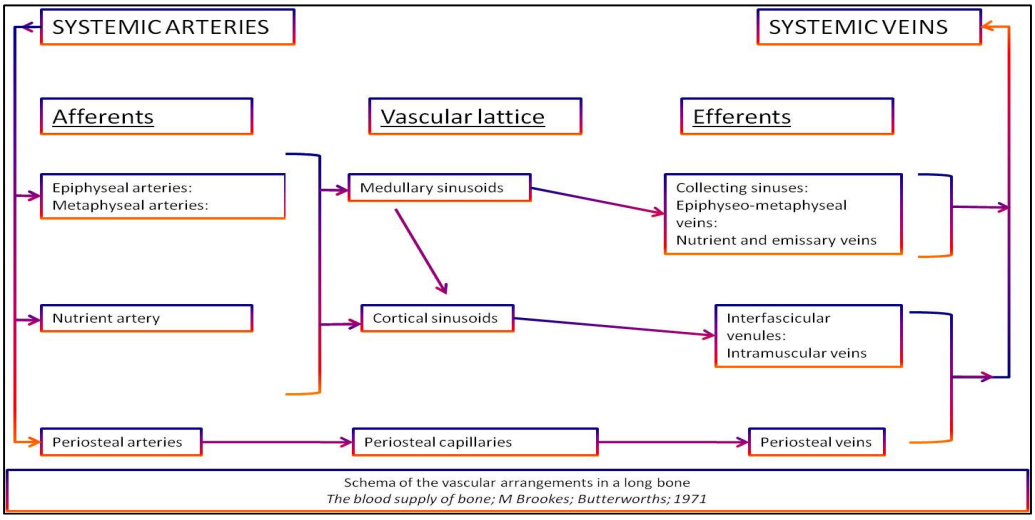

Figure 8: Schematic of vascular arrangement in the long bone

The vascular supply to the knee joint in the lower limb is largely through descending branches from the femoral, popliteal, lateral circumflex arteries in the thigh, the circumflex fibular artery and recurrent branches from the anterior tibial artery in the leg [4]. These vessels form an anastomotic network around the joint. Blood supply to the tibia comes from the popliteal artery branching into the anterior and posterior tibial artery. The nutrient artery arises from the posterior tibial artery before entering the oblique nutrient canal. The artery also divides into four branches; namely 3 ascending and 1 descending artery. The descending branch leads to the endosteal surface providing blood to the inner tibial cortex. The anterior tibial artery provides the periosteum with a blood supply as it branches out to the interosseous membrane. The posterior tibial artery brings oxygen and nutrient dense blood to the muscles and tissues in the posterior lower leg. Bones transmit the force of muscular contraction from one part of the body to another during movement. They do not work on their own. They are surrounded by muscles, fluids and a vascular system as mentioned above. Muscles play a very crucial part in the biomechanical energy generation mechanism. Bone shapes are implicated in joint leverage, the amount of muscles that can be attached and the size of the articulation surface [4].

2.5 The tibia in relation to the lower limb

The tibia is anatomically positioned in the lower limb, inferior to the vertebral column. The lower limb consists of two major long bones, the femoral bone and the tibia. The femoral bone is

connected at the thigh proximally and distally attached to the tibia at the knee joint. The leg has two long bones, the tibia is medially connected and the fibula laterally positioned. The tibia is the larger bone and is the main articulating bone with the femur at the knee joint. Figure 9 below illustrates the major long bones in the lower limb from the distal end of the vertebral column onwards.

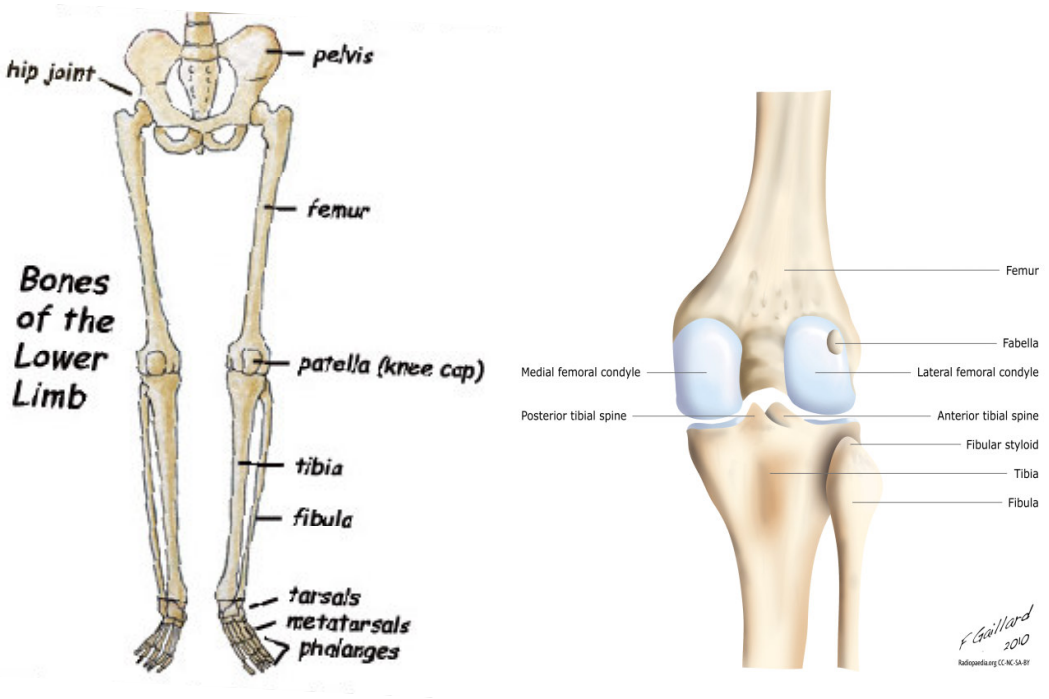

Figure 9: Lower anatomy and posterior view of a knee [12, 13]

At the proximal end, the tibia expands transversely to act as the main weight bearing bone. The transverse plane consists of medial and lateral condyles which are articular and separated by an intercondylar region as illustrated in the right-hand diagram of Figure 9. The intercondylar region is the site where the cruciate ligament and the menisci of the knee joint sit. Ligaments link bone to bone across articulations. Tibial condyles are thick horizontal discs of bone attached to the top of the tibial shaft. The tibial tuberosity is based on the anterior aspect of the tibia below the junction between the two condyles. The tibial shaft has three surfaces, namely the posterior, medial and lateral surface [4, 14]. The medial surface is smooth and subcutaneous and is palpable along almost its entire extent. The medial and inferior to the tuberosity, the medial surface bears to the roughened elevations. This elevation site is the area of the collective attachment of three main muscles which descend from the thigh; sartorius, gracilis and semitendinosus [4, 14]. Figure 10 below shows the various muscles that envelope the femoral, tibial and fibular bone.

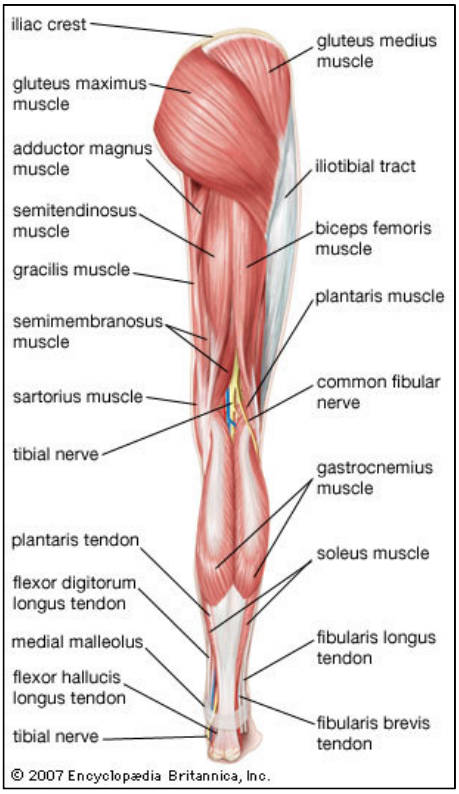

Figure 10: Muscles in the lower leg [15]

The sartorius muscle is the most exterior muscle in the anterior compartment of the thigh. The muscle descends from the anterior superior iliac spine to the medial surface of the proximal shaft of the tibia [4]. Its attachment to the tibia is anterior to that of the gracilis and semitendinosus. Gracilis is positioned in the medial compartment of the thigh and descends vertically down the medial side of the thigh [14]. Its insertion lies between the tendon of the sartorius in front and the tendon of the semitendinosus behind. The semitendinosus muscle is medial to the biceps femoris in the posterior compartment of the thigh. The tendon curves around the medial condyle of the tibia and inserts into the medial surface of the tibia posterior to the tendons of the gracilis and sartorius muscles [4, 14]. The semitendinosus is responsible for knee joint flexion and extension of the thigh at the hip joint. Sartorius, gracilis and semitendinosus muscles are combined and attached on the tibia and their combined tendons of insertion are often termed as the pesanserinus [4, 14].

2.5.1 Vascular supply and innervations

The knee joint is innervated by branches from the obturator, femoral, tibial and common fibular nerves [4, 5]. The tibia is served by the tibial nerve and the sural nerve. The sciatic nerve descends from the proximal part of the femur, right under the posterior cutaneous nerve thigh into the common peroneal nerve. Figure 11 below illustrates the description given above.

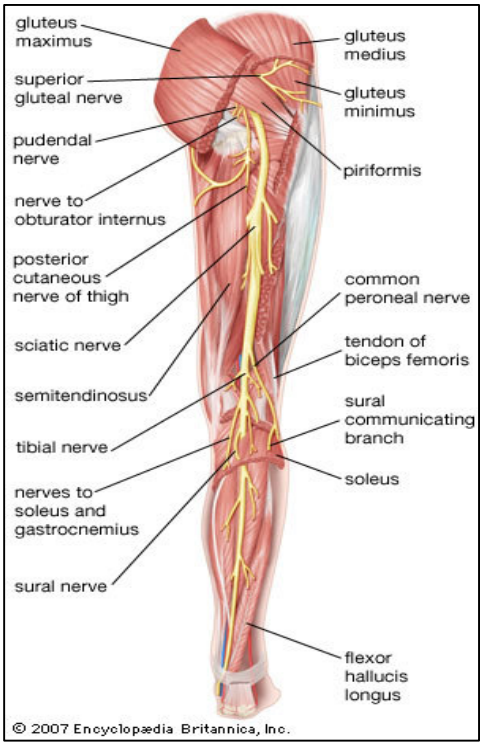

Figure 11: Muscles and nerves in the lower leg [15]

The muscles, nerves and vascularity described above have a vital role to play collaborating with each other to perform day to day activities. And if a connection is broken such as when a bone is fractured and causing trauma to the system around, the body has its own safeguarding mechanism that begins the repair process immediately within matter of seconds before any other sort of intervention happen externally. The next section will examine what happens at the microscopic level when bones fracture. However before going in depth of bone fracture repair, a review of one the most common way to identify fractures to ease trauma management in hospitals is described.

2.6 Bone fracture classification

In 2010 it was reported that in every 100,000 people of the population, 26 suffered a tibial fracture every year [17]. The estimated resident population of the UK in mid-2009 was 61,792,000 [16]. A simple calculation shows the annual incidence of tibial shaft fractures to approximately 16,000. Bone fractures are generally classified according to one of the four most comprehensive and widely used system in the world which is the AO (**A**rbeitsgemeinschaft für **O**steosynthesefragen), the Tscherne, the Gustilo and the Winquist-Hansen classification. During this study the **A**rbeitsgemeinschaft für **O**steosynthesefragen/**O**rthopaedic **T**rauma **A**ssociation group – AO/OTA classification will be used to describe the fractures. Fractures are coded in a four digit code, for example: 42-A1. Figure 12 illustrates the AO classification breakdown.

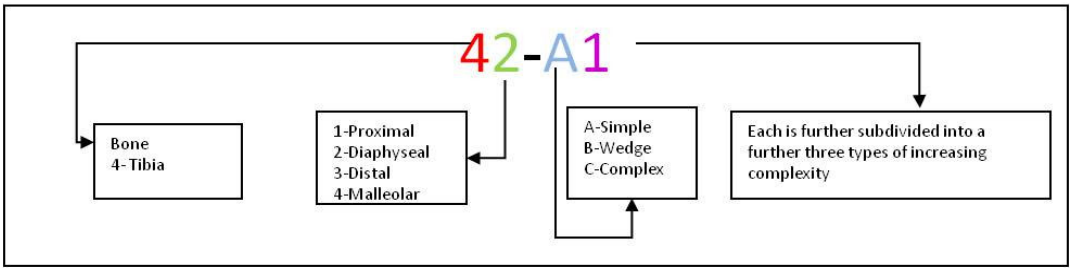

Figure 12: AO Classification breakdown to illustrate the four digit code [1]

2.6.1 AO - Arbeitsgemeinschaft für Osteosynthesefragen classification

The AO Classification was started by Maurice E Müller and his associates [1]. During the early years of the AO group, in order to document the fracture cases treated for quality control purposes to gauge the effectiveness and risks of fracture management; the requirement to have a classification system was felt with the increasing volume of information generated. According to the AO Foundation, the classification is "a system based on well defined terminology, which allows the surgeon to consistently describe the fracture in as much detail as required for clinical situation. This description is the key to classification and forms the basis for the alphanumeric code that allows documentation and research [1]". Since this study is targeted to examine the efficacy of using telemetry on a tibial bone, the next section looks at the fracture classification as described by the AO foundation for the tibia and fibula.

2.7 Fractures of the tibia

A bone fracture is commonly described as a break in the continuity of the bone. Causes of bone fracture may be due to several reasons such as:

- Trauma – falls, accidents
- Pathological reasons – bone cancer
- Fatigue – repetitive overloading which leads to high stresses in the bone
- Fragility – due to bone loss in cases such as osteoporosis

The fracture occurs within a fraction of a millisecond. It results in a predictable damage to the soft tissues due to a break. A fracture produces a loss of bone continuity that results in pathological deformation, loss of the support function of the bone, and pain. Since the AO classification is the system used in this study, the following sets of figures (13-15) will describe the various tibial fractures that can occur. Assessing the right fracture can help in efficient fracture treatment and management. In the AO classification fractures for the tibia are normally divided into proximal, diaphyseal and distal. The figures below are an extract of the AO classification tables for tibial fractures.

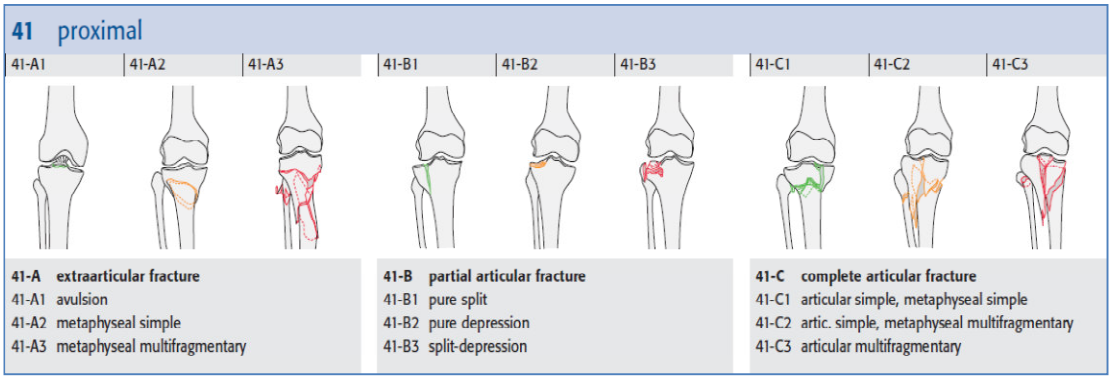

Figure 13: Proximal fractures [1]

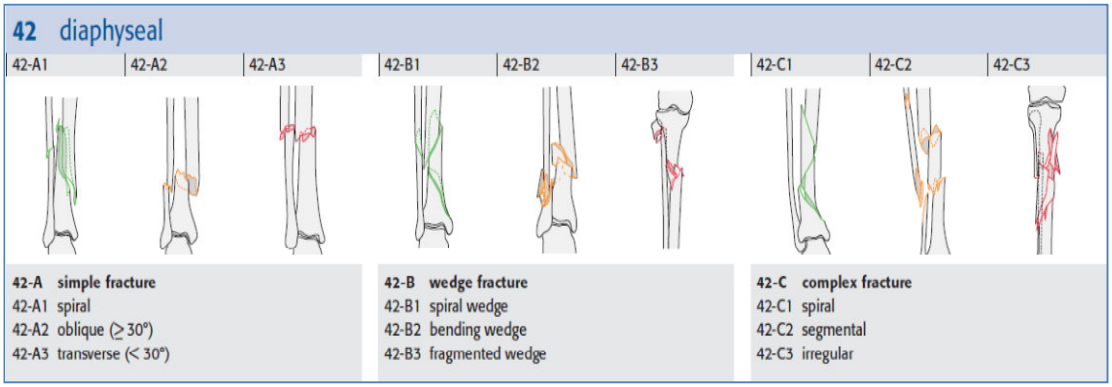

Figure 14: Diaphyseal fracture [1]

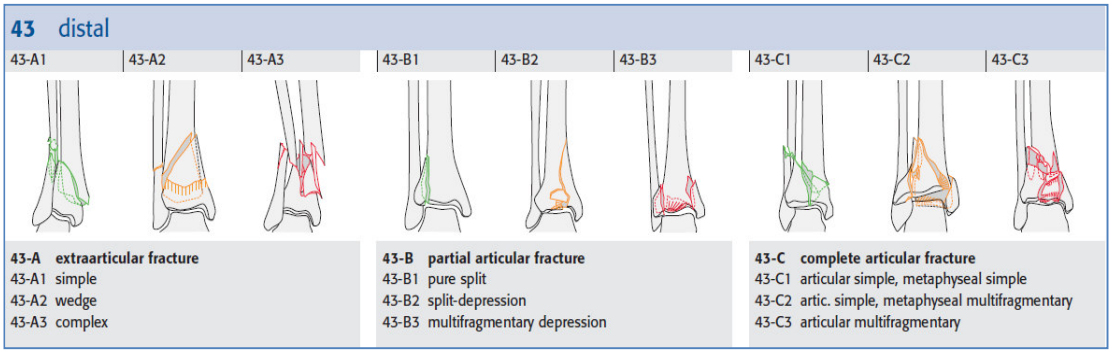

Figure 15: Distal fracture [1]

When a bone is broken, the immune system will normally set in motion a number of processes in order to begin the repair process. The next section will examine in detail the various stages of the bone fracture healing processes.

2.8 Bone fracture repair: stages of the healing process

The process of bone healing is complex and is usually broken down into a chain of events for simplification. Bone fracture healing mechanism is often described as primary or secondary bone healing. Primary or direct bone healing normally refers to direct cortical healing between rigid and opposed fractured ends of a bone [4-6, 8]. Primary healing normally occurs without the formation of cartilaginous tissue which leads to callus formation. Primary healing tends to occur in

cases where rigid fixation such as bone plates has been used. This reduces the gap between the fractured ends, giving rise to good vascularisation for blood and nutrients. The repair is initiated by the Haversian system of the lamellar bone. Osteoclasts resorp necrotic bone and new lamellar bone is then synthesized and laid parallel to the old cells eliminating the need for additional remodelling. However, cases of a complete gap reduction in fractures are not very common [1, 5, 6, 8, 10].

Secondary healing involves healing processes within the bone marrow, periosteum and surrounding soft tissues of the bone. The sequence of the callus healing is divided into four stages: inflammation, soft callus, hard callus and remodelling. Callus is the term used for proliferative physiological bone healing. Secondary healing tends to occur in fractures treated by closed methods such as intramedullary fixation amongst other. These fractures are likely to cause broken tissue which results in haematoma formation at the fracture site. The blood vessels at the fracture site thrombose causing bony necrosis at the edges of the fracture [4-6, 8]. This increases capillary permeability resulting in swelling of the tissue. Within the haematoma there is a network of fibrin, reticulin fibrils and collagen fibrils [4-6, 8]. The haematoma is steadily replaced by granulation tissue. Further chemical and mechanical factors stimulate the callus formation and mineralisation. Ultimately pain and swelling decreases and soft callus is formed. The stages of fracture healing are illustrated in Figure 16 on page 66.

According to Claes et al. [36] after fracture, this process lasts until between 1-7 days post fracture. Soft callus formation or immature bone is formed corresponding approximately to the time when the bone fragments are no longer able to move about freely which is around 2-3 weeks post fracture [1]. This soft callus stage is usually characterised by an increase in vascularity and cellularity into the fracture callus [4-6, 8]. Fibrous tissue replaces the haematoma and new bone formation starts. When the end of the fractured bone is linked by the soft spongy callus, the stage of hard callus starts and lasts about 4 months. Callus forms at the fracture site through endochondral ossification at the haematoma.

Endochondral ossification is the process by which embryonic cartilaginous model of most bones contribute to longitudinal growth for remodelling. Bone resorption occurs leading the cartilaginous model to be gradually replaced by bone by appositional growth. The process of endochondral ossification starts with the formation of the bone collar around the hyaline cartilaginous model. A primary ossification centre is formed within the hyaline cartilage leading to the cavitation of the cartilage model. This further leads to the formation of spongy bone through the invasion of the internal cavities by the periosteal bud and the deteriorating cartilage matrix. As the cavity ossification formation continues, secondary ossification starts appearing in

preparation to the ossification of the epiphyses. As the ossification of the epiphyses is completed, the hyaline cartilage remains only on the epiphyseal plates and on the articular cartilage completing the endochondral ossification process [1, 5, 6, 8, 10]. An illustration of the stages of endochondral ossification can be found in the Section 2.10 Figure 17 (Page 74).

Periosteal callus forms along the periphery of the fracture site to commence the repair process by intramembranous ossification which is initiated by pre-osteoblasts. Intramembranous ossification is the process by which flat bones are formed. In the fibrous connective tissue membrane, an ossification centre is formed. The ossification centre is formed by the centrally located mesenchymal cells cluster and differentiating into osteoblasts. Within the fibrous membrane, osteoblasts begin to secrete osteoid which is mineralised in a few days. The trapped osteoblasts become osteocytes. A network of trabeculae is formed by the accumulated osteoid laid between the embryonic blood vessels. Vascularised mesenchyme condenses on the outer surface of the woven bone and becomes the periosteum. The trabeculae lead to the formation of the woven bone collar which is later replaced by mature lamellar bone. Spongy bone which consists of distinct trabeculae persists internally and this leads to the formation of the red marrow by its vascular tissue [1, 5, 6, 8, 10]. Remodelling to cortical bone begins once the fracture has solidly united with mature or woven bone. The woven bone is then slowly replaced by lamellar bone through various processes such as surface erosion and osteonal remodelling. This part of the process can take several months to several years until the bone has returned to its original morphology and the complete restoration of the medullary canal [1,4-6, 8]. Figure 16 below is a representation of the different stages of bone fracture healing as described above.

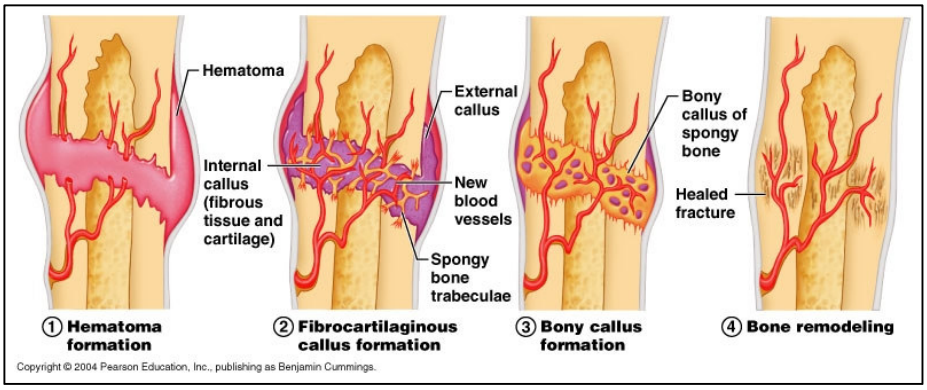

Figure 16: Stages in the process of bone fracture healing [18]

2.9 Bone callus: a review

Callus has been researched and studied at length in terms of its biological properties and how the proliferation occurs. However, there are very few studies that have been conducted and understand the mechanical properties of callus and how it affects clinical union. Callus is not

usually taken into account when testing medical devices designed for fracture fixation. Studies have been conducted on the callus proliferation with time to better understand the mechanical properties of bone fracture healing only *in-silico* [21]. Anatomically correct bone models to test medical devices are widely used but do not reflect the mechanical properties of real bone.

Aro *et al.* [22] designed an experiment to predict the properties of fracture callus by measuring the mineral density using micro-bone densitometry. The study conducted used rat tibiae with closed fractures to acquire standardised specimens of fracture callus at progressing stages of healing. *In-vitro* indentation was performed and the bone tissues were biopsied in order to establish the hardness and calcium content of a standardised area. The study showed that hardness of callus was correlated with the mineral density of the local tissue. This meant that the hardness had a non-linear relationship with mineral density per volume of tissue as measured by the micro bone densitometry [22]. 3D imaging and bone mineral quantification gives additional information about the quality and geometry of the fracture callus. The latter may be useful clinically to monitor healing. Micro-bone densitometry may allow clinicians to detect the degree of mineralisation non-invasively and accurately, however it is more complicated to be applied in practice. Conventional single or dual photon absorptiometry is used to display 2D images of 3D structures; applying these techniques to fracture healing monitoring may be more complex *in-vivo* due to the assumptions that are required for extrapolation to 3D [22].

Powell *et al.* [23] proposed an experimental study to examine rat metatarsals to investigate whether the callus calcium content is an indication of the mechanical strength of the bone repair during healing. The study showed that the mid-fracture callus calcium content increased. This coincided with the beginning of recovery of the ultimate tensile stress, elastic and torsional modulus of the fractured bone. The changes were determined using micro-interferometry in order to ascertain if a chronological correlation existed between fracture stability and callus calcium content. However, monitoring the calcium content requires a needle biopsy in order to examine the fracture callus and ability forecast when the fracture is mechanically healed. Needle biopsy requires sample cells from the patient's body for laboratory testing [24]. And as any other procedure it carries the risk of bleeding and infection at the site of entry where the needle is inserted which will cause further trauma to the patient.

In a study conducted by Markel *et al.*, the link between the biology of the repair process and the gradual increase of mechanical function experienced by the healing bone is linked by the quantification of the callus tissue material properties [25]. The study examined bilateral tibial transverse osteotomies on 32 dogs divided into 4 groups to be euthanized at week 2, 4, 8 and 12. Torsion properties of each pair were determined and each bone was analysed for indentation

stiffness, calcium content and histomorphometric data at various sites. Change was observed during the study period: indentation stiffness of periosteal callus increased up to 8 weeks before a plateau was observed, while the endosteal callus indentation stiffness peaked at 8 weeks and decreased by week 12. The result shows a linear increase over time in the gap tissue stiffness and the cortical bone stiffness decreasing. The change in the data correlates to the histological changes in bone ossification and porosity of the tissues. The study concluded that the combination of mineral density of every region within the bone volume with the distance of the region from the bone's torsional axis may be the best technique of describing the torsional properties of healing fractures [25]. However, since the study was conducted on canines, it is not directly comparable to humans.

Cui *et al.* [26] proposed to study an evolutionary model of the external callus. Callus samples from different stages of healing were obtained from volunteers after a diaphyseal long bone fractures. X-Ray diffraction (XRD), scanning electron microscopy (SEM) and transmission electron microscopy (TEM) analysis were conducted and the results suggest that the fracture healing depends on the proper alignments of collagen matrix and mineralisation in a sequential process. Other common mineral phase di-calcium phosphate dehydrate (DCPD) other than hydroxyapatite (HA) was observed in the early stage healing callus. However, it was not very clear as to what actually controls the sequence of events in healing.

Moorcroft *et al.* [27] designed an experiment to examine the mechanical properties of callus from tibial fractures that are treated with external fixation. The properties were measured using a specially designed system to determine load and displacement. Stiffness was measured in different places and at various loading rates. Creep properties were assessed by the application of a constant load. The results suggest that fracture stiffness was found to vary between planes and the viscoelastic characteristics of callus changed with time. In early measurement, energy absorption was observed when a load was applied on the callus. The callus absorbed less energy during later tests progressively. Moorcroft *et al.* [27] have been able to demonstrate that the properties of callus change with time as the viscous element decrease and the elastic element increase. The author does suggest that further study is required to develop a more consistent technique in order to establish clinical union.

Ford *et al.* [28] conducted an experiment in order to understand the outcome of soft callus chondrocytes during long bone fracture repair. Transmission electron microscopy was used to study the detailed structure of the chondrocytes. The results show that the chondrocytes of the soft callus were engulfed by the matrix rich in collagen. This is a result of the progressive production of bone matrix which eventually leads to remodelling and repair.

Shefelbine *et al.* [29] led an experiment designed to develop a technique using micro-computed tomography and finite element (FE) method to assess fracture stiffness. This technique was developed and validated using phantoms. The method was applied to 3-4 weeks healed rat femur. Micro CT was used to determine the 3D geometry and material properties for the finite models. The *in-vitro* and *in-silico* results were compared; FE method predictions for the callus rigidity correlated significantly better with the experimental method than any other technique used to monitor healing. The study suggests that the use of FE analysis can be beneficial to predict mechanical properties of healing callus in fracture healing studies.

The interfragmentary strain theory by Perren [54] states that the magnitude of interfragmentary strain determines subsequent tissue differentiation of fracture gap tissue. The theory examines how the mechanical environment impacts tissue differentiation in a fracture gap. Each tissue type has different strain tolerances; applied interfragmentary strain has to be smaller than the strain tolerances of a tissue for it to form. Strain below 2% allow for direct fracture healing. The interfragmentary strain below 10% allow for cartilage differentiation and leads to endochondral ossification. The strain between 10% and 100% leads to granulation tissue and eventually non union. The theory proposed that pluripotential cells are responsive to local deformation within the fracture gap [55]. Tissue cells have the ability to withstand specific levels of deformation and the above values states that with strains higher they are unable to survive.

Stems cells are defined by their ability to remain undifferentiated for a prolonged period while retaining the potential to differentiate along one lineage (unipotent), multiple lineages (multipotent) or in all three germ layers (pluripotent) [57]. Mesenchymal stem cells are multipotent because they have the ability to exhibit the potential for differentiation into a variety of different cells/tissue lineages. Mesenchymal stem cells are a population of stromal cells present in the bone marrow and most connective tissue, capable of differentiation into mesenchymal tissues such as bone and cartilage [57].Mesenchymal cells have the potential to differentiate into chondrocytes, osteoblast, fibroblasts, marrow stroma and other tissues of mesenchymal origin [56, 57]. Embryonic stem cells are pluripotent; this means that they have the ability to differentiate into almost any cell in the body. They are derived from the inner cell mass of the embryonic blastocyst. Embryonic stem cells can be maintained *in-vitro* indefinitely without losing its potential to differentiate. Studies conducted on embryonic stem cells are mostly conducted on mouse according to Tuan et *al.* [58].

Finite element method has been used to better understand the complex relation between mechanical environment and tissue formation. Garcia-Aznar *et al.* [30] examined the influence of interfragmentary movement on the growth of callus. The study used mathematical models that

can predict tissue growth and differentiation patterns from local mechanical signals. The model predicted several geometric features of callus. The finite element results were in agreement with the experimental observations. The spatial and temporal tissue differentiation patterns were said to be in qualitative agreement with other well known experimental results. The investigation concluded that local mechanical signals can almost certainly clarify the shape and size of fracture calluses. The author suggests that the technique may be applicable to other areas of tissue biomechanics.

The extent to which a fractured bone can regain stability and strength depends on the mechanical properties of the tissues that are formed during healing. The quantification of the overall mechanical behaviour of the fracture calluses may help understand the properties better. There are a few existing sets of data on the material properties of individual calluses but more in depth data is required in order to help in clinical studies. Fracture callus material properties have been measured via nano-indentation by Leong *et al.* [31]. Nano-indentation was conducted on longitudinal sections of rat fracture callus at 5 weeks post fracture. There are several factors that can alter one or more phases of healing such as disease and drug treatment. A positive correlation was observed between the modulus and mineral content in woven bone at multiple locations. Nano-indentation however cannot be conducted *in-vivo*. Measurement of fracture callus is definitely a way of understanding the mechanical behaviour and properties of fracture calluses.

Understanding bone callus formation has developed over the years, swapping between *in-vitro, in-vivo* and *in-silico*. Naturally, bone callus is affected by many other factors biologically and mechanically. Muste *et al.* [32] designed a study to examine the formation, evolution and completion of the bone callus after elongation in sheep. The study was conducted using 2 to 4 years old sheep. A mandible osteotomy was created in the central zone of the symphysis and was maintained close using an osteodistractor device. Fibrous tissue was observed during the formation of primary callus. From week 4/5 to week 8, the elongation process was completed and bone remodelling completed. The study concluded that the organisation and progression of bone healing remained a complex process influenced by postoperative and post traumatic factors which last for a variable period of time depending on the number of factors.

Among the numerous questions in orthopaedic, along with the subject of when does clinical union is said to occur, new questions such as, is osteoclast activity the key to age-related impaired healing, has been raised. Mehta *et al.* [33] hypothesised whether calcified callus microstructure and composition is impaired due to the influence of advanced age. The study conducted revealed that callus mineralisation was less in young animals with semi-rigid fracture fixation but remained unchanged in the aged group. It was observed that callus bridging and callus microstructure and

mineralisation were diminished in advanced aged individuals. The study demonstrated the dominating role of osteoclastic activity in age-related impaired healing while illustrating the optimisation of fixation parameters. The experimental results can be beneficial in understanding and assessing healing in aged individuals with fixation devices. However, a further investigation is needed to establish a better set of parameters to assess physical healing.

In order to conduct a histological evaluation of the callus in the treatment of tibial fracture, osteosynthesis were conducted on 11 sheep, aged 10-22 months by Adamiak *et al.* [34]. The latter used a semicircular fixator as the operative technique. Callus and bone samples were obtained and analysed histologically. All the animals survived for 6 to 18 months post removal of the fixator. Bone union was observed in all the treated animals. The histo-pathological examinations confirmed complete healing of the tibial bones. Evaluation of bone callus samples showed a thick layer of compact bone tissue with fully developed blood vessels and bone marrow [34].

Since finite element modelling is becoming more in use to validate experiments, a study to better understand the mechanical change of the hard callus that influences local tissue strains during bone healing is required. Vetter *et al.* [35] conducted a finite element (FE) study to investigate the above based on sheep experiments. The strain patterns were conducted at six successive healing stages and the input derived was from an experimental sheep study. The strains obtained were compared with the outcome of the hypothetical FE models [35]. The difference in spatial distributions was interpreted using mechanobiology theory. It showed that taking into account the heterogeneity of the hard callus is crucial at the intermediate stages of healing when cartilage convert to bone via endochondral ossification [35]. The implementation of *in-vivo* data in an *in-silico* study can be beneficial in validation processes.

Non-union or mal-union is a major setback for patients with bone fractures. It is vital to find a way to monitor healing in order to make clinical decisions as early as possible if healing is not as predicted. Claes *et al.* [36] examined inducing bone formation using distracting plates from the lateral bone surfaces. 20 sheep were operated on at the medial site of the tibia. Strain-induced bone formation is likely between two bony surfaces established by an osteotomy but also connecting a bony surface and a suitably designed implant. However, the bony surface must be accessible to suitable blood supply and cells. This new technique may allow for bone apposition in a large number of bones which could not be appropriately treated previously. It can be an effective technique to address bone defects such as mal-union. The author also suggests that it may also be a method to assess healing and defect early on during post-operative treatment. However, there is no published data about the use of this particular method as a way to monitor healing.

A study carried out by Oni [37] investigated the bony callus to examine the healing of an experimental fracture of a rabbit tibia. The experiment was conducted using period acid Schiff reaction and Van Gieson staining method to differentiate between woven and lamellar bone. The results show that the callus consisted of two connected but different type of bone. A double refraction observed in the periosteum and callus cartilage showed dissimilar sized collagen fibres aligned vertically to the axis of the diaphysis.

Bone callus has been investigated and analysed in various ways by many experts. However, there is still a dearth of understanding of how internal trauma fixation devices aid in the callus growth and development. There is also no published data where bone callus has been taken into consideration during the testing phase of internal fixation devices. Moreover, there is a lack of information on how bone callus can be used with success to monitor bone healing.

In this study, an experiment was initiated to create a set of composite materials that replicate the different tissues simulating the tissues that develop during bone healing from early soft callus to mature callus. The idea is to use the different composites and simulate healing on a fractured Sawbone® instrumented with an intramedullary nail while monitoring the strain measurement. More details about the design of experiment and its outcome is described and discussed in Chapter 4. The next section examines the significance of the nature of healing callus at the biological level.

2.10 Mechanobiology of fracture healing

The principle of mechanobiology is the understanding of the biological processes that are regulated by signals to cells generated by mechanical loading, a concept dating back to Roux, 1881 [37]. Meulen et al. [39] explained the importance of skeletal mechanobiology from the traditional skeletal biomechanics focussing on how the load bearing tissues are produced, maintained and adapted by cells as an active response to biophysical stimuli in their environment. The author also stated that an improved understanding of mechanobiology using the knowledge and tools already available can be beneficial to the medical arena. The mechanobiology of bone development and growth can be relevant for prevention and treatment of congenital deformities; however understanding the processes of bone development during regeneration in fracture healing and the bone adaptation to implants can aid further understand the gradual process that can be influenced over time [39].

Bone development involves two critical phases; the first starts *in-utero* when bone tissue starts to form. A foetus is normally born with various ossified precursors of adult bone. The development of the second phase happens post natal [38]. The schematic illustration in Figure 17 below shows the development of long bones from embryonic until mature. Bone formation is commonly

classified into two main types, namely intramembranous and endochondral bone formation. During intramembranous ossification, bone is formed and replaces existing membrane of embryonic connective tissue.

Figure 17 illustrates the processes encountered during endochondral formation. The processes involve tissue differentiation from granulation tissue through to fibrous tissue and cartilage to bone. During the ossification process, the mechanical and morphological status of the tissue changes completely. Bone differentiation continues beyond the ossification stage. Osteoclasts and osteoblasts are the cells responsible for the outline of the microstructures of cortical or cancellous bone tissue. The above described process of structural growth is the modelling process. Once the tissue has matured, osteoclastic resorption and osteoblastic formation maintains the bone continually by the remodelling process [37, 38, 39].

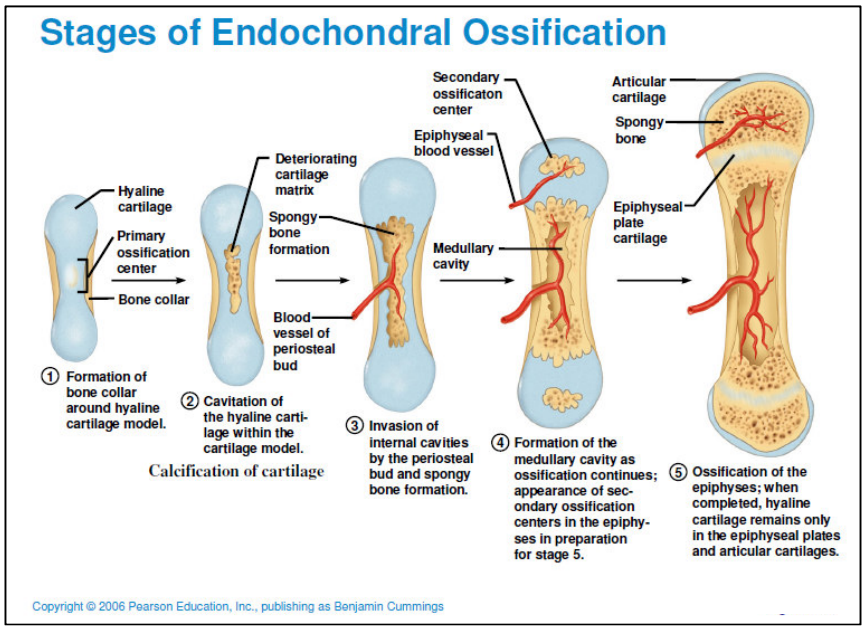

Figure 17: Stages of Endochondral ossification [40]

Fracture healing is a natural tissue differentiation process which may benefit from further understanding the interaction between mechanical and chemical stimuli. Bone fracture triggers a series of biological responses that leads to new tissue generation. This is normally achieved by the multiplication and differentiation of mesenchymal stem cells of the granulation tissue into cells forming cartilage, fibrocartilage, fibrous tissue or bone [39, 41, 42].

Mechanobiology has been discussed in both experimental and computational studies. Computational studies were initiated with a purpose “to determine the quantitative rules that govern the effects of mechanical loading on tissue differentiation, growth, adaptation and maintenance by trial and error” [39]. Pauwels introduced a new perspective based on

observations *in-vivo* on the mechanobiology of tissue differentiation [41]. His perception on tissue differentiations were based on observations from histological patterns in cases of pseudarthroses and angulated fractures. Pauwels suggested that critical evidence for tissue differentiation is contained in the stress and strain invariants of hydrostatic stress and octahedral shear stress however he was not equipped to measure or calculate the stresses or strains accurately.

Carter et *al.* [43, 44] tested Pauwels theory of endochondral bone formation using finite element analysis. High values of the osteogenic index were found in the cartilage where osteogenesis is expected to occur during *in-vivo* skeletal development was reported [43, 44]. Osteogenic index was defined as the combination of the peak cyclic hydrostatic stress and the peak cyclic octahedral shear stresses over a number of loading cycles. Similar positive predictions were performed for other skeletal sites for bone regeneration in fracture healing and around interfaces of orthopaedic implants [39].

Carter et *al.* [43] describes fracture healing as a regenerative process displaying tissue differentiation characteristics during skeletal morphogenesis. His hypothesis regarding tissue differentiation and fracture healing was consistent with previously theories about morphogenesis. The perspective used in his theories states that tissues develop under cyclical loading of undifferentiated mesenchymal tissue. Carter suggests that the “entire” loading history of a bone over a period of time will determine the tissue response during the healing process. The presence of high shear or tensile hydrostatic stresses in the history may help to encourage the formation of fibrous tissues.

His theory proposed was that, fracture will bring forth an osteogenic stimulus. If cyclic strain or stresses are created along with a good blood supply, bone formation will commence. The presence of high stress magnitudes will encourage the tissue propagation. As healing occurs, the incidence of high shear and/or tensile hydrostatic stresses promotes fibrous tissue formation. Chondrogenesis in turn is promoted by high compressive hydrostatic stresses. He also states that if cartilaginous tissue forms, compressive hydrostatic stresses will inhibit endochondral ossification.

Carter also hypothesised that the influence of mechanical stresses histories in the ossification of callus is similar to what occurs during the skeletal morphogenesis process. The cyclic compressive hydrostatic stresses prevent ossification and cyclic shear stresses encourage proliferation and ossification. Carter [43] tested this hypothesis using finite element modelling and the theory was used to predict variation in early callus characteristics and where the initial ossification process is likely to begin. The FE modelling indicated that fracture healing patterns are controlled by intermitted hydrostatic pressure in the initial callus than by shear intermittent stress. The results

presented confirm the histological findings stated in the literature. The study conducted by Goodship and Kenwright [43] showed that the periosteal surface near the interfragmentary gap is the area where the tensile principal stresses are highest and replicates initial bone formation created in an experimental osteotomy. Carter also observed that the strongest stimulus for the formation of bone is directly outside the interfragmentary gap at the periosteal surface where high compressive dilational stresses are absent. The study also indicates that the initial callus formation may be caused by the role of intermittent hydrostatic pressure in inhibiting vascular in-growth. The process of revascularisation and ossification has been shown to appear first in areas where there is an absence of high compressive hydrostatic stresses.

In relation to a bone-implant interface and fracture healing, the mechanobiology is discussed briefly as follow. For bone formation to thrive there should be minimal movement at bone-implant interface. This allows for the process of osseointegration [42]. Motion at the interface of implants creates high stresses in tissue regeneration hindering new bone formation causing fibrous tissue formation which is consistent with expectations based on the principles presented above.

In fracture healing cases, the regenerative process involves inflammation, proliferation, differentiation, ossification and bone remodelling. However, these processes do not necessarily occur in linear progression around the trauma site. They may take place simultaneously around the site. The 3D distribution of the processes and tissue formation is primarily controlled by the stress, strain and local vascularity [42]. Loading instigated by the method of fixation and physical activity of the patient determines the distribution of the tissue formation. Variation in these factors can result in vital metamorphosis in healing patterns [39, 42].

When a surgeon uses a rigid internal fixation, the primary goal is to lessen sporadic motion at the fracture site that normally occurs due to muscular activity. The formation of granulation tissue during the regeneration process is thus shielded from distortional strains that would be expected to promote proliferation hence resulting in a small fracture callus [42]. The mesenchymal tissue is also protected from significant hydrostatic stresses. The formation of bone directly throughout the tissue is therefore consistent based on the mechano-biological ideas presented above. Cartilage and fibrocartilage are unlikely to form unless there is vascular disruption since significant hydrostatic pressure is not created.

The idea of mechanobiology tend to lead us away from biomechanics, however in an evolutionary world of multidisciplinary models, the objective in order to make key advances in the area of orthopaedics, should be the integration of both these models. This leads to the end of this section

on mechanobiology. The next section explores the mechanical properties of the bone concentrating on long bones for the purpose of the study.

2.11 The mechanical properties of bone

The mechanical properties of bone depend on the tissue it is made from and how the latter is organised structurally to execute its mechanical function. For mechanical testing, long bones are often used as a whole bone or tailored into beams or rods. A whole diaphyseal bone is most commonly tested using bending and torsional tests. The dense nature of cortical bone determines its strong and stiff mechanical properties compared with cancellous bone. For comparison, Figure 18 below shows the elastic modulus and ultimate tensile strength of the bone and several other tissues and biomaterials [45]. The mechanical properties of bone depend on the type of mechanical testing. Bone is elastic, anisotropic, heterogeneous and a composite material. The determinants of bone mechanical properties include its density, porosity, microscopic structure and collagen fibre orientation [45].

Bone is an organic material that has been considered in the same way as a synthetic engineering material. In terms of fracture healing, one needs to consider the mechanical properties of the bone from being a soft tissue to a mature cortical bone. The different levels of bone callus relate to the different level of progression of healing tissue at the fracture site. Lacroix et *al.* [21] described the generation of tissues involved in the repair process such as fibrous connective tissue, cartilage and woven bone before the mineralisation to mature cortical bone. The latter study included a summarised table with the material properties of the various tissues extracted from published sources (see Figure 19 page 68). The data from Figure 19 shows the Young's modulus of the incrementing generation of tissues involved in the fracture repair from granulation tissue to cortical bone.

Bone is known to be a dynamic tissue; its structure can change in response to loading patterns. This concept between the form and mechanical function was first observed by Roux but it was eventually established and became known as Wolff's law [46].

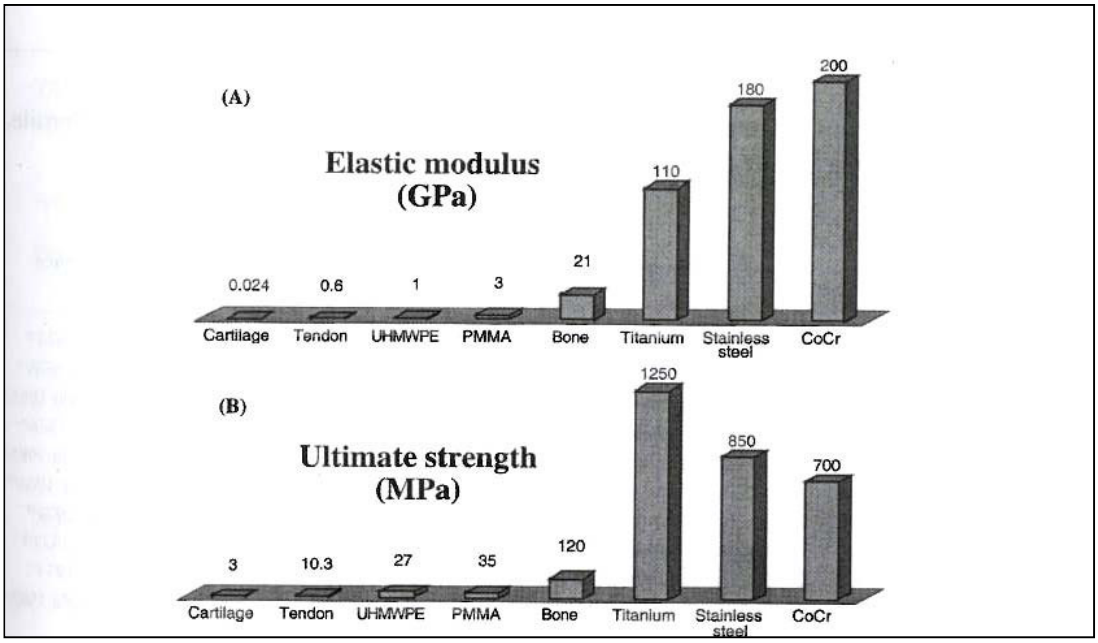

Figure 18: Illustrations of the elastic modulus (A) and strength (B) of bone and other common tissues and biomaterials [45]

	Granulation tissue	Fibrous tissue	Cartilage	Marrow	Immature bone	Mature bone	Cortical bone
Young's modulus (MPa)	0.2	2[a]	10	2	1000	6000[b]	20000[b]
Permeability (m^4/Ns)	1E-14	1E-14[a]	5E-15[c]	1E-14	1E-13	3.7E-13[d]	1E-17[e]
Poisson's ratio	0.167	0.167	0.167	0.167	0.3	0.3	0.3
Solid compression modulus (MPa)	2300	2300	3400[f]	2300	13920	13920	13920[e]
Fluid compression modulus (MPa)	2300[g]	2300[g]	2300[g]	2300[g]	2300[g]	2300[g]	2300[g]
Porosity	0.8	0.8	0.8	0.8	0.8	0.8	0.04[h]

[a] Hori and Lewis (1982).
[b] Claes and Heigele (1999).
[c] Armstrong and Mow (1982).
[d] Ochoa and Hillberry (1992).
[e] Cowin (1999).
[f] Tepic et al. (1983).
[g] Anderson (1967).
[h] Schaffler and Burr (1988).

Figure 19: Extracted from Lacroix et al. illustrating the mechanical properties of various bone tissue [21]

Wolff's law states that every change in the form and the function of a bone or in the function of the bone alone, leads to changes in its internal architecture and in its external form. Structural adaptation of the bone occurs when the bone is placed under compressive or tensile stress which leads to remodelling. Bone is formed where stresses require it and resorp where stresses do not require it [5, 6].

The physical properties of bone depend on the geometry and the type of load applied; alternatively, a machined sample of bone with known geometries can be tested. The data from Figure 18 and 19 would have been machined samples of known geometries tested for consistency. Loading of the bone would normally occur within the elastic range during any type of loading process when the bone is in use within the musculoskeletal system. For ease of understanding, using a simpler system to analyse the mechanics of materials, it is probable to

approximate the stresses for a given loading arrangement. During locomotion, four types of loading may occur which are, axial loading, bending, torsion and transverse loading [45, 46]. The consequent total load applied throughout the structure may vary combining total stresses which can be either compressive or tensile and shear stresses. The most common types of loading are compression, bending and torsion although transverse loading plays more of a minor role. Compressive and tensile stresses are generated in different sections of the bone during loading.

Bone has been described above as dynamic and often described as an isotropic homogeneous elastic tissue. However, this simplification has often been made for its mechanical properties. Bone is in fact an anisotropic homogeneous tissue exhibiting viscoelastic properties. This viscoelastic characteristic of the bone simply suggests the stress depends not only on the strain but also on the time history of the strain. This behaviour can sometimes also be observed as creep which is the gradual increase in strain under constant stress or stress relaxation which is the gradual decrease in stress held at a constant strain. Bone is viscoelastic and the properties vary with the speed of loading, showing up as an effect of strain rate in a stress/strain curve and the effect of frequency in fatigue tests. Loading a viscoelastic material has a typical response where the following is observed; there is a dependence on the strain rate that is, the faster the stretching, the larger the stress requires. Also the loading and unloading curves do not coincide instead there is the formation of a hysteresis loop. After complete loading, there is the potential that permanent deformation may or may not occur.

Nigg *et al.* [46] stated that daily activities would normally results in strains of the order of 2000 to 3000 με. These strains are considered to be within the elastic limit hence qualifying bone as an elastic tissue. The viscosity in bone is accountable for the stiffness on strain rate, the capability to disperse energy, for stress relaxation and creep behaviour observed. The experimental testing of bone or artificial bone uses the standard mechanical testing approaches such as axial compression, tension, torsion and bending in order to determine the mechanical behaviour of the bone. In the case of natural bone testing, the organisation of the bone tissue provides more insight into the structural loads to derive mechanical behaviour rather than invasive tests [42].

The mechanical adaptation of bone is synonymous with bone remodelling which is a continuous process that occurs. If there is an increase in physical loading of the bone, an increase in bone mass is likely to be observed. Similarly, if there is lack of activity, bone mass may decrease changing the architecture of the mechanical environment. The regulations of these processes are normally conducted by osteocytes termed mechanosensors. The Mechanostat Theory was first recognised by Frost in 1986 [47] to explain the changes that occur biomechanically as a function of the strain environment. The theory has been experimentally verified and has proven useful for

understanding bone adaptation. The concept suggests that there is a physiological window of normal strains. Below 200 με remodelling response is likely to occur while if it reaches the upper limit of 2500 με in compression or 1500 με in tension a modelling response will occur [48]. Currently strain is considered the most significant mechanical factor in regards to bone remodelling [47]. Strain theories have been studied and tested both experimentally and using finite element analysis by many experts. Strain can either be in compression or in tension but both have osteogenic potential [49, 50]. The strain direction has been suggested to control osteonal remodelling in the cortical bone, so that the configuration occurs in the principal strain directions [51]. Static and dynamic strain induces different responses in bone. Dynamic loading has been documented to induce osteogenic responses which led to numerous studies investigating strain rate and frequency in the adaptation of bone [47].

The mechanical properties of bone have to be closely monitored throughout as any changes in activity can induce response in the structural arrangement in the bone cells. This chapter started with a review looking in details at the structure of the bone, the various cells involved as well as the vascular and muscular system within the skeletal system. It reviewed fractures and the fracture repair processes with details about bone callus tissue and formation which is a major component within this study. Finally, the mechanobiology and the mechanical properties were examined before moving to a more detailed review of the tibia, its structure and it's loading in relation to the main aims of the project. This concludes the end of this chapter. The next Chapter examines the loads and forces the tibial anatomy is subject to.

2.12 References

[1]. T P Rüedi, R E Buckley, C G Moran. AO Principles of Fracture Management. Thieme Publishing. 2007

[2]. http://abcfromfl.wordpress.com/2010/05/27/abcfromfls-anatomy-anatomical-terms-body-reference-planes/ (last accessed: 24/04/201212:40)

[3]. http://www.squidoo.com/intro_anat1 (last accessed: 24/04/2012 12:28)

[4]. R Drake, A W Vogl, A W M Mitchell, A Mitchell. Gray's Anatomy for students: with StudentConsult Access.1st edition Churchill Livingstone, 2004

[5]. S C Cowin. Bone Mechanics Handbook. 2nd edition, Informa Healthcare, 2001

[6]. J D Currey. Bone: Structure and Mechanics. Princeton University Press, 2006

[7]. http://training.seer.cancer.gov/anatomy/skeletal/tissue.html (last accessed: 24/04/2012 13:02)

[8]. J P Bilezikian, L G Raisz, G A Rodan. Principles of bone biology, Two volume set. Academic Press,2nd edition, 2002

[9]. Martin TJ, Sims NA, Ng KW. Regulatory pathways revealing new approaches to the development of anabolic drugs for osteoporosis. Osteoporosis International, 2008, 19, 1125–1138.

[10]. Murray Brookes. The blood supply of bone: an approach to bone biology. Butterworth – Heinemann, 1971

[11]. LJ Donaldson, IP Reckless, S Scholes, JS Mindell, NJ Shelton.The epidemiology of fractures in England. Journal of Epidemiology & Community Health, 2008, 62, 174-180.

[12]. http://thesebonesofmine.wordpress.com/category/anatomical-terms/ (last accessed: 25/04/2012 12:43)

[13]. http://radiopaedia.org/images/408102 (last accessed: 25/04/2012 12:57)

[14]. Elaine N Marieb. Human Anatomy and Physiology., 5th Edition, Benjamin Cummings ,2001

[15]. http://www.britannica.com/EBchecked/media/101369/Posterior-view-of-the-right-leg-showing-the-muscles-of (last accessed: 25/04/2012 13:29)

[16]. 2008 World Population Data Sheet, Population Reference Bureau; http://www.prb.org/Publications/Datasheets/2008/2008wpds.aspx (last accessed: 15/05/2011 11:42)

[17]. C.M.Court-Brown, J.McBirnie. The epidemiology of tibial fractures. Journal of Bone and Joint Surgery [Br], 1995, 77-B, 417-21.

[18]. http://apbrwww5.apsu.edu/thompsonj/Anatomy%20&%20Physiology/2010/2010%20Exam%20Reviews/Exam%202%20Review/Ch%206%20Bone%20Fractures.htm (last accessed: 25/04/2012 15:28)

[19]. PL Leong, EF Morgan. Measurement of fracture callus material properties via nano-indentation. Acta Biomaterialia, 2008, 4, 1569-1575.

[20]. Markel MD, Wikenheiser MA, Chao EY. A study of fracture callus material properties: relationship to the torsional strength of bone. Journal of Orthopaedic Research, 1990, 8,6, 843–50.

[21]. D.Lacroix and PJ Prendergast. A mechano-regulation model for tissue differentiation during fracture healing: analysis of gap size and loading. Journal of Biomechanics, 2002, 35, 9, 1163.

[22]. HT Aro, BW Wippermann, SF Hodgson, HW Wahner, DG Lewallen, EY Chao. Prediction of properties of fracture callus by measurement of mineral density using micro-bone densitometry. Journal of Bone and Joint Surgery (Am). 1989,71,1020-1030.

[23]. ES Powell, PV Lawford, T Duckworth, MM Black. Is callus calcium content an indication of the mechanical strength of healing fractures? An experimental study in rat metatarsals. Journal of Biomedical Engineering, 1989, 11, 4, 277-81.

[24]. http://www.mayoclinic.com/health/needle-biopsy/MY00088 (last accessed: 27/04/2012 17:15)

[25]. MD Markel, MA Wikenheiser, EYS Chao. A study of fracture callus material properties: relationship to the torsional strength of bone. Journal of Orthopaedic Research, 1990, 8,843-850.

[26]. FZ Cui, Y Zhang, HB Wen, XD Zhu. Microstructural evolution in external callus of human long bone. Materials Science and Engineering, 2000, C 11, 27-33.

[27]. CI Moorcroft, PJ Ogrodnik, PBM Thomas, RH Wade. Mechanical properties of callus in human tibial fractures: a preliminary investigation. Clinical Biomechanics, 2001, 16, 776-782.

[28]. JL Ford, DE Robinson, BE Scammell. The fate of soft callus chondrocytes during long bone fracture repair. Journal of Orthopaedic Research, 2003, 21, 54-61.

[29]. SJ Shefelbine, U Simon, L Claes, A Gold, Y Gabet, I Bab, R Müller, P Augat. Prediction of fracture callus mechanical properties using micro-CT images and voxel-based finite element analysis. Bone, 2005, 36, 480-488.

[30]. JM Garcia-Aznar, JH Kuiper, MJ Gomez-Benito, M Doblaré, JB Richardson. Computational simulation of fracture healing: Influence of interfragmentary movement on the callus growth. Journal of Biomechanics, 2007, 40, 1467-1476.

[31]. P.L.Leong, E.F.Morgan. Measurement of fracture callus material properties via nanoindentation. Acta Biomaterialia, 2008, 4, 1569-1575.

[32]. A Muste, I Papus, FL Betec, R Lacatus, A Donisa, M Marius. The study of posttraumatic bone callus formation in sheep. Lucrări Stiinłifice Medicină Veterinară, 2010, Xliii (2), Timisoara.

[33]. M Mehta, P Strube, A Peters, C Perka, D Hutmacher, P Fratzl, GN Duda. Influences of age and mechanical stability on volume, microstructure, and mineralization of the fracture callus during bone healing: Is osteoclast activity the key to age-related impaired healing? Bone, 2010, 47,219-228.

[34]. Z Adamiak, T Rotkiewicz. A histological evaluation of bone calluses in the treatment of tibia fractures in sheep with the use of a semicircular fixator. Veterinarni Medicina, 2010, 55,11, 547-550.

[35]. A Vetter, Y Liu, F Witt, I Manjubala, O Sander, D R Epari, P Fratzl, GN Duda, R Weinkamer. The mechanical heterogeneity of the hard callus influences local tissue strains during bone healing: A finite element study based on sheep experiments. Journal of Biomechanics, 2011, 44, 3, 517-523.

[36]. L Claes, A Ignatius, S Schorlemmer, D Horvath, A Veeser. Transverse callus formation by implant induced strain application. Presentation O-111,Institute of Orthopaedic Research and Biomechanics, University of Ulm, Germany

[37]. OA Oni. The bony callus. Injury: International Journal of the Care of the Injured, 1997, 28, 9-10, 629-631.

[38]. Alastair J.S. Summerlee. Available at: www.aopublishing.com/bone/bonesample.pdf (last accessed: 12/07/2012 22:29)

[39]. Marjolein C.H. van der Meulen, Rik Huiskes. Why Mechanobiology? A survey article. Journal of Biomechanics, 2002, 35, 4, 401-414.

[40]. http://www.kean.edu/~jfasick/docs/Fall%20Semester%20Lectures%20Chapt.%201-15%20%20%2707/Chapter%206B.pdf (last accessed: 12/07/2012 23:05)

[41]. Dennis R. Carter, Gary S. Beaupré. Skeletal Function and Form: Mechanobiology of Skeletal Development, Aging, and Regeneration Cambridge University Press, 2007

[42]. Stephen C Cowin. Bone Mechanics Handbook. 2nd edition, Informa Healthcare, 2001

[43]. Carter D.R. Mechanical loading history and skeletal biology. Journal of Biomechanics, 1987, 20 , 1095-1109.

[44]. Dennis R Carter, Marcy Wong. The role of mechanical loading histories in the development of diarthrodial joints. Journal of Orthopaedic Research, 1988, 6, 6, 804-816.

[45]. Yuehuei H. An, Robert A. Draughn. Mechanical Testing of bone and bone implant interfaces. CRC Press, 1999

[46]. Benno M.Nigg, Walter Herzog. Biomechanics of the musculoskeletal system. 3rd edition, Wiley , 2009

[47]. J P Bilezikian, L G Raisz, G A Rodan. Principles of bone biology. Academic Press,2nd edition, 2002

[48]. Martin RB & Burr DB. Structure, Function and Adaptation of Compact Bone. Raven Press, 1989

[49]. LE Lanyon. Experimental support for the trajectorial theory of bone structure. Journal of Bone and Joint Surgery, 1974, 56-B, 1, 160-166.

[50]. Maquet, P. and Furlong, R. Biomechanics of the Locomotor Apparatus: Contributions on the Functional anatomy of the Locomotor Apparatus. Springer Verlag

[51]. L E Lanyon, Sheila Bourn. The influence of mechanical function on the development and remodelling of the tibia. An experimental study in sheep. Journal of Bone and Joint Surgery, 1979, 61, 2, 263-273.

[52]. http://varmaanatomy.blogspot.co.uk/ (last accessed: 15/01/2013 16:38)

[53]. HK Vaananen, H Zhao, M Mulari, JM Halleen. The cell biology of osteoclast function. Journal of Cell Science, 2000, 113, 377-381.

[54]. Perren SM. Physiological and biological aspects of fracture healing with special reference to internal fixation.Clinical Orthopaedics and Related Research, 1979, 138, 175-196.

[55]. SM Perren. Evolution of the internal fixation of long bone fractures, The scientific basis of biological internal fixation: choosing a new balance between stability and biology. Journal of Bone and Joint Surgery [Br], 2002, 84-B, 1093-1110.

[56]. BV Johnson, N Shindo, PD Rathjen, J Rathjen, RA Keough. Understanding pluripotency – how embryonic stem cells keep their options open. Molecular Human Reproduction, 2008, 14, 9, 513-520.

[57]. Andrea Augello and Cosimo De Bari. The regulation of differentiation in mesenchymal stem cells. Human Gene Therapy, 2010, 21, 1-13.

[58]. Rocky S Tuan, Genevieve Boland, Richard Tuli. Adult mesenchymal stem cells and cell-based tissue engineering. Arthritis Research Therapy, 2003, 5, 32-45.

3 Anatomical loads and forces in the tibia

This section will examine the anatomical loads and forces experienced during activities in the lower limb but also more specifically in relation to the tibial forces. What and how the forces in the tibia are measured will also be reviewed before moving on to analyse the literature at hand on the concept of strain and how telemetry has been used to measure forces in the tibia combined with what has previously been discussed in Section 1.4.

The tibia is found in the lower limb, which is anatomically positioned inferior to the vertebral column. The anatomical placement of the tibia has been discussed in Section 2.4. The tibia is larger than the fibula in size and the main weight bearing bone. At its proximal end, the tibia expands in the transverse plane for weight-bearing. Loading of the tibia is of specific interest in this project as the device being developed is a tibial intramedullary nail.

Komistek *et al.* [1] examined the techniques that have been used in the past as well as currently methods used in determining the *in-vivo* loads transmitted in knee mechanics. The latter investigated the loads acting across the femoro-tibial joint. Using telemetry, the loads for multiple activities were determined. Intersegmental forces and torsional forces calculated from inverse dynamics were due to muscle, ligaments and contact forces. The axial force measured by the team using telemetry post operatively were 0.5 times the patient's bodyweight at month 3 and 1.8 times at month 23. Torsional force of magnitude 7Nm was observed in the axial direction. However, the largest force recorded was the interaction between the femur and tibia during stair descent activity. The study by Komistek *et al.* is not the first time that telemetry was used in determining the *in-vivo* loads acting in the body.

Wehner *et al.* also investigated internal loads in the human tibia during gait using telemetry [2]. Based on internal fixations deformations, *in-vivo* experiments using telemetry was successfully used in determining internal loads acting inside the implant during the healing process. Using this information, a musculoskeletal model of the lower extremities developed by Anybody Research Group were modified to determine the 3D internal loads along the tibial axis during gait. The forces were measured in bodyweight (BW) and the moments in bodyweight times millimetre (BWmm). Axial force of magnitude 4.7 times the BW was the highest internal load recorded and the bending moment in the sagittal plane was observed up to 71.6 times BWmm [2]. The author concluded that the findings of this study could be used to improve the mechanical behaviour of current implant designs for the treatment of tibial fractures to avoid implant failures under *in-vivo* loading conditions [2].

D'Lima *et al.* [3] instrumented tibial prosthesis to measure *in-vivo* forces after total tibial arthroplasty. The forces were measured postoperatively during rehabilitation. The tibial forces

observed during walking averaged at 2.2 times the bodyweight post operatively by week 6. On day 6, the stair climbing activity recorded tibial forces on 1.9 times the bodyweight which increased to 2.5 times the bodyweight as healing occurred on week 6. Understanding the influence of increased forces hence increasing bodyweight during activities seems to positively influence healing.

Early weight bearing is commonly prescribed and encouraged by clinicians to produce strains essential to encourage callus formation. Aranzulla *et al.* [4] conducted a study that used weight bearing as a monitoring system during tibial fracture healing. According to the study, the magnitude and frequency of weight bearing will determine the load transferred at the fracture site, the movement and the strain produced will therefore have an influence on healing. Weight bearing was found to be less than 50% of the body weight during the first two months post fracture in patients treated using external fixators for their tibial fracture [4]. These measurements were taken with patients stepping onto a force plate.

Another study conducted by Joslin *et al.* [5] investigated the use of weight bearing after tibial fracture as a guide to healing. The assessment of fracture healing remains a matter of clinical verdict based upon a subjective impression of fracture pain, stiffness made by loading and assessment of radiological union by the presence of bridging callus and the absence of the fracture line. It has been observed that weight bearing increases with time post fracture. The ability to weight bear has been suggested to be controlled by a biofeedback mechanism relating fracture site strain to the stiffness of the fracture.

Meggitt et al. [6] also used weight bearing as a guide to fracture healing. They concluded that the biofeedback mechanism facilitated by the mechano-receptors in the fracture callus was the most likely reason how the damage to load bearing by the limb was prevented. Wardlaw *et al.,* who used the same methods as Meggitt et al., reached the same assumption that there was likely to be physiological response mechanism [7]. Joslin *et al.* found that in this study, fracture stiffness was found to increase to 15Nm/deg before removal of the external fixator. Two patients failed to reach union by 20 weeks with stiffness measurements of less than 5Nm/deg. Joslin *et al.* concluded that increases in weight bearing reached post fracture seem to moderately associate with increase in fracture stiffness and the return to normal values of weight bearing largely show that there is clinical union.

Using experimental *in-vitro* testing and mathematical modelling of an external fixator, Beaupre *et al.*[8] predicted that up to 95% of the axial load can be supported by a fracture callus with the modulus of elasticity only half of that of healed bone. Gardner *et al.* [9] conducted a similar study using external fixators and predicted that 99% of the tibial load can be carried by early osteogenic

soft callus with only 1% modulus of a healed bone. However, a study conducted by Vijaykumar *et al.* [10] disagrees with Gardner *et al.* [9]. The study conducted by Vijaykumar *et al.* [10] aimed to investigate the actual load sharing in a real fracture during gait at different healing stages. The study showed that as healing progressed, average tibial resultant force and peak magnitude were observed to increase in addition to the return of the mechanical integrity of the limb. Forces recorded were found to be in tune with the *in-vivo* forces recorded by Taylor *et al.* [11] with peak numbers reaching that of normal subject as healing evolved.

Muscular forces are often considered as forces that are registered during *in-vivo* loading forces. Lu *et al.* [12] performed *in-vivo* experiments using instrumented telemetered proximal femoral prostheses. The forces transmitted were processed and indicated that the axial force in long bones is a response to muscle activity. The results indicated that the bending moments along limbs was by a combination of tensile forces in muscles and compressive forces in bones. This proved that muscle forces are important in experimental and theoretical investigations of load transmissions along bones and should be taken into consideration when designing implants.

Telemetry, which had previously been discussed in Section 1.4, seems to have a recurring theme in the review above. Telemetry has been successfully used in measuring loads and forces in the lower extremities in various studies. Section 1.4, also examined the history and beginnings of telemetry in orthopaedics. However, in order to gain a better understanding as to how telemetry relates to the forces experienced, the next section looks at the basic concepts of strains and strain gauges.

3.1 Basic concept of strain, strain gauges in relation to telemetry

Strain represents the dimensional changes of a subject or body under the action of a force or several forces. When force is applied, the object changes its dimension. This change in dimension is termed deformation (ΔL). Deformation per unit length (L) is strain (ε):

$$\varepsilon = \frac{\Delta L}{L} \qquad [3.1]$$

Strain is a dimensionless measure since it is the ratio of two quantities, both in units of length. Strain is defined as the geometric change in a material in response to force application and is also known as a normalized displacement. The types of strain in a body are the same as the types of force producing them: normal strain (compressive and tensile) and shear strain. Normal strain is analogous to normal stress. Ultimate strain is the strain that occurs at fracture. Strain can be measured directly and is recorded as length per unit length or can sometimes be also reported as a percentage. Positive strain occurs when a material is subjected to tensile stress in the direction of the applied load, reflected as an increase on the length of the material. If the material is

compressed the length is decreased and the strain is negative. Strain rate is the deformation per unit time, which is an important parameter for viscoelastic materials such as bone.

Strain Gauge measurement in Biomechanics

The fundamental principle underlying the electric resistance strain gauge is that when a wire is stretched, its length increases and its cross-sectional area decrease causing a change in its electrical resistance. The equation relating the length change to the resistance change is,

$$R = \frac{\rho L}{A} \qquad [3.2]$$

Where R is the resistance, ρ is the material property of the conductor called resistivity, L is the length of the conductor and A is the cross sectional area of the conductor [14].

In-vitro, strain gauges have been used for bone strain measurements since the late 1950s. Lambert reported that gauges could be attached directly to the surface of moist cortical bone and described methods of water proofing the gauges and lead wires. In the study, the deformation and weight bearing functions of the fibula and tibia were measured [15].

Strain gauges are transducers whose resistance varies under an applied stress. There are three categories, metallic, semiconductor and mechanical. Metallic gauges have a gauge factor G of approximately 2; semiconductor gauges have a higher gauge factor, of approximately 100, but also have a high temperature coefficient, which tends to limit their application [14]. One type of metallic gage commonly used consists of an etched metal foil pattern on a suitable base. This is attached to the test piece by a suitable adhesive. The actual adhesive used should suit both the sensor and the surface on which it is mounted and due consideration should be given to the humidity, temperature of the operating environment [14, 16]. The unstressed resistance of the strain gauge equals ρl/a where ρ is the resistivity of the gauge material, l and, a, are the length and cross sectional are of the track. When a test piece undergoes strain, the gauge attached to it is strained by the same amount. Tensile strain causes the gauge to stretch, which increases the gauge resistance. Compressive strain produces the opposite effect and decreases the gauge resistance. This variation in resistance with strain is linear over the operating range of the gauge.

Strain Gauge Bridges

For the strain to be measured, it must be translated from a variation in resistance to a variation in DC voltage. This is done by connecting the strain gauge into a bridge circuit and energizing the bridge from a constant voltage or constant current supply. The reason for having a bridge is that the changes in resistance with strain, especially with the metallic gage, are inherently small and

the bridge allows the resultant small changes in voltage to be read directly; strain voltages may thus be measured at the best possible at increased resolution. [14, 16]

3.2 Hypothesis of monitoring fracture healing using telemetry

This study aims to produce a biomechanical model for the simulation of fracture healing in an *in-vitro* environment, using a customised artificial model. This model will then be used for biomechanical testing of several generations of prototyped instrumented tibial nail.

Measurement of strain changes in the nail aims to allow better understanding of load sharing, in both the fractured and intact bone. This will act as a base, allowing for the design of a clinically applicable instrumented nail. The telemetry should be able to show small strain changes in the nail, as the fracture heals, thus allowing monitoring of the repair process as well as early prediction of delayed-union and non-union.

An ideal instrumented nail for clinical use would use a minimum number of strain gauges whilst providing sensitive data for a maximum number of clinical environments. We have thus over instrumented our nail to start with and loaded it under different conditions, with the hope of high-lighting the optimum location and number of strain gauges before designing the second generation nail.

- Hypotheses:
  - Strain gauges implanted in a tibial IM nail are able to provide sensitive data, showing a relationship between strain and axial force.
  - Strain gauges implanted in a tibial IM nail are able to provide sensitive data, showing a relationship between strain and axial torque.
  - A single site for the positioning of strain gauges to provide sufficient data to predict fracture healing.

3.3 References

[1] Richard D. Komistek, Thomas R. Kane, Mohamed Mahfouz, Jorge A. Ochoa, Douglas A. Dennis. Knee mechanics: a review of past and present techniques to determine *in-vivo* loads. Journal of Biomechanics, 2005, 38, 215-228.

[2] Tim Wehner, Lutz Claes, Ulrich Simon. Internal loads in the human tibia during gait. Clinical Biomechanics, 2009, 24, 299-302.

[3] Darryl D.D'Lima, Shantanu Patil, Nikolai Steklov, John E.Slamin, Clifford W.Colwell. Tibial forces measured *in-vivo* after total knee arthroplasty. The Journal of Arthroplasty, 2006, 21, 2.

[4] P.J. Aranzulla, D.S.Muckle, J.L. Cunningham. A portable monitoring system for measuring weight-bearing during tibial fracture healing. Medical Engineering & Physics, 1998, 20, 543-548.

[5] C.C.Joslin, S.J.Eastaugh-Waring, J.R.W.Hardy, J.L.Cunningham. Weight bearing after tibial fracture as a guide to healing. Clinical Biomechanics, 2008, 23, 329-333.

[6] Meggitt, B.F., Juett, D.A., Smith, J.D. Cast-bracing for fractures of the femoral shaft. Journal of Bone and Joint Surgery, 1981, 12–23.

[7] Wardlaw, D., McLauchlan, J., Pratt, D.J., Bowker, P. A biomechanical study of cast-brace treatment of femoral shaft fractures. Journal of Bone and Joint Surgery, 1981, 63-B, 7–11.

[8] Beaupre, G.S., Hayes, W.C., Jofe, M.H., White, A.A. Monitoring fracture site properties with external fixation. Trans. ASME, 1983105, 120–126.

[9] Gardner, T.N., Evans, M. Relative stiffness, transverse displacement and dynamisation in comparable external fixators. Clinical Biomechanics, 1992, 7, 231–239.

[10] V.Vijaykumar, L. Marks, A.Bremmer-Smith, J.Hardy, T.Gardner. Load transmission through a healing tibial fracture Clinical Biomechanics, 2006, 21, 49-53.

[11] Taylor, S.J.G., Walker, P.S., Perry, J.S., Cannon, S.R., Woledge, R. The forces in the distal femur and the knee during walking and other activities measured by telemetry. Journal of Arthroplasty, 1998, 13, 428–437.

[12] Tung-Wu Lu, Stephen J.G.Taylor, John J.O'Connor and Peter S.Walker. Influence of muscle activity on the forces in the femur: an *in-vivo* study. Journal of Biomechanics, 1997, 30, 11/12, 1101-1106.

[13] G.Bergmann, F.Graichen, A.Rohlman. Hip joint loading during walking and running measured in two patients. Journal of Biomechanics, 1993, 26, 8, 969-990.

[14] 3535D, F & G Scorpio Data Logger, Solartron Instruments, User Guide, 1993

[15] Kenneth L Lambert. The weight bearing function of the fibula: A strain gauge study. Journal of Bone and Joint Surgery, 1971, 53, 507-513.

[16]Yuehuei H. An, Robert A. Draughn. Mechanical Testing of bone and bone implant interfaces, CRC Press, 1999

4 In-Vitro testing

4.1 Biomechanical testing

In-vitro biomechanical testing is the standardized laboratory tests to validate the implant prior to any clinical study. The *in-vitro* testing provides the platform for the implant to be tested under extreme conditions and to ensure the implant complies with regulations and the standards of specific countries where the implants are intended for sale. *In-vitro* testing is conducted for practically all medical devices at some stages of development or the other to ensure that the device is functioning without incurring any failure as it would be expected to function in the body. However, this is not always the case; recent failure of hip resurfacing metal-on-metal devices show that devices that have been tested successfully *in-vitro* have failed to function efficiently over the duration of time expected [15].

In this study, the *in-vitro* testing is broken down into several components; each component will have a description of the methodology used, the results and discussions. The testing starts with the design of the bone callus mimic leading to the testing of the first generation of the smart nail to the third generation nail used in the cadaveric and *in-vivo* study. The data recorded were processed using Excel and statistical analysis was performed.

4.2 Synthetic bone callus

Bone callus as described in previous chapters' referring to the bone repair and growth process that is initiated after trauma. Current trends in the manufacturing industry dictates, that any orthopaedic device have to undergo rigorous testing before any approval is given for clinical trial. Trauma devices are currently tested in systems that simulate the actions the device will be subjected to in the human body. This type of testing is very important as it helps understand the forces and the limits the device can be subjected to. A series of composites have been designed with the aim to take into perspective the various different properties of bone and associated tissue during healing while testing trauma fixation devices. The next section looks at composites in more details and the basic properties that need to be taken into account when designing a new material for special purposes.

4.2.1 Composites

A composite is said to be a multi-phase material that exhibits a significant proportion of the properties of both constituents' phases. The constituent phases must be chemically dissimilar and separated by a distinct interface [1]. Most composites are created to develop an amalgamation of mechanical characteristics, for example stiffness and toughness. The properties of composites are a function of the properties of the constituent phases, their volumes and spatial relationships of the dispersed phase. There are several types of composites namely particle reinforced

composites, fibre reinforced composites and polymer matrix composites. In this study, we are going to concentrate on the particle and fibre reinforced composites.

Particle reinforced composites

There are further two subdivisions of particle reinforced composites as large particle and dispersion strengthened composites. The distinctions between these are based on reinforcement or strengthening mechanism. The hard and stiffer particles tend to restrain movement of the matrix phase in the vicinity of each particle. The matrix (softer phase) transfers some of the applied stress to the particles which bear a fraction of the load. The degree of reinforcement or improvement of mechanical behaviour depends on strong bonding at the matrix particle interface.

In dispersion strengthened composites, reinforcing particles are much smaller having diameters between 0.01 and 0.1µm. The mechanism of strengthening is similar to that for precipitation hardening, the matrix bears the major portion of applied load and the small dispersed particles delay the motion of dislocations which results in plastic deformation and leads to improved yield, tensile strength and as well as hardness of the composite.

Fibre reinforced composite

The most important composites are those in which the dispersed phase is in the form of a fibre. Design goals of fibre reinforced composites often include high strength and stiffness to weight. These characteristics are expressed in terms of specific strength and specific modulus parameters. Fibre reinforced composites are sub-classified by fibre length.

Influence of fibre length

The mechanical characteristics of a fibre reinforced composite depend not only on the properties of the fibre but also on the degree to which an applied load is transmitted to the fibres by the matrix phase. The extent of the load transmittance is the magnitude of the interfacial bond between the fibre and the matrix phase. A critical fibre length is necessary for effective strengthening and stiffening of the composite material. The critical fibre length l_c is dependent on the fibre diameter d, its ultimate tensile strength σ_f and on the fibre matrix bond strength τ_c as,

$$l_c = \frac{\sigma_f d}{2\tau_c} \qquad [4.1]$$

If the fibre length is ($l > 15\ l_c$), it is termed as continuous fibre reinforcement. For discontinuous fibres of length significantly less than l_c the matrix deforms around the fibre such that there is virtually no stress transference and little reinforcement by the fibre [1].

Influence of fibre orientation and concentration

Longitudinal loading and transverse loading

The properties of a composite having its fibres aligned are highly anisotropic. Taking the deformation of a composite in which a stress is applied along the direction of alignment, the total load sustained by the composite F_c is equal to the loads carried by the matrix phase F_m and the fibre phase F_f,

$$F_c = F_m + F_f \qquad [4.2]$$

A continuous and oriented fibre composite may be loaded in the transverse direction; the load is applied at a 90° angle to the direction of fibre alignment. The stress σ to which the composite as well as both phases are exposed is the same,

$$\sigma_c = \sigma_m = \sigma_f = \sigma \qquad [4.3]$$

This is termed as iso-stress state. The strain of the entire composite ε_c is,

$$\varepsilon_c = \varepsilon_m V_m + \varepsilon_f V_f \qquad [4.4]$$

but since $\varepsilon = \sigma/E$ replacing in equation 4.4,

$$\frac{\sigma}{E_{ct}} = \left(\frac{\sigma}{E_m}\right) V_m + \left(\frac{\sigma}{E_f}\right) V_f \qquad [4.5]$$

Where E_{ct} is the modulus of elasticity in the transverse direction and dividing by σ yield [1],

$$E_{ct} = \frac{E_m E_f}{(1-V_f)E_f + V_f E_m} \qquad [4.6]$$

The fibre phase

On the basis of the diameter and character, fibres are grouped into three different classifications: whiskers, fibres and wires. Whiskers are very thin that have extremely large length to diameter ratios. Materials that are classified as fibres are either polycrystalline or amorphous and have small diameters. Fine wires have relatively large diameters.

The matrix phase

The matrix phase of fibrous composites may be a metal, polymer or ceramic. In general metals and polymers are used as matrix materials because some ductility is desirable. For the fibre reinforced composites the matrix phase serves several functions. First it binds the fibres together and acts as the medium by which an externally applied stress is transmitted and distributed to the fibres. The second function of the matrix is to protect the individual fibres from surface damage as a result of mechanical abrasion or chemical reactions with the environment. Finally the matrix separates the fibres and by virtue of its relative softness and plasticity prevents the propagation of brittle cracks from fibre to fibre, which could result in catastrophic failure [1]. It is essential that adhesive bonding forces between fibre and matrix to be high to minimise fibre pull out. The theory of the composites described above gives an insight in the background before launching into the design of the bone callus tissue composites.

4.2.2 Bone callus mimic design

To date, there has been no published study of *in-vitro* testing using simulated healing regimes. The literature on bone callus is very limited and has been reviewed in Chapter 2. Lacroix [2] published a thesis on the simulation of tissue differentiation during fracture healing where fracture healing is described as a complex biological process. The study examined in great details the concept of simulating tissue differentiation during fracture healing; however, the experiment was *in-silico.* Despite the increasing use of virtual testing as a validation tool, it is still a prediction tool that has to be utilised in conjunction with established knowledge of fracture gap sizes and the effect of loading on healing. However, experimental analyses of the effect of loading on healing using callus mimic composites would be more effective in terms of the testing of medical devices *in-vitro*.

A new material design was initiated to develop a series of composite materials simulating the properties of healing tissues, designed to be applied on a fractured bone *in-vitro*. This would be used during the developmental stages of testing fracture fixation devices. This particular phase of the study was started during the post graduate studies dissertation.

Summary of previous work conducted in the postgraduate dissertation

A standard intramedullary nail was wired with strain gauges at the distal, midshaft and proximal sites of the nail, with the wires coming out at the proximal end of the nail. The nail was implanted in a 3rd generation Sawbone® with a midshaft 10mm osteotomy and potted in FastCast® polyurethane on both sides. The construct was loaded on an Instron compression machine and offset axial compression induced bending was applied to it. In order to simulate fracture healing, a composite material was designed. Due to time limitation within the project, only six samples were investigated. Hydroxyapatite (HA) and macerated Sawbone® were used as filler in percentages of 5%, 10% and 25% to epoxy resin by approximate volume. The samples were carefully measured, mixed and left to cure in an oven at 55°C. The samples were tested for compression strength using the Instron Machine. The results were then compared to the compressive strength of bone in the longitudinal direction as published in Bones: Structure and Mechanics [3]. Table 2 below shows the result from the test [4]. This data was compared a table of Modulus of Elasticity given by Currey [3]. The table contained the results of elastic moduli for bone in the radial, circumferential and longitudinal direction. When compared, the 5%HA to epoxy mixture as the callus composite material gave 111MPa, which is around 0.6% of the modulus of elasticity of bone taken at 18.2GPa. The composite was applied to the proximal fracture osteotomy in 8 separate steps to simulate internal and external cortical bridging in the four anatomical planes. The construct was allowed to cure at room temperature for 24 hours after each step before axial compression measurement was taken again. The results showed there was a decrease in strain after callus bridging. The study demonstrated the simulation of early fracture healing in an idealised scenario without the effect of any muscular activity which plays a significant role in the fracture healing process [4].

Sample	Compressive strength/MPa
Control Araldite Only	68.4
25% Sawbone	83.4
10% Sawbone	92.1
5% Sawbone	87.4
25% HA	105.8
10% HA	111.3
5% HA	111.3

Table 2: Compressive Strength of bone in longitudinal direction [4]

The results from the initial study conducted in the postgraduate dissertation showed the dearth of data available in the literature regarding to simulation of bone tissues for *in-vitro* testing. This

led to the idea of developing a biological mimic to simulate the different tissues that occur during fracture healing within the doctoral study. Extensive literature search showed that there was no such experiment or study about *in-vitro* simulation of fracture healing, hence this was considered to be novel and an application for a GB patent [5] was filed with Patent Application Number GB 0907766.1. The next section describes the new set of composites in more detail along with the materials selection, mechanical and microscopic analysis of the raw materials and end products.

4.2.3 Materials selection for synthetic callus material design

From a basic understanding of composites as described in the above sections, a set of composites were designed to simulate early spongy bone callus to hard mature osteogenic bone. This mimicked the different stages of healing which would be used *in-vitro* in order to simulate healing on a fractured tibial Sawbone®. Numerous materials were assessed in terms of their physical properties and carefully selected to achieve the closest match for the bone callus mimic. Amongst the material considered were, glass fibre, beech wood, hydroxyapatite, stainless steel, tin, chromium alginate and bone cement. In order to be able to find the modulus of the matrix to be used, reverse engineering of the elastic behaviour in discontinuous and randomly oriented direction equations of composite was used. The equation was the closest to what the hypothesis set to achieve. Despite, the number of challenges it presented to produce such a composite, the theory was used only as a background to identify the selected range of matrix that would help achieve the modulus required. The equations were mathematically transposed to find the approximate range of the matrix modulus for the estimated mechanical properties. With the approximate modulus range known and the different stages of healing identified, the material selection was undertaken accordingly. The discontinuous and randomly oriented equation is more likely to fit the purpose of this composite is given by the equation below:

$$E_{CD} = \left(k \times E^f \times V^f\right) + (E^m \times V^m) \quad [4.7]$$

- E_{CD} = Young's modulus of bone = Young's modulus of composite
- E^f = Young's modulus of fibre or particulate
- E^m=Young's modulus of matrix
- V^m= Volume of matrix
- V^f= Volume of fibre or particulate
- k = fibre efficiency parameter [1]

The above equation was rearranged and the estimated range of materials modulus was calculated. Different materials were researched and tested to approximate the different stages of the healing process. Numerous epoxies, silicones and resins with the approximate mechanical properties were identified as the matrix. A specific set of fillers were identified composed of metals and ceramic powders and particulate. The experimental protocol used was the same as used in the previous study [4] except for the percentage mixtures. It was deemed prudent to set the percentages at 5%, 10% and 15% in order to make the mixing process uniform depending on the size of the filler material.

In order to use the reverse engineering process to mathematically calculate and approximate as accurately the range of values for material selection, the end values for the modulus of bone was taken from Figure 20 below extracted from a paper by Lacroix et *al.* [2].

	Granulation tissue	Fibrous tissue	Cartilage	Marrow	Immature bone	Mature bone	Cortical bone
Young's modulus (MPa)	0.2	2[a]	10	2	1000	6000[b]	20000[b]
Permeability (m^4/Ns)	1E 14	1E 14[a]	5E 15[c]	1E 14	1E 13	3.7E 13[d]	1E 17[e]
Poisson's ratio	0.167	0.167	0.167	0.167	0.3	0.3	0.3
Solid compression modulus (MPa)	2300	2300	3400[f]	2300	13920	13920	13920[g]
Fluid compression modulus (MPa)	2300[g]	2300[g]	2300[g]	2300[g]	2300[g]	2300[g]	2300[g]
Porosity	0.8	0.8	0.8	0.8	0.8	0.8	0.04[h]

Figure 20 : Physical properties of bone extracted from Lacroix et al. [2]

The Young's modulus was used in equation 4.7 and the formula was tested using the mechanical properties of hydroxyapatite as the particulate. Table 3 below shows the calculated values of the modulus of the matrix for the different bone tissue. This table is an illustration of the sample of reverse engineering conducted to gain an understanding of the type of matrix that can be used in this experiment. Hydroxyapatite was used for this part of the modelling since it is a mineral found in bone, the mechanical properties were considered to be appropriate for use in this experiment.

Bone tissue	Ecd/GPa	Ef/GPa	K	Vf	K*Ef*Vf	Vm	Em/GPa
Granulation	0.02	77	0.2	0.1	1.54	0.9	-0.55
Fibrous	0.2	77	0.2	0.1	1.54	0.9	3.89
Cartilage	10	77	0.2	0.1	1.54	0.9	8.34
Immature	100	77	0.2	0.1	1.54	0.9	12.78
Mature	600	77	0.2	0.1	1.54	0.9	17.23
Cortical	2000	77	0.2	0.1	1.54	0.9	21.67

Table 3: Calculated values for modulus of the matrix with hydroxyapatite as particulate

Taking that approach and proceeding with a complete modelling reverse engineering, using a range of preferred materials, a series of trial of the experiments were started. Hydroxyapatite (HA), powdered tin, powdered steel and beech wood shavings were used as the particulate and in

the various composite mixtures. Hydroxyapatite is a mineral that is found in bone. Beech wood has a Young's modulus between 10 and 18GPa which is similar to the mechanical properties of mature to cortical bone. Steel is known to have a modulus of around 200GPa and it is widely used in the medical industry for its mechanical properties. Tin has a modulus of approximately 50GPa which makes it softest material chosen. These four materials were chosen to act as particulates in the composite as they have the mechanical properties the callus material was aiming to achieve.

The materials were sourced and analysed for particle size using a light microscope and an Able Image Analyser. A series of high strength polymeric materials were selected according to their manufacturer's specification of the elastic modulus and tested on their own to assess the suitability for the experiment. The particulate materials were mixed with the polymeric resins such as epoxies and were selected according to their elastic modulus. Four different layers of healing from granulation tissue to immature bone were approximated. The particulate materials were analysed using light and scanning electron microscopy technique.

4.2.4 Microscopy analysis

Several techniques have been developed for materials characterisation analysis. Light and scanning electron microscopy are two important methods. Light microscopy is the use of visible light to detect small objects. It is a widely recognized technique and is used in laboratories within biomedical research and material science field. Scanning Electron Microscope (SEM) uses electrons instead of light to form an image. Figure 21 below shows a schematic of an SEM.

The SEM used was a Zeiss Supra 35VP, a field emission SEM that can operate with both high vacuum and variable operating pressure capability. This allows for non-destructive examination samples in their natural state. The system is equipped with a suite of analytical techniques for material composition and phase detection such as energy dispersive x-ray analysis (EDX), back scattered detection (BSE) and electron back scattered diffraction (EBSD).

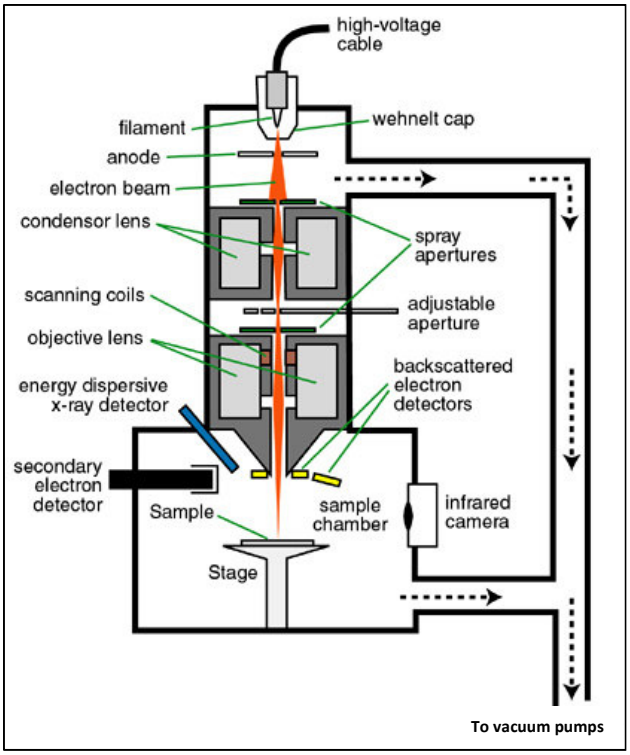

Figure 21: Schematic of an Scanning Electron Microscope [6]

SEM uses high energy electrons to generate signals at the surface of solid specimens. These signals reveal information about the sample such as chemical composition, morphology, crystalline structure and orientation of the material the sample is made up of. The SEM is normally used to produce high resolution images. In this instance, SEM has been used to analyse the particulate materials prior to making the composites. This is because of the microscopic size of the particulate materials to the naked eye. When analysed the materials sizes were aggregates rather than the size of a single particle. This is due to the fact that when mixed to epoxy resin, the particulates would tend to distribute randomly hence forming an aggregate size. The sample preparation in this experiment was very straightforward. A sticky carbon disc (tab) is mounted on a stub that fits onto the stage of the chamber in the SEM. The particulate materials are dispersed on a clean surface and the carbon disc mounted stub is pressed down onto the powder. For non conductive surfaces a gold or platinum coating can be applied. Figure 21 below shows the SEM pictures of the four chosen particulates used in the composites.

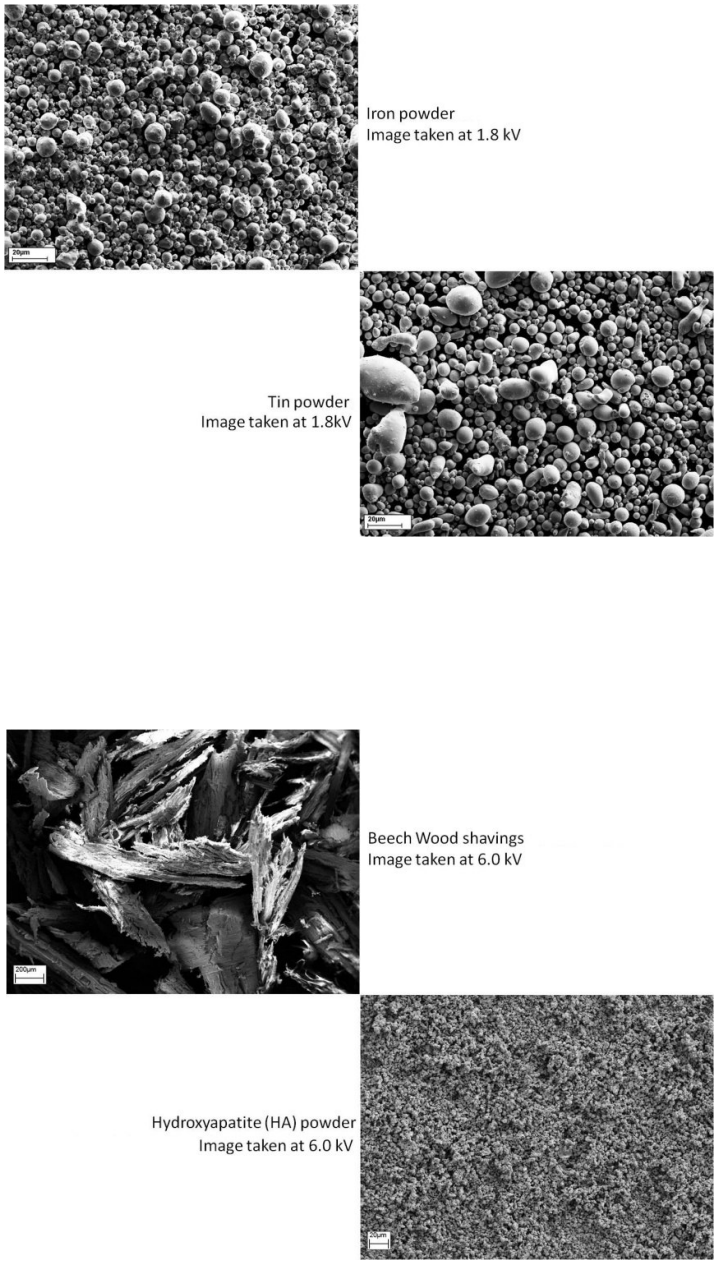

Figure 22: SEM images of selected particulates for callus composite

SEM helps to understand the shape and spatial arrangement of the particulate aggregates. But in order to have an understanding of the size of the aggregates and its distribution when mixed with resins, light microscopy has been used. The particulate samples were prepared by dispersing them in either an aqueous or non-aqueous mountants on a glass slide and protected by a cover slip. Several images were taken and analysed using Able Image Analyser and Excel. A graticule was used for spatial calibration. The images were processed and the particle sizing of the aggregates were measured in square microns. Images were taken for each material and the average taken overall. With these details in-hand, the composite design experiments were carried out as per the set protocol.

4.2.5 Experimental protocol for callus composite

The particulates, fibres and matrix material were weighed accurately using a calibrated Denver electronics balance model APX-60 capable of measuring to 0.1mg. A standard method of preparation was established. The different components were weighed, mixed by manual stirring for one minute, resting for another minute and stirring again for one minute before allowing the mixture to rest for a minimum of 10 minutes, in order to allow the air bubbles to dissipate, before being poured to set in moulds. Cylindrical silicon moulds were used to allow the composites to set. All the composites were allowed to set for 24hrs at room temperature in a fume cupboard before being mechanically tested. Compression testing was performed on a calibrated Instron 8501 test machine. The samples were measured in diameter and height before a 5kN load was applied and Young's Modulus was calculated. The results were compared to bone callus healing data as shown in the table above. From a set of over 70 samples, 4 distinct composites were selected to simulate granulation tissue, fibrous tissue, cartilage and immature bone respectively. Table 4 shows the different resins used for the matrix in the samples. The results from the samples are shown below in Table 5.

DePuy CMW – Polymethyl Methacrylate
E2 – Polurethane potting compound
E3 – Araldite 2026 polyurethane adhesive compound
E4 – Devweld 530 -2 part methacrylate adhesive
E5 – Araldite 2014 – 2 part epoxy paste adhesive
E6 – Beuhler Epo Thin Hardner
E7 - Trihardner

Table 4: Resins used for the matrix

The particulates shown in Table 5 are denoted as follows: beech wood (BW), glass fibre (GF), hydroxyapatite (HA), tin (SN), stainless steel (SS).

Sample Composition	Epoxy	Percentage	Diameter/mm	Height/mm	Height immediately after testing/mm	Youngs Modulus (MPa)
ACRYLIC PERSPEX			25.44	26.3	26.3	1632
BW1	E2	5	X	X	X	0
BW10	E5	5	28.81	12.09	12.05	1066
BW11	E5	10	28.46	14.67	14.69	1239
BW12	E5	15	28.85	13.16	13.16	1134
BW13	E6	5	28.24	15.57	13.19	1.373
BW14	E6	10	28.96	15.81	12.26	57.63
BW15	E6	15	28.52	17.9	17.85	656.6
BW16	E7	5	28.21	13.52	13.45	707.7
BW17	E7	10	28.51	13.51	13.44	849.2
BW18	E7	15	27.67	15.52	15.5	777.8
BW2	E2	10	X	X	X	0
BW3	E2	15	X	X	X	0
BW4	E3	5	28.86	18.03	15.71	32.98
BW5	E3	10	28.3	20.56	18.81	36.75
BW6	E3	15	29.43	21.02	19.85	36.82
BW7	E4	5	27.87	20.39	20.21	365.2
BW8	E4	10	28.46	20.03	20.71	531.4
BW9	E4	15	28.84	19.54	19.45	284.1
CHROMIUM ALGINATE			24.48	15.28	SPLIT	55.65
CMW 1			29.36	19.12	19.11	0
CMW 2			29.28	19.41	19.41	1242
GF10	E5	5	28.52	12.44	12.38	587.6
GF11	E5	10	29.14	13.2	12.99	967.4
GF12	E5	15	29.21	17.3	17.3	729.4
HA1	E2	5	28.49	16.32	SPLIT	23.89
HA10	E5	5	28.95	9.24	9.19	1404
HA11	E5	10	29.18	11.2	11.11	737.5
HA12	E5	15	29.07	10.24	10.41	575.4
HA13	E6	5	29.07	14.35	14.33	1515
HA14	E6	10	28.34	13.7	13.69	906.3
HA15	E6	15	29.19	15.24	15.15	639.5

HA16	E7	5	29.22	10.24	10.24	638
HA17	E7	10	28.32	11.57	11.56	696.8
HA18	E7	15	28.25	11.59	11.54	585.9
HA2	E2	10	28.59	21.45	21.43	0.7281
HA3	E2	15	28.17	19.61	19.61	1.52
HA4	E3	5	28.65	14.37	14.14	46.95
HA5	E3	10	28.95	14.85	13.9	45.94
HA6	E3	15	29.96	13.63	13.56	50.79
HA7	E4	5	27.63	20.08	19.62	169.6
HA8	E4	10	27.27	17.3	17.28	210.6
HA9	E4	15	27.77	17.75	17.75	345.3
SN1	E2	5	27.25	16.1	16.4	43.05
SN10	E5	5	28.98	11.25	11.24	752.5
SN11	E5	10	29.01	11.69	11.69	821.8
SN12	E5	15	29.34	11.39	11.1	562.9
SN13	E6	5	28.17	15.56	15.49	649.9
SN14	E6	10	28.67	13.88	13.86	719.7
SN15	E6	15	29.26	14.31	14.29	509.8
SN16	E7	5	28.31	13.06	13.01	592.1
SN17	E7	10	28.66	12.09	12.09	609.8
SN18	E7	15	27.9	12.38	12.35	694.2
SN2	E2	10	28.71	16.59	16.59	56.45
SN3	E2	15	28.01	17.42	17.25	11.38
SN4	E3	5	28.82	12.95	12.18	43
SN5	E3	10	28.71	15.41	14.68	32.99
SN6	E3	15	28.19	14.36	13.1	41.56
SN7	E4	5	28.7	20.41	20.14	157.4
SN8	E4	10	27.73	17.31	17.31	27.72
SN9	E4	15	27.67	15.93	15.9	313.2
SS1	E2	5	27.88	16.24	15.92	227.9
SS10	E5	5	28.93	11.34	11.28	697.9
SS11	E5	10	28.7	13	12.82	948.1
SS12	E5	15	28.19	12.98	12.94	1086
SS13	E6	5	29.18	14.72	14.7	864.9
SS14	E6	10	28.6	13.73	13.72	1221
SS15	E6	15	29.04	15.7	15.7	680
SS16	E7	5	28.89	13.26	13.26	684.1
SS17	E7	10	28.3	13.4	13.39	579.7

SS18	E7	15	28.13	14.04	14.04	1122
SS2	E2	10	29.08	18.56	18.35	18.03
SS3	E2	15	28.64	18.15	18	0.3598
SS4	E3	5	27.26	20.43	20.22	133
SS5	E3	10	28.77	13.26	13.05	41.43
SS6	E3	15	28.42	14.09	13.56	43.82
SS7	E4	5	28.67	17.85	17.39	38.76
SS8	E4	10	27.91	18.1	15.62	115.1
SS9	E4	15	28.46	12.82	12.38	299.8
TRIHARDNER 1			28.69	15.07	14.86	1701
TRIHARDNER 2			27.91	16.27	16.24	1076

Table 5: Samples of composite tested for in compressive loading using an Instron

Table 6 below shows the type of tissue and the modulus of the composites compared to data extracted from a study conducted by Lacroix [2]. The matrix materials specification used are available in Appendix B. The result above was analysed carefully and the nearest match for the modulus of the tissue type was selected.

Callus Level	**Tissue type**	**Young's Modulus (MPa) [2]**	**Young's Modulus of bone callus composite (MPa)**	**% Filler Material (Fibre or Particulate)**	**Matrix Material**
L1	Granulation tissue	0.2	0.3598	15% SS (stainless steel)	Polyurethane potting compound
L2	Fibrous tissue	2	1.52	15% HA (hydroxyapatite)	Polyurethane potting compound
L3	Cartilage	10	11.38	15% SN (tin)	Polyurethane potting compound
L4	Immature bone	1000	1239	10% BW (beech wood)	Araldite 2014 –two component epoxy paste adhesive

Table 6: Compression modulus of composite callus compared to bone tissue modulus

The load vs. extension curves for the four selected composites are shown below in Table 7. Since the load applied during the compression test of the composite was constant, the graphs show a linear elastic behaviour during the test. However, the viscoelastic properties of the selected composites were not tested. Viscoelastic behaviour is characterised by hysteresis in the response of the material to load or strain with respect to time whereas elasticity relates to the material deformation to the applied load.

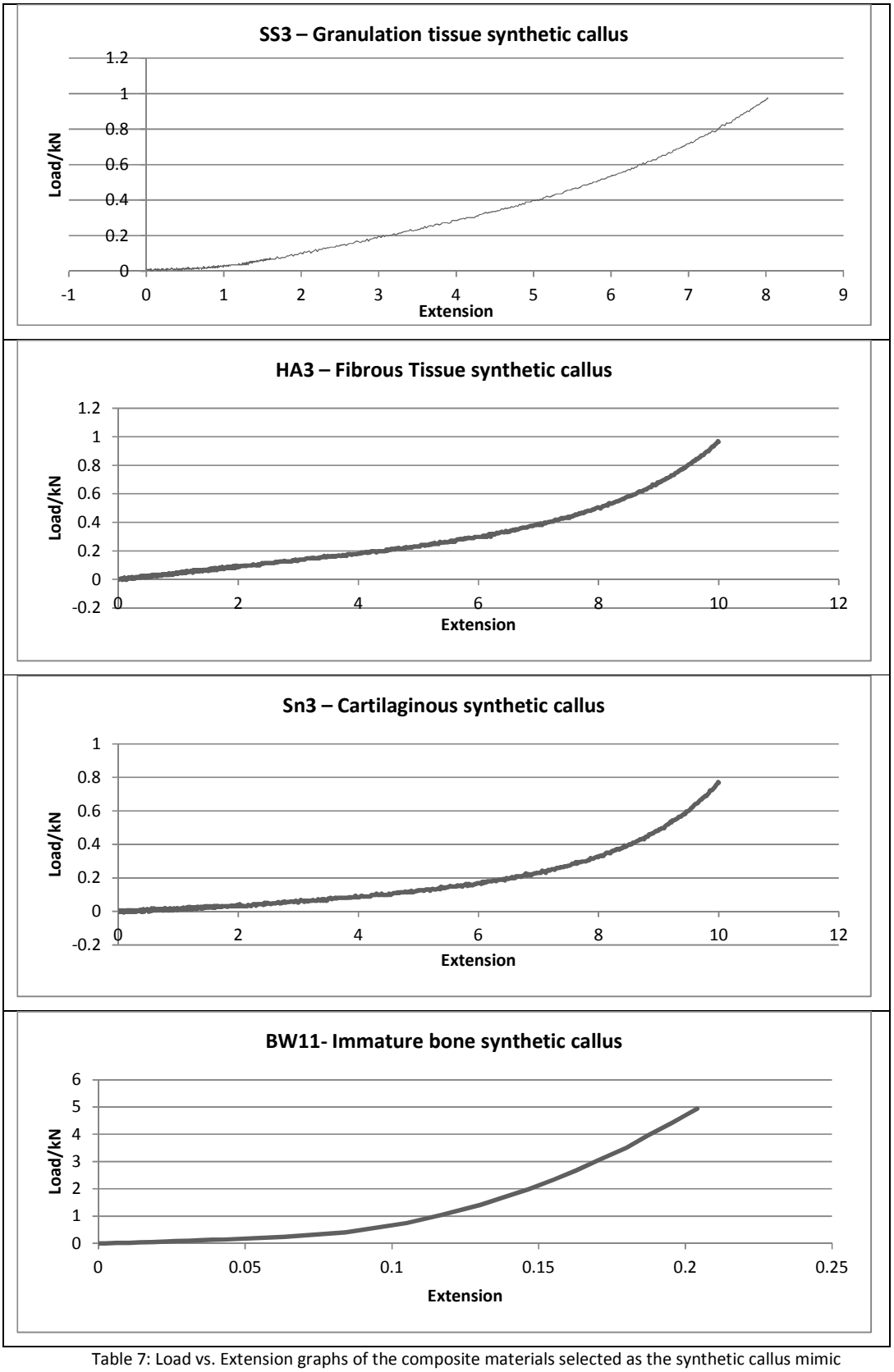

Table 7: Load vs. Extension graphs of the composite materials selected as the synthetic callus mimic

The graphs were loaded to a maximum of 5kN; however from the graphs it can be observed that some of the composites with lower modulus had a lower compressive strain.

4.2.6 Curing and repeatability

In order to ensure the modulus of the selected composites were within range of experimental errors, the set of composite for granulation tissue and cartilaginous tissues were prepared repeatedly using the above described methodology and compression tested using the Instron test machine. The results of the tests are published in Appendix C. During the experiment some sample using polyurethane did not cure as expected within the time given on the manufacturer's specification. Samples from the same batch were repeated with the same curing problem. It was thought to be a defective batch of polyurethane. This was corrected by using a new batch of polyurethane.

Granulation tissue callus mimic	Cartilaginous tissue callus mimic
0.628407	0.633205
0.609425	0.536374
0.543125	0.544649
0.598290	0.539301
0.581963	0.551631
0.575122	0.539301
Standard Deviation = 0.029672	Standard Deviation = 0.037522

Table 8: Compressive modulus repeatability and standard deviation

Table 8 shows the repeated testing of the compressive modulus of two of the tissue types with a low standard deviation.

4.3 Biomechanical tests

All the biomechanical tests follow the same protocol as described below. The *in-vitro* testing consist of testing 3 generations, GEN I to GEN IIIa, of the telemetrised nail each with a different arrangement of strain gauges mounted on its surface along with the other electronic components. Figure 23 below is a schematic diagram showing the details of the different generation of nails. The next section will look at the protocol set for the *in-vitro* biomechanical tests to be carried out for all three nail generations. The next sections will also explain the differences within the nail as the experiment were carried out. All the changes in the tibial nail to accommodate the strain gauge arrangements were taken into consideration in regard to fatigue the nail will have to withstand during its functional lifetime. Finite element analysis (FEA) was conducted by University of Hull experts part of a collaboration with Smith & Nephew to ensure that the pockets of material removed does not affect the fatigue strength of the nail and the data was compared to a standard nail. The result of the analysis concluded showing that the pocket did not have significant impact on the bending stiffness. However, the peak stresses were shown to have

increased 2 fold at the base of the pocket when the nail was subjected to gait moment. The inclusion of a dovetail in the design of GEN II pocket shows a significant reduction in mechanical stress in the pocket area [16]. The results shown by the finite element was still within specification for a standard nail hence it was considered safe to go ahead with material removal for the placement of the strain gauges and associated components.

320 x 10 mm	340 x 10 mm	180 x 10 mm	340 x 10 mm	Multiple sizes
Spiral configuration	1 extended pocket	1 short pocket	1 extended pocket	1 short pocket
Wired energizer/reader	Wired energizer/reader	Wireless energizer/reader	Wireless energizer/reader	Wireless energizer/reader
9/8 slave stations	5 slave stations	2 slave stations	3 slave stations	1 slave stations
24-27 gauges	20 gauges	6 gauges	12 gauges	1-2 gauges
3 gauges per slave site aligned at +45°, 0° and -45° to nail axis	4 gauges per slave site aligned at 0° (x3), and 45° (x1) to nail axis	3 gauges per slave site aligned at 0° (2), and 45° (1) to nail axis	4 gauges per slave site aligned at 0° (3), and 45° (1) to nail axis	1-2 gauges per slave site aligned at 0° and/or +45° to nail axis
Establishing loading protocols, validating fracture models, & understanding gauge sensitivity to fracture location	User experience on software and hardware components prior to GEN III nail. Soft encapsulant & biocompatibility testing	User experience on software and hardware components in animals prior to GEN III nail. 8 patients in vivo study of strain changes during fracture healing	User experience on software & hardware components in patients prior to commercial GEN IV; 5 patients in vivo study of strain changes during fracture healing	Verification & Validation of GEN III nail. Pocket will be shorter than 70 mm (GEN IIIa).

Figure 23: Schematic Diagram from project plan

4.3.1 Tibial construct

Biomechanical testing of the first generation – GEN I telemetrised nail was conducted *in-vitro* on a 4th Generation Sawbone® - an artificial bone mimic. The Sawbone® was prepared using orthopaedic surgical tools and the entry point was located medially to the lateral tibial in the anterior posterior (AP) view. The entry point was positioned in line with the anterior cortex and the intramedullary canal in the lateral view. The guide wire was connected to the drill via the mini connector and inserted into the proximal tibia and drilled approximately 4-6 cm in depth to reach the medullary canal. The tibial bone mimic was then fractured approximately 140mm from the distal end to simulate an oblique fracture about 36° to the vertical starting from the frontal plane. This type of fracture is described as a 42-A2 oblique fracture by the AO (**A**rbeitsgemeinschaft für **O**steosynthesefragen) Foundation. The fracture was then reduced before the insertion of the nail. The Sawbone was reamed approximately 2mm over the nail diameter to ease insertion into the medullary canal. The nail was secured using fixation screws both at the distal and proximal end

once in position. Figure 24 below shows an instrumented GEN I intramedullary nail with the pockets visible on the anterior side of the nail. At the distal end some wires can be seen exiting the cannulation.

Figure 24: GEN I showing the pockets on the anterior side of the nail

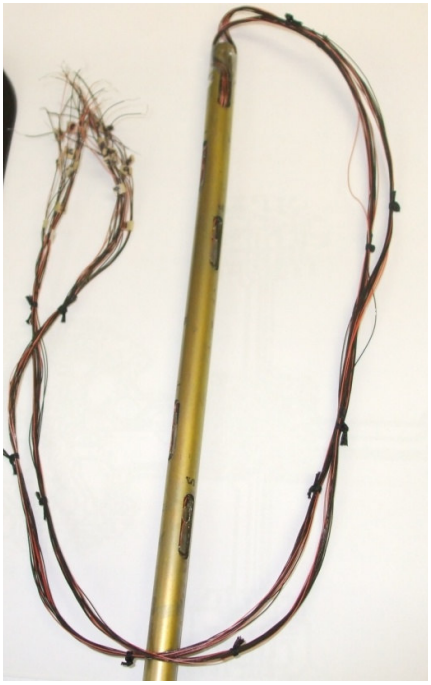

Figure 25: GEN I showing the wires exiting the distal end of the nail

Figure 26 below shows a series of images illustrating the fractured Sawbone® (A) , the IM nail inside the bone (B) and the distal end showing where the connecting wires exit (C).

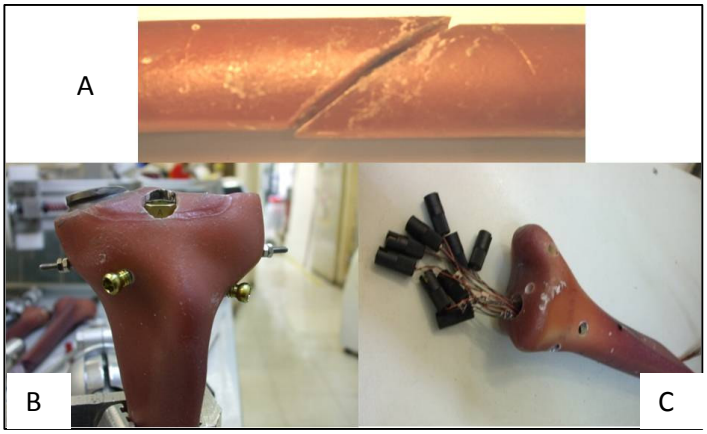

Figure 26: Figure A shows the fracture induced replicating 42 A2 fracture; B shows the proximal part of the tibial bone with the nail inserted and the screws in place; C shows the distal end with the wires from the instrumented nail exiting

The nail was a Ti6Al4Va 38cm TriGEN META Nail from Smith & Nephew Plc. The nail had 8 pockets machined on its surface in a spiral arrangement along the longitudinal axis. The pockets are 15mm long x 6mm wide x 34mm pitch. Each pocket had 3 set of strain gauges with 4 wires each that are channelled through the distal end of the pocket to the cannulation and exits at the proximal of the most distal screw holes with a 500mm wire extension to connect to the amplifier. In each pocket the strain gauges were positioned in relation to the longitudinal axis with gauge A at 45°, gauge B at 0° and gauge C at -45° (see Figure 23).

The strain gauges were bonded to the base of the pocket with MBond-600 adhesive and were protected with MBond-43B coating. The instrumentation of the GEN I nails were carried out by Vishay Micro-Measurements. The gauges were wired as quarter bridges with a single return wire in each pocket. The wires were joined to 8mm diameter connectors which fed into the amplifying box connected to the Labview V8 software on a standalone laptop.

Figure 27 on the next page shows a close up image the strain gauge arrangement visible in their different angles in the machined pocket. Only one GEN I instrumented nail was tested in this project. This was due to the fact that the other instrumented GEN I nail was damaged on insertion in the tibial Sawbone®.

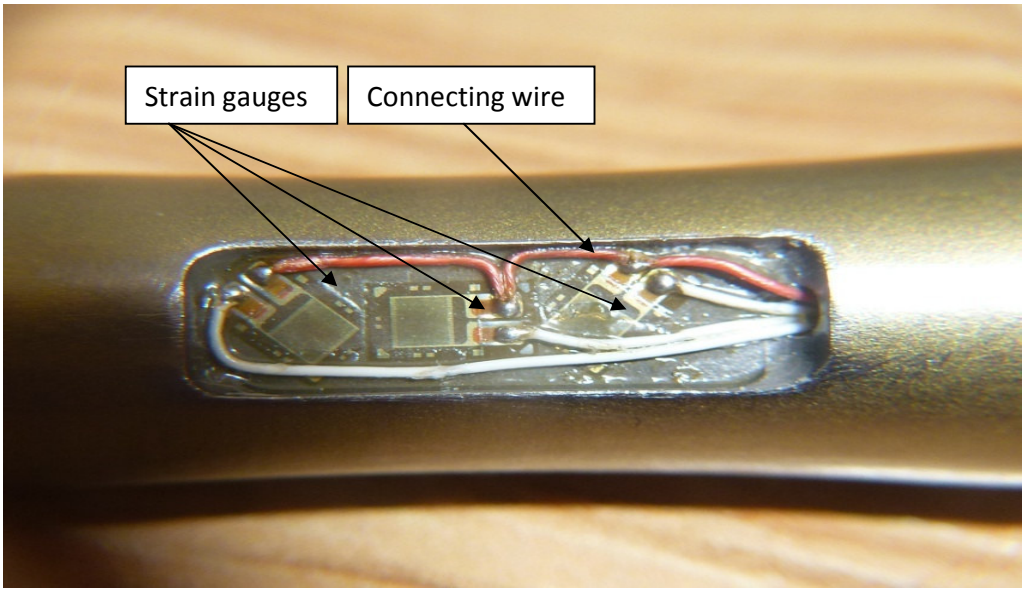

Figure 27: Strain gauge arrangement in a machined pocket

4.3.2 Experimental protocol

The Sawbone®- nail construct was then placed in a custom-made aluminium frame as shown in Figure 28. The frame has an adjustable top platform to accommodate axial compression loading. The load cell was at the bottom of the frame with a set of anti-rotation cross bar to reduce any potential rotation occurring at the distal end during testing. The load cell was designed for bending, torque and axial compression loading.

Figure 28: Custom made aluminium frame for axial compression and torque testing

The Sawbone® sits in the frame as shown below in Figure 29. The load cell was calibrated with a set of known loads. The Sawbone® had a washer inserted at both the proximal and distal end to act as an interface facilitating load transfer between the steel ball, the adjustable screw for loading and the bone surface. The Sawbone® was placed in the frame with the proximal loading interface 23mm offset from the medial midline and 9mm offset distally based on a study by Hutson *et al.* [7] to simulate a single legged stance. Distally a metal cap was designed to fit below

the bone with a hole along the midline axis overlapping the medullary canal for the wires to exit. It also housed a distal ball which interfaced with the top of the load cell. Figure 29 shows the aluminium frame with the instrumented intramedullary nail along with the amplifying box and an image of the connectors exiting the nail to the amplifying box.

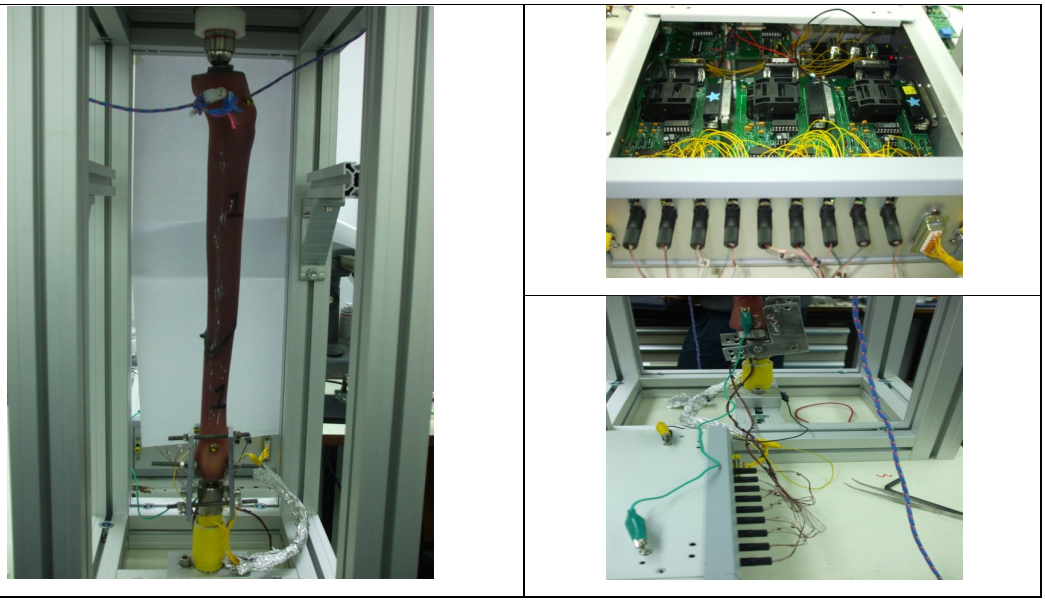

Figure 29: (Left) Pictures of the frame with an artificial bone in the loading position, (Right) Images of the amplifying system with the connectors from the wires from the instrumented nail

4.3.3 Loading protocol and data capture

The test protocol for biomechanical testing using the aluminium frame was described as follows. For axial compression bending, the Sawbone® was loaded from 0N to 1000N with incrementing steps of 50N. The increment of 50N was achieved by adjusting the screw fixed to the top of the frame while connected to the software where the graphical user interface allow the user to see the force applied (see Figure 30). The unloading was recorded as well in order to look at the hysteresis effects.

The torque testing was designed to be applied in both an internal and external rotation. The aluminium test frame was accommodated with a pulley system. A 100mm cross bar was placed horizontally through the proximal end of the bone in a medio-lateral direction. At each end, a set of strong wires able to withstand 10kg, were attached on both sides as shown in Figure 31. Switching the sides of the rope, opposite torque can be applied. The torque was applied to the Sawbone® in different axial compression modes at, 0N, 500N and 1000N. Torque applied was up to 5Nm, to simulate internal and external rotation (see Figure 31). This was done by applying weights from 500g to a maximum of 5kg.

A separate set up was used to apply a 4-point bend test to the instrumented Sawbone®. Two laboratory retort stands were secured on table top using G-clamps and the rod and clamp were set to about 45cm above table top. The instrumented tibial Sawbone® was removed from the aluminium frame while still connected to the amplifiers and the bone was set vertically with its proximal and distal end secured by the clamp of the stands. A custom-made supporting device made with two rings connected with a metal rod was placed on the tibial bone with the rings at either side of the fracture. The load for the 4pt bend test was applied across the metal rod, straight below the fracture line as shown in Figure 32. The test was conducted by hanging dead weights to the metal rod across the fracture simulating a 4-point bend test starting with 0.5kg up to 10kg.

It would have been ideal to repeat the loading in order to get a better understanding of the positioning of the strain gauges and the measurement, however the amount of data generated that require analysing and since this was a developmental nail, it seemed viable to conduct one run using this nail. Only one type of fracture pattern was investigated using GEN I instrumented nail. However, due to the fragility of the nail it was not possible to extract the nail from the bone model to simulate several fracture patterns.

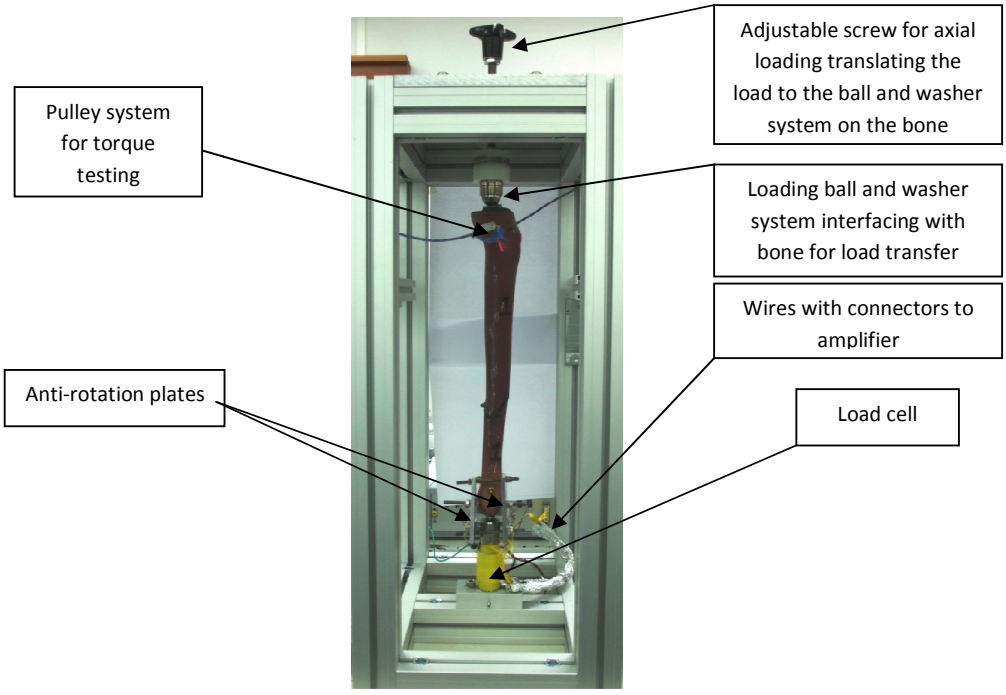

Figure 30: Tibial Sawbone® with an implanted instrumented GEN1 intramedullary nail

Figure 31: Left picture shows the loading contact point for axial compression and the right picture showing the pulley system for the internal and external torque

The instrumented Sawbone® was wired to the amplifier which was connected via an RS 232 to a laptop using Labview V8. The software recorded 512 counts in 5 seconds. The data collected was processed using a matrix and the average counts were converted to micro strains by diving by 6.8 (see section 4.4.1). The results were plotted and the gradient taken. The next section discusses more on the biomechanical test results before and after callus simulation testing.

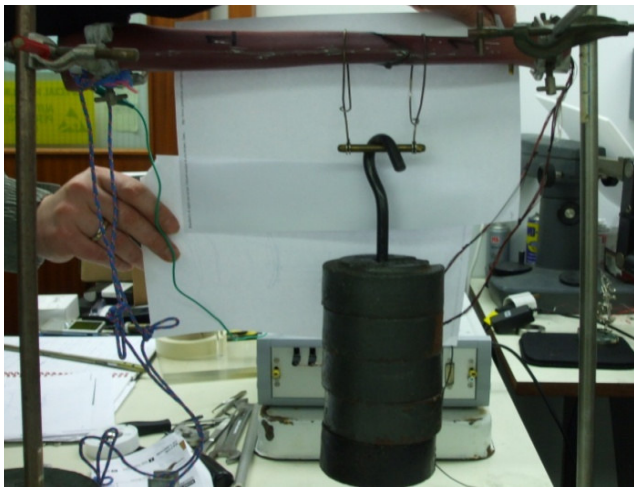

Figure 32: Four point bend test

4.4 First generation (GEN I) telemetrised intramedullary nail

GEN I was designed in order to establish loading protocols, validate fracture models but mainly to understand the gauge sensitivity to the fracture locations. GEN I was subjected to all the tests described in the test protocol above. It was also the first IM nail to undergo *in-vitro* fracture healing simulation using the four different composites created to replicate several layers of bone callus. The next sections described GEN I in more details as well as the biomechanical tests and different protocols in establishing the healing pattern on the fractured surface.

4.4.1 Strain gauge arrangement

GEN I nail consisted of eight separate pockets each containing three strain gauges, making a total of 24 strain gauges. The strain gauges used were foil gauges from Vishay Micromeasurements Ltd (N3K-XX-S022H-50C/DP), bonded at the base using MBond-600 adhesive and protected with a coating of MBond-43. The eight pockets have an anticlockwise spiral arrangement in order to balance the bending stiffness down the length of the nail, whilst being able to estimate the 6 degrees of freedom load vector at any given level by interpolation. This arrangement means that some gauges were under compression whilst others were under tension. There were three anterior pockets (1, 4, 7), two medial pockets (3, 6), three lateral pockets (2, 5, 8).

Each group of three gauges were arranged at +45°, 0° and -45°, with respect to the nail's longitudinal axis, in the plane of the pocket. Gauges were wired as quarter bridges with a single return wire in each pocket. Each of the eight pockets gives rise to four wires which travel inside the cannulation of the nail and exit to its outer surface by the most proximal of the distal locking screw holes. The 32 wires exit the Sawbone® through the distal end of the cannulation, and feed raw strain data to a digital amplifier by means of eight connectors. Strain data for each of the 24 gauges was quantified and displayed on a computer using Labview v8® software. 512 strain count measurements were recorded for each strain readings taken.

The average value is used for data analysis. The strain count can be converted to microstrain by dividing by a factor of 6.8. This value was determined both empirically by shunting the strain gauge with a known resistance to simulate a known strain, and also by calculation of the "strain to counts" process path; both values agreed. To increase accuracy of the measurements, electrical noise was reduced by earthing all metallic components of the experimental set up including the gauge wires and switching off the mains power supply, using only the computer battery during loading of the nail and data collection. The schematic for the design for the instrumentation of the GEN I nail is shown in Figure 33 and 34 can be seen on page 106. This instrumentation was done by Vishay Micromeasurements. The software interface used for the data collection was developed by UCL as part of the TSB project.

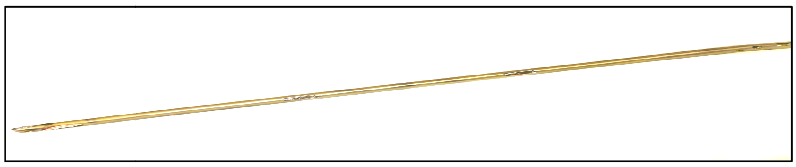

Figure 33: GEN I instrumented IM nail

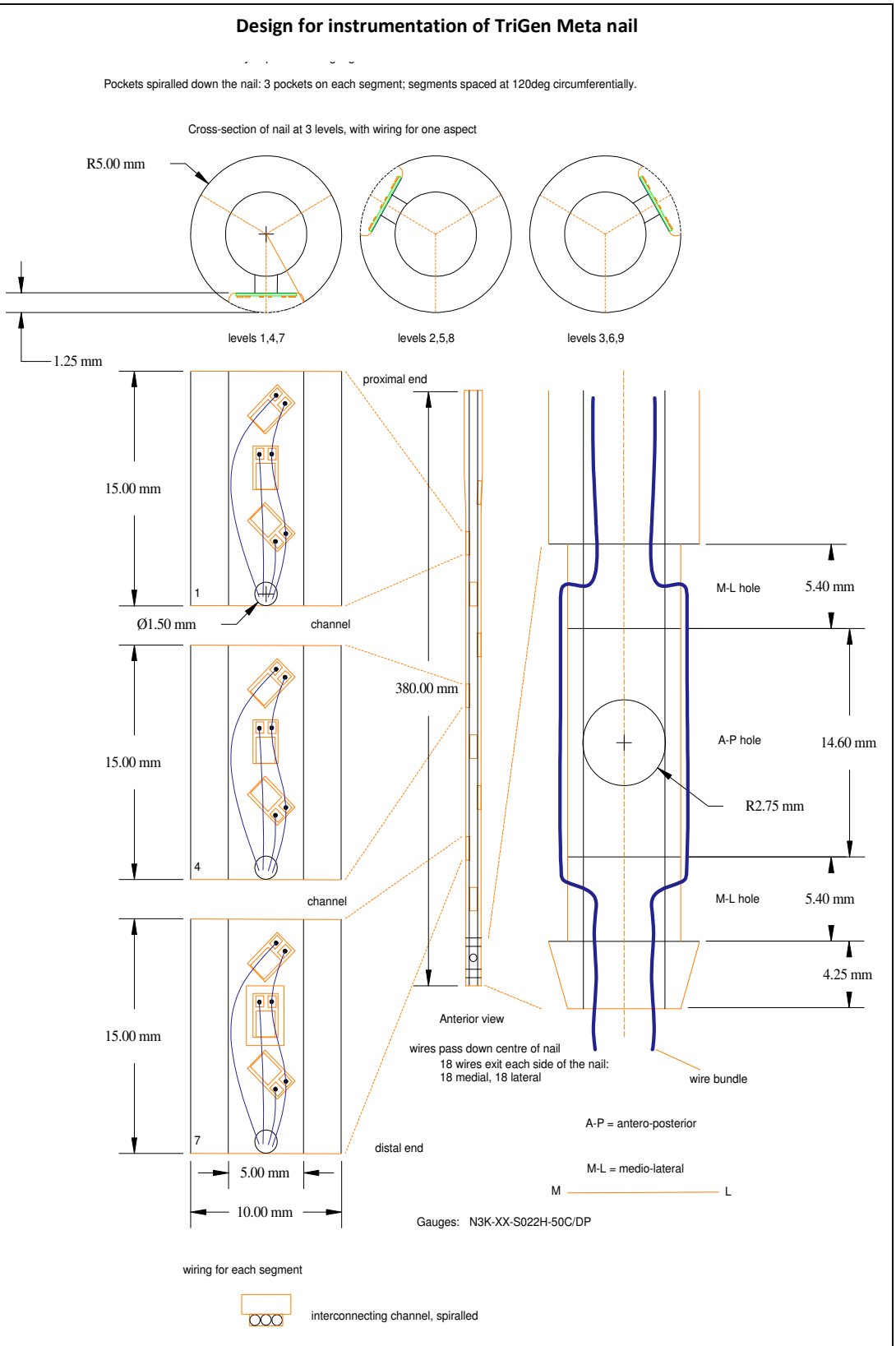

Figure 34: GEN I Instrumentation Design Schematic [8]

4.4.2 Bone callus composite application

The selected composites were used in the testing of the GEN I telemetrised intramedullary nail. Biomechanical testing of the nail was conducted for all required loading protocol using the simulated callus composite material. The composites were applied in two different forms to the fractured bone; circumferentially and in quadrants. Since there is no extensive literature that describes the geometry callus formation takes, the segmental geometry was decided upon based on a pilot study conducted by Wilson *et al.* [9].

But as there is no data to relate to the geometry callus formation takes in every single case and in order to see if there is any difference in the strain readings, it was decided that a change in the application of the artificial callus geometry to a circumferential application would help understand the variation of the sensitivity of the strain gauges between the two geometries. For the application of the different artificial callus, the steps taken in the making of the composite described above was taken. The only variation before application was that the callus mixture was allowed to thicken for a couple of hours before application as the fresh mixture had a low viscosity leading to potential settling of particulates/fibres. The composite material in both circumferential and segmental application were prepared following the same protocol, and allowed to dry for 24hrs at room temperature in a fume cupboard before testing.

Circumferential application method

Circumferential application of the composite material was achieved by applying the thickened mixture in a thin layer on all four anatomical planes at the same time. In order to ensure that the distribution of the thickened material does not settle in only one direction, the instrumented Sawbone® was allowed to rest for 15 minutes each on a separate anatomical plane. This was repeated for another an hour before it was allowed to rest until testing. The circumferential test was performed over 4 days.

Due to time limitation and restricted number of instrumented nails, the same instrumented Sawbone® had to be used for the segmental application tests. A rotary mini drill was used with a selection of burrs to remove the first layers of composite material before the segmental application of the callus mimic. Proper reduction of the fracture ensured that no composite material bled through the fracture reaching the nail. Figure 35 shows a schematic of the circumferential callus application technique used. Figure 36 below shows the four levels applied on the sawbone. The picture was taken 24 hours after the composite was allowed to dry and ready to be tested biomechanically.

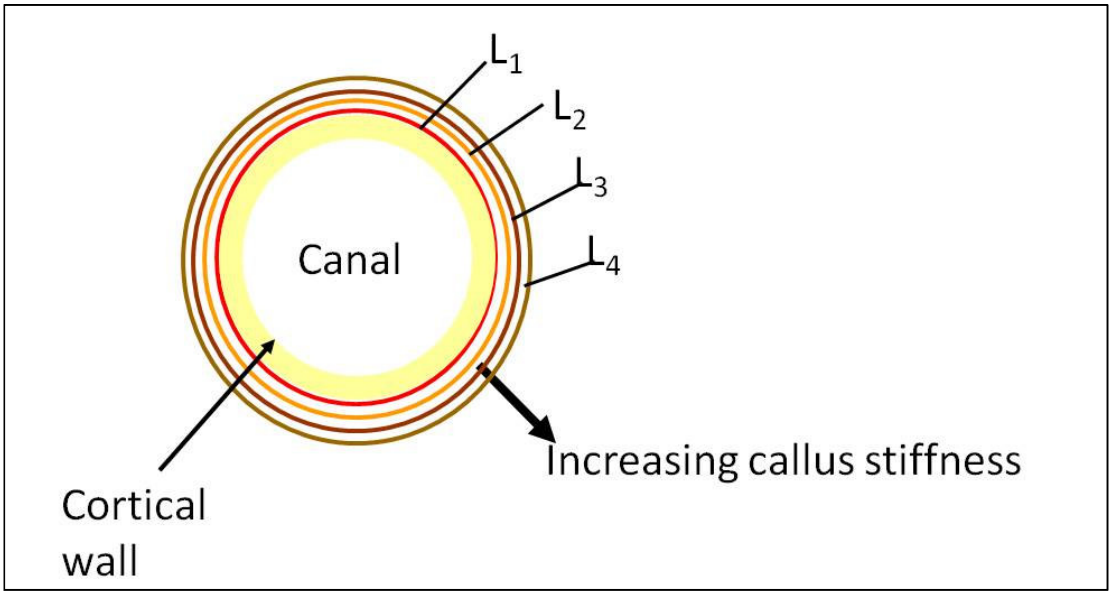

Figure 35: Circumferential callus application schematic

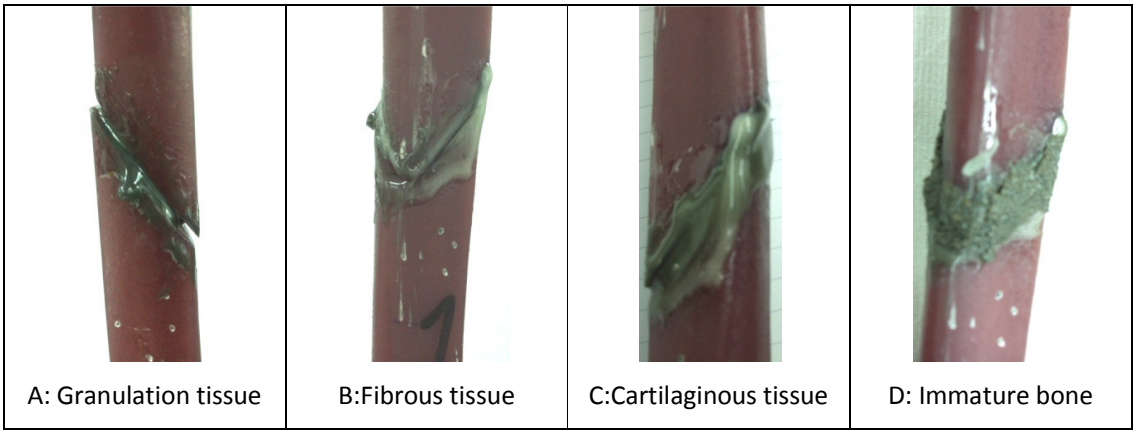

Figure 36: Circumferential application of the callus on the artificial bone

Segmental application method

In the case of the segmental application of the callus, based on the study by Wilson *et al.* [9], the composite mixtures were applied starting on the posterior side of the fracture, leading on to the medial, lateral and anterior position. Once the first layer was applied all round the fracture, the same process was applied for the second, third and fourth layer of composite callus material simulating the incremental tissue healing and mineralization. Figure 37 shows a schematic of the application of the callus material to simulate the segmental application method.

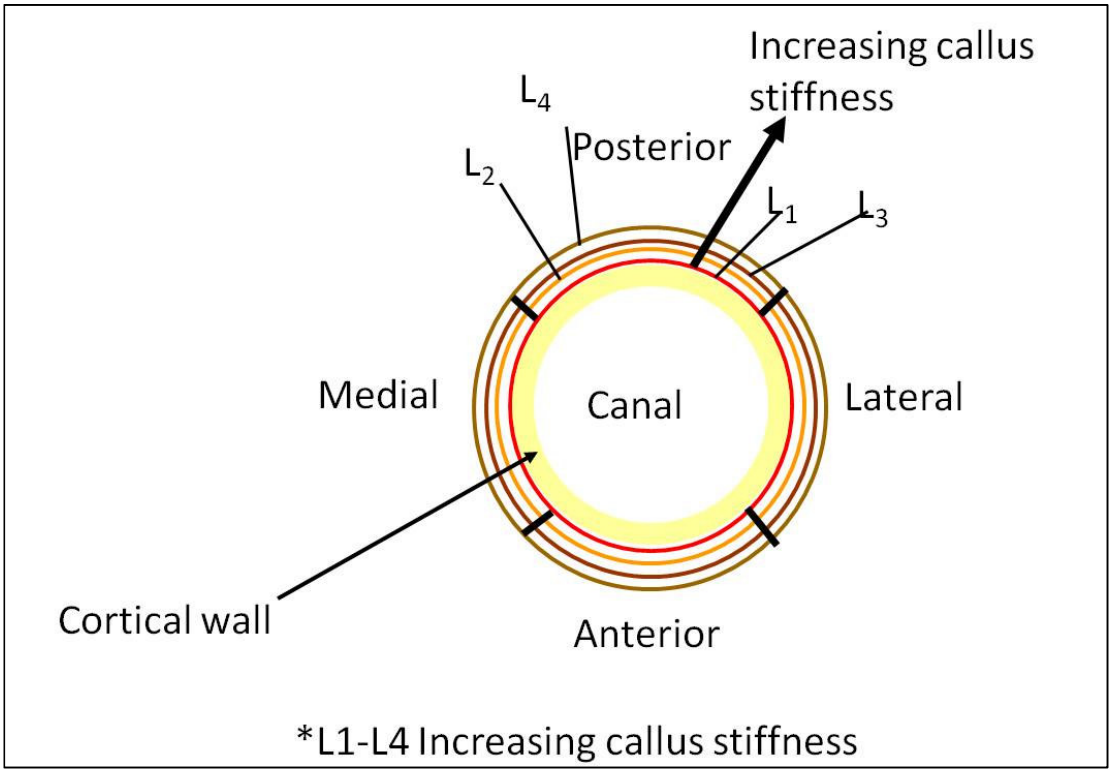

Figure 37: Segmental application of the callus material following Posterior, Medial, Lateral, Anterior (PMLA)

The results of both circumferential and segmental application of the artificial bone callus material are described in the next section.

4.4.3 Results and discussion

The results presented in this section will be according to the biomechanical test conducted, namely, compression testing, clockwise and anticlockwise torque, and 4 point bend test. The results will be presented starting from a fractured bone all through to L4 healing callus composite application. The fracture site created simulating a 42-A2 AO classification fracture was situated 140mm from the distal end of the bone. The strain gauges found nearest to the fracture sites are Gauges 4 and 5 as shown in the Figure 38 below. Gauges 1 and gauges 9 were the farthest from the fractured area hence understanding their sensitivity was crucial for the further development of GEN II onwards.

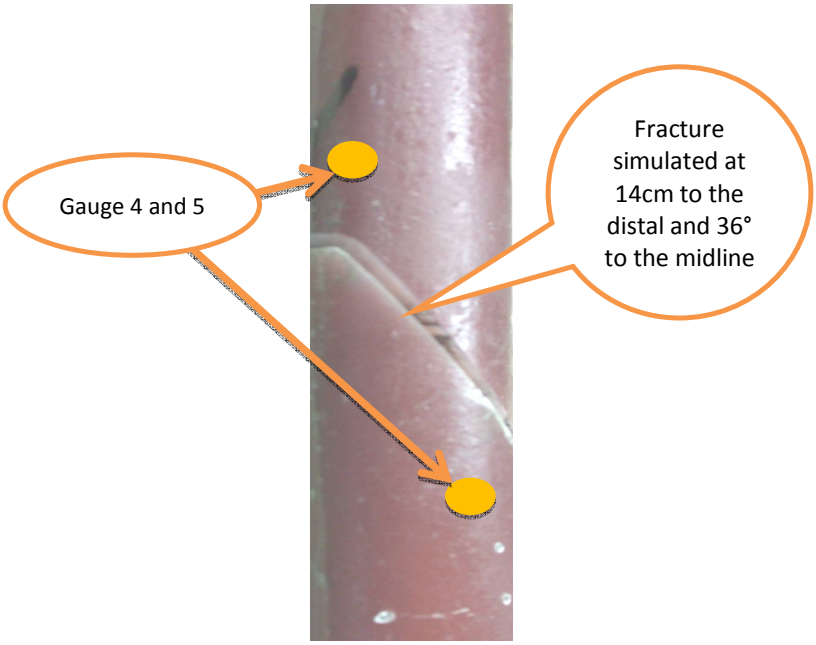

Figure 38 – Fracture site with indication to the two nearest strain gauges in GEN I

The biomechanical tests were conducted on the instrumented fractured Sawbone® before the application of the bone callus in segmental and circumferential application techniques. During both techniques, data was collected and processed as described above. The next sections will analyse the results of the segmental application and the circumferential application separately before discussing the strain gauge sensitivity for both and which one was the best technique to proceed further with instrumentation and design of GEN II IM nails.

4.4.4 Segmental application of callus composite results and discussion

The results for the segmental application of the callus will be analysed and discussed as per the biomechanical test protocol. Starting with the compression tests, the discussions will be followed by the torque testing at 0N and 1000N in compression and concluding with the 4-point bend test across the fractured area.

4.4.4.1 Compression testing

Compression testing was conducted while the instrumented bone was secured attached to the aluminium frame simulating a single legged stance. The load was applied incrementally by 50N starting from 0N up to a 1000N. The data was logged and processed as described above in Section 4.4.1. The data was graphically represented by plotting microstrain (µstrain) against load (N) for each gauge. Figure 39 on page 112 shows a graphical representation of compression loading of GEN I for all the gauges on the fractured Sawbone®. Most gauges registered a strain ranging from approximately 1750 and 2500 microstrain at 0N. As the load was applied, the gauges registered a change in strain varying from 500 to slightly above 4000 microstrain. The change in strain

registered per gauge is dependent on the orientation of the gauge. During axial compression bending simulating a single legged stance, both tension and compression would be observed. As the load applied increased on the fractured bone, the strain increased.

L1 callus composite was applied straight after the whole set of biomechanical tests were carried out. Starting on the posterior side, a thin layer of L1 was applied as per the protocol described in Section 4.4.2. The set of biomechanical tests were carried out 24hr after before the next segmental application on the medial side. The application followed a pattern which is referred as Posterior, Medial, Lateral and Anterior – PMLA before L2 was applied in the same pattern as well as L3 and L4.

Figure 40 (page 112) shows the graphical representation of the compression loading of GEN I for all the gauges after the application of the Posterior L1 callus composite followed by Anterior L4, Figure 41 (page 113). The graphical representation of the readings for the application of the callus in between can be found in Appendix D. As it can be observed from Figure 39-41 the volume of data generated by the strain gauges meant that further processing had to be conducted in order to quantitatively analyse the results. The plotted graphs were used to generate the gradients which resulted in further graphical representation of N $\mu strain^{-1}$ against the callus growth over time. The results presented for GEN I in this thesis focused on the gauges nearest to the fracture site, the most proximal set of gauges and the most distal set.

Figure 42 (page 113) shows the graphical representation of the Gauge 4A and 5B of the axial loading against the simulated callus level (see Table 6 on page 95) in segmental (S) application as denoted on the graph. Gauges 4 and 5 has been represented here as they are the closest to the fractured area as well as the A and B oriented gauges have been observed to show more sensitivity to the fracture healing simulation. 5B shows there is a decrease as healing occurs while 4A gauge registered a decrease but lesser than 5B.

The positioning of 4A refers to the strain gauge positioned at +45° to the axis of the nail on the anterior side. When the axial compression load is applied, the entry point of the load is on the medial side of the bone. The position is also proximal to the fracture site. The model represented a completely reduced fractured bone with an internal fixation device. At this point in time, the percentage of the implant load is very high. The hypothesis states that as healing is simulated, the percentage load will shift from the nail to the bone. Figure 42 on page 113 shows the gradual decrease in the implant strain as healing is simulated segmentally. 5B is positioned at 0° to the nail axis on the medial side nearest distally to the fracture site. With the load applied on the medial side of the nail, 5B is directly in line with the loading of the nail hence experiencing higher compressive strains.

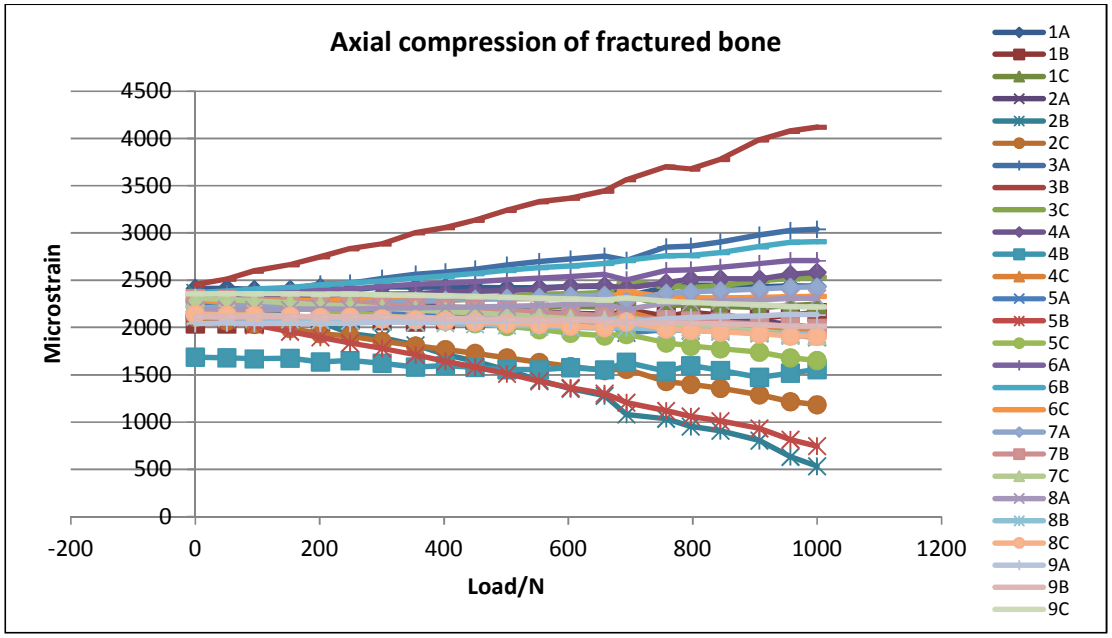

Figure 39 – Axial compression graph showing measurement from all the strain gauges in the fractured bone as it is loaded from 0N to 1000N

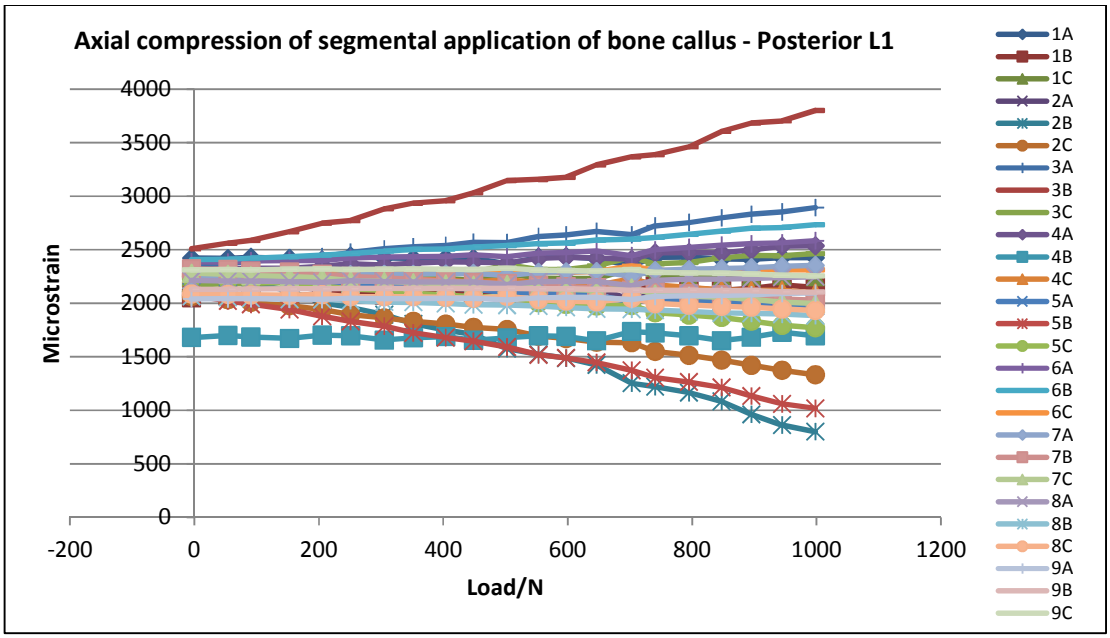

Figure 40 – Axial compression graph showing measurement from all gauges after the application of the first level of synthetic bone mimic simulating granulation tissue on the posterior side

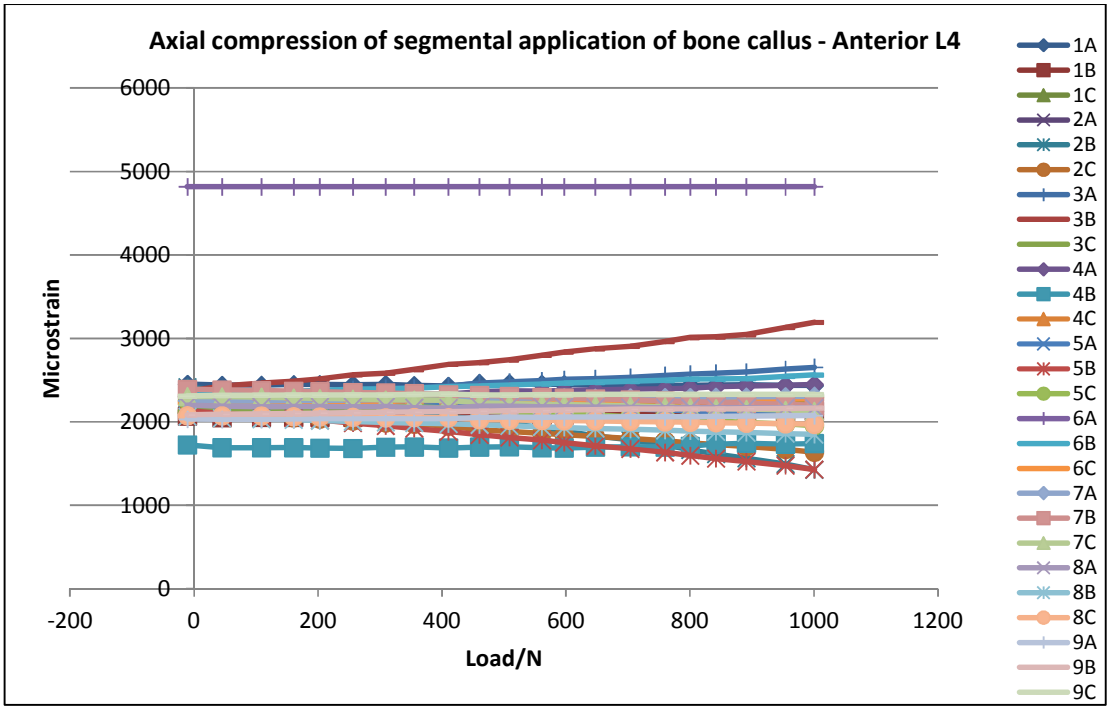

Figure 41 – Graph illustrating the axial compression loading of all the gauges after the application of the last layer of callus mimic simulating immature bone of the segmental method on the anterior side

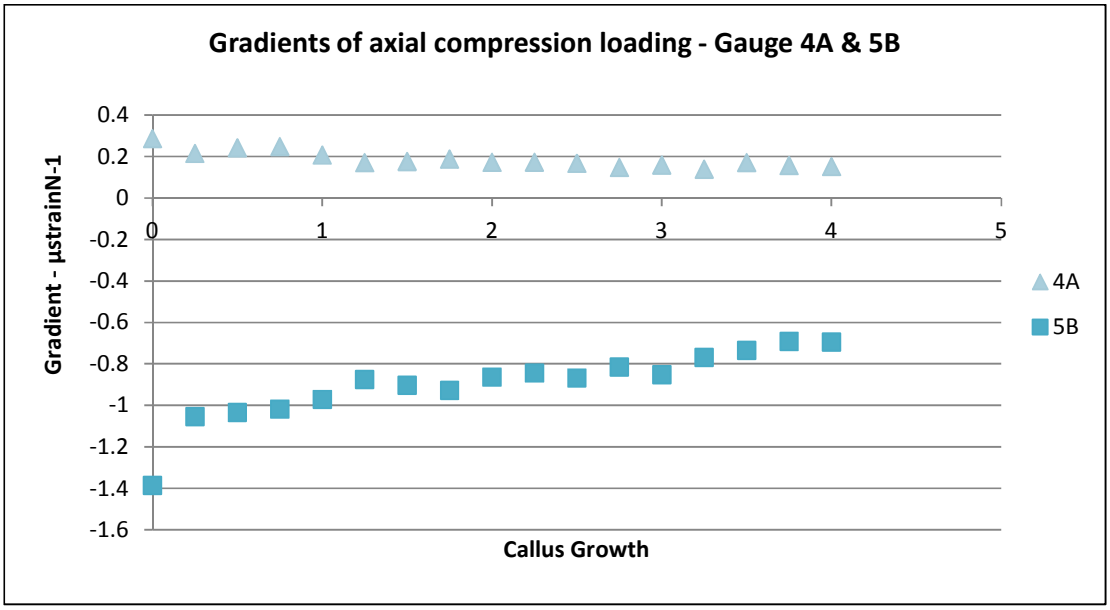

Figure 42 – Graph illustrating the gradient of gauges 4A and 5B over the axial compression loading from 0N to 1000N

Figure 43, 44, 45 shows the gradient of the axial compression testing for gauges 1, 4, 5 and 9 A, B and C respectively. As a reminder, A, B and C denotes the orientation of the gauges from the longitudinal axis of the nail. With the load applied travelling on the medial side of the nail, some gauges experience compression while others tension. This is illustrated in the graphs of Figure 43, 44 and 45. As the callus growth is applied, either an increase or a decrease of strain per load is

observed. The observations from gauge 5 from Figure 43-45 shows the gauge in compression with high compressive strains and as the healing is simulated the strain decreases. Gauges 1, 4 and 9 however show tensile strain. This is the result of loading on the medial side as gauges 1, 4 and 9 are found on the anterior and posterior side.

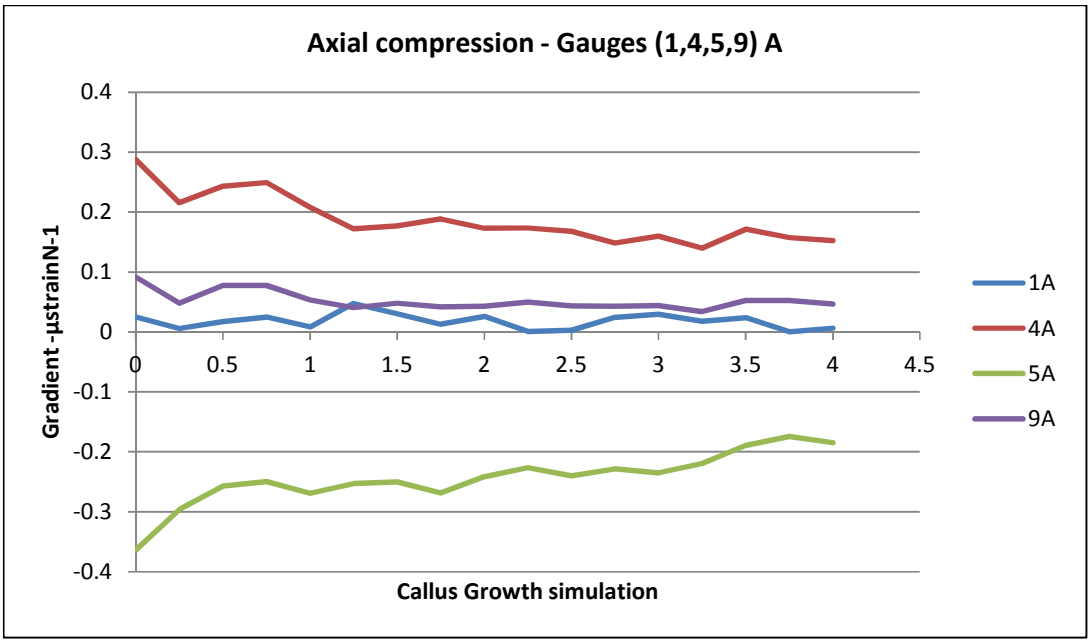

Figure 43 – Graph illustrating the strain change in the gradient of Gauges (1,4,5,9) A in the segmental application of synthetic callus

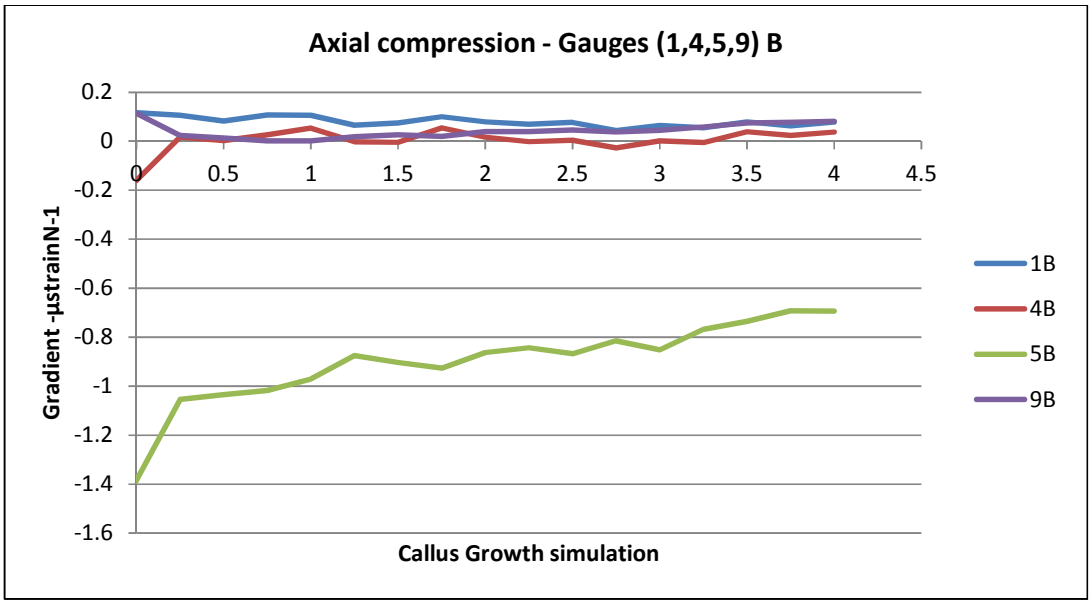

Figure 44– Graph illustrating the strain change in the gradient of Gauges (1,4,5,9) B for segmental callus application

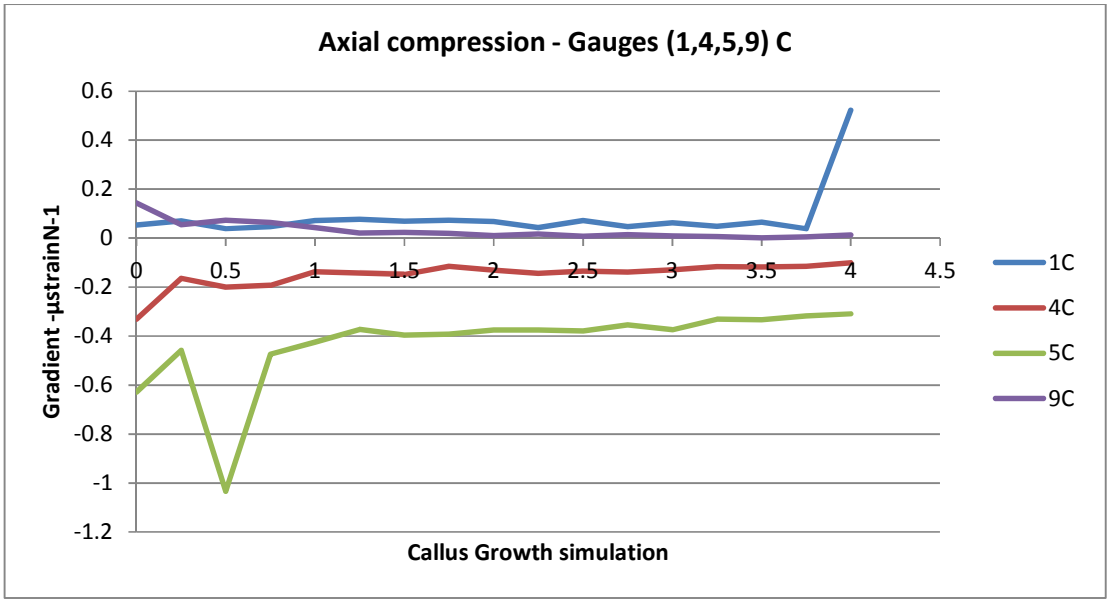

Figure 45– Graph illustrating the strain change in the gradient of Gauges (1,4,5,9) C for segmental callus application

5C in Figure 45 shows an increase in the compressive strains after the application of L2 callus. This could be due to the elastic properties of the callus synthetic material however if this was the case, similar trend would be observed from the other gauges. The loads applied were not kept at a constant rate for a long period of time for this type of behaviour to develop. The time taken between loading and taking a measurement was not more than 15 seconds. Consequently the sudden increase in the compressive strains, despite being in line with the applied load, can also be associated with instrumental error. Instrumental error in the system can also be observed from Figure 41 on page 113 regarding gauge 6A which had ceased to work hence showing a straight horizontal line at around 4800 microstrain.

4.4.4.2 Torque testing

Torque testing was conducted as described in Section 4.3.4. The torque was carried out to simulate internal and external rotation at three specific axial compressions load, namely 0N, 500N and 1000N. Because of the sheer amount of data generated, only internal torque at 0N and 1000N axial load will be presented. Starting 0N, the Figure 46 shows the internal torque readings of the fractured tibia. The strain measurements at 0Nm varied between 1750 and 2500 microstrain. At 5Nm, the strain changes varied from 1500 to approximately 3200 microstrain. Both tension and compression forces are observed in on Figure 46.

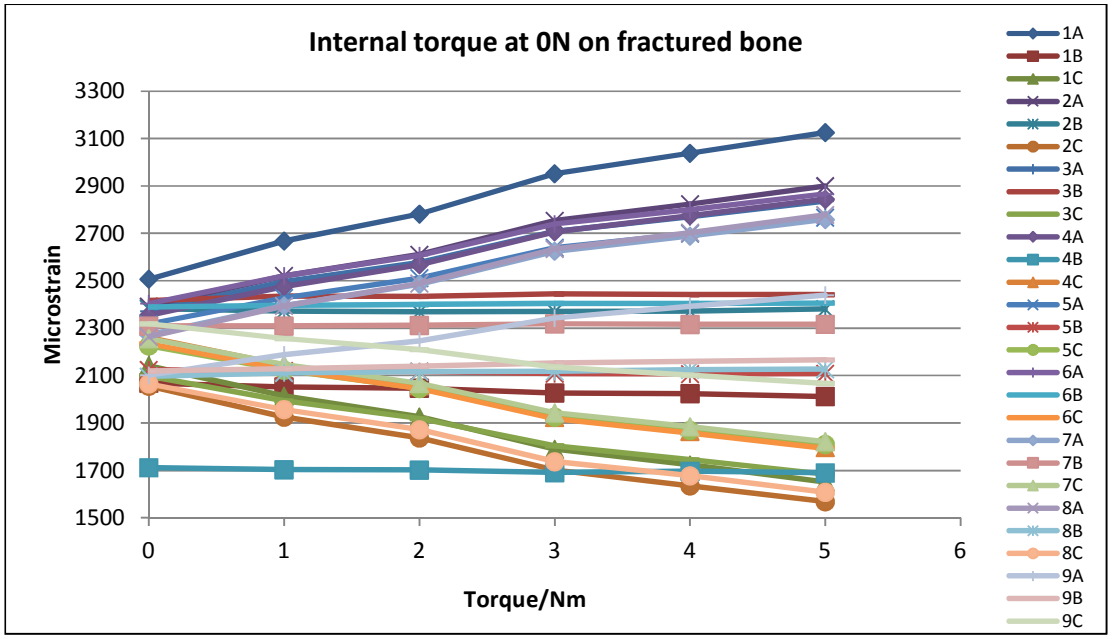

Figure 46 – Graph illustrating internal torque at 0N in compression

Figure 47 to 49 show the results of applied internal torque plotted as the calculated gradient for all the gauges from fractured through to the simulation of healed bone against the callus growth timeline.

It is quite clear from Figure 47 gauges A (oriented at +45 °) at all four positions that there is a gradual decrease as the fracture heals. Gauges A at all four sites were experiencing tensile strains during the application of internal torque and as the callus was applied segmentally, the decrease can be observed. Similar observations can be made on Figure 49 where the strain gauges are oriented at -45°, tensile strains are seen decreasing consistently from fractured bone to healed using the segmental application method. However, the observations for Figure 48 show very low strains from fractured to immature bone simulation for gauges positioned at 0°. A spike in the strains can be observed after the application of L3 simulating cartilaginous tissue. This sudden change is more likely to be associated with instrumental error as previously seen in Figure 45 for the axial compression loading.

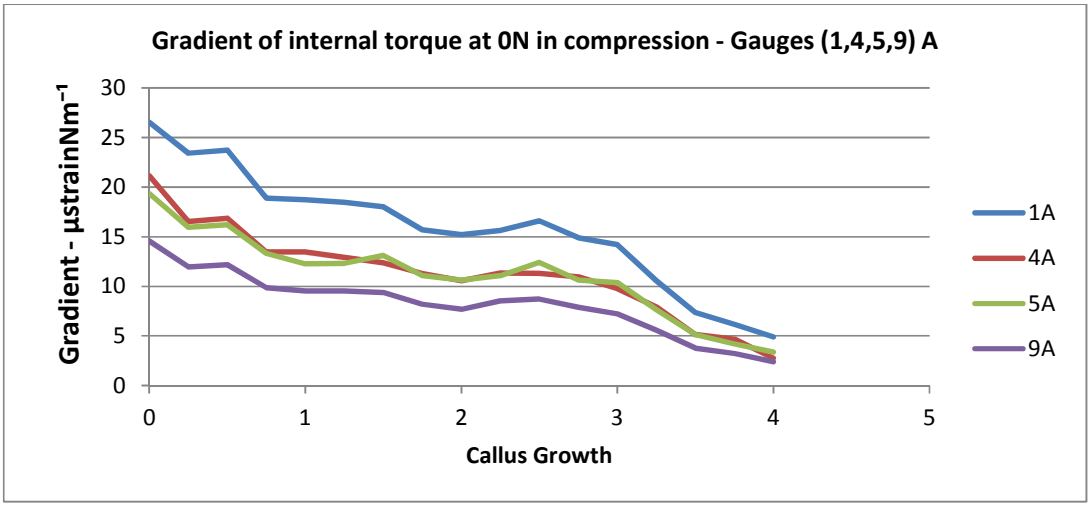

Figure 47 – Graph illustrating the internal torque at 0N in compression for the four gauges

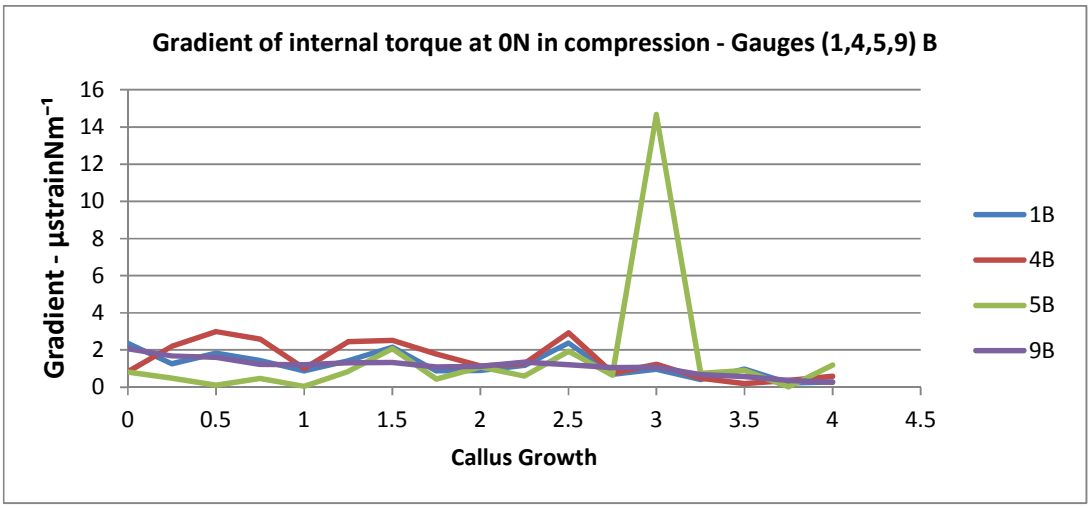

Figure 48- Graph illustrating the internal torque at 0N in compression for gauges 1,4,5,9

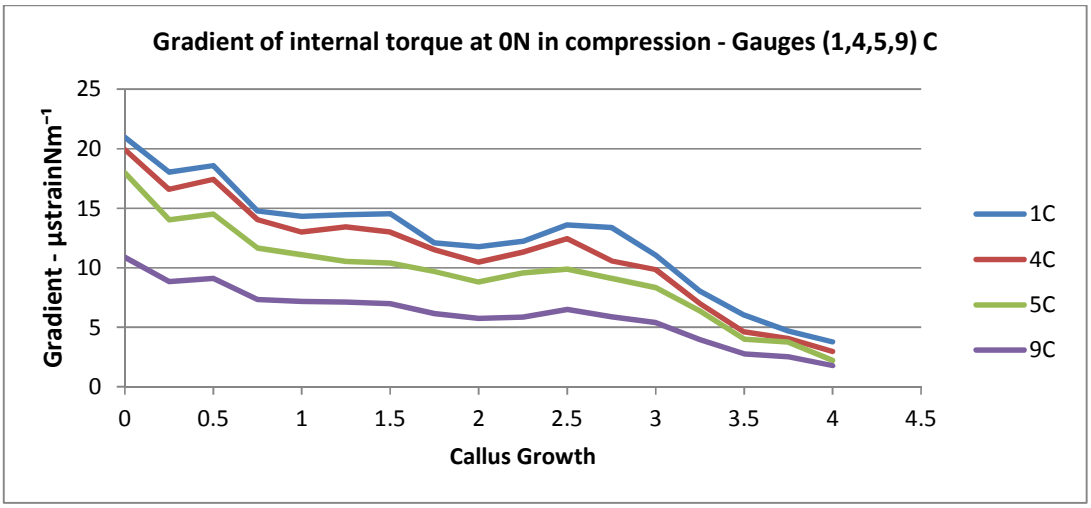

Figure 49 – Graph illustrating the internal torque at 0N in compression for gauges 1,4,5,9

Figure 50-52 shows the gradient of the internal torque at 1000N in compression for gauges 1, 4, 5 and 9. Since the original set of data is very condensed, the graphs are shown in Appendix D. The gradient graphs show the change in strain for the above mentioned gauges over the time of simulated healing. Figure 50-52 shows the gauge (1, 4, 5, 9) A and C oriented at +45° and -45° to the axis of the nail respectively. A gradual decrease in strain is observed over time as the fracture heals. This is consistent with previous results seen above for the application of the torsional force at 0N in compression. Tensile strains are observed on the graphs of internal torque in compression at 1000N for all three gauge positions (A,B,C).

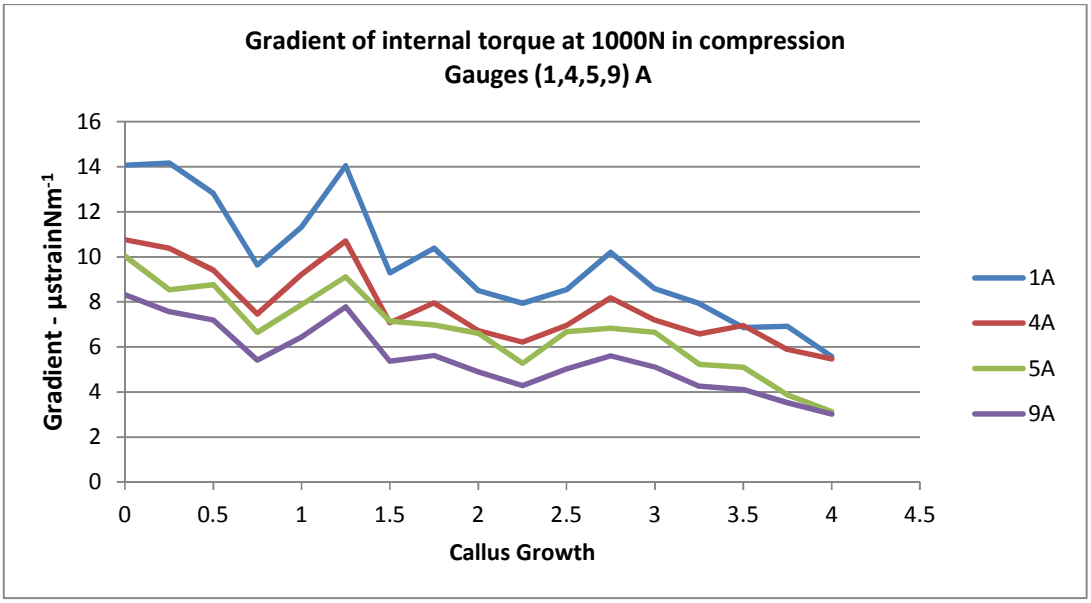

Figure 50 – Graph illustrating the gradient of the internal torque during loading at 1000N in compression

Figure 51 (page 119) shows an anomalous spike for gauge 4B which in terms of the timeline seems around the callus growth mark 2.75. Unlike the previous spikes seen in the result, this particular one seems to keep consistent through the other gauges from Figure 50 and 52. The distribution Figure 51 is not very consistent which seems to suggest that there may be some instrumental error. However, it is highly likely that without the instrumental error, the results at gauge B could follow the same trend as A and C. The tensile strain observed in Figure 50 and 52 show a gradual decrease however there are specific points where there is an increase in the strain before it decreases again. This could be due to the callus material deforming under 1000N in compression from the medial site while simultaneously having an internal torque of 5Nm applied to it. The results from the internal torque under 0N compression and 1000N compression shows that if this was replicated *in-vivo* there would be an obvious change in strain depending on the compression bending the bone is under. While the bone is under compressive load, the readings

seem to suggest that the 5Nm torque is powerful enough to register tensile strain in the opposite direction.

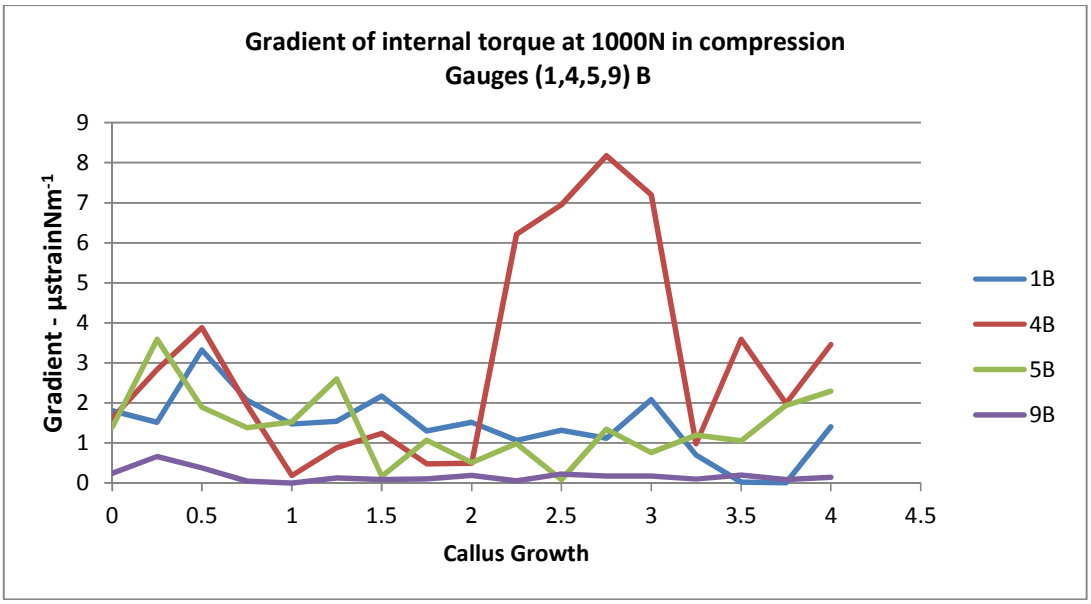

Figure 51: Graph illustrating the gradient of the internal torque during loading at 1000N in compression for gauges B

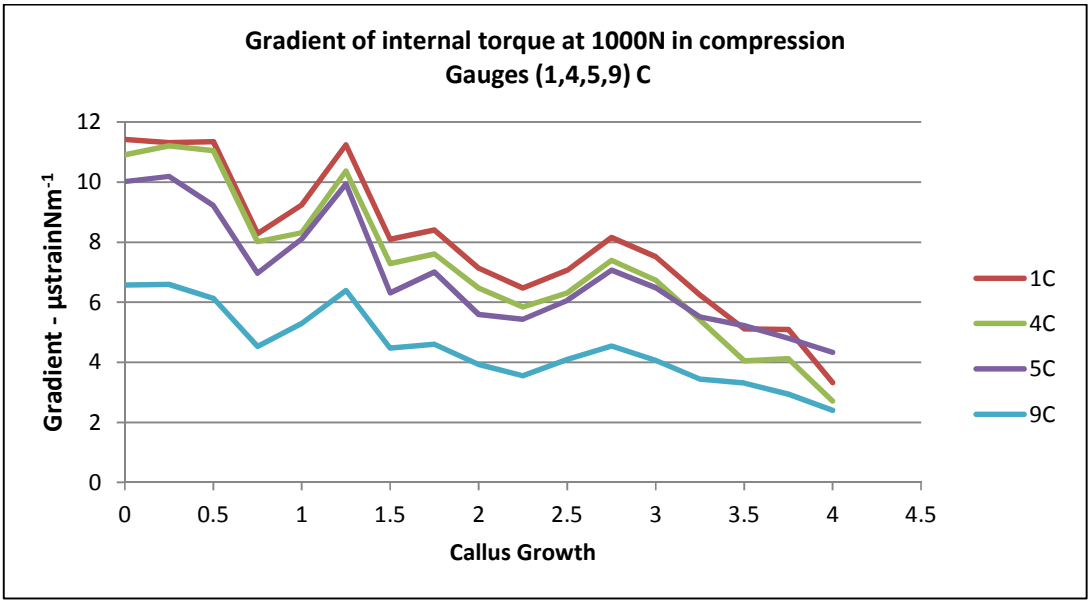

Figure 52: Graph illustrating the gradient of the internal torque during loading at 1000N in compression for gauges C

4.4.4.3 Four point bend test

The four point bend test was conducted on a custom made set up using retort stands and a custom-made ring for the load application. The load was applied directly at the fracture site with the bone anterior surface in the upward direction (see Figure 32 Page 104) and the recorded data was processed and calculated as described for the other biomechanical testing. A maximum of 100N was applied with a steady increment of 10N starting with an initial 5N. The results were

plotted similarly and Figure 53 shows the initial observations taken of the fractured bone. On the fractured bone, the strain readings initialised between 1600 and 2500 µstrains and the readings varied between 1000 and 2750 µstrains at 100N. The gradients of all the plotted data (see Appendix D) was calculated and plotted for gauges (1, 4, 5, 9) A, B and C.

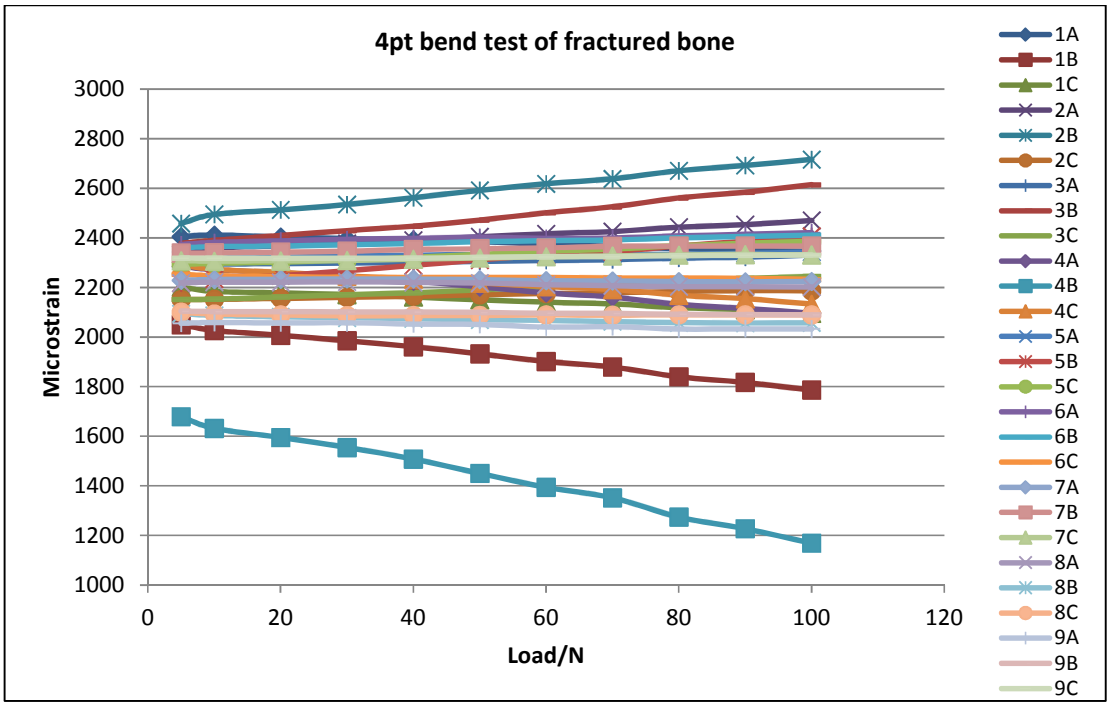

Figure 53 – Graph illustrating the loading of the fractured bone up to 100N on a 4pt bend test

Figure 54 – 56 show the gradient of gauges 1, 4, 5 and 9 (A, B, C) for the four point bend test with the segmental application of the callus growth. Throughout the three graphs, there is a consistency in the trend of the tensile strain observed as well as the drops and spikes at specific points along the callus growth timeline. Since the bone was positioned clamped with the anterior side facing up and the load was applied across the fracture site, gauge 1 and 4 (A, B and C) positioned on the anterior side has the highest tensile strain observed. This is consistent with the mechanics of the experiment with the medial and lateral side experiencing much lower strain readings as shown in Figure 54-56. The directionality of the gauges (+45°, 0° and -45°) does not really show any more of the behaviour experienced during the four point bend test. However, the decrease in strain as the fracture heals can be observed as previously suggested in the hypothesis. This leads to the end of the biomechanical testing with the application of the synthetic callus using the segmental method. The next section will analyse the results of the same loading protocol for the circumferential application method.

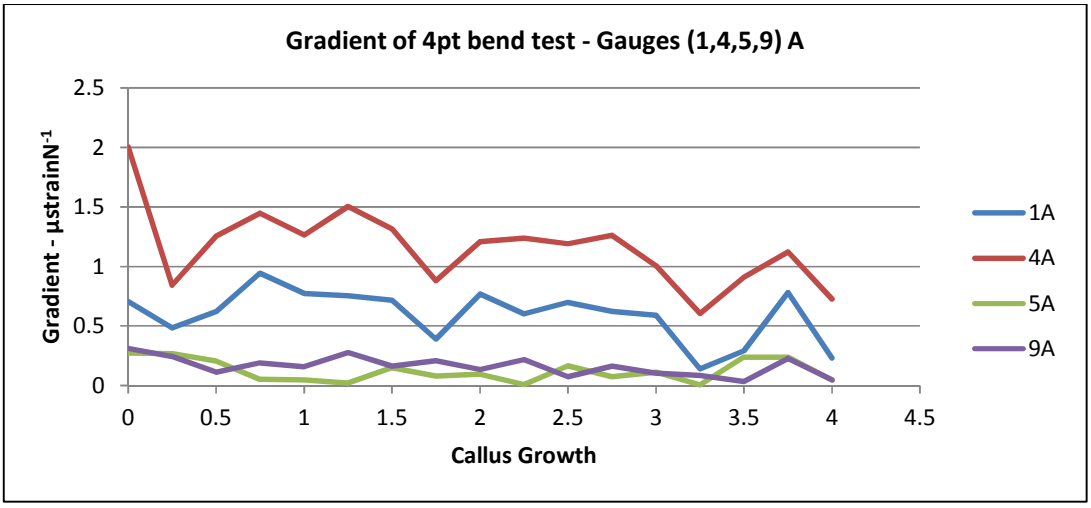

Figure 54 – Gradient of gauges 1,4,5,9 A in a four point bend test

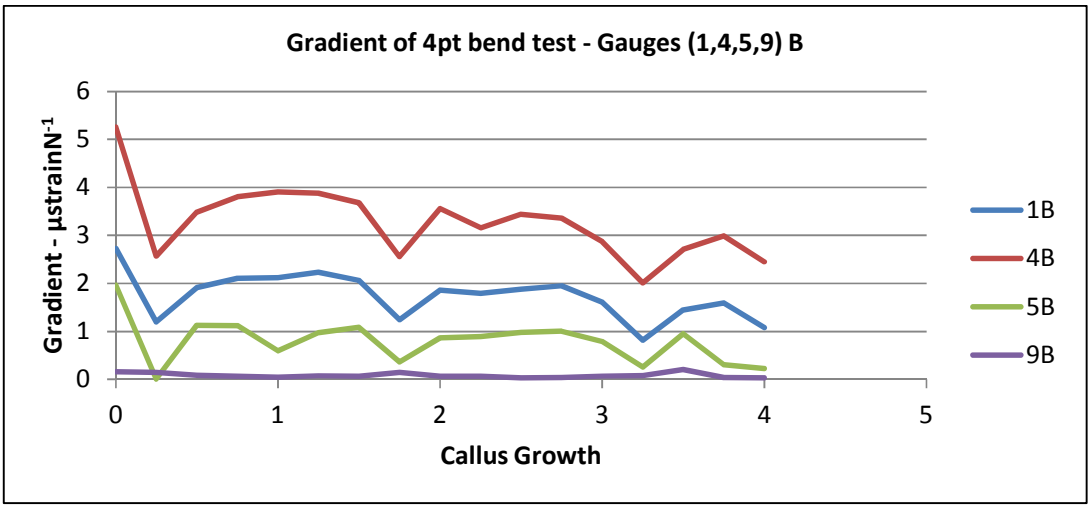

Figure 55- Four point bend test gradient for the gauges 1,4,5,9 B

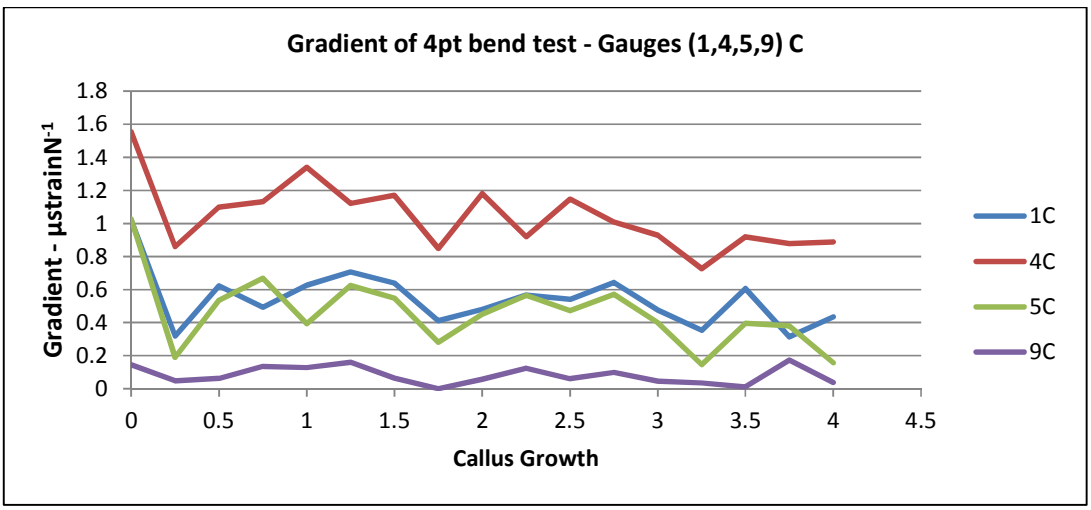

Figure 56 – Four point bend test gradient for the gauges 1,4,5,9 C

4.4.5 Circumferential application of callus composite results and discussion

After the completion of the biomechanical tests for the segmental application of the callus composite layers, a small rotary drill was used to remove the composite material layers with care from the surface of the Sawbone®. Once the material removed, the artificial bone was placed back in the aluminium frame and a new baseline set of data was recorded for the biomechanical tests. This was to ensure that in case there is any material residue across the fracture site but the probability of callus composite seeping through the microscopic gap once the fracture is reduced is very unlikely. After baseline testing, the circumferential application of the callus composites protocol described in section 4.4.2.

4.4.5.1 Compression testing

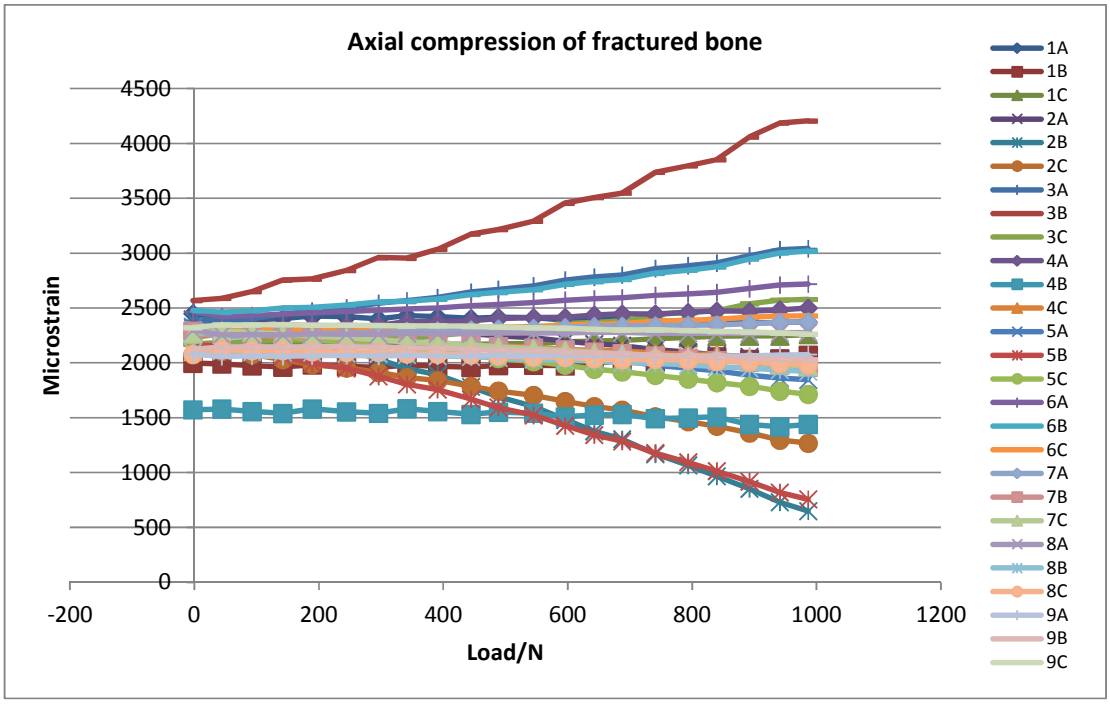

Figure 57: Graph illustrating the axial compression loading from 0N to 1000N of the fractured bone after the removal of the callus composites from the segmental application method

Figure 57 shows the baseline axial compression loading of the fractured bone after the removal of the synthetic callus used in the segmental application method. The strain measured range from approximately 500µstrain to 4250µstrain. This is consistent with the strain measurement taken before the segmental application as seen in Figure 39 (page 112).

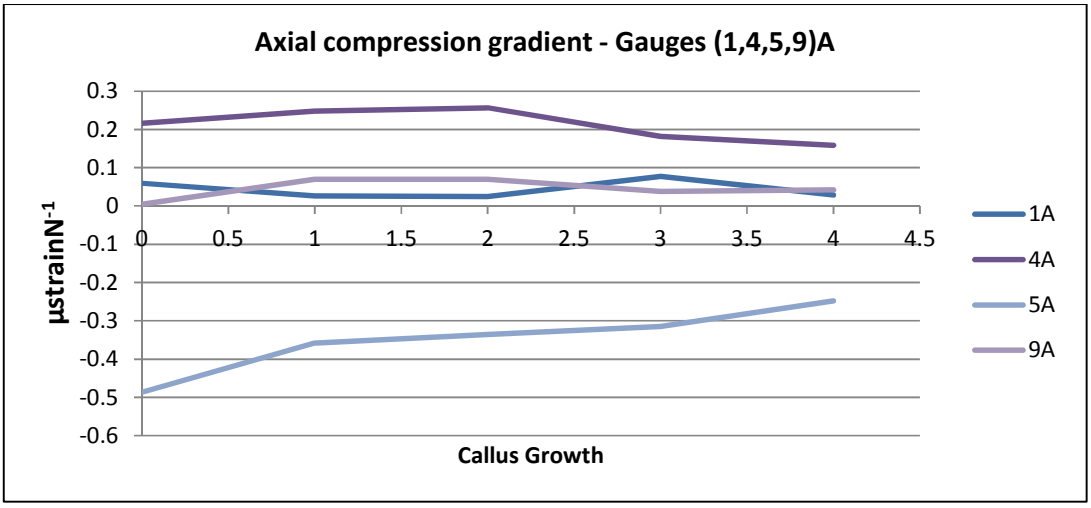

Figure 58 – Axial compression gradient as callus growth increases for gauges 1,4,5,9 A

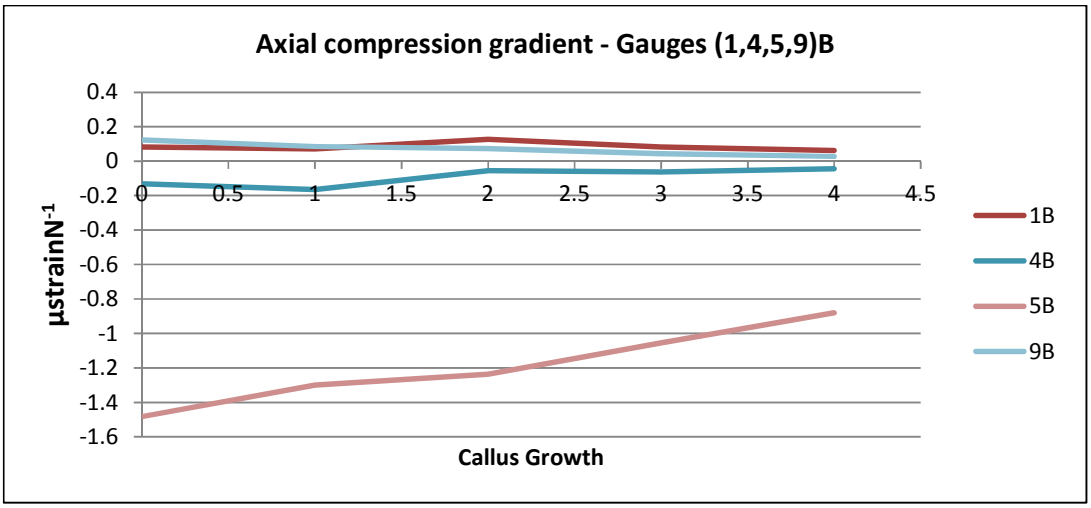

Figure 59 – Graph illustrating the axial compression gradient of gauges 1,4,5,9 B as healing progresses for the circumferential method

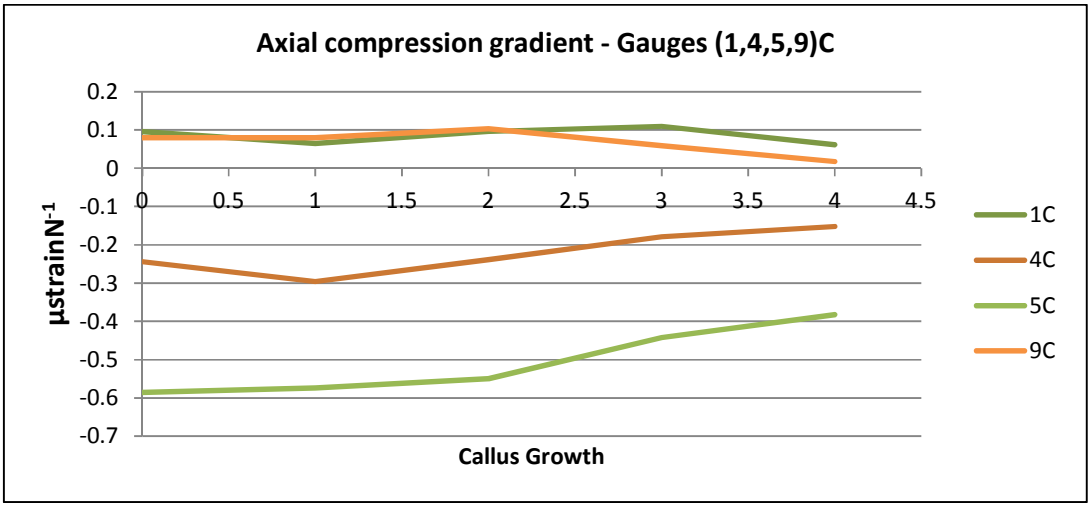

Figure 60 – Graph showing the axial compression gradient of gauges 1,4,5,9 C during loading as healing progresses

Figure 57-60 shows the gradient of the axial compression test over the circumferential application of the simulated healing process. As it can be observed from Figure 58, gauges 1A and 9A which are the farthest away from the fracture site registers the smallest change in strain per load as healing is simulated. The high compressive strains observed in gauges 5 are consistent across the three graphs in all the directions (+45°,0°,-45°). Gauge 5 is found on the medial side of the nail and is bound to have the highest compressive strains as the axial compression loading is medially offset, this is consistent with the mechanics the system. Gauges 1 and 9 are shown to experience tensile forces. This is consistent with their positions being on the anterior and lateral side as well as the direction of the forces applied. Regardless of the callus application process which is replicating the way healing occurs, the result is consistent with the axial compression from the segmental application within the limits of experimental errors.

4.4.5.2 Torque testing

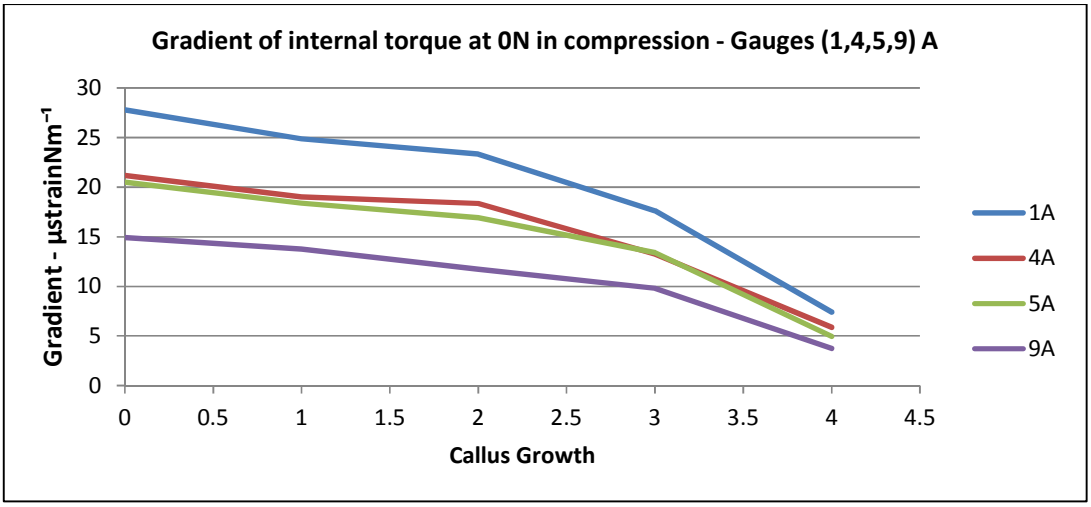

Figure 61 – Graph illustrating the gradient of the internal torque at 0N in compression for gauges 1,4,5,9 A

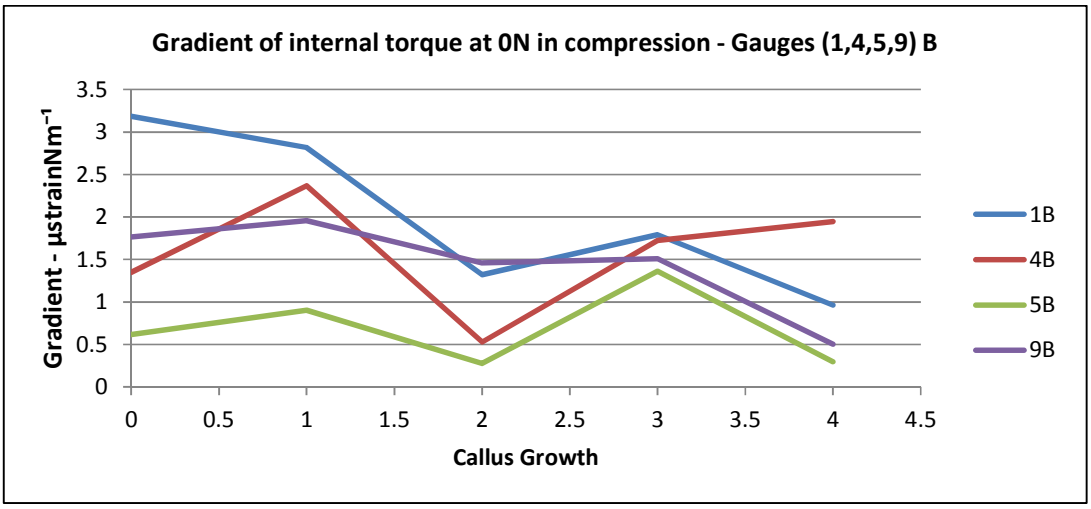

Figure 62-Graph illustrating the gradient of the internal torque at 0N in compression for gauges 1,4,5,9 B

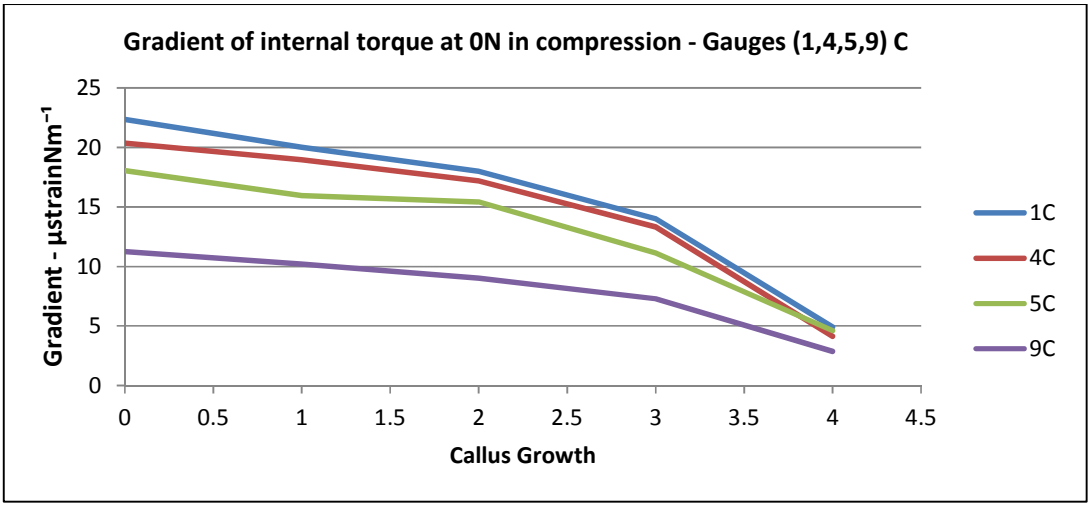

Figure 63- Graph illustrating the internal torque gradient at 0N in axial compression for gauges 1,4,5,9 C while simulating fracture healing

Internal torque at 0N in compression loading was conducted as per the loading protocol. Graphs of strain against load were plotted for each test and after each callus composite application. The gradients were calculated and plotted. Figure 61-63 shows the gradients over the callus healing timeline for the gauges nearest to the fracture site (4 and 5) and gauges at the proximal and distal ends (1 and 9). The gradients in Figure 61 and 63 show a gradual decrease that is recorded of the strain over time. These gauges show consistency in the tensile strain observed as an internal torque of up to 5Nm is applied. However, Figure 62 which represents the strain gauges at 0° does not have the same trend. Tensile strains are present however there seems to be some changes in the material behaviour which may be settling causing the dips and spikes. Bearing in mind that the application of the circumferential callus method suggests that at that same point in time more callus material is applied compared to the segmental application method.

The next set of Figures 64-66 (page126) shows the gradient of the internal torque at 1000N in compression for gauges at the proximal and distal as well as the gauges on the sides of the fracture site. Figure 64 and 66 is very similar to Figure 61 and 63 observing a decrease in strain as the torsional loads are applied during the fracture healing simulation. Figure 65 also show a decrease in the tensile strain observed however gauge 4B shows a drop to nearly zero after the application of the second level of callus material and the strain increases again for level 3. This could potentially be associated with instrumental error. Gauge 9B yields very limited activity in Figure 65. Hardly any change is recorded at the most distal gauge in the 0° orientation to the nail axis as the loads are applied.

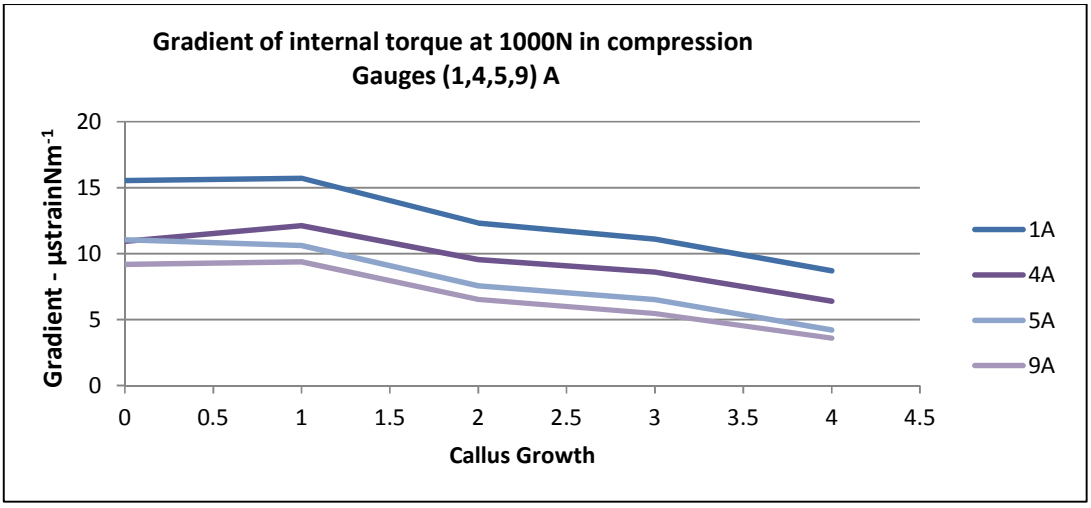

Figure 64 – Graph illustrating the gradient of internal torque at 1000N in compression for gauges 1,4,5,9 A

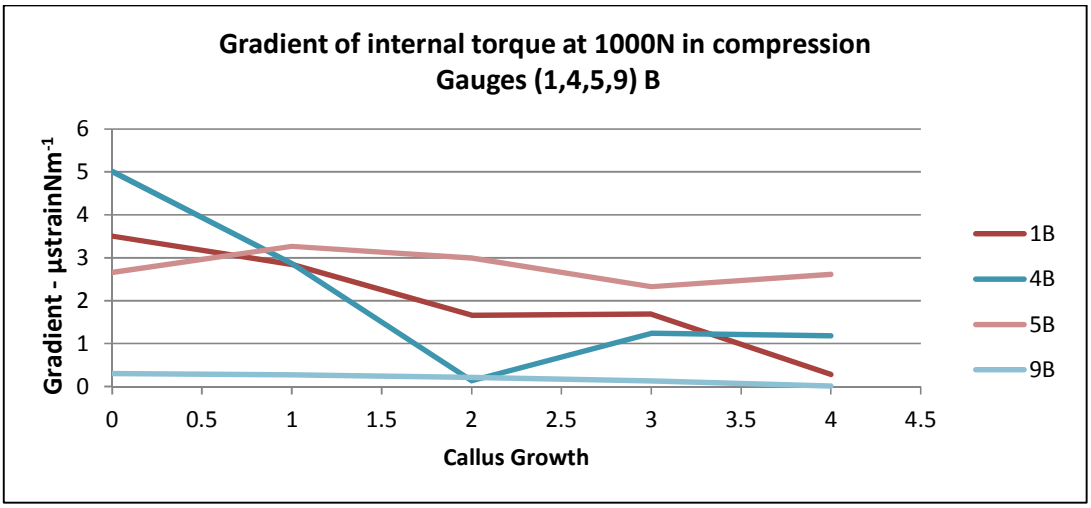

Figure 65- Graph illustrating the gradient of internal torque loading at 1000N in compression for gauges 1,4,5,9 B

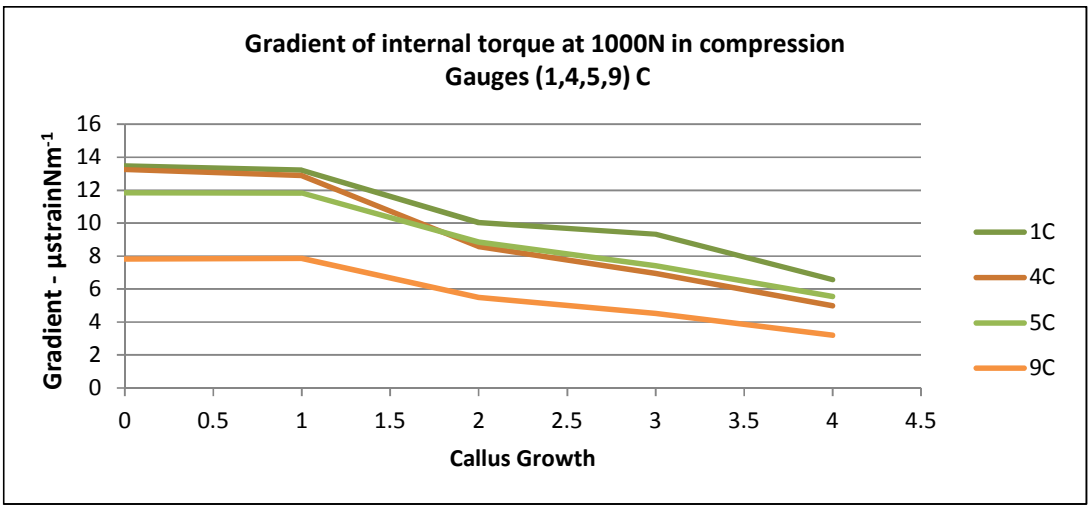

Figure 66- Graph illustrating the gradient of the internal torque at 1000N in compression for gauges 1,4,5,9 C

4.4.5.3 Four point bend test

The four point bend test was performed as per the experimental protocol described. The results have been graphically represented and gradients were calculated. All the gradients during the callus healing application regime were plotted and have been graphically represented on Figures 67-69 for the most proximal and distal gauge as well as the gauges on either side of the fracture site. All three graphs show a gradual decrease as the callus healing composite is applied.

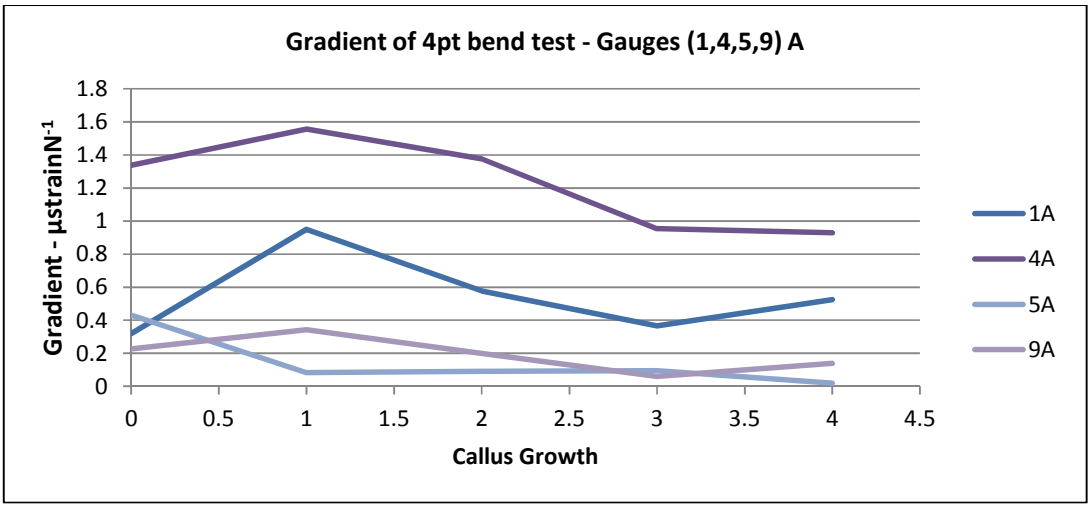

Figure 67- Graph illustrating the gradient of gauges 1,4,5,9 A during the four point bend test loading against callus growth

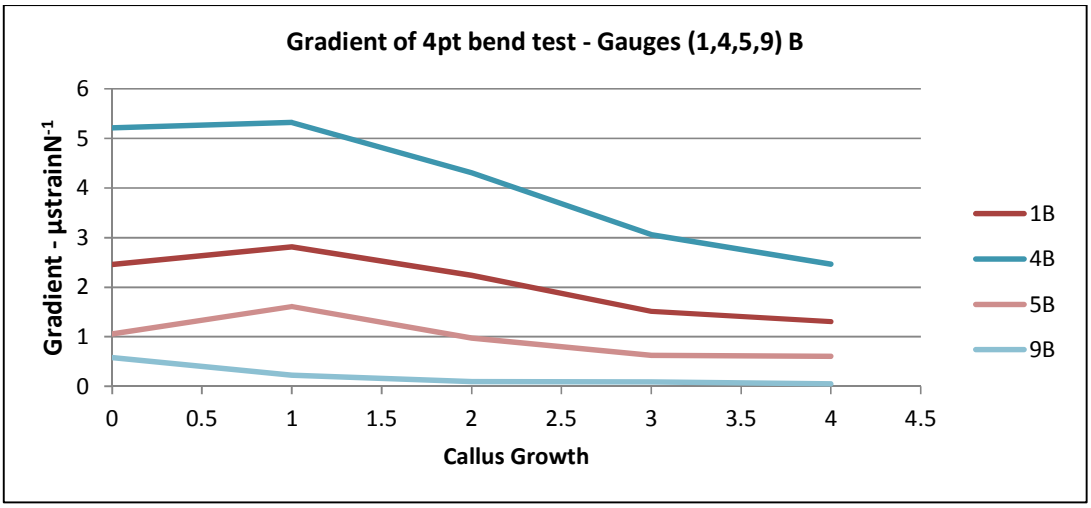

Figure 68- Gradient of gauges 1,4,5,9 B against the callus growth during four point bend test loading

Figure 67 -69 shows tensile strains present during the 4-point bend test. Gauges 1 and 4 are positioned on the anterior surface of the nail and facing upwards during the testing show consistency in decreasing tensile strain. Gauges 1A and 1C however both seems to have low tensile strain in the fractured bone, increasing strain after the application of the first callus level and then leading to decreasing tensile strain as healing is simulated. This could potentially be due

to the positioning of the gauges in +45° and -45° as the 0° oriented gauge in Figure 68 seems to have a smoother strain trend as load was applied.

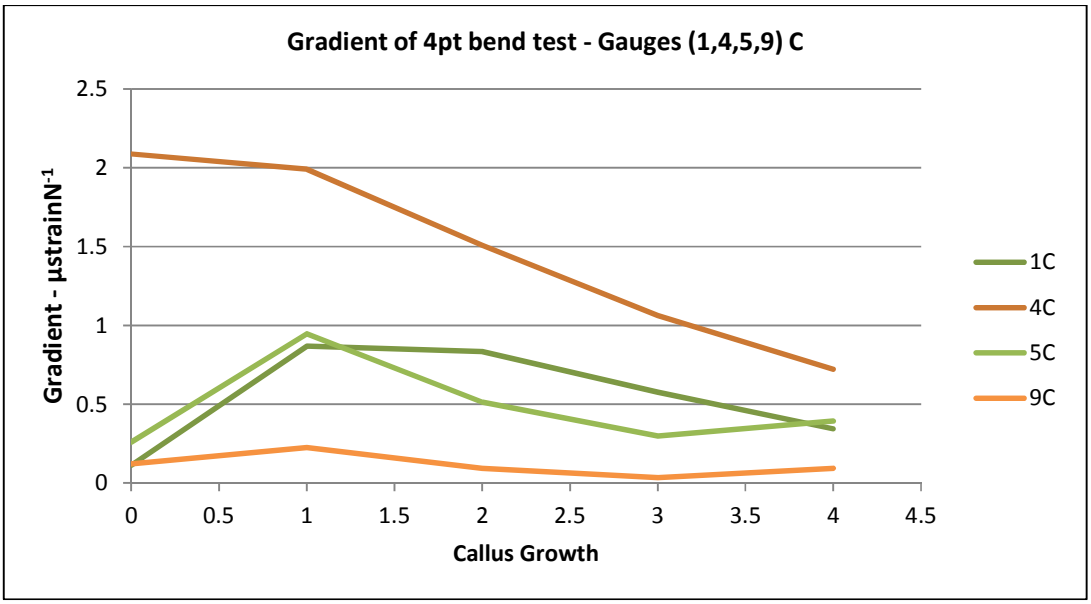

Figure 69 – Gradient of gauges 1,4,5,9 C during four point bend test loading against callus growth

4.4.6 Discussion

The values of each oriented gauge at each strategic anatomical position seemed to have followed the same trend all the way through the biomechanical tests. The original aim was to understand the sensitivity of the gauges in order to decide on the placement of the gauges. Gauges positioned farthest from the fracture site based in the distal third of the tibial bone, was still able to record data and was sensitive enough to measure the healing simulation conducted both segmentally and circumferentially. In this *in-vitro* biomechanical experiments that had been conducted only once due to mechanical damage to the wires, the decrease in the strain both compressive and tensile seemed to have followed through both during circumferential and segmental application of the bone callus composite. The composite replicated soft bone material of 0.2GPa all the way through to 1GPa. The application of the first level of callus composite replicating granulation tissue at 0.2GPa shows a slight change in strain measurement in both application techniques. After L4, replicating immature bone, gauge 1 showed a significant change in the strain, both compressive and tensile depending on the biomechanical test and bearing in mind the medial application of axial compression load.

Physiologically this scenario of callus morphologically may not apply as described in the biomechanical tests, however using the above data, clinicians can understand and predict what can be expected for similar fractures or healing morphology. This could act as a predictor to

further understand the mechanical integrity of the callus in relation to internal fixation and loading regimes for treatment.

The hypothesis proposed is that the forces experienced by an intramedullary nail, normalised by the ground reaction force will progressively decrease in a sigmoidal manner as fracture heals. This is illustrated in Figure 70. This experimental work carried out appears to support the above hypothesis. Loading during healing has been previously investigated in the animal model; this indicates a decrease as healing progresses. The biomechanical experimental tests for GEN I IM nail has highlighted the importance that bone healing plays in the loading regime of an IM nail.

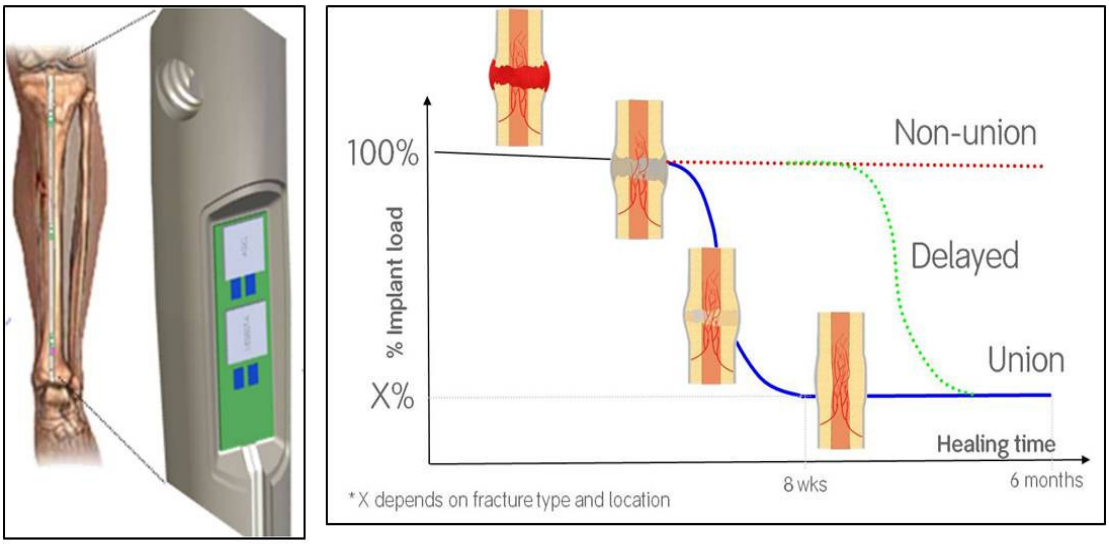

Wireless sensors embedded in implant measuring biomechanical forces

Sigmoidal decrease in force when normalised to an external load during bone fracture healing. Schneider et al. reported 50% drop in nail load for a multi-fragmentary midshaft femoral fracture

Figure 70: Illustrating the hypothesis of how a decrease in percentage implant load over time can be monitored using telemetry

However, this experiment should be repeated for various fracture patterns as well as with various callus morphologies. So far, this experiment has been conducted once for each callus application method, further understanding the type of forces that the tibial bone experience during healing would help change treatment for more efficient methods. And with the use of telemetry, non-union and mal-union can be avoided.

4.5 Second generation (GEN II) telemetered IM nail

GEN II was designed in order to establish user experience on software and hardware prior to GEN IIIa nails as well as to validate the encapsulant to be used on the nail and its biocompatibility. GEN II was subjected to all the tests described in the test protocol above. The next sections described

GEN II in more details in terms of the strain gauge arrangement; the different test method and reasoning behind the callus mimic application.

4.5.1 Strain gauge arrangement

The strain gauges used in GEN II nails were thin film gauges and were instrumented at Strain Measurement Devices (SMD) under the UCL work-packages. The thin film gauges specifications were 5kΩ and 100ppm/deg C for temperature count. There were 20 gauges on GEN II divided in subsets of 4 gauges over 5 slave stations. The first three were aligned at 45° and the fourth one at 0° aligned to the nail axis. The strain gauges arranged as shown in Figure 71 below in an extended pocket on the anterior side. The slave stations were connected to a master microcontroller on a PCB. The whole system had a regulated power supply of 8-9V to power 2 PCB (Overseer & TIMk2) and one GEN II flexi.

The overseer board generated power for the functioning of the nail while also generating the clock to control the master microcontroller and slaves. The TIMk2 board in turn powered the overseer board. The strain data from the overseer board is then transmitted to TIMk2 which is transmitted via an RS232 to a dedicated laptop with LabView interface. TIMk2 is initiated using a customised software designed by UCL (Wildcroft Software) and sends the signal to the master microcontroller and slaves for programming and for standard operating. Figure 71 is a picture of GEN II taken prior to implantation in Sawbone®. Figure 72 illustrate in more details the schematic of the strain gauges arrangement on GEN II. The next section will describe the test method to be used for GEN II testing.

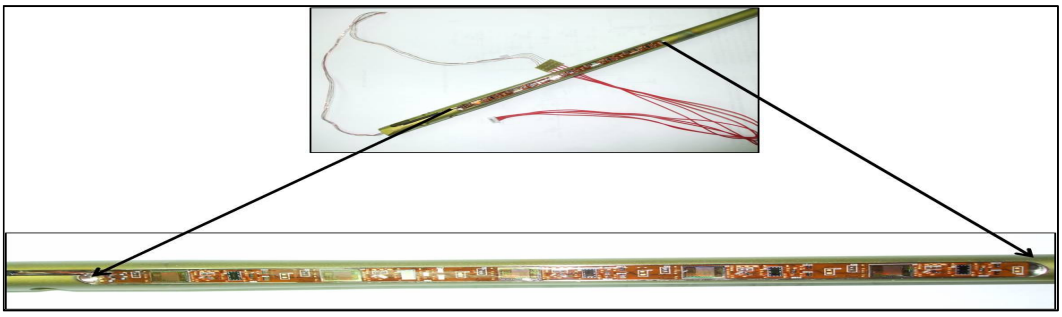

Figure 71- Instrumentation area of GEN II nail

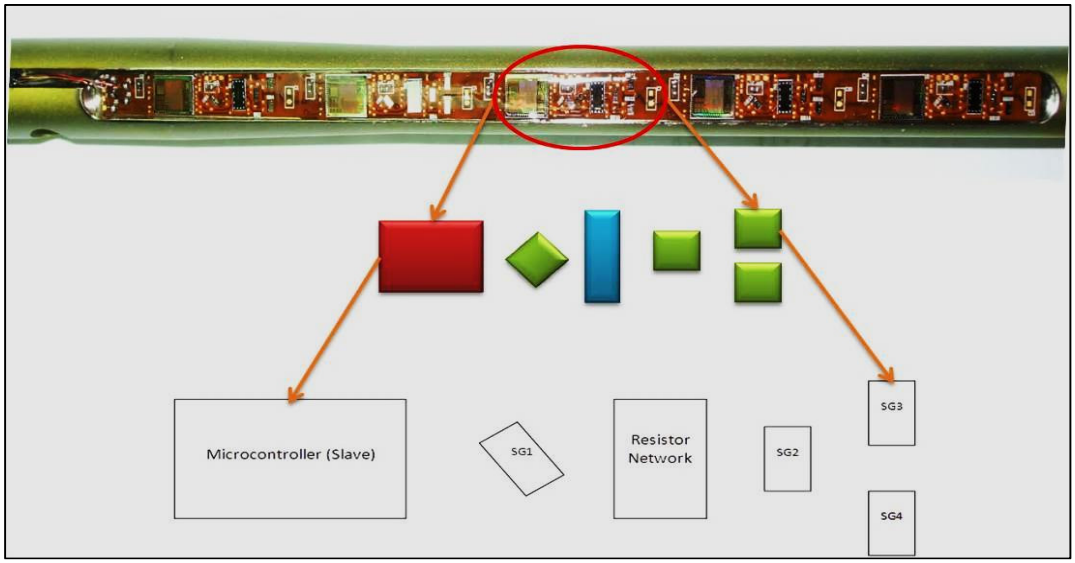

Figure 72 – Schematic of GEN II nail

4.5.2 Test method

The test method used for GEN II was different from that used in GEN I. Two instrumented nails and artificial tibial bones were available for use during biomechanical testing. In order to run more than two simulations, the idea was to re-use the instrumented nails and bones. Using GEN II, the aim was to simulate:

- A control – An instrumented nail in an un-fractured bone
- An instrumented GEN II in a 42-A2 fracture
- An instrumented GEN II in a 42-A3 fracture
    - OR366 – Callus composite application protocol
    - OR381 – Callus composite application protocol
    - OR451 – Callus composite application protocol

Biomechanical tests on an un-fractured bone were decided in order to gain an understanding of the type of strains that can be observed in a bone that is fully healed. The 42-A2 fractured Sawbone® was to replicate the fracture in GEN I experimental set up that will allow direct comparison taking into consideration the change in strain gauge arrangement. The 42-A2 was artificially healed using the circumferential healing regime as applied in GEN I experiments. The decision for choosing this healing technique is further discussed in the next paragraph.

A biomechanical torsional testing of the simple diaphyseal ovine tibial fracture model fixated with a human TRIGEN META nail was conducted as a pilot study at Smith & Nephew Research Centre [14]. The objective of that particular study was to determine torsional strength and stiffness of sheep tibiae fixated with TRIGEN META nails after 3 months. Three of the ovine models used

namely, OR366, OR380 and OR451 were monitored closely and x-ray imaging was taken at week 4, 6, 8 and 10. The x-ray images have been tabulated for all three animals and can be found in Appendix E. The x-rays were analysed and the observations of the callus healing regime was recorded. The observation of the healing was closer to the circumferential healing rather than the segmental healing regime hence the circumferential healing technique for the 42-A2.

After taking measurement on the un-fractured bone, the bone was fractured with the nail in-situ producing a 42-A3 fracture. The 42-A3 fracture is a transverse fracture that was induced at the midshaft of the tibial bone and the three different healing regimes recorded from the *in-vivo* study were mimicked using a GEN II nail. The callus composite material was applied as describe in Table 9 below. The biomechanical tests applied were the same as described in GEN I, axial compression, torque and 4pt bend test using custom made rigs.

The nails were instrumented under instructions from UCL at SMD. The instrumented nail had to be implanted in the Sawbones® that were pre-reamed by 1.5-2mm over the diameter of the nails and some of the screw holes were already in place. However, the nails used were shorter in length for the pre-drilled holes. New holes had to be drilled as normally done in surgery. This technique will be discussed in details in Chapter 5.

During implantation, extreme precaution had to be taken as the components were wire bonded under the encapsulant which held the flexi in place. Wire bonding is the process to connect integrated circuits to printed circuit boards. This process is a delicate and specialised process. Ultrasonic vibration was used during the process. The slightest pressure on the encapsulant may mechanically damage bonds hence damaging the connections between components. Despite the slightly over-reamed medullary canal, the nail insertion was a very delicate procedure. The slight bend in the nail does not make the task easier as the nail section becomes larger due to a curvature designed into the device. One of the nails slid easily in the bone and was screwed securely in place, proximally and distally. However, when connected to system, there was no response at all. This unfortunately showed how fragile and delicate the wire bonds were. Fortunately the two other nails, despite being a tight fit in the medullary canal, they were in good working conditions when connected to the system. This mechanical damage of GEN II nail already showed that there could be an issue during testing. However, optimistically the gauges streamed live data without any incident at the beginning. The reliability of the instrumented GEN II will be discussed in this chapter as the results are presented.

Key to Table 9: AP – Antero-posterior, ML- Medio-lateral, P- Posterior, M- Medial, L- Lateral, A- Anterior

Animal	Week	View	Callus growth	Callus Level	
OR380	4	AP	M	L2	L2 PM
	6	AP	ML	L2	
	8	AP	ML	L3	L2 PMLA
	10	AP	ML	L4	
	4	ML	P	L2	L3 PMLA
	6	ML	PA	L2	L4 PMLA
	8	ML	PA	L3	
	10	ML	PA	L4	
Animal	Week	View	Callus growth		
OR366	4	AP	L	L2	L2 L
	6	AP	ML callus but bridging only on L	L2	
	8	AP	ML callus but bridging only on L	L3	L2 LA
	10	AP	ML callus but bridging only on L	L4	
	4	ML	PA	L2	L3 L slight A
	6	ML	PA Callus but no bridging	L2	
	8	ML	PA callus but bridging only on A	L3	L4 L
	10	ML	PA callus but bridging mainly on A	L4	
Animal	Week	View	Callus growth		
OR451	4	AP	L	L2	L2 PML
	6	AP	ML	L2	
	8	AP	ML	L3	L2 PMLA

	10	AP	ML	L4	
	4	ML	PA	L2	L3 PMLA
	6	ML	PA	L2	L4 PMLA
	8	ML	PA	L3	
	10	ML	PA	L4	

Table 9: Observations of callus morphology from ovine models

Wire bonds were chosen as the connection in between components by Smith & Nephew, according to their project specification. GEN II was the most realistic prototype of GEN IIIa in terms of strain gauge arrangement and the technological components used. Once the nails were implanted, the bone was connected to the circuit and the biomechanical tests were started. As the tests progressed, not all of them functioned fully to the end of the tests. The different failure modes were recorded and will be discussed in the results as well as illustrated graphically in the coming sections.

4.5.3 Results and discussion

The biomechanical tests were conducted as described in the experimental loading protocol and the test method followed was the GEN II test method as described in the section above. The results were processed and analysed using similar post processing methods used in GEN I. The order of the results presented will follow the test method and the illustrations of the changes observed will be graphically represented using the gradients. The results will examine the strains of the un-fractured bone before moving on to the 42-A2 fracture and comparing the results to the GEN I results obtained. This then leads to the results of the 42-A3 midshaft fracture with the callus composite application from the x-ray observations of three different ovine models.

4.5.3.1 Results and discussion of unfractured bone

Compression Testing

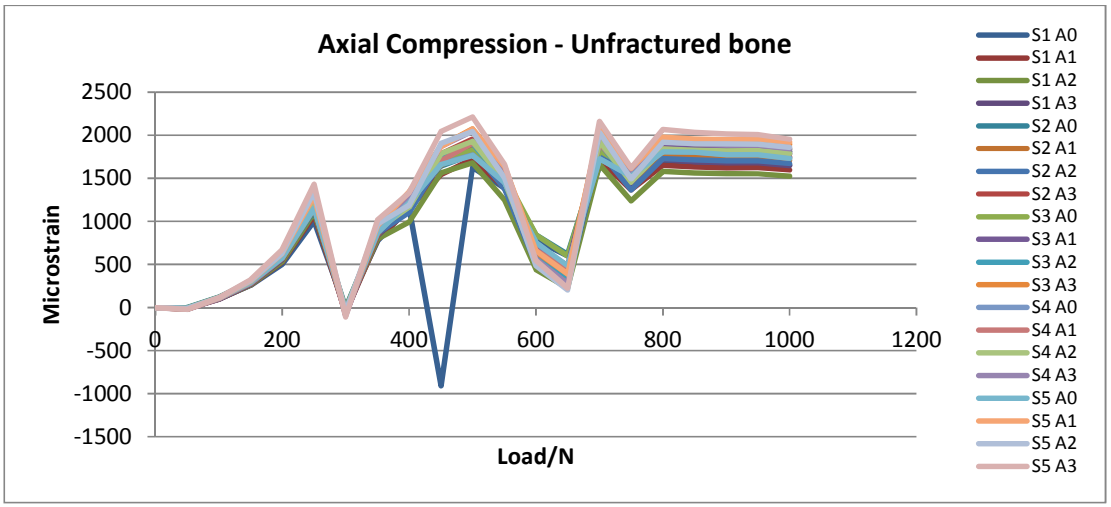

Figure 73: Axial compression loading of an unfractured artificial bone with an instrumented nail

Figure 73 illustrates the 20 strain gauges of the un-fractured bone on a graph recording the strain measurements as load is applied as described in the loading protocol. The graph shown here, presents some anomalies as load is applied. There is a gradual increase in the strain from 0N to 200N after which a sudden drop in strain is observed. This anomaly appears again just after 600N and slightly at 800N. Taking the different arrangement of the strain gauges into consideration, the odd graphical representation of strain in an un-fractured bone can only be associated to a number of variables such as a relaxation in the test rig, relaxation of the callus mimic or instrumental error.

Loading an instrumented IM nail in an un-fractured artificial bone to understand the strains present in a tibial bone, simulating a healthy functioning bone has not been experimentally tested and published before. The hypothesis is that the forces experience by an IM nail when normalised by the ground reaction force will progressively decrease as healing occurs in a fractured bone. The above results are from axial compression loading on the medial side of the tibia and should consequently show low strains as it is in an un-fractured bone model. The maximum strain reading that can be observed starts at around the 500N load application. If the instrument error can be subtracted from this experiment, the highest strain reading as a bone is loaded up to a 1000N seems to be around 2000N. Finlay *et al.* [15] conducted compressive loading on cadaveric tibial bones to understand the strain distribution in the lower leg. A maximum load of about 1000N was centrally loaded which produced a maximal, compressive principal strains of about 500 µstrain. Observations from Figure 73 show strains with magnitude around 500 µstrain at 200N compressive load. Due to lack of time and Sawbone® available the experiment was not

repeated as the same artificial bone was fractured along the midshaft to simulate a 42-A3 fracture.

Torque testing

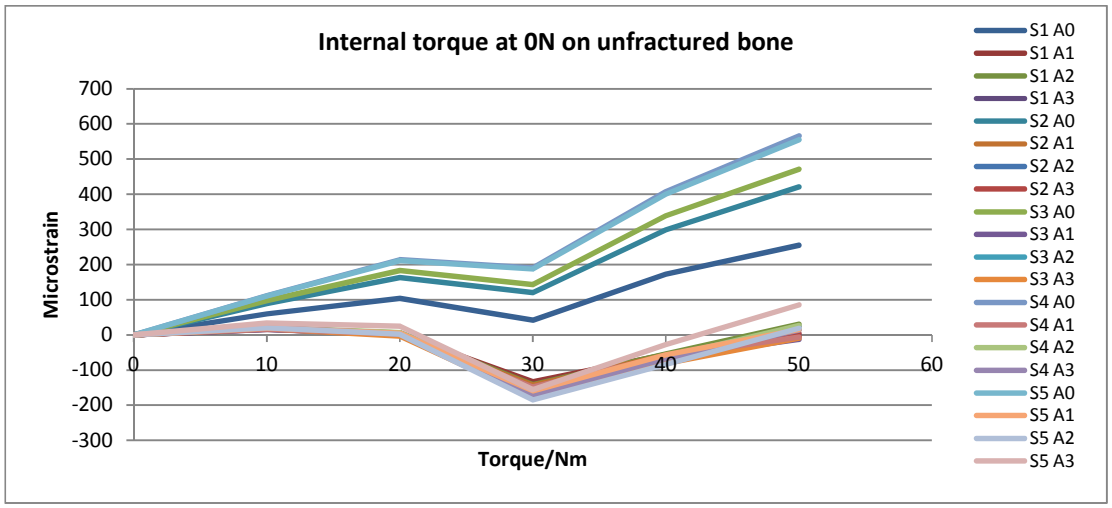

Figure 74: Internal torque loading at 0N in compression on an unfractured bone

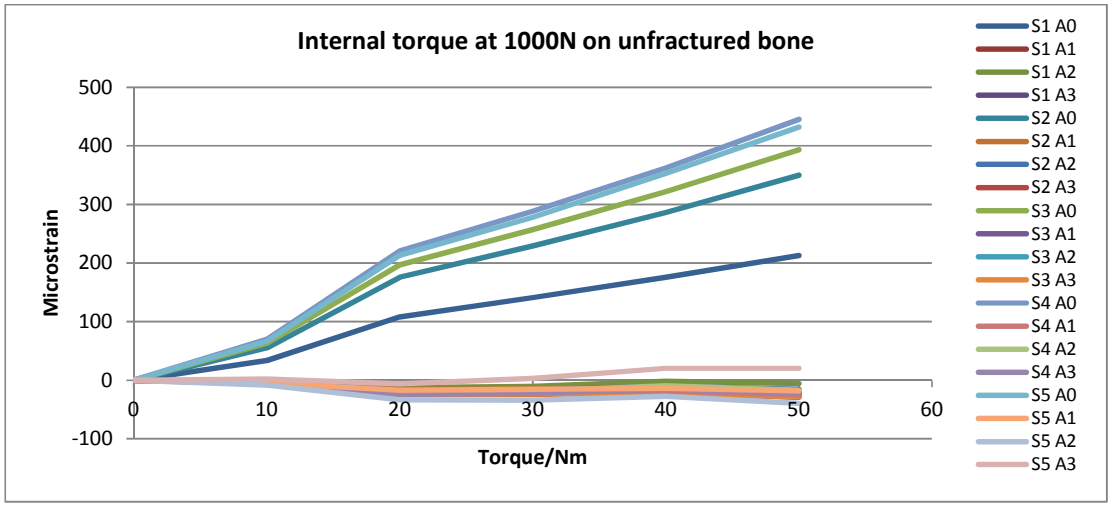

Figure 75: Internal torque at 1000N in compression on an unfractured bone

Leading on from the axial compression testing results, the internal torque testing both at 0N and 1000N in compression on the un-fractured bone is presented in Figure 74 and 75. The magnitude of both graphs shows the maximum strain measured is 550 and 450 µstrain respectively. This value is nearer to the values recorded by Finlay *et al.* [11].

3 and 4 -point bend test

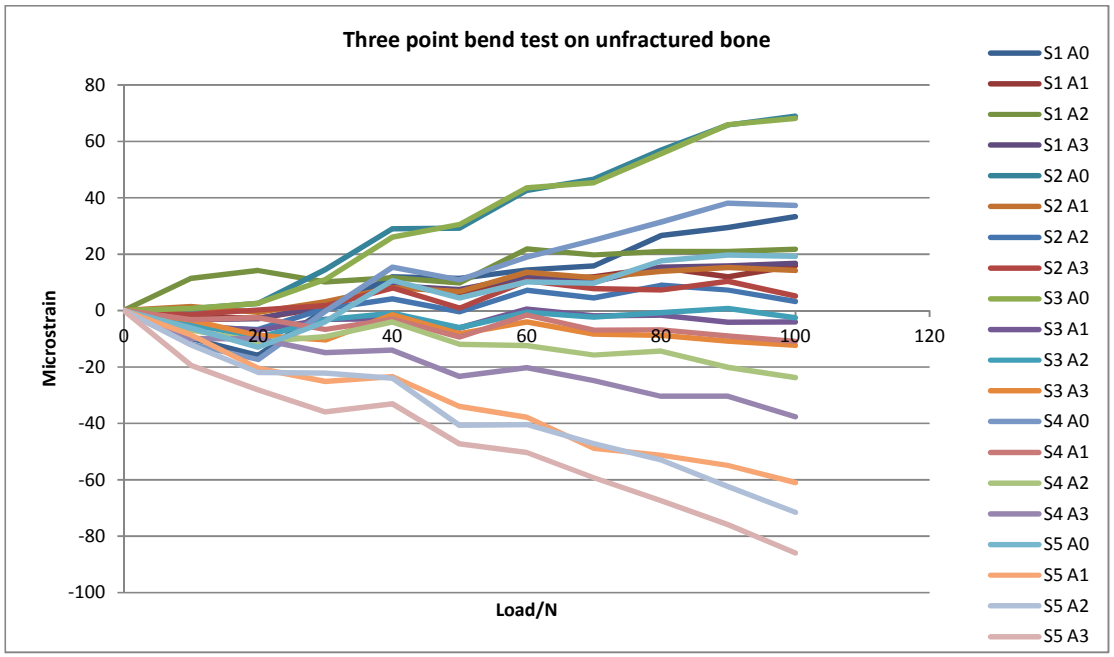

Figure 76: Three point bend test loading from 0N to 100N on an unfractured bone

Figure 76 shows the result of a three point bend test on the un-fractured bone. Since it was an un-fractured bone, it was deemed sensible to conduct both a 3 –point and a 4-point bend test. The 3-point bend test experimental set up was similar to the 4-point bend test as described in the experimental protocol. However, instead of the custom made rings used for the rest of the experiments, tested wire used for the pulley system which can withstand 10kg the maximum load, was used as the wire to apply the load across the bone. Figure 76 was generated and the strain readings vary from around -80µstrains to +70µstrains. Figure 77 representing the 4pt bend test, sees a similar trend as the 3pt bend test. However, this trend is observed only until the 60N load applied across the bone. Similar sudden change in strain readings as observed during the axial compression test is observed during the four point bend test which can be associated with a number of varying factors such as instrumental error across the flexi or mechanical damage to the wire bonds.

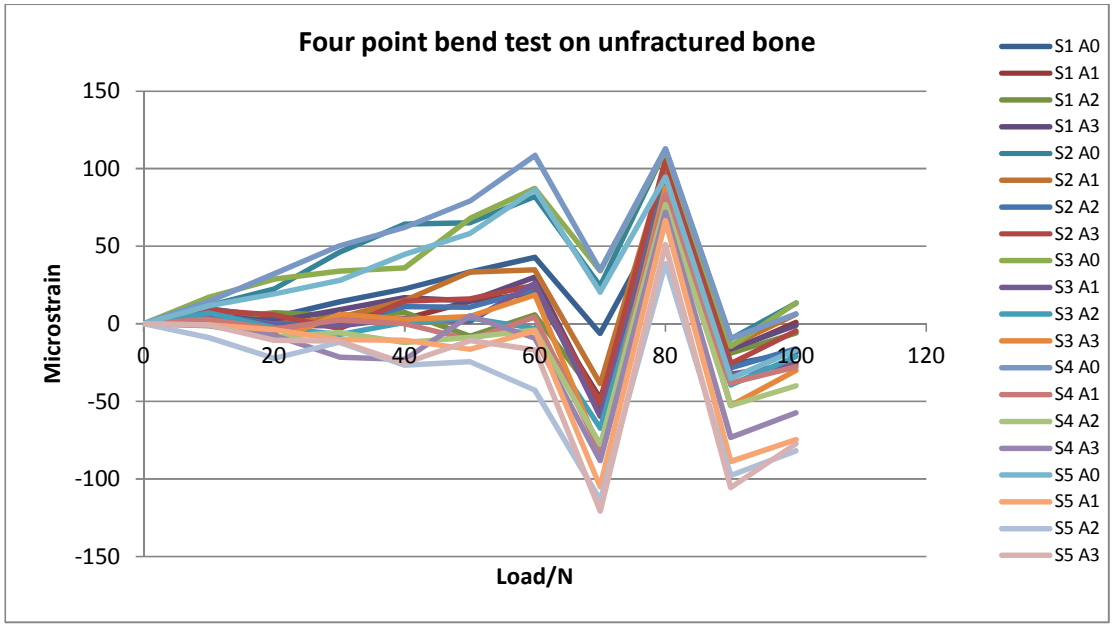

Figure 77: Four point bend test loading from 0N to 100N on an unfractured bone

Strain reading measured on the unfractured bone should give an indication of the strain that can be encountered in a healthy bone. However, this system lacks the intricacy of the muscular and vascular complexities which would otherwise add to the strain measured in the unfractured bone. The anomaly shown in Figure 73 and 77 may be due to the fragile nature of the GEN II nail however, since this was an unfractured bone, all the load should realistically be on the bone and not on the nail. This anomaly at this particular point in time was unknown as the results from the torque and three point bend test seem to show nonlinear behaviour.

4.5.3.2 Results and discussion for 42-A2 fracture

An instrumented GEN II nail was used in a Sawbone® replicating a 42-A2 fracture. The bone was subjected to the same set of loading protocol as described in section 4.3.3 and 4.4.2 for the circumferential application of the callus material.

Axial Compression

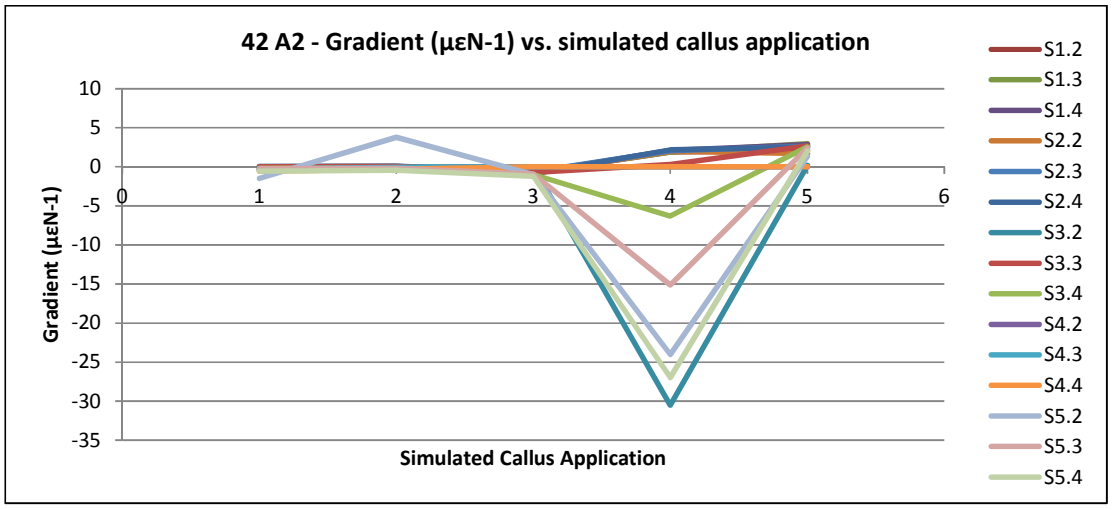

Figure 78: Axial compression loading gradient vs the simulated callus on a 42-A2 fracture

Figure 78 represents the gradient of simulated callus application on GEN II with all the gauges oriented at 45° to the nail axis. The nail has suffered some sort of interference or damage at L3 during the simulated application. Figure 79 shows a similar trend for gauge 1 at slave site 3. However it can also be observed from Figure 79, gauge 1 at slave site 4 seems to have stopped working from the fractured bone all the way to the application of L4 callus material. Because the strain gauge arrangement is different, direct comparison with GEN I is unlikely to explain the anomaly observed so far. A very slight tensile strain can be observed from the gauges in both figures however the behaviour of the electronic components make it difficult to rely on the data sets produced in this test.

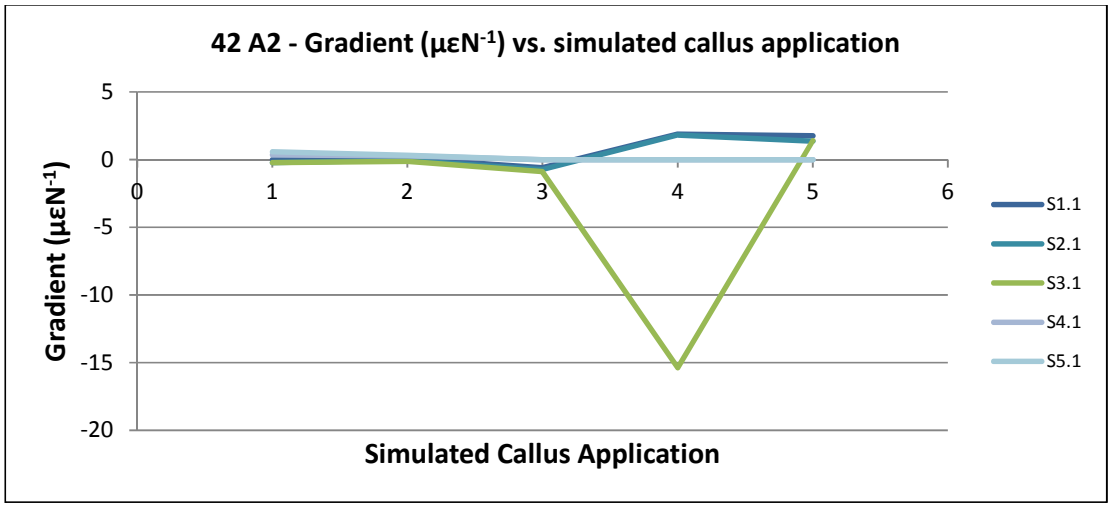

Figure 79: Graph illustrating the gradient of gauges at 0° against simulated callus during axial compression testing

Torque Testing

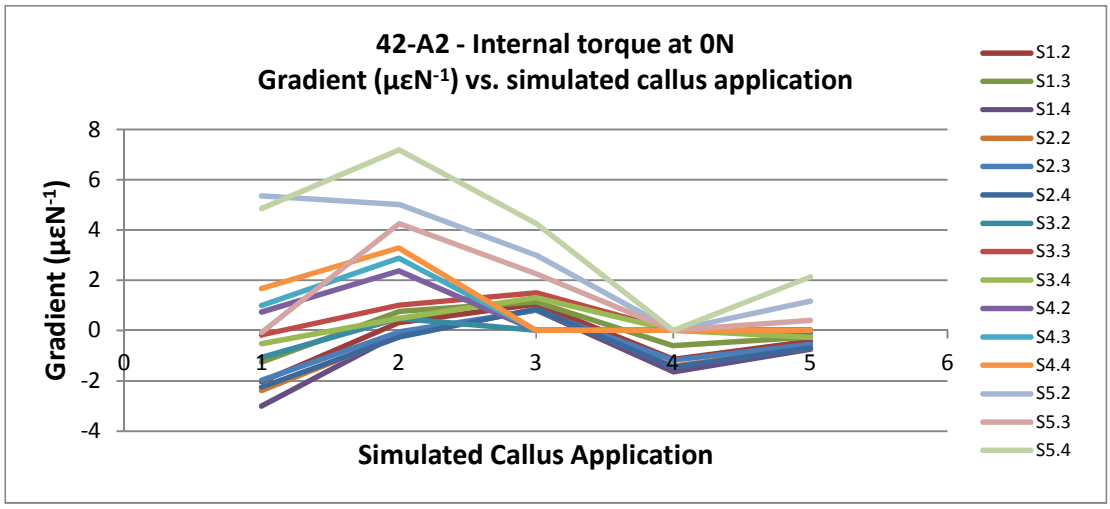

Figure 80: Gradient of internal torque at 0N for gauges placed at 45°

Figure 80 is illustrating callus simulation for the 45° oriented gauges. The gradient shows an increase in tensile strain after the application of the first layer of the callus composite according to the protocol set above. The increase is observed throughout all gauges before a decrease is seen for some gauges as healing progresses. Some gauges are shown to be experiencing bending forces as the torque is applied.

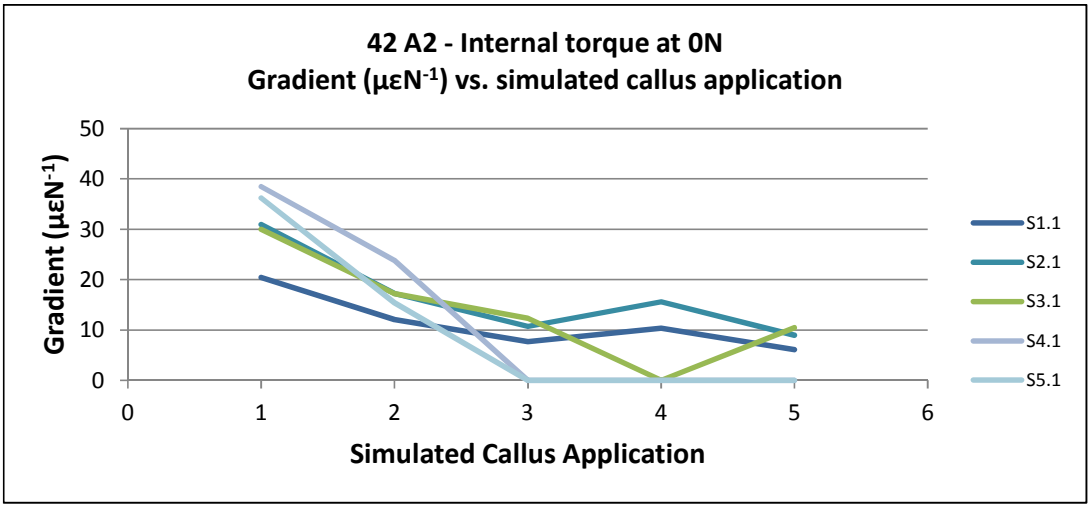

Figure 81: Gradient of internal torque at 0° vs simulated callus application on a 42-A2 fracture

Figure 81 sees high tensile strain readings on the fractured bone and a decrease is observed as callus healing progresses when it reaches a plateau or even increases after the application of L3 callus which is consistent with what is observed during the axial compression test.

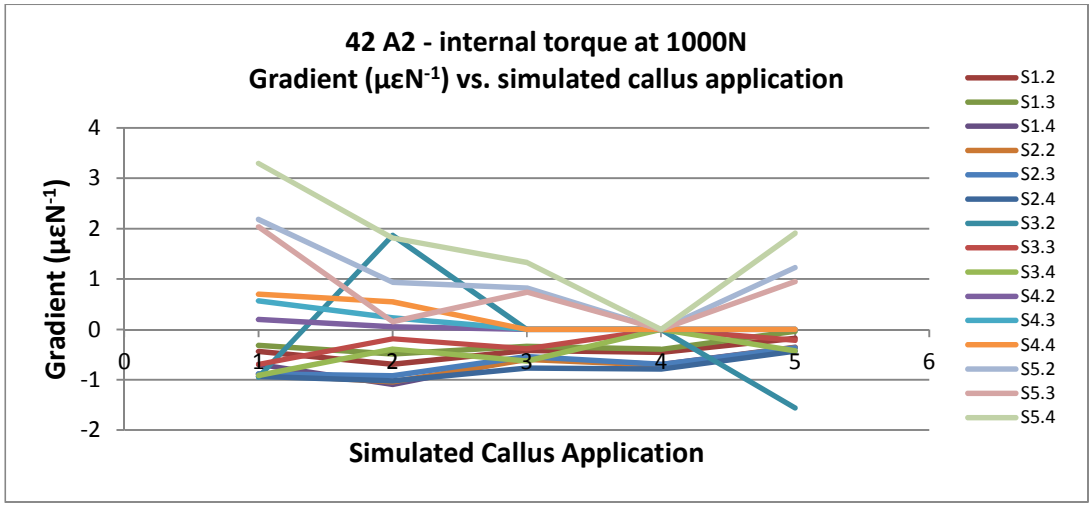

Figure 82: Gradient of Internal torque at 1000N in compression for a 42 A2 fracture

Figure 82 shows internal torque at 1000N in compression with a varied set of readings. Tensile strain is observed at high magnitude for some gauges in compression while others are slightly in tension. However, it has to be taken into account that at this point in time, when the biomechanical tests were being conducted, some gauges were transmitting high level of noise as well as suffering temporary drop in data transmission all together. This again could be associated to instrumental damage or error. However, bearing in mind that the pocket where the strain gauges are positioned is found on the anterior side of the nail. While the axial loading itself is being translated medially from the midline, it is not surprising that the strain readings are low.

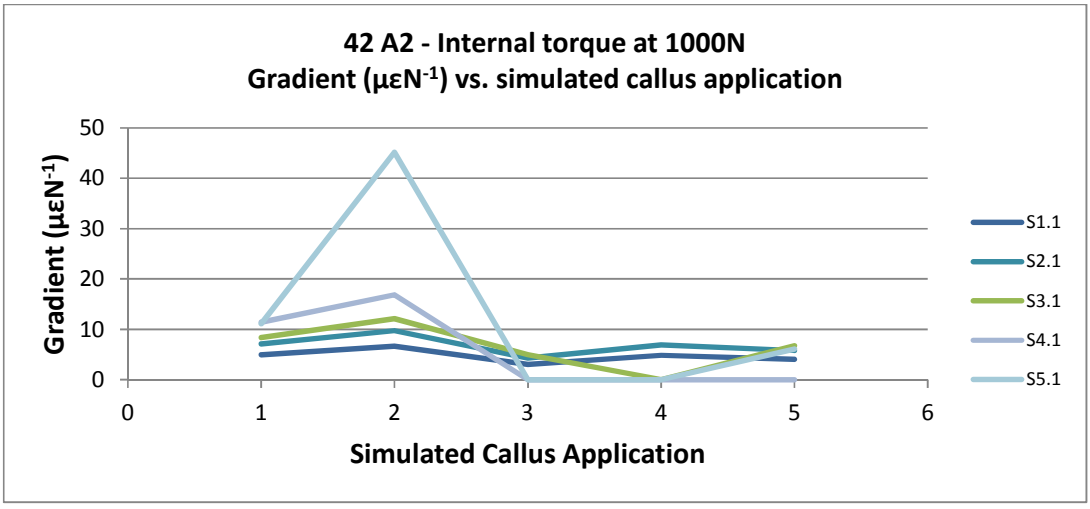

Figure 83: Gradient of internal torque at 1000N in compression for the gauges at 0° vs simulated callus application

In Figure 83, it is obvious that gauge 1 at slave site 5 has an error that occurred which induced this spike in gradient at stage 1 of the simulated callus application. The rest of the gauges seem to be following similar trends but in a more uniform direction. The tensile strain is more or less stable;

no sudden increased or decreases are observed however so far the data has not been reliable and is not comparable due to difference in strain gauge arrangement

Four point bend test

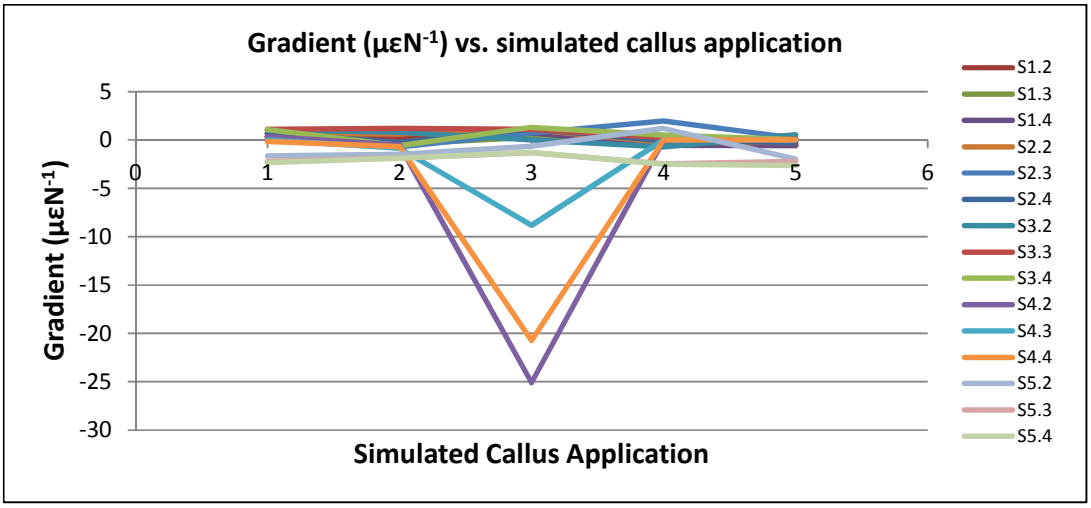

Figure 84: Gradient of the four point bend test vs simulated callus application on a 42 A2 fracture

From the graph of Figure 84 we can observe a spike in compressive strain for gauge 2, 3 and 4 at slave site 4. At stage 2 of healing callus, these three gauges seemed to have experienced instrumental or experimental error. Similar trend is seen in Figure 85 gauges 1 at slave site 4 and 5 is seen to have experienced very high strain at stage 1 and 2 of callus application.

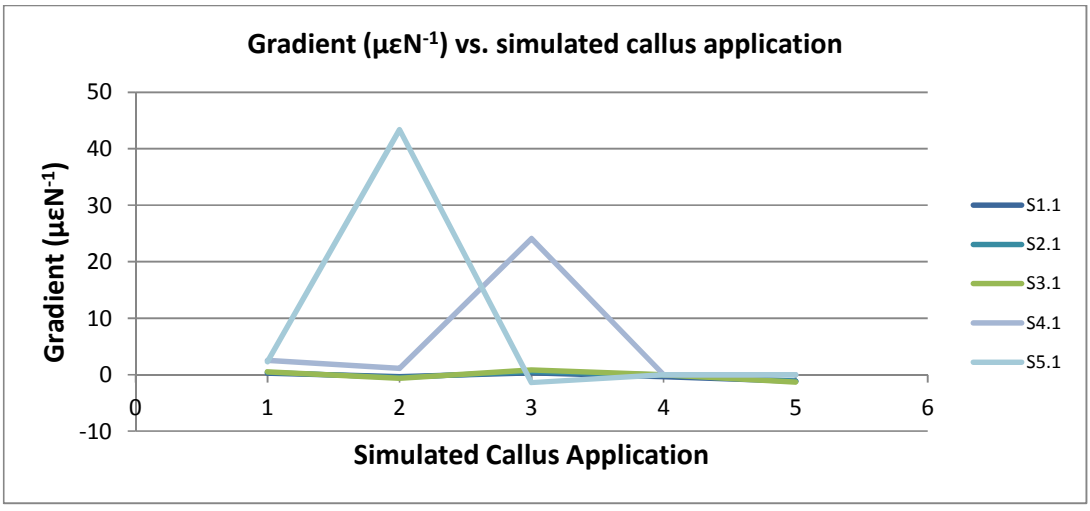

Figure 85: Graph illustrating the gradient for a 4pt bend test for the gauges placed at 0°

Despite the difference in strain gauge arrangement, a reliable nail could have possibly shown some more mechanically apt behaviour in regards to the loading protocol. However, there has been some consistent unpredictability in the strain measurement during testing of 42-A2 fracture

and the simulation of healing using the circumferential method. This particular nail was used only 42-A2 fracture which meant that the instrumental damage happened on insertion in the medullary canal. This will be discussed in more details in the discussion section on GEN II nailing system.

4.5.3.3 Results and discussion for 42 – A3 fracture

The 42-A3 fracture biomechanical tests have been discussed in the test method as well as the callus application techniques. The nail that has been used for this part of the testing is the same nail from the un-fractured bone. This means than that there may be some anomalous sets of data which have been associated with increasing instrumental error and damage caused to the wire bonds. Unfortunately these errors could not be prevented once the instrumented nail was damaged; however biomechanical tests for all three different simulations were completed with at least part of the nail still in working condition.

This simulation can help understand and predict what magnitudes of strain are to be expected as healing progresses. Among the three different callus application technique used for this fracture, OR366 was the less healed bone while OR380 and OR451 had similarly healed patterns (Figure 86-91 on pages 144 -146). By comparing these biomechanical tests to the *in-vivo* x-ray images of these ovine models, a lot of information can be extracted in terms of the direction of the loads and forces. This said the importance of muscles, ligaments and vascularity in fracture healing *in-vivo* has to be acknowledged and could not be simulated within these *in-vitro* experiments. However the different fracture callus patterns show potentially what the approximate strain that can be expected if the nail was a fully functioning instrumented nail. The strain measurement recorded and analysed for all three simulations showed similar anomalies as previously seen from the graphs above using GEN II nail. Due to this particular aspect, the results presented for the three ovine model callus healing simulation will concentrate on the axial compression testing results.

OR366 Axial Compression Results

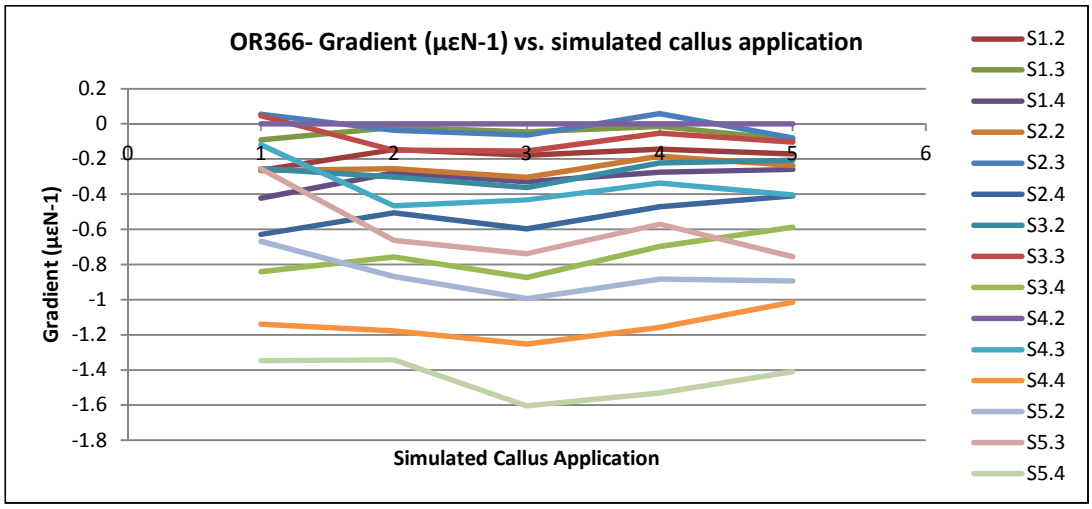

Figure 86 : Axial compression results for gauges at 45° simulating callus healing of OR366

The axial compression gradient observed show a non-changing strain at gauges aligned 45° on the anterior face to the nail axis. Gauges 1 (Figure 87) at all the slave site seem to experience a decrease in tensile strain as healing progressed before a slight increase simulating healed bone. Slave 1, gauge 1 is the most proximal gauge hence the farthest from the fracture site. The load applied is transferred to the bone on the medial side which is more likely to affect strain gauges oriented at 0°. However the gauge at 0° on the anterior side was sensitive enough for the forces from the medial side.

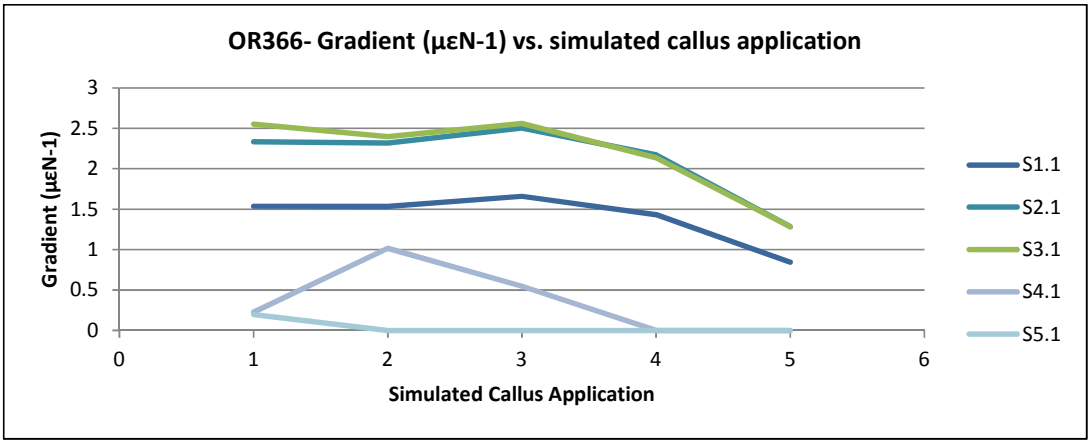

Figure 87: Axial compression gradient of gauges placed at 0° simulatinng callus morphology of OR366

OR380 Axial Compression Results

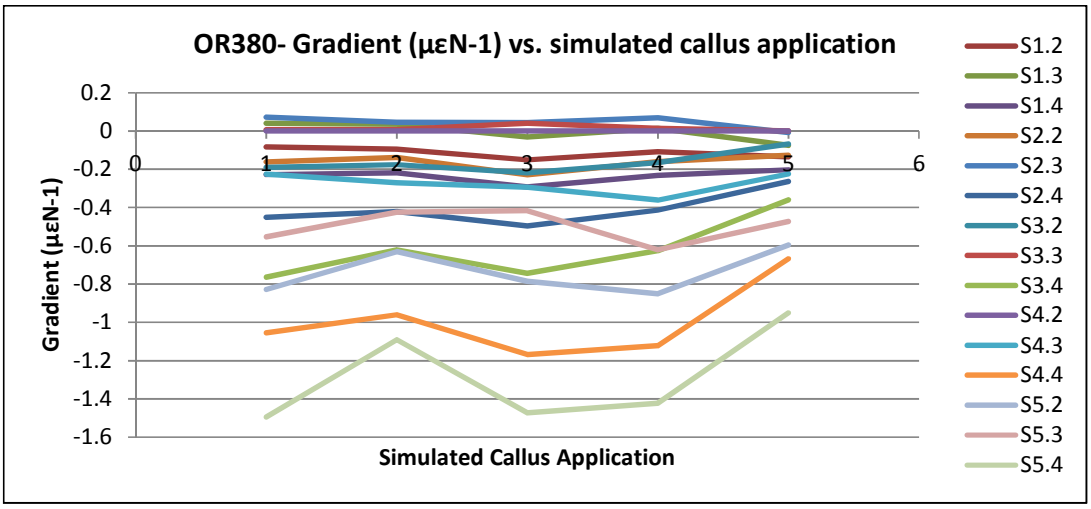

Figure 88: Axial compression gradient of gauges placed at 45° simulatinng callus morphology of OR380

OR380 simulated a more complete healing pattern with callus growth observed on the posterior, medial and lateral side at week 4. Figure 88 and 89 shows the axial compression gradient over the simulated callus application. The 45° gauges shows compressive strains decreasing as the load from the nail shifts to the fractured bone as healing progresses. Gauges 1 start with higher tensile strain than the other gauges. From the fractured bone there is a slight increase in the tensile strain carried by the nail which then decreases as healing progresses. However, the strain springs back to the nail before decreasing again. This leads to believe that there may be evidence of creep in the callus material which induces the load material behaviour accordingly. However this can be argued as creep is a function of time and since the loading is not time dependent, this behaviour is unlikely to be material related but more likely to be instrumental error.

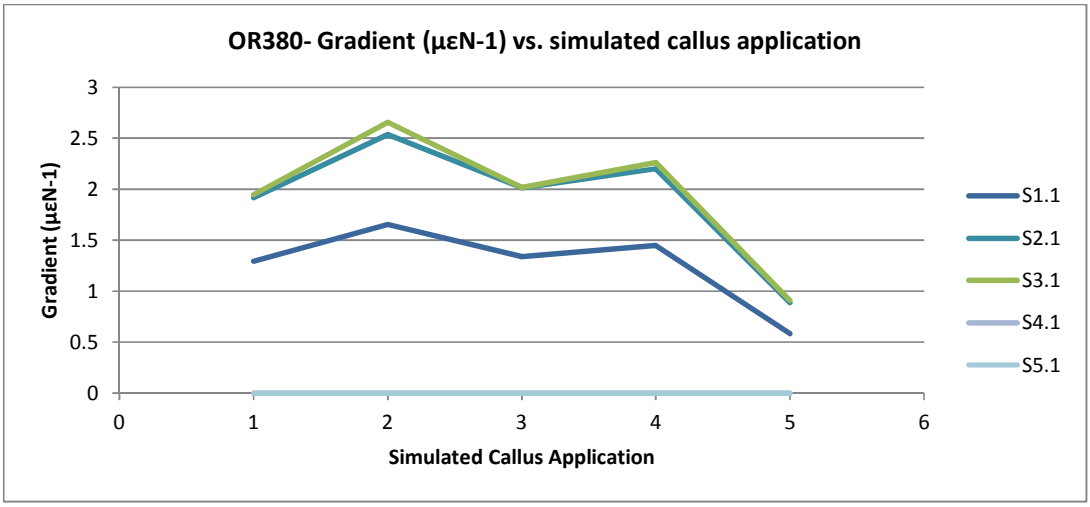

Figure 89 illustrating the gradient of gauges 1 from OR380 in axial compression loading

OR451 Axial Compression testing

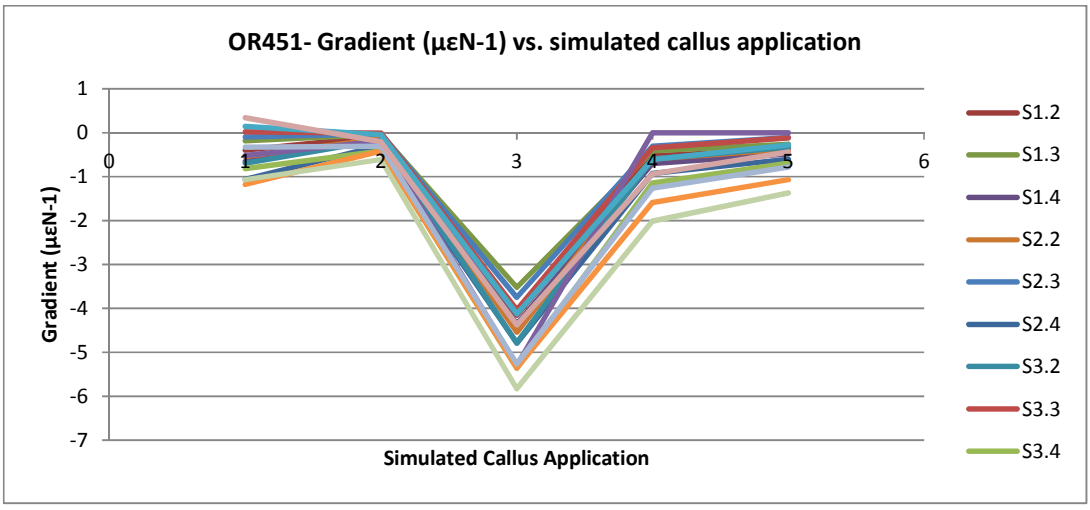

Figure 90 Axial compression gradient of gauges placed at 45° simulatinng callus morphology of OR451

Figure 90 and 91 showed the axial compression gradient of simulated OR451 as healing progresses. Simulation of OR451 produced callus growth bridging three quadrants of the bone at week 4 and all four quadrants from week 6 onwards. Both graphs show a drop in strain from the nail at stage 2 of the callus application which could be associated to either the elastic response as seen previously or as instrumental interference.

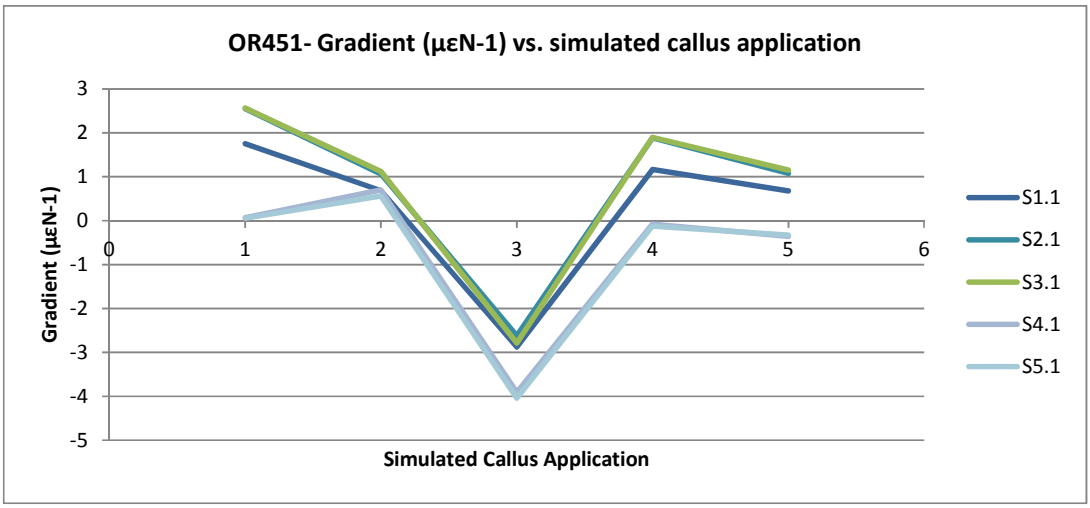

Figure 91: Axial compression gradient of gauges placed at 0° simulatinng callus morphology of OR451

The results generated by GEN II were far from being reliable. This will be further discussed in the next section as GEN II strain gauge arrangement is a mock up of what the clinical nail aims to be. This brings an end to the results of *in-vitro* biomechanical tests before moving onto the discussion and conclusion of the chapter.

4.6 Discussions and conclusions

The results of GEN I and GEN II *in-vitro* biomechanical tests are the firsts set of data with *in-vitro* simulation of fracture healing. There are currently no published data about the simulation of fracture healing with composite materials mimicking natural biological callus. The design and development of the bone callus material is another aspect of this study which will be discussed in relation to its application on both GEN I and GEN II but also on its own.

The bone callus has until now been simulated only *in-silico* by many investigators. However, the study conducted by Lacroix [2] was the closest tissue differentiation technique used during fracture healing simulation *in-silico*. Several groups have researched the various properties of the different stages of bone callus and so far this has added to the knowledge available on bone callus; however the information is very limited.

There is currently no study to compare the design and use of the callus composites but there is further work required on the preparation protocol of the composites for use *in-vitro*. The composites themselves are yet to be refined. The distribution of the materials in the final composite is crucial to its modulus. The curing and repeatability experiment has shown that it can be reproduced within limits of experimental errors. However, a better technique needs to be established in order to manipulate the distribution of material particulates in the matrix thus having a better ability to manipulate the mechanical properties of the composite. This can even lead to the fabrication of more physiologically accurate artificial bone to be used *in-vitro* for implant testing.

GEN I IM nail has been tested in a fractured Sawbone® on its own before any fracture healing simulation techniques. Two different simulation techniques have been tested; the first was a segmental application which was derived from an *in-vivo* study conducted by Smith & Nephew Research Centre, York. While there is hardly any data as to the pattern the callus follow as healing progresses: in order to have a comparison from a different technique, circumferential application was selected. Both segmental and circumferential application of callus composites on GEN I produced different sets of results but both are as equally important. This is because there is a lack of data that will enable clinicians to predict how the bone callus will grow and at what rate. However, in an ideal physiological system, the process of callus production starts from the seconds after the fracture happens and it is strongly correlated to the immediate mechanics action that the bone undergoes. This means that the description from the graphs showing strains from a fractured bone followed by healing strains starting immediately may not be the most accurate system however this is the beginning of an indication of what we can learn from a telemetered intramedullary nail.

The use of a telemetry nail will certainly aid for a better understanding of how healing is progressing. Some patients may have a circumferential growth of callus while others may have a segmental growth of callus. Understanding both is equally crucial however, for further biomechanical tests; circumferential application was selected due to time restrictions.

The literature reported results by Schneider *et al.* [12] which were *in-vivo* measurements that are unique and cannot be compared. Manley *et al.* measured the *in-vivo* tensile and compression loads in a canine femur but could not measure the complete set of load components. Additionally the loading condition in a quadruped is not comparable to human [13]. Obara *et al.* measured the *in-vivo* strains of an intramedullary nail during fracture healing in goats, a decrease in implant strains were noted, but again the comparison to human was questionable [14]. There is no direct comparison in the literature for the sets of data produced above. However, understanding the structural characteristics of the loading will aid in understanding the strain readings in relation to healing. Hypothetically, the load on the nail would shift from the implant back to the bone if healing is progressing successfully within the expected time frame. But as every patient is different, callus growth will be different hence healing pattern and strain analysis would differ.

By analysing the material property distributions and loading conditions, we can determine the possible approximations of the mechanical response of the bone *in-vivo*. Taking the example of the axial compression test, compression forces are applied to both ends of the long bone. With the bone held firmly straight in the mechanical test frame, the load was applied at the proximal end on the medial side. In an idealised situation, using GEN I nails with a 42-A2 fracture, the compressive stresses axially directed in the z-y plane will cause bending in the diaphysis about the x-axis. This will also cause the midshaft to compress in length with a slight increase in bone diameter. The highest strain will be in the midshaft region but proximal to the fracture site.

Translating this to the biomechanical test conducted using GEN I the highest strain recorded were around gauges 5 (ABC) which was the nearest distal gauges. GEN I was also used to assess the sensitivity of all the gauges. Most of the graphs shown in the results section show gauges 1,4,5 and 9 as they were the most strategically positioned: most proximal, one on each side of the fracture site and most distal.

The fact that all four showed enough sensitivity should be helpful to select the appropriate position of the gauges for the clinical nails. With distal third fractures being the statistically most common non-union cases, the 42-A2 fracture is roughly 14cm from the distal end thus making this case a close approximation of distal third fracture. Gauge 1 being the farthest from the fracture was sensitive enough to measure the strain readings on the fractured bone but also observed a decrease in strain as healing composites was applied. This was observed for all three

biomechanical tests, some more than others, but the gauges were sensitive to the first layer of callus composite added simulating healing of granulation tissue. Looking at a broader aspect of the investigation, enabling clinicians to assess and understand the healing at an early stage would help ensure early non-union cases can be avoided or diagnosed earlier.

Results from GEN I testing was optimistic as a tool to monitor healing. However the tests should be repeated following the same set of protocols in order for the results to be statistically significant. The results from GEN I should have also been an indicator as to the placement of the strain gauges that are more sensitive to the lowest modulus of synthetic callus. Bearing in mind that in the body, musculature and vascularity takes a major part in the healing process, the experiments should be validated using finite element models simulating muscle forces to understand the strains that will be incurred.

Gen II strain gauge arrangement were configured in sets of four, over five sites in a long pocket proximally placed on the anterior side of the nail. GEN II biomechanical tests were a challenge themselves due to the fragility of the nail developed. With a different strain gauge arrangement, the fragility of the flexi PCB with a soft encapsulant was the challenge of the nail insertion in the Sawbone®. Soft encapsulant was used instead of the widely approved industry electron beam welding in order to reduce manufacturing costs. The instrumental damage was due to breaks in the wire-bonding used in the circuit between the electronic components and the strain gauges were the cause of many issues. Circumferential application of callus composites was chosen for GEN II as it is less time consuming and would make good comparison with GEN I. However the results of the biomechanical tests in GEN II is not reliable as the wire bonds breakage cause the data set to skew from the expected values during some of the tests.

However, summarising what GEN II results show a non linear behaviour which implies there is a change in the structural stiffness of the system. Results from GEN II have shown compressive and tensile strains where the information could be interpreted. However care should be taken in doing so as the graphs shown for GEN II show obvious signs strange material and mechanical behaviour. Non linear behaviour of structural materials can be due to several aspects such as a direct relation to the load applied, large deformations happening at the structural level or in response to material nonlinearities such as load history, creep or relaxation response and possible environmental conditions which are all time dependent. In the case of GEN II none of the above could possibly explain the non linear behaviour as the loading of instrumented nail in the bone tests were conducted in seconds. Nevertheless, since the loading was applied medially to the nail axis and the gauges were all placed on the anterior side, there is the possibility of mechanical

delamination of the gauges from the surface of the machined pocket due to the bending forces experienced by the nail.

Gen II results show major instrumental errors and cannot be used to validate this study. In order to consider GEN II strain gauge arrangement as template for pre-clinical *in-vitro* testing further and more rigorous development and tests needs to be repeated on sets of reliable instrumented nails. This would also be helpful in order to recreate more than one callus morphology on different fracture types in order to understand the variations that can be expected in *in-vivo* situations.

With the 42-A2 fractures in both GEN I and GEN II, there was most likely a high point contact during the compression and torsion testing. This would be associated with the slippage of the bone which resulted in strain readings jumping from extreme highs to lows and vice-versa during loading. However, some results from GEN II did support results presented by Finlay et al. [11] regarding the valued of torque present on the unfractured bone. Despite all the strange anomalous graphs seen throughout the results, the hypotheses stated below have all been satisfied.

Hypotheses that:

- Strain gauges implanted in a tibial IM nail are able to provide sensitive data, showing a relationship between strain and axial force.
- Strain gauges implanted in a tibial IM nail are able to provide sensitive data, showing a relationship between strain and axial torque.
- A single gauge site is able to provide sufficient data to predict fracture healing

However, a recommendation for further work is necessary with different fractures and a more reliable system in order to establish a set of predictions as to the strain readings that can be used as guides for clinicians in the long run. This will be discussed in the conclusions and recommendations for further work.

4.7 References

[1]. Dr S T Hassan .Composites materials technology. Division of Product Design. Faculty of Arts, Computing, Engineering and Sciences, Sheffield Hallam University, 2004

[2]. Damien Lacroix. Simulation of tissue differentiation during fracture healing. University of Dublin, Dec 2000

[3]. John D.Currey. Bones: Structure and Mechanics, Pg56, Table 3.1. Princeton University Press, 2002;

[4]. Jaya L Nemchand. MSc Biomedical Engineering Dissertation 07/08. Smart implants – Multi-channel strain gauge telemetry for monitoring fracture healing *in-vitro*, Brunel University

[5]. Jaya Luxshmi Nemchand, Anthony Walter Anson. UK Patent Application GB 2470034 A,.A biological mimic test composite; Undergoing substantive examination.10th November 2010

[6]. http://www4.nau.edu/microanalysis/Microprobe-SEM/Instrumentation.html (last accessed: 16/07/2012 5:29)

[7]. Zych GA, Cole JD, Johnson KD, Ostermann P, Milne EL, Latta L. Mechanical Failures of Intramedullary Tibial Nails Applied without Reaming Clinical Orthopaedics,1995, 315, 129-137

[8]. Waheed Mahmood (SN:50316397) ; UCL iBSC Orthopaedic Science 08/09. Instrumented Tibial Intramedullary nail, Direct strain measurement in simulated in-vitro fracture healing

[9]. Darren Wilson. Project Number: TO024/95/02. Smith &Nephew Research Centre, Review report of the biomechanical testing of an instrumented META tibial nail equipped with axial aligned strain gauges carried out by the Trauma GBU biomechanics group under various static loading conditions and fracture patterns.

[10]. Smith & Nephew Research Centre Work Report, Biomechanical torsional testing of the simple diaphyseal ovine tibial fracture model fixated with a human TRIGEN META nail; Work report reference no.: WRP-TO024-320-14, Work coordinator : Martin Galfe

[11]. J.B. Finlay, R.B. Bourne, J. McLean. A technique for the *in-vitro* measurement of principal strains in the human tibia. Journal of Biomechanics, 1982, 15,10,723- 739

[12]. Erich Schneider, Markus C.Michel, Martin Genge, Kurt Zuber, Reinhold Ganz & Stephan M.Perren. Loads acting in an intramedullary nail during fracture healing in the human femur. Journal of Biomechanics 2001, 34, 849-857

[13]. Manley P.A, Schatzker J, Sumner-Smith G. Evaluation of tension and compression forces in the canine femur in-vivo. Archives of Orthopaedic and Trauma Surgery, 1982, 99, 213-216

[14]. Obara T., Nippon Seikeigeka Gakkai Zasshi . A biomechanical study on the fracture treatment – intravital measurement of the strain on an intramedullary nail in the healing process of the femoral fracture in goats. 1979, 53, 2, 199-212

[15]. Alison J Smith, Prof Paul Dieppe, Peter W Howard, Prof Ashley W Blom. Failure rates of metal-on-metal hip resurfacing: analysis of data from the National Joint Registry for England and Wales. The Lancet,2012, 380 , 9855, 1759-1766

[16]. Smith & Nephew Research Centre Review Report. Review report outlining the mechanical torsional testing of a simple diaphyseal ovine tibial fracture model fixated with a human TRIGEN META-NAIL carried out by Hull University. T0024/320/06. July 2010

5 In-Vivo testing

In-vivo testing is widely conducted within medical research. In the UK, animal experimentations are conducted under the Animals (Scientific Procedures) Act 1986 [1]. This act is regulated by the Home Office and requires specific licenses. It safeguards the laboratory animal welfare while allowing medical research to take place. For orthopaedic medical device testing, it is crucial to use models where the implant dimensions can be compared to those used in humans. Species and breed of animals chosen for an i*n-vivo* study are directly influenced by the number and size of the implants [2, 3]. According to Pearce *et al.* [2], the use of dogs for orthopaedic research is still greater than sheep however between 1990-2001 sheep have been used in 9-12% orthopaedic research involving fractures. He also states that the increase may be related to more public acceptance in the use of larger animals such as sheep rather than companion animals for medical research.

In terms of the macrostructure of the bone, the literature reports that dog bone is a more appropriate comparison to human bone in terms of the biology; however, the adult sheep bear a similar body and weight as human adults and have bones more dimensionally appropriate for human implants [2, 4]. In terms of histology, sheep bone structure is different to human; sheep bones have more primary bone structure consisting of osteons compared to secondary bone of humans. Sheep bone is denser hence the higher strength compared to humans. Despite the physiological differences, several studies argue that the sheep is still a valuable model for human bone remodelling activity [2, 5, 6, and 7].

Within this study, Blue Faced Leicester Cross Suffolk sheep of approximately 2.5 years old were selected. The next section describes the controlled pilot study conducted as a welfare study for the design and use of specialised external loading fixtures as well as the trial of a dummy reader and energiser system.

5.1 Pilot and live phase animal study

The pilot study was been approved under the Animals (Scientific Procedures) Act 1986 and the Animal Study Authorisation document can be found in Appendix F. The study was coordinated by a specialist from Smith and Nephew, York Research Centre. The project license number and the work request number associated are 60/3643 and WRQ-TO024-320-09 respectively. The three animals selected for the study were ovine Blue Faced Leicester Cross Suffolk ranging from 2 to 2.5 years old.

The pilot sheep study was designed as a welfare study. Its main aim was to determine the effect of repeated application of an external loading jig and a dummy reader and energiser system during general anaesthetic on animal welfare. It was also designed to monitor the effect of

refining the surgical technique on the time required for fracture healing. This pilot study will help to lessen any welfare issues experienced in the live phase study which will focus on collecting implant strain data. This second pilot study follows on from the success of an initial pilot study whereby three animals were treated with a human TRIGEN tibial nail after being subjected to a midshaft osteotomy. This study will be followed by a live phase study which will gather strain data to validate the use of a device to predict fracture healing. The live phase study will consist of using an external loading rig under general anaesthesia bi-weekly and applying prescribed loading protocols to soft tissue and controlling the load/torque applied without causing re-fracture. The potential welfare issues for the live phase study warranted the need for a pilot study.

The three animals selected were subjected to the same surgical protocol as described below including a pre-operative screening, surgery for implantation of device and the simulated loading of the implant during the post-operative phase. Pre-operative screenings are performed ahead of the surgical procedures. The sheep were radio- graphically assessed to determine their suitability for the study. The cortical wall thickness, length and diameter of the bone canal at the isthmus are the most important criteria in the animal selection process. The animals were then trained and familiarized to a number of carers at the test facility to ensure that the strain measurement protocols can be applied without any major welfare issues.

5.2 Surgical protocol

The surgical protocol followed has been described as observed and according to the narration during the operation by the surgical team. The surgery is illustrated in several distinct phases to help understand the technique using the TriGEN META-NAIL™ surgical manual [8]. Before the animal was anaesthetised, the leg and its immediate surrounding areas were prepared in order to avoid any risk for infections as shown in Figure 92.

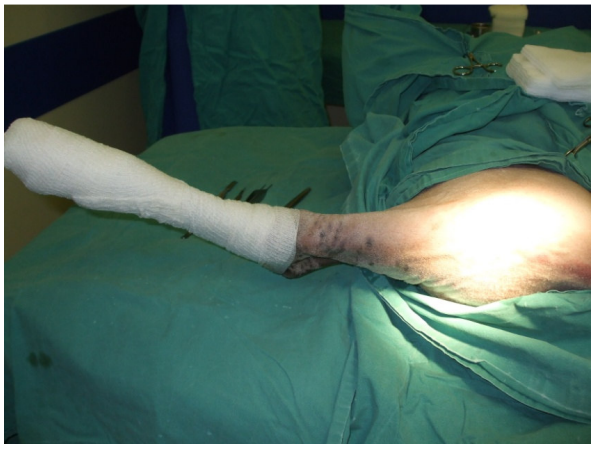

Figure 92: Preparation of the left hind limb with the animal in supine position. The distal end of the leg with the hoof are held

During the surgical procedure a number of tools are used from a dedicated specialist set for the TriGEN Meta Nail. Figure 93-96 shows the main tools as mentioned in the surgical procedure manual for opening the tibia, reaming, nail insertion, fracture reduction and locking of the screws.

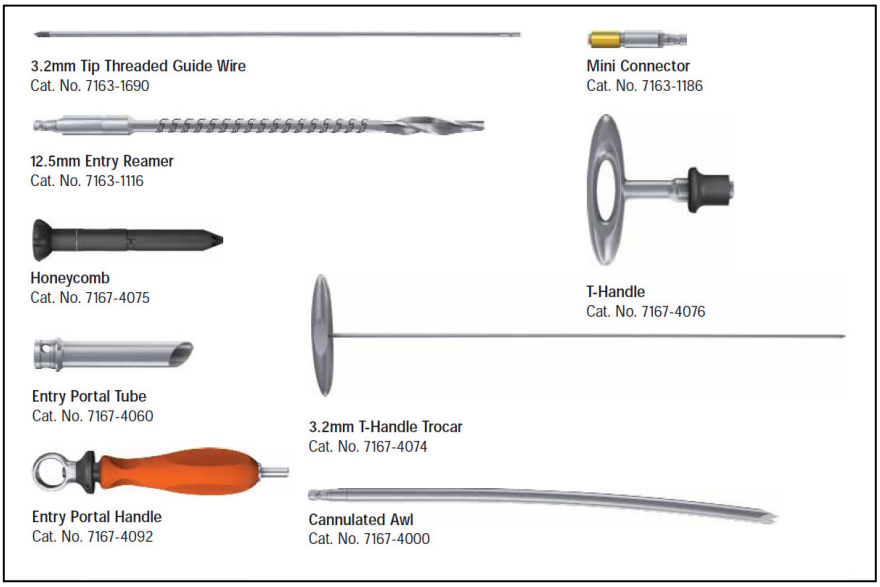

Figure 93: Instruments for Opening the Proximal tibia [8]

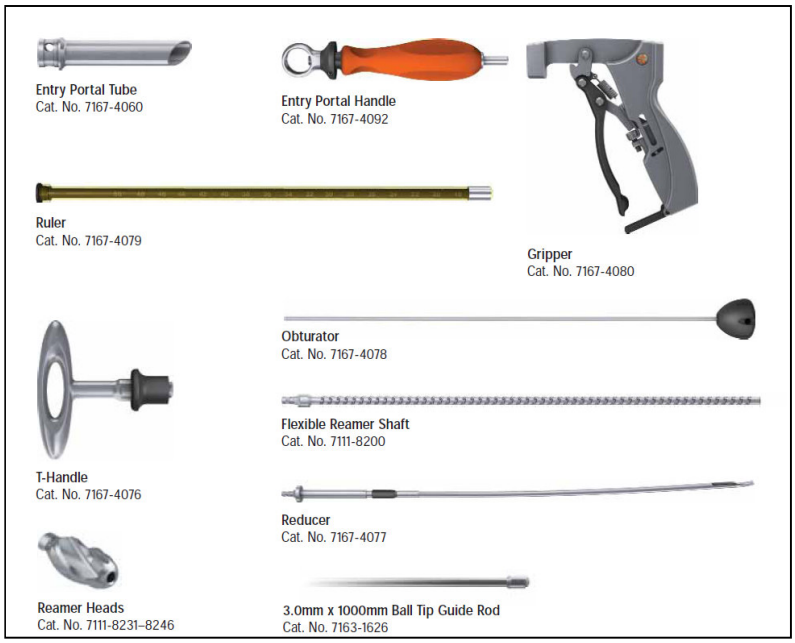

Figure 94: Instruments for Fracture reduction and reaming [8]

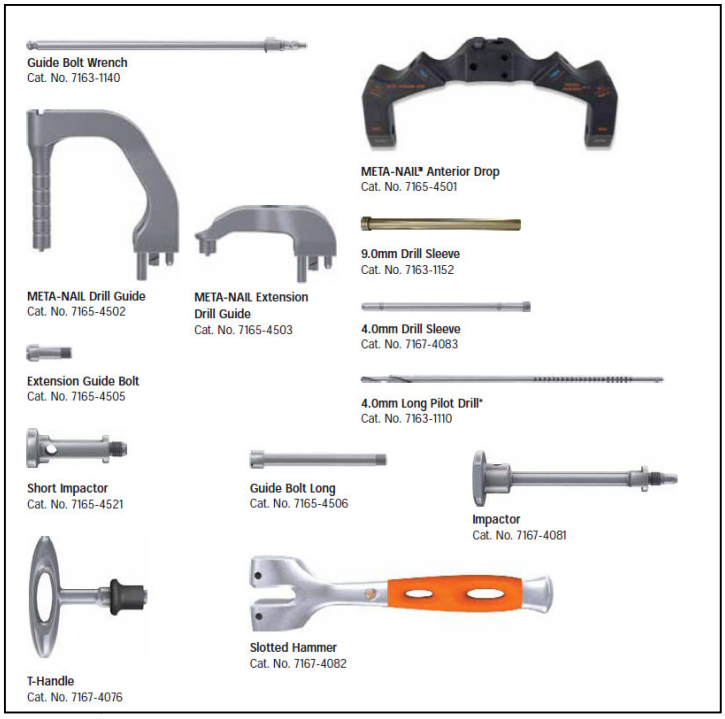

Figure 95: Instruments for nail assembly and insertion [8]

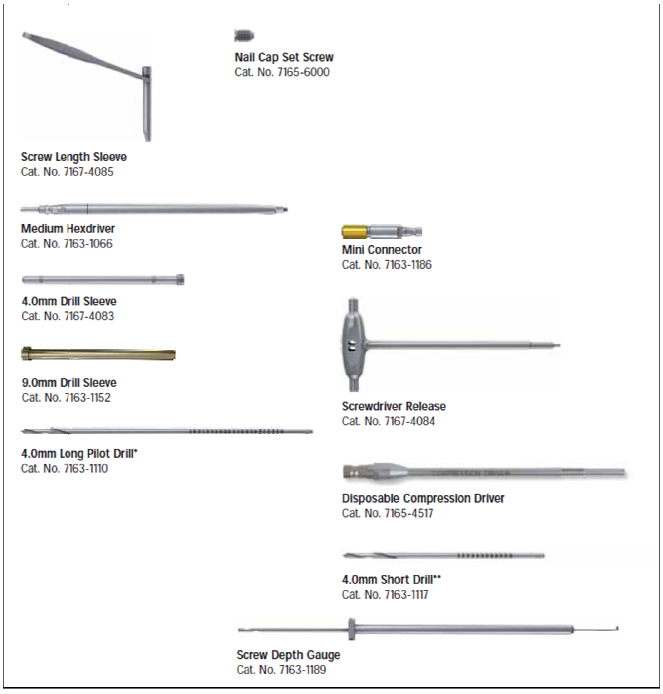

Figure 96: Instruments for standard, dynamic and compression locking [8]

Creation of access point for the IM nail

The animal was held in the supine position with the left tibia elevated between 80-90°. A longitudinal incision about 1-2cm medial to the midline was performed. The incision started at the level of between 1 and 3cm proximal to the superior pole of the patella and until the level of the

tibial tubercle. The muscle layer is incised between rectus femoris and the vastus laterallis. The joint capsule is opened with the insertion point for the nail at the anterior part of the tibial plateau immediately in front of the medial meniscus ligament attachment point. The approach is medial to the patellar ligament and lateral eminence. The patellar is luxated primarily to get access to the entry point. Intercondylar fat padding covering the anterior aspect of the crest is removed appropriately to allow access to the articulating structures. The initial incision for the entry point depends on the animal. The aim is for a reduced length which ensures the patella tendon is sufficiently luxated laterally but also reducing any trauma to the nearby tissue.

Entry portal acquisition – left hind limb

The 3.2mm tip threaded guide wire is joined to the drill via the mini connector and inserted into the proximal tibia to a depth of between 2 and 6cm. The path of the wire is established in the anterior-posterior (AP) and medial-lateral (ML) position. The honeycomb is used to deploy multiple guide pins to ensure that the trajectory is optimised in the AP and ML views. After placing the guide wire, the honeycomb and guide wires are removed and the 12.5mm flexible entry reamer is attached to the drill and advanced over the guide wire through the entry tube to a depth of 3-6cm. Figure 97A and 97B shows the x-ray fluoroscopic images acquired from the left tibia, highlighting the insertion of the guide wire. Figure 98 and 99 shows the flexible entry reamer attached to the drill placed at the entry point.

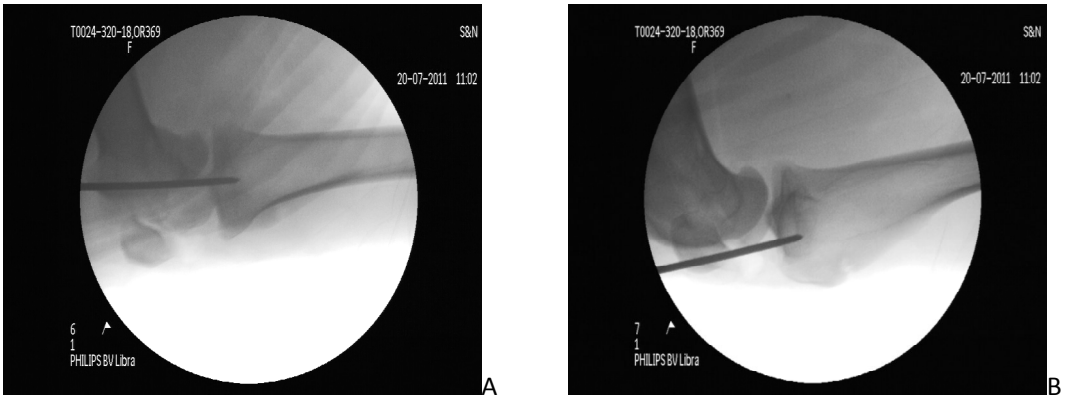

Figure 97: X-ray fluoroscopic images acquired from the left tibia highlighting the 3.2mm, Tip threaded guide wire inserted into the proximal tibia (A) A/P view, (B) M/L view

Fluoroscopy imaging is completed to ensure the position of the reamer is kept to avoid penetration of the posterior cortex. A flexible 10mm reamer is used throughout the medullary canal. The reaming is then increased to a maximum of 11.5mm to ensure the implant can be inserted into the canal whilst maintaining 3 point of contact.

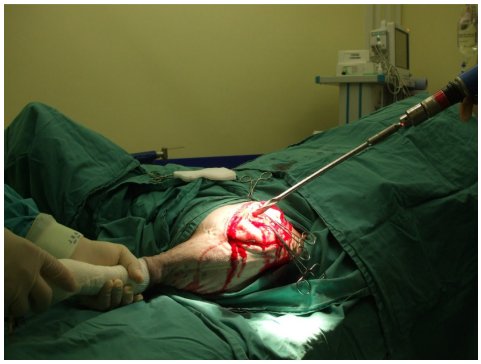

Figure 98: Flexible reamer entry positioned at the entry point with the leg in full extension

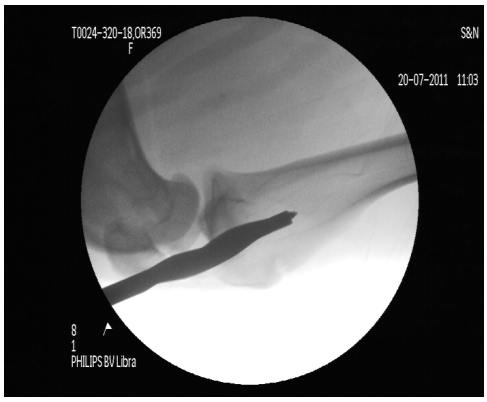

Figure 99: X-ray fluoroscopic image acquired from the proximal tibia in a lateral view highlighting the placement of the entry reamer

Creation of the midshaft osteotomy

The anterior drop is attached to the drill guide and targeting accuracy verified by inserting a titanium nitride coated 9.0mm drill sleeve and a 4.0mm drill sleeve into the drop. A 4.0mm long pilot drill is then passed through the assembly. A trial nail of 8-9 cm proximal section of a META nail is then attached to the anterior drop and distal targeter, which has a calibrated slot that lines up the midpoint of the nail. The drill guide assembly is orientated in either the AP or lateral position and the trial nail advanced over the guide rod using the slotted hammer to the desired depth. With the trial nail countersunk approximately 2-15 mm from the surface of the tibial plateau, a 1 mm wide osteotomy is created over the midpoint of the nail using a 1 mm thick oscillating saw. The action of the saw is controlled using a cutting guide and the bone held rigid using a pair of turkey clamps. The trial nail is not fixated to the bone enabling more freedom to control the version of the implant and the final position of the distal screws. Figure 100 and 101 shows the above described procedure.

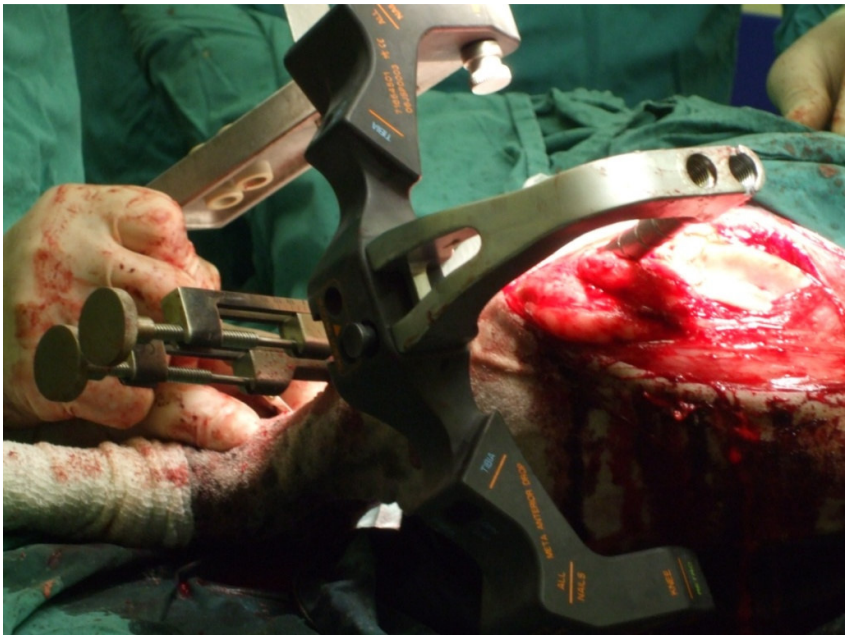

Figure 100: Insertion of a dummy nail attached to the anterior drop and the distal targeter for the creation of the osteotomy

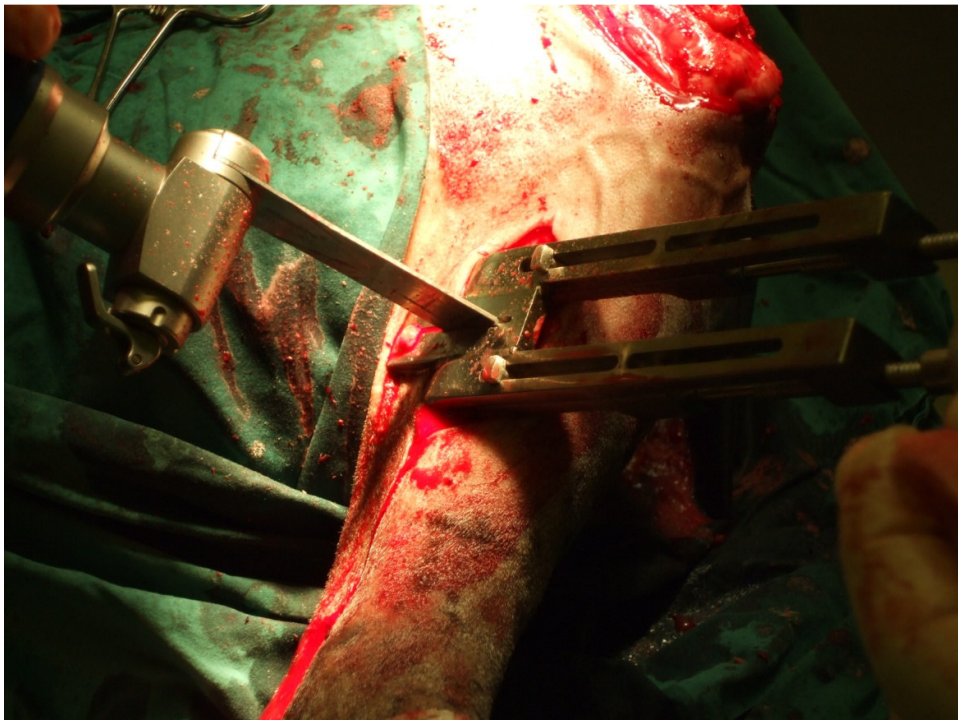

Figure 101: Creation of the osteotomy using the oscillating saw

Figure 102 shows an x-ray fluoroscopy of the osteotomy created on the midshaft in the diaphyseal region of the tibia. At this stage in the surgery, fluoroscopy is crucial to ensure bone integrity after the creation of the osteotomy.

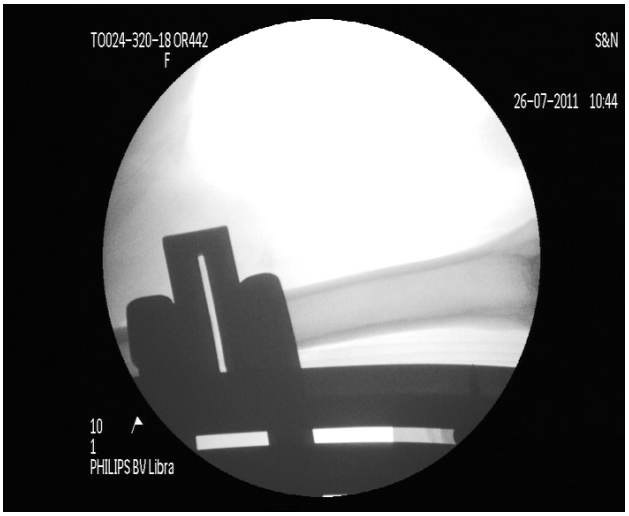

Figure 102: X-ray fluoroscopic image acquired from the diaphyseal region of the tibia indicating the position of the osteotomy

Insertion of implant

Once the osteotomy has been created, the implant is inserted in the medullary canal to a certain depth while being verified by the fluoroscope imaging. The nail is checked using the C-arm X-ray to ensure that it is anatomically aligned with respect to the mechanical axis of the tibia and the distal screw holes. Figure 103 shows the insertion of the telemetry nail after the creation of the osteotomy. Figure 104 shows the x-ray image used for the verification of the anatomical alignment of the nail.

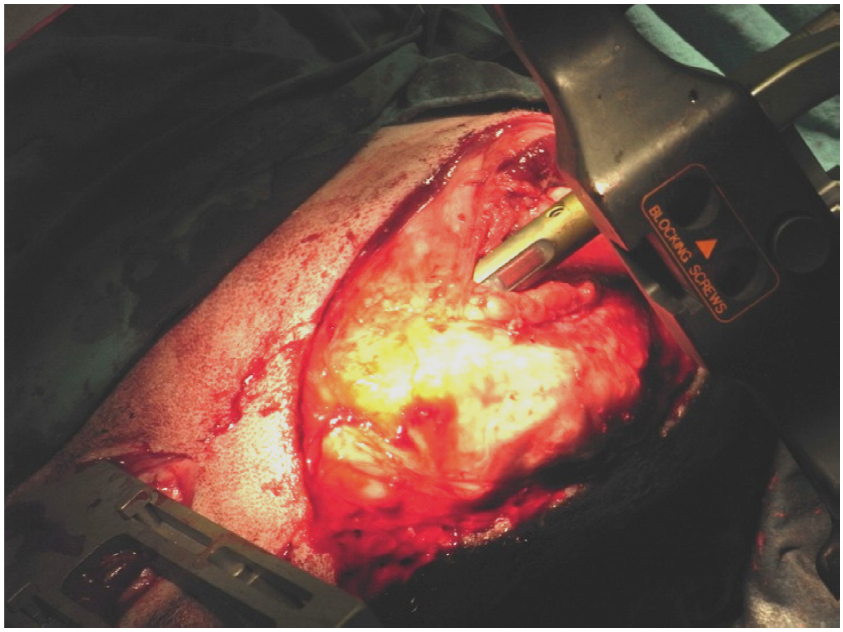

Figure 103: Insertion of the telemetric nail after the creation of the osteotomy; on the bottom left the distal targeter where the osteotomy is can be seen

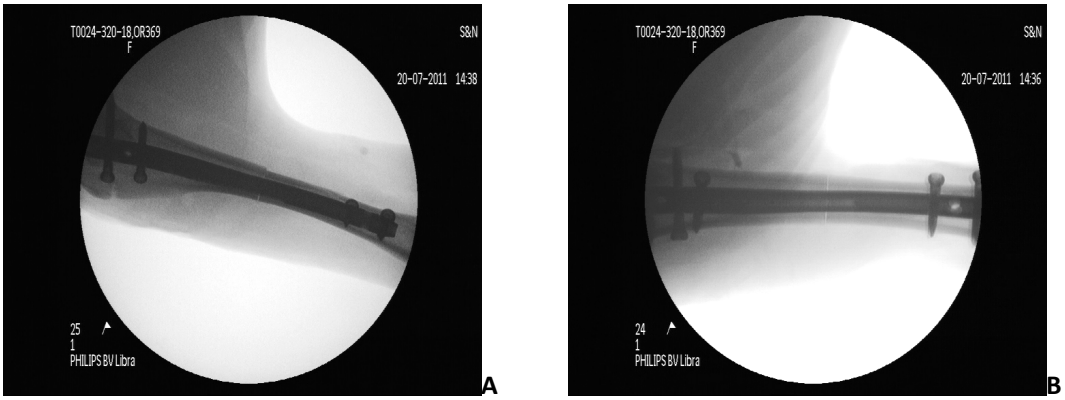

Figure 104: Digital X-ray images acquired immediately after surgery (A) lateral view, (B) A/P view

Proximal and distal screw locking and reduction of fracture

The distal locking screw is inserted first using the mechanical targeting guide. Incisions are made on the skin once the ML holes are located using the guide. The distal locking screws are inserted and measured using one of the techniques outline below as described in the TriGEN META-NAIL ™ Surgical Manual:

- "Gold" titanium nitride, 9.0mm drill sleeve, "silver" titanium oxide, 4.0mm drill sleeve and the 4.0mm long pilot drill
- Screw depth gauge
- Screw length sleeve and 4.0mm short drill

The most distal ML hole is threaded for stability. The compression drive is attached to the T handle and the assembly guide inserted through the guide bolt into the top of the nail until it contacts the most proximal 5.0mm locking screw. The compression driver is turned clockwise to drive the locking screw distally and compress the fracture. A dynamic locking screw is inserted through the proximal dynamic slot. Two additional interlocking screws are inserted in the proximal end of the nail using the medial and lateral slots in the Anterior Drop. Figure 105 and 106 are schematics of the distal and proximal screw locked in position from the surgical manual. Figure 107 and 108 shows the insertion of the distal and proximal locking screws respectively.

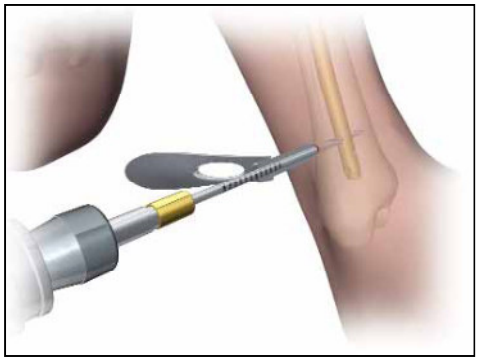

Figure 105: Distal locking screw

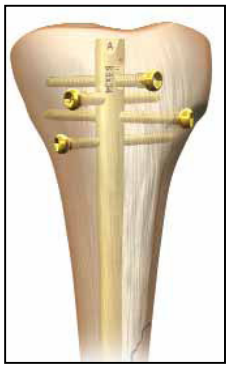

Figure 106: Proximal locking screws

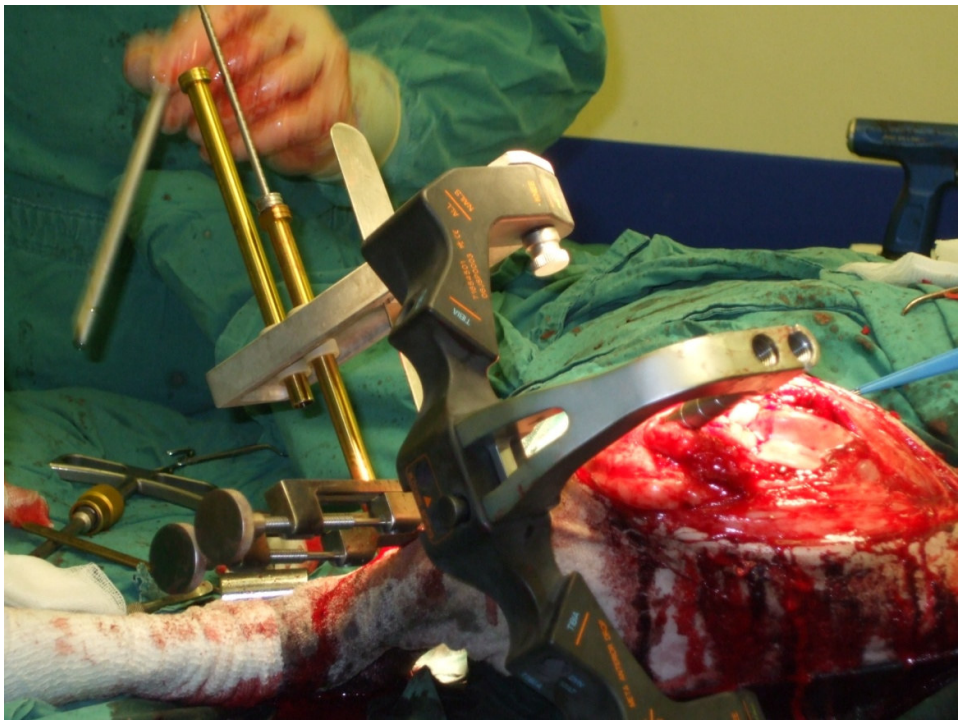

Figure 107: Positioning of the distal locking screws using the gold and silver sleeves

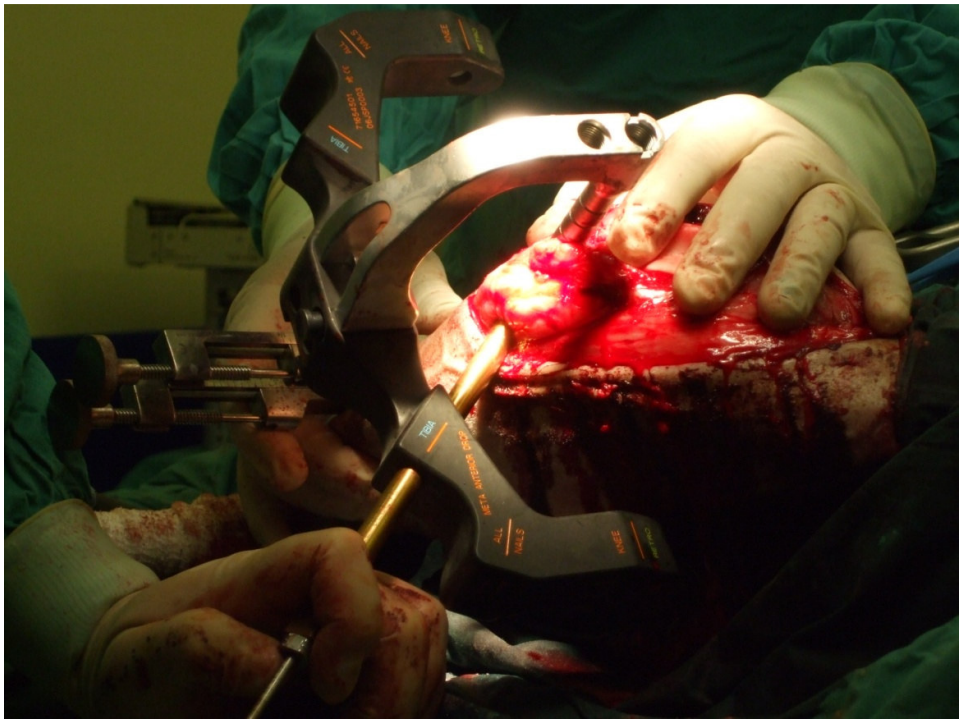

Figure 108: Positioning of the proximal locking screws using the anterior drop

Once the screws were in place, a final x-ray was taken to ensure everything was in place and the access point was closed. The animal was taken to recover in their pen and monitored by the hour ensuring the animal is fine. These animals were selected to assess the welfare issues that may be taken into consideration while designing the loading rig that would be in use for the live phase study. The next section will examine the tests that need to be conducted and the evaluation of designs that have been prototyped before choosing the actual final design to be refined and used.

5.3 Rationale of loading rig design

The three testing described in Chapter 4, have been proposed to evaluate the progression of the fractured bone healing *in-vivo*. These tests would require the animal to be under general anaesthetic on the X-ray table to ensure patient compliance is attained. The aim of the rig is to simulate all the test performed *in-vitro* so as when applied *in-vivo*, the data can be compared and hence gain better understanding of the progression of healing. The tests to be performed *in-vivo* are as follow:

- Torsion testing under general anaesthetic using a customised loading rig
- Axial compression bending under general anaesthetic using a customised loading rig
- 3 point bend test under general anaesthetic using a customised loading rig

The review and design components of this rig were distributed between UCL and Brunel University respectively. The tests to be performed as mentioned above had to be reviewed before any design could be initiated.

5.3.1 Torsion testing

According to Nordt *et al*. [9], torsional loading can help better understand the biomechanics of the knee *in-vivo* by recreating the mechanics of a normal knee. The rationale behind the torsional load testing is that this loading technique has the benefit of isolating the output from the strain gauges bonded onto the intramedullary nail from the relative position of those gauges with respect to the fracture. Though the application of this load required the used of adjacent anatomy to effectively apply the torsional load along the long axis of the tibia, both in the ovine and human model, this technique has proven to be effective for load transference as described by Nordt *et al.* [9].

Experimental studies by Wallace et al. [10], describes the fracture repair in an ovine tibia fracture model in which the osteotomy is fixed with an external fixation device of known stiffness. He introduced a gap during fixation to investigate the effects of fracture micromotion. Interfragmentary movement during gait was assessed and recorded at day 7 ranging from 0.8 to 1.4mm and decreasing to 0.2mm by week 5 as fracture healing started. These displacements were induced by the ground reaction forces of around 30% of bodyweight. Torsional stiffness was observed to increase from 0.06Nm/degree on the 14^{th} day to 1Nm/degree on the 42^{nd} day, compared with 2.55Nm/degree in intact bones. Seebeck *et al.* [11] used gait analysis to monitor tibial fracture repair in sheep. External fixators were used to fix the fractures and in order to allow micromotion a 3mm gap was introduced. Axial compression observed at the fracture site during gait analysis was initially between 0.4 and 0.7mm before decreasing to 0.3mm 5 weeks postoperatively. Torsional movement of 1° decreased to about 0.6° when healing progressed.

Schneider *et al.* [12] also studied femoral healing with an instrumented IM nail, using various loading protocols. Partial weight-bearing at was performed at 150N and 250N and axial load induced by voluntary isometric quadriceps contraction was also measured. A torque test was performed with the hip and knee flexed to 90°, and an orthogonal force of 35N was applied at the ankle, resulting in a torque of 11 Nm.

5.3.2 Axial compression

Axial compression has been conducted in many studies with successful outputs during fracture healing. Strain output is independent in relation to the positioning of the strain gauges and the fracture if there is no bending. However, the sensitivity will be dependent on the fracture reduction and the bony contact at the fracture site.

Studies conducted by Seebeck *et al.* [11] shows axial displacement of 0.4 to 0.7mm while Wallace *et al.* [10] recorded displacement of 0.8 to 1.4mm during the early fracture healing. These displacements are related to ground reaction forces. Seide *et al.* [13] used an axial force of 100N in clinical trial evaluating a telemetric plate during stance phase of the gait cycle.

5.3.3 Three point bend test

Three or four point bending test should be a fairly straightforward test to perform *in-vivo*. This is because the antero-medial aspect of the tibia is covered only by a soft but thin covering of tissue. However, measurement will strongly depend on the orientation of the callus relative to the plane of bending and the strain output will be dependent on the positioning of the gauge and fracture site.

Published studies using sensors connected to external fixating devices have been conducted by Claes *et al.* [14]. The experiment consisted of an orthometer attached to an external fixation device to measure the bending of the fracture. 15Nm/degree was the stiffness required to help in clinical decision making regarding the removal of the frame. However, there is still difficulty to get accurate load and angle to replicate the simulated experiment in practice.

Taking into consideration all the above rationale and previous studies conducted *in-vivo* for the tests to be performed; a design was created originating from Brunel University. The next section will look at the detailed design of the *in-vivo* loading rig.

5.4 Design and description of loading rig

The design was initiated by taking some cadaveric measurements of the sheep leg as the main user of the rig would be during the live phase study. Figure 109 shows measurement being taken on a cadaveric ovine leg at the test facility.

Figure 109: Ovine Measurements

Once the necessary measurements were taken, solid modelling and assembly was conducted using Solidworks 2010-2011 Student version. Figure 110 show two different orientation of the assembled loading rig.

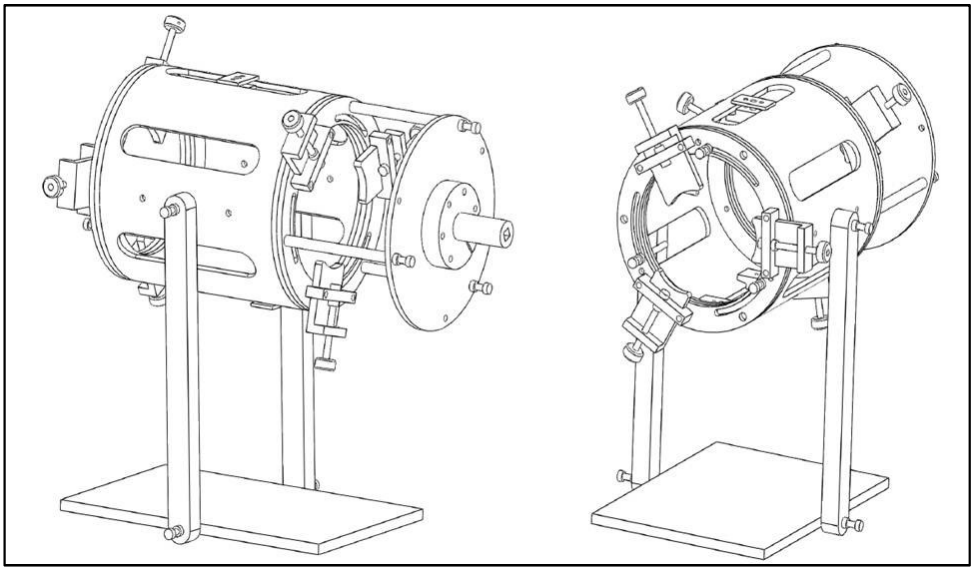

Figure 110: Loading rig assembly

This assembled model was prototyped using glass reinforced polymer (GRP) for the cylindrical housing and the rest of the components were made of either aluminium or stainless steel where more strength was required. Aluminium was chosen because of its light weight. The cylindrical form structure was designed to pass over a leg unhindered. GRP was chosen for the cylindrical housing so that any electrical fields are not trapped due to Faraday cage effects. This was the only way to ensure that the coil for the instrumented nail is not hindered in its function. The cylindrical structure had two circular sub-structures each concentrically placed at either ends with a rotatable ring fitted to them. The rings were equi-spaced and able to rotate through an excursion of 40° each. Both rotatable rings had a minimum of three radially extending or contracting components changeable by means of a screw thread arrangement. The radial movement is engaged to the central axis of the cylindrical structure to compress against soft tissues. The radially applied compressive force is transmitted through the soft tissue to the bone structure. The distal ring is kept in fixed position in relation to the fracture site and the proximal ring is fitted with equidistant extending or contracting jack can be manually adjusted to accommodate different anatomical geometry and aspect. The point of contact between each jack and the soft tissue on the leg is concave and equipped with a silicone elastomer to allow uniform distribution of forces.

The cylindrical housing is attached to a platform that supports the assembly by means of a parallel oriented plate with two pivotable arms secured using screw and nut fixation. The arms can move

transversely in an arc of 180°. This assembly allows both angular adjustment and elevation providing the flexibility for the leg to maintain a natural physiological position. The design was given more flexibility when the tubular spacers placed on the distal end were manufactured in three different sizes of length 6cm, 10cm and 20cm. The dimensions of all the components are shown in the manufacturing drawings that can be found in Appendix G. At the end of the spacers, a metal plate, the same size as the distal rotatable ring was fitted secured with nuts and flat washers. At the centre of the round plate another set of holes are generated and a custom-made transducer holder with a matching set of holes as the plate is fitted on the distal end.

The transducer itself was developed and manufactured at UCL. Every component of the rig was manufactured at Brunel University. The prototype was tested on a step by step basis on an ovine model. Figure 111 shows the GRP housing being tested for dimensions on the ovine leg. Figure 112 and 113 shows the whole assembly as a prototype being tried out on the ovine model. The external loading rig was inserted through the GRP housing and the jacks locked against the soft tissue. It was immediately noted that the static plate with the transducer holder had to be oriented obliquely to match the soft tissue. It was also noted that the GRP housing was too closely positioned to the static ring. The end faces of the jacks also did not engage with the soft tissue surfaces. The distal jacks were also too close to the medial malleolus.

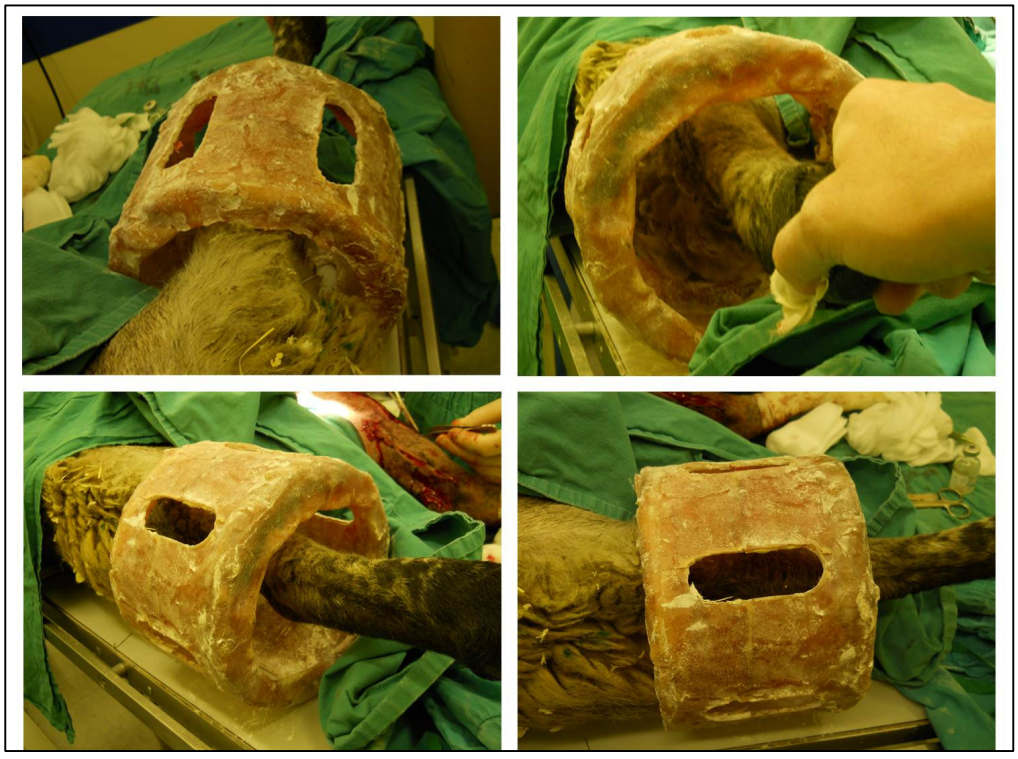

Figure 111: The glass reinforced polymer housing being trialled on its own on an ovine model left hind limb

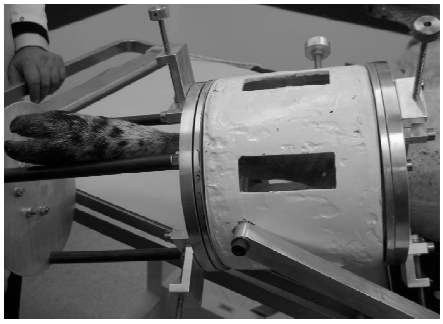

Figure 112: The whole construct together modelled on the ovine model left hind limb

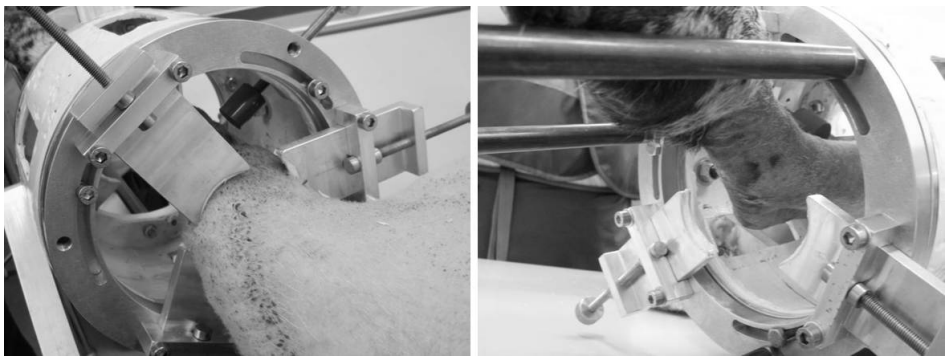

Figure 113: A close-up on the area where the jacks meet with the skin of the ovine model

The GRP housing was eventually removed to enable the distal and proximal support plates positioned in the optimum locations. Figure 114 shows the try out without the GRP housing.

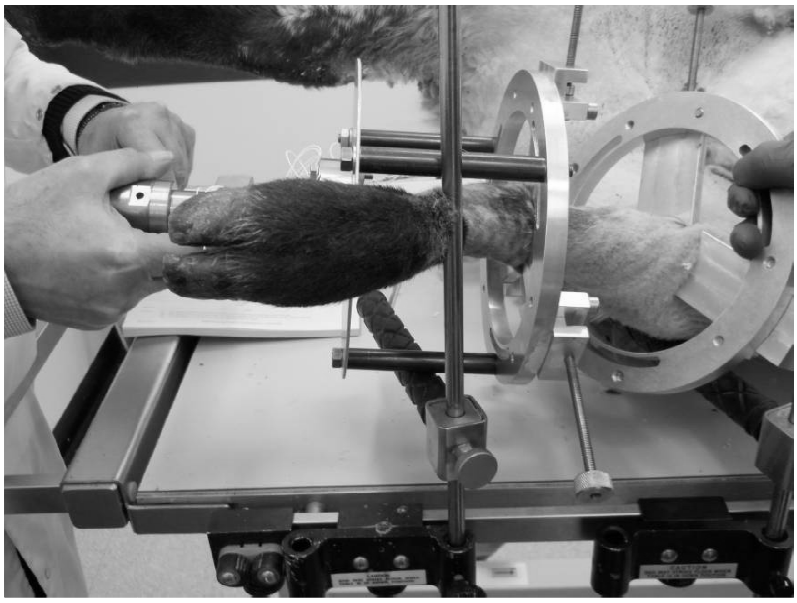

Figure 114: Trying the construct without the support of the GRP housing to assess its feasibility without the housing component

Again it was immediately noted that the contact between the jacks and the soft tissue needed to be adjusted. The design changes were made but in the meantime a less bulky and more straightforward design was created by Smith & Nephew, Memphis, USA. It was in the shape of an orthotic shoe where by some parts such as the transducer holder and transducer could still be used on this design. Figure 115 shows the new orthotic shoe design with the transducer and torque wrench placed on the alignment jig developed from the platform that was attached to the original loading rig design.

Figure 115: Orthotic shoe with velcro straps design by S&N Memphis to simulate and apply the torsion on the ovine leg

The original loading rig design may not have been suitable for ovine use but it was modelled on a human leg and Figure 116 shows illustrates the potential use in clinical settings.

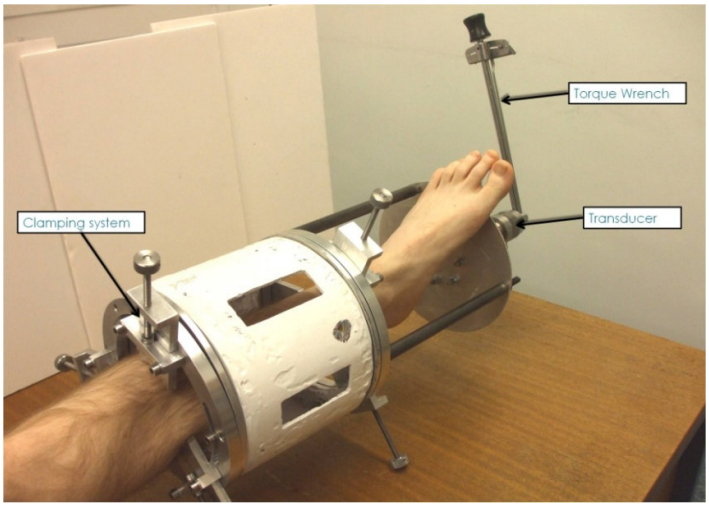

Figure 116: The device was modelled on a human leg showing the potential for use in clinical settings

The design prototype shown above has been submitted for a GB patent application; Patent application number 1104239.7, A post physical trauma physiological test instrument. The whole assembly as presented in Figure 116 had just been put together and modelled on a human leg without the application any torsional forces on the actual tibial model. It fits the human tibia

without any concerns and can potentially be used in the future as a torsional testing device for human subjects.

The compression and 3 point bend test for the ovine model was consequently modelled in close collaboration between Brunel University and Smith & Nephew, Memphis, USA. The transducer was the only component manufactured at UCL for all the tests components. Figure 117 and 118 shows the axial compression rig and the 3 point bend test respectively.

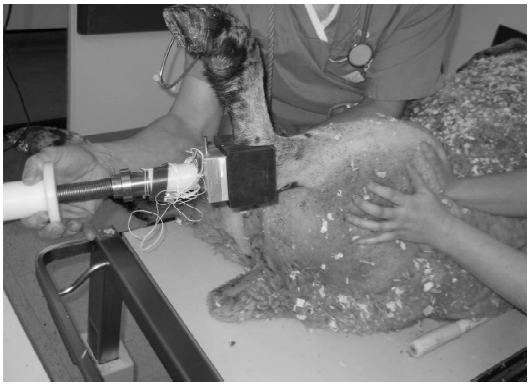

Figure 117: Axial compression test equipment being tested on an ovine leg

The orthotic shoe was designed and manufactured by S&N, Memphis, USA while other than the transducer the rest of the components were designed and manufactured at Brunel University. Figure 118 shows 3 point bend test that was used during this pilot study.

Figure 118: System simulating a three point bend test on an ovine leg

A custom made stable platform for a 3pt bend test was used. The distance between each leg support was set at approximately 16 cm. Placing the tibia across the loading supports parallel to the reference bar was challenging and took a great deal of time. Furthermore, the combined weight of the leg with the dead weights tends to cause the apparatus to sag at the distal end. This was addressed by ensuring the leg is more stable and secured before the test.

This pilot study led to the next phase of the project which involved the *in-vivo* testing of GEN IIIa instrumented wireless nails in an ovine model. However, prior to *in-vivo* testing, the nail was tested in a cadaveric model with the coil on an excised leg was done.

5.5 GEN IIIa wireless telemetered nail and reader/energiser system

GEN IIIa nails were designed in three stages, GEN 3a, 3b and 3c. GEN 3a to 3c saw the changes of materials used for the flexi to a more compatible and medically compliant material. The nail used is a paediatric nail of 150mm in length. The system is made up of the nail, a reader and an energiser coil. The nail has 1 master site and 1 slave station. There were 6 thin film strain gauges that were instrumented by SMD. Four gauges were oriented 0° and 2 gauges at 45° to the nail axis. Figure 119 shows a UniGraphics close up of the machined pocket. Figure 120 shows anterior pocket with instrumentation of a GEN III nail.

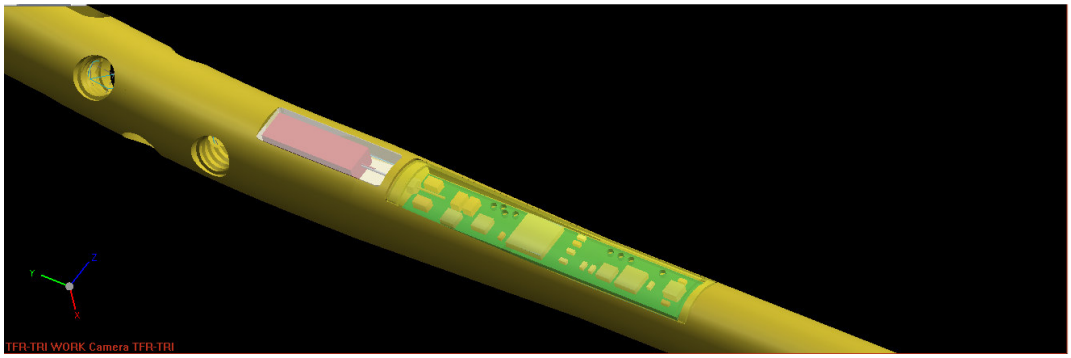

Figure 119: GEN III machined pocket with instrumentation schematic

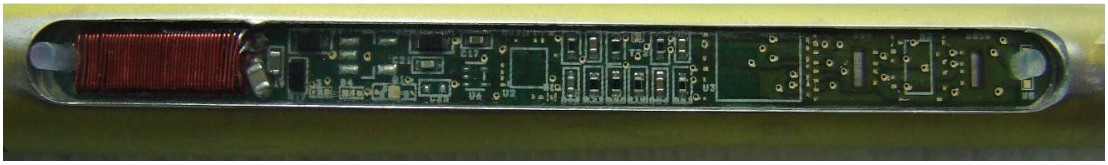

Figure 120: Instrumented pocket of GEN III Nail

The nail showed in Figure 119 is connected to a wireless system with an energiser and detector to a laptop where the raw data is streamed live. The energiser/reader system is found in the patient box which powers the implant and then demodulates the signal from the nail back to the receiver which is connected to a laptop via an RS232. The external coil is connected to the patient box. The data is received in LabView as raw data. The processing of the raw data from GEN 3a is much

simpler than GEN I and II. The user has to subtract each channels count from the baseline count (zero load count) and then divide by 46. A special Graphical User Interface (GUI) has been developed for this study. The GUI is also being tested and validated for ease of use by clinicians. Prior to the implantation of the nail for pre-clinical trials in the ovine model, the system underwent a pre-implantation testing in a cadaveric limb.

5.6 Cadaveric trial for telemetered nail and coil

The cadaveric trial for the telemetered nail and coil system has been conducted at UCL for the pre-implantation testing of GEN III nails. The trials were performed on an excised left hind limb of a sheep, surgically prepared to receive the nail. This trial was being conducted in order to verify the functionality of the energiser/reader system and an attempt to record strain data. Figure 121 & 122 on page 173 shows the various loading conditions applied to the model. The first recorded measurement of the wireless system was a reading taken of the nail inserted in the bone without any load applied. The next reading had the nail in the bone with compression loading manually applied simulating as closely as possible the axial compression loading described for the biomechanical tests of GEN I & II. The third and final set of data using this set up was the application of a 10kg load across the midshaft of the bone with the nail implanted simulating a 3pt bend test. The microstrain results were plotted and presented in Figure 121. Figure 122 presents the fluctuations in the 10 seconds recorded strain readings. Only one GEN III nail was tested in a cadaveric limb prior to implantation.

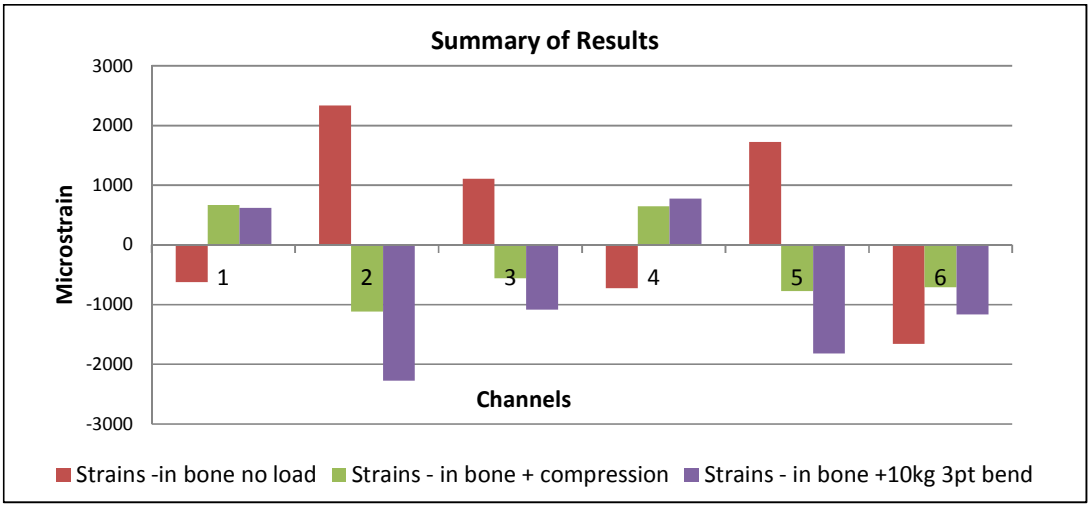

Figure 121: Loading of a GEN III nail in a cadaveric left hind limb to assess the functionality of the system

Key for Figure 123:
SD: Standard deviation,
IBNL: nail in bone no load,
IBC: nail in bone compression loading applied,
IB10kg3PBT: Nail in bone with a 3pt bend test of 10kg loading

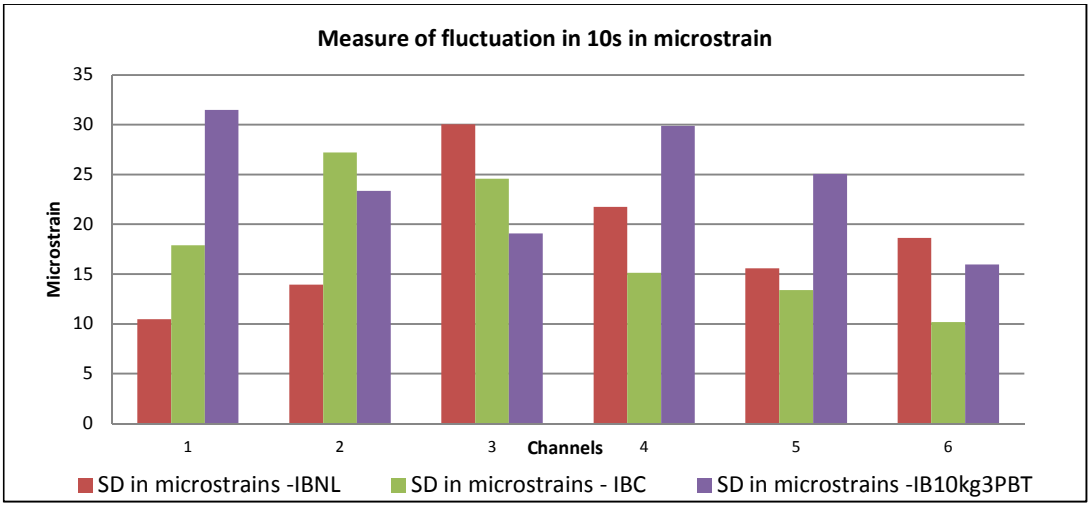

Figure 122: Standard deviation of strain measurement for three different loading protocol to assess the fluctuations in the strain for 10s

As it can be observed in Figure 122, the graph illustrates the different loading of the bone and the strains measured. This experiment was conducted on an excised limb prepared to receive a nail. The strains were measured once the nail was implanted with no load. Three of the gauges are observed to be compression and the other three in tension. As soon as some compression forces were applied, the strain readings show a change with previously compressive forces now in tension and vice versa. The strain readings were similar to compression readings when subjected to a 3pt bend test with a load of 100N. Standard deviations were conducted on all three sets of readings for the 10 seconds of data recorded ensuring there is no anomalous data. A set of readings were taken for the nail in air without any load as a baseline measurement. The strains measured were high, reaching magnitudes of above 80,000 microstrain. This successful pre-implantation testing led to the pre-clinical trials conducted by Smith and Nephew. Despite, the optimistic perception of the system at this point in time, it should be noted that the system was being tested in a cadaveric limb without the association of any muscle forces and bodily fluids. This cadaveric trial is very important at this phase; however it would be better if this same pre-implantation testing was conducted more than once using more than one nail in saline in order to have a statistically significant set of data validating the functionality of the whole system.

5.7 Pre-clinical trial

The live phase study was designed to gather information to power a future study with the objective to demonstrate that fracture healing status can be determined by taking strain measurements from an instrumented nail. The study was conducted in accordance to the Animal Study Authorisation document can be found in Appendix F. The study was coordinated by a specialist from Smith and Nephew, York Research Centre. The project license number and the work request number associated are 60/3643 and WRQ-TO024-320-18 respectively.

The animals selected for the study were ovine Blue Faced Leicester Cross Suffolk ranging from 2 to 2.5 years old. 12 sheep were selected for the study. Their medullary canals were measured under general anaesthetic and the animals were trained for the different prescribed loading activities. 3 out of 12 sheep were euthanized during surgery due to complications associated with the surgical procedure. Another sheep died approximately 12hrs after surgery due to excessive bleeding into the intestines. Instrumented nails were successfully inserted into 8 sheep. However, one of the 8 remaining sheep had to be euthanized at 31 days due to persistent lameness in the operated limb cause by a damaged ligament. The nail was left in the limb and the bone was excised and subjected to mechanical loads described in section 5.8. All the sheep followed the same surgical protocol as described in Section 5.2.

The remaining instrumented nails were successfully implanted. Strain readings were going to be taken at various stages of the healing process. Strain readings were taken prior to implantation in air and immediately after surgery. Figure 123 shows the intra-operative strain data, the change between pre-operation and post-operation. The maximum post-operative strains observed are 1800µstrains. Nail 7, channel 1 and 4 were ineffective during pre-operation, so the data was invalid while channel 3 and 6 were observed with moments of 25-30Nm in the out of plane direction. Nail 9, channel 2 was ineffective post-operation hence the unrealistic high strain value. Similarly large strains were observed in Nail 6 at 45° which is difficult to explain but would most probably be due to large torque of 30Nm. However, this is unrealistic as the nail is most likely to break from such torque.

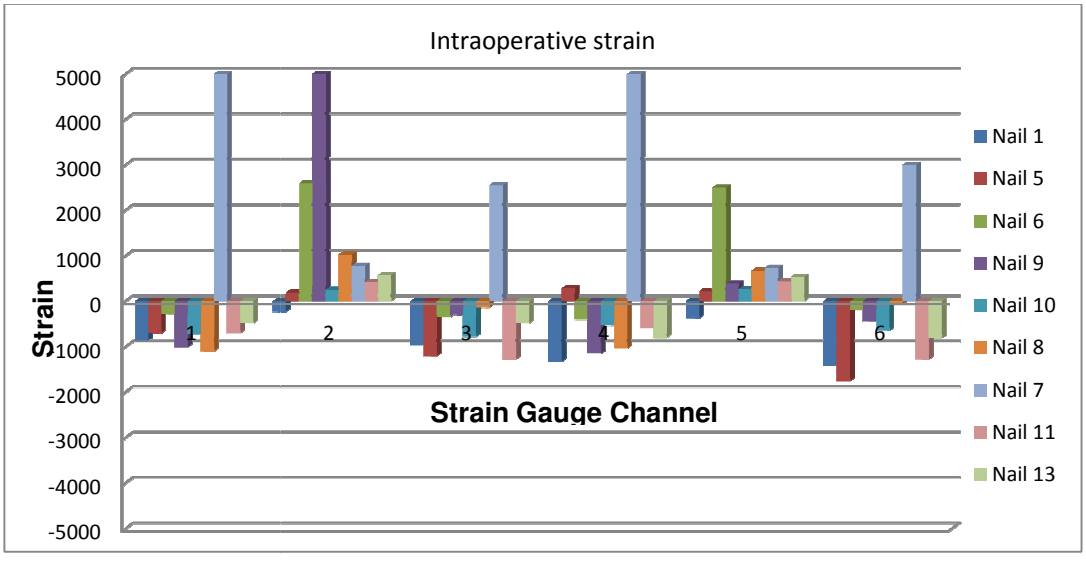

Figure 123: Intra-operative strain of the implanted wireless nails measured before and after surgery

The aim of this live phase study was to monitor healing while conducting a set of loading protocols using custom-made loading rigs and interfaces. However, 2 weeks post-op, when the

readings were taken, there was no signal received from the nail. This factor was repeated throughout the study with some sheep receiving very weak signals and some data could be recorded while others seem to have failed. The failure was associated to be most likely due to instrumental error caused by mechanical failure. It was assumed that this was due to the wire bonds which were the most fragile component in the system and the tight fit space for the implantation without over-reaming could have caused its failure. This mechanical failure is similar to what occurred in the biomechanical testing of GEN II nails. The machined pocket where the instrumentation was placed was encapsulated using medical grade adhesives instead of the industry approved electron beam welding. The use of a soft encapsulant as well as the wire bonding processes for the electronic components were decisions taken by the manufacturer in order to reduce the manufacturing cost in the long term.

The nails were left in the sheep, the x-ray images were taken according to schedule and the sheep were euthanized as previously planned. Temperature counts were taken when the signal was available and strong enough to record data for at least 5 seconds. The temperature data were calculated when available. Temperature can be interpreted in terms of healing as if there is a sudden spike in the temperature reading; there is most likely an inflammation of the tissue. The temperature data can be found in Appendix H.The sheep that was euthanized due to lameness had its tibial bone excised and it was one of the fully functioning nails. The nail was used in an *in-vitro* biomechanical study to try to assess at what point or how the nail is failing so as to prevent the same technical issues in the next generation system.

There was no data to be analysed from this live animal study. This was due to the failure of obtaining any live signal for data streaming when the energiser was used to activate the nail. This was the case for all the remaining nails. The few readings taken of temperature is beneficial however, this study did not complete what it was set to do. The nail design and development had to be reassessed. The excised tibial bone with the GEN IIIc still implanted was tested biomechanically to further understand the failure incurred in the other nail.

5.8 Excised cadaveric nail trial

The tibial bone was excised, frozen and sent to UCL where the biomechanical tests were to be conducted. Figure 124 is a picture of the excised bone instrumented nail. The screws are visible and the fracture line is not visible anymore which shows that in 31 days healing have occurred and the callus have bridged but the question remains as to how mechanically ready is it.

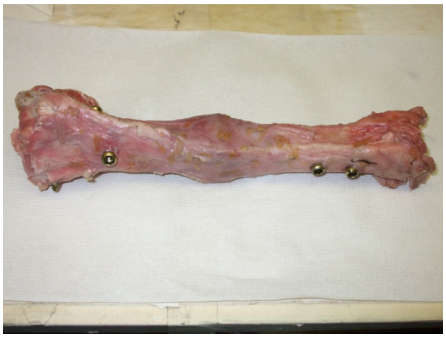

Figure 124: 5 Weeks old excised ovine tibia with nail in-situ and the screws visible

The bone was subjected to be both static and dynamic loading while with the healed and bridged callus. The nail was then removed from the bone and the bone was re-fractured at the original fracture site before the nail was re-implanted and tested biomechanically again. The distal end of the bone had to be cast in using bone cement for a stable fixation on a Zwick compression testing machine. Figure 125 shows the bone cemented to provide a platform.

A load of 200N, 500N, 1kN and finally back to 200N were applied. The nail was pre-soaked in saline and then inserted into the medullary canal. Strain measurement was recorded from immediate removal from saline through to insertion in the canal and after locking the screws in place before being placed onto the Zwick compression machine as shown in Figure 125.

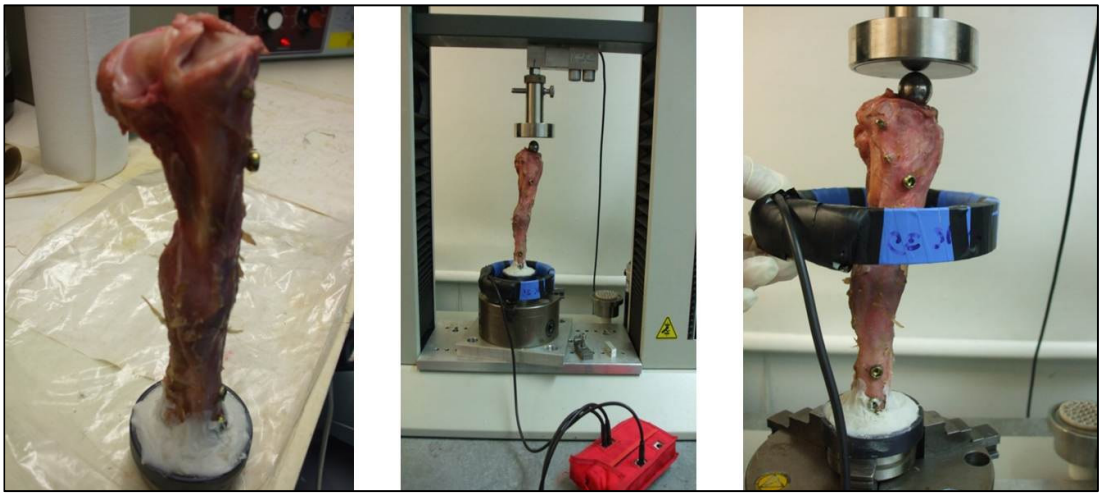

Figure 125: Excised bone set in bone cement at the distal end before being placed in a Zwick test machine with the induction coil and the patient box connected to monitor strain reading

The nail was dried in an oven at 60°C for 48hrs in an attempt to remove the hysteresis from the strain gauges. The nail bone construct was exposed to cyclic compression load from 200N to 1500N. Each strain gauge could detect a change in load from its baseline position (no load) up to 1000N and back to the original no load position as shown in Figure 126.

The fact that the nail still implanted was still functioning without any sign of failure seemed to be a positive aspect. However, it should be noted that the nail has been in a live animal for approximately 5 weeks and would have probably been the only functioning system had the animal healed without lameness. The cyclic loading shows that the nail has the ability to function as it was designed to perform and that there is still an unexplained aspect that requires further investigating as to what would cause the failure.

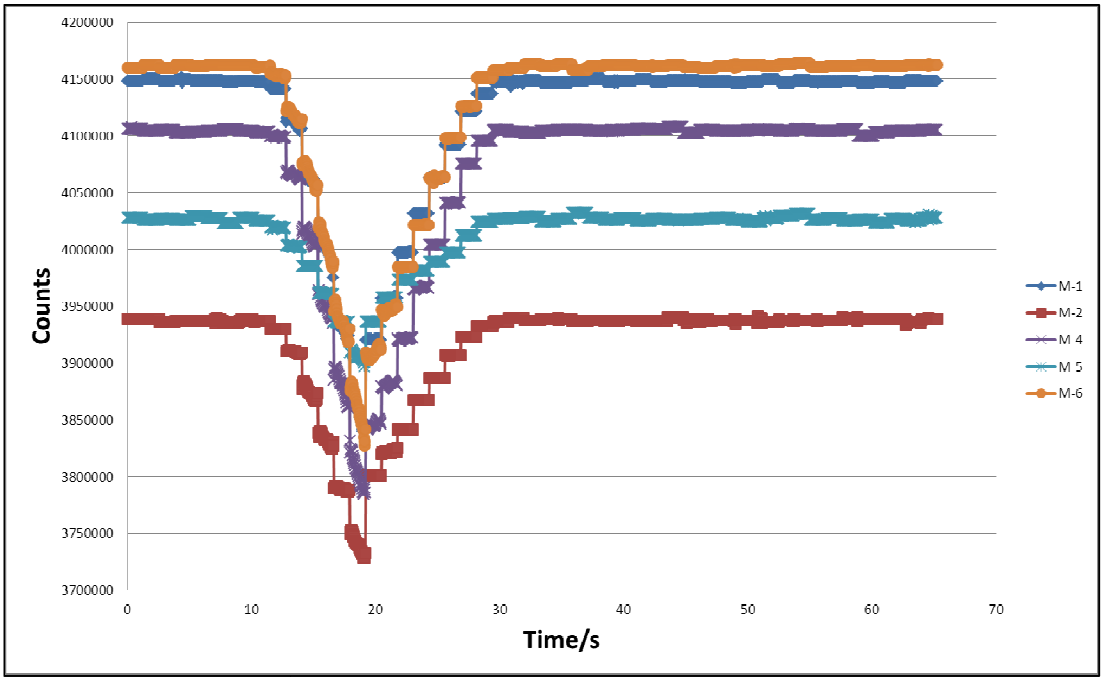

Figure 126: Cyclic compression loading of the excised bone up to 1000N for 60s

Prior to a transverse cut was made through the callus to the original fracture site, the bone was subjected to an x-ray computed tomography imaging analysis (XCt) over 50mm of the callus. 25 sliced imaged were taken at 2mm intervals. The images are shown in Figure 127. The series of picture show the medullary canal with surrounding tissues in four different colours. The colours in the pictures are further explained; grey denotes the soft granulation tissue of the bone callus. The red and blue mixture illustrates the fibrous tissue which is slightly harder. The white area show mineralisation has occurred which is harder immature bone tissue.

This is a very interesting and crucial finding regarding callus tissue of a healed bone at approximately 5 weeks old. Without the lameness, this animal would have healed and achieved clinical union as scheduled. This data is particularly interesting since Chapter 4 investigate the idea of creating composites to mimic those same tissues as observed in the CT images. Due to time restriction, this bone callus tissue would have been an excellent candidate to test the different tissues mechanically in an SEM showing the characteristics of the fibres holding it together.

Lameness of the animal was due to a ligament that could not be treated. With the right prescribed set of loading regime, the nail has the ability to function and monitor healing however this is yet to be tested. The CT images are also particularly interesting as it shows yet another variation in relation to the distribution of the callus morphology. These images show the challenges that are present in predicting callus morphology without the knowledge of the forces the tissue are sustaining.

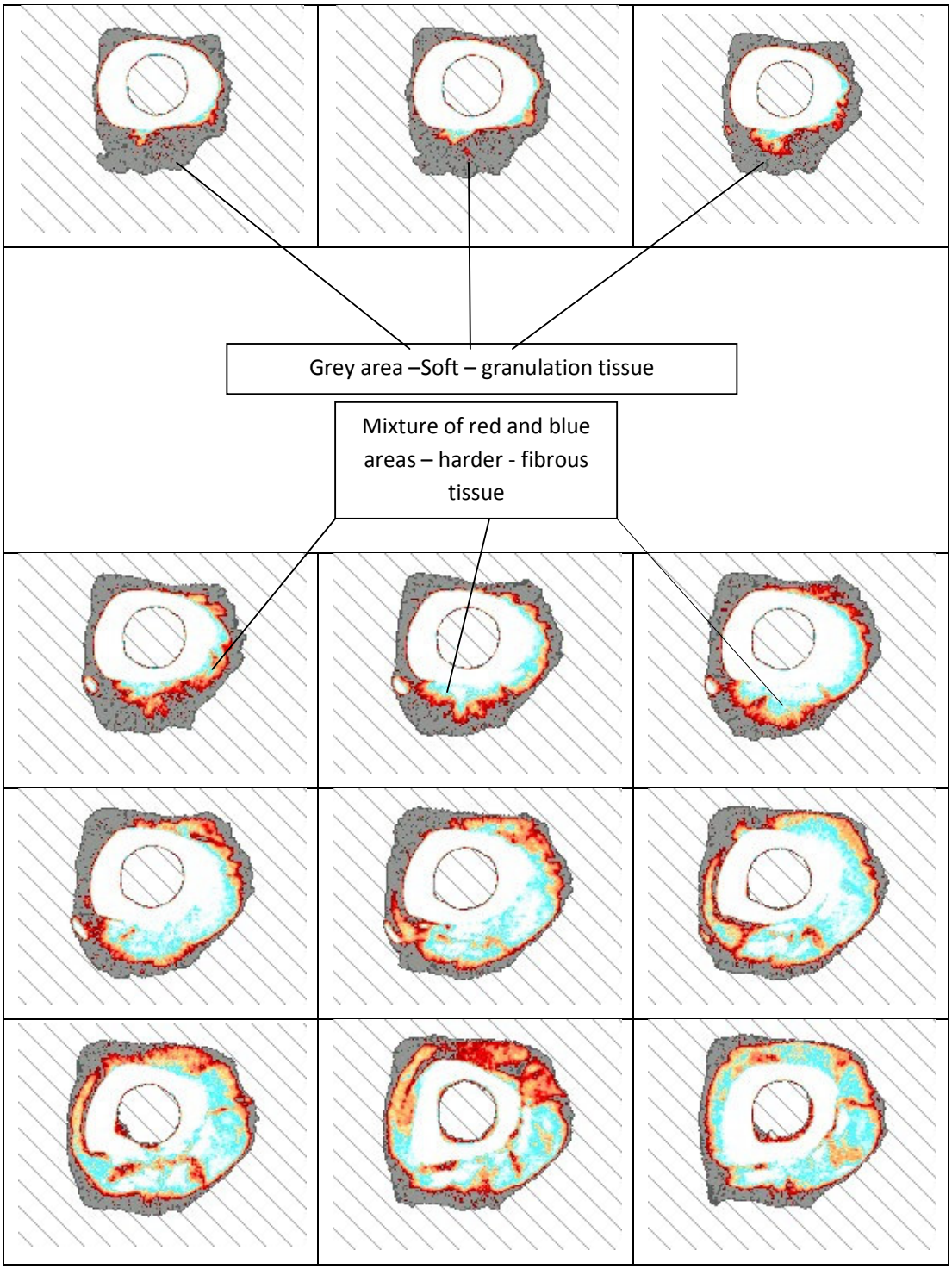

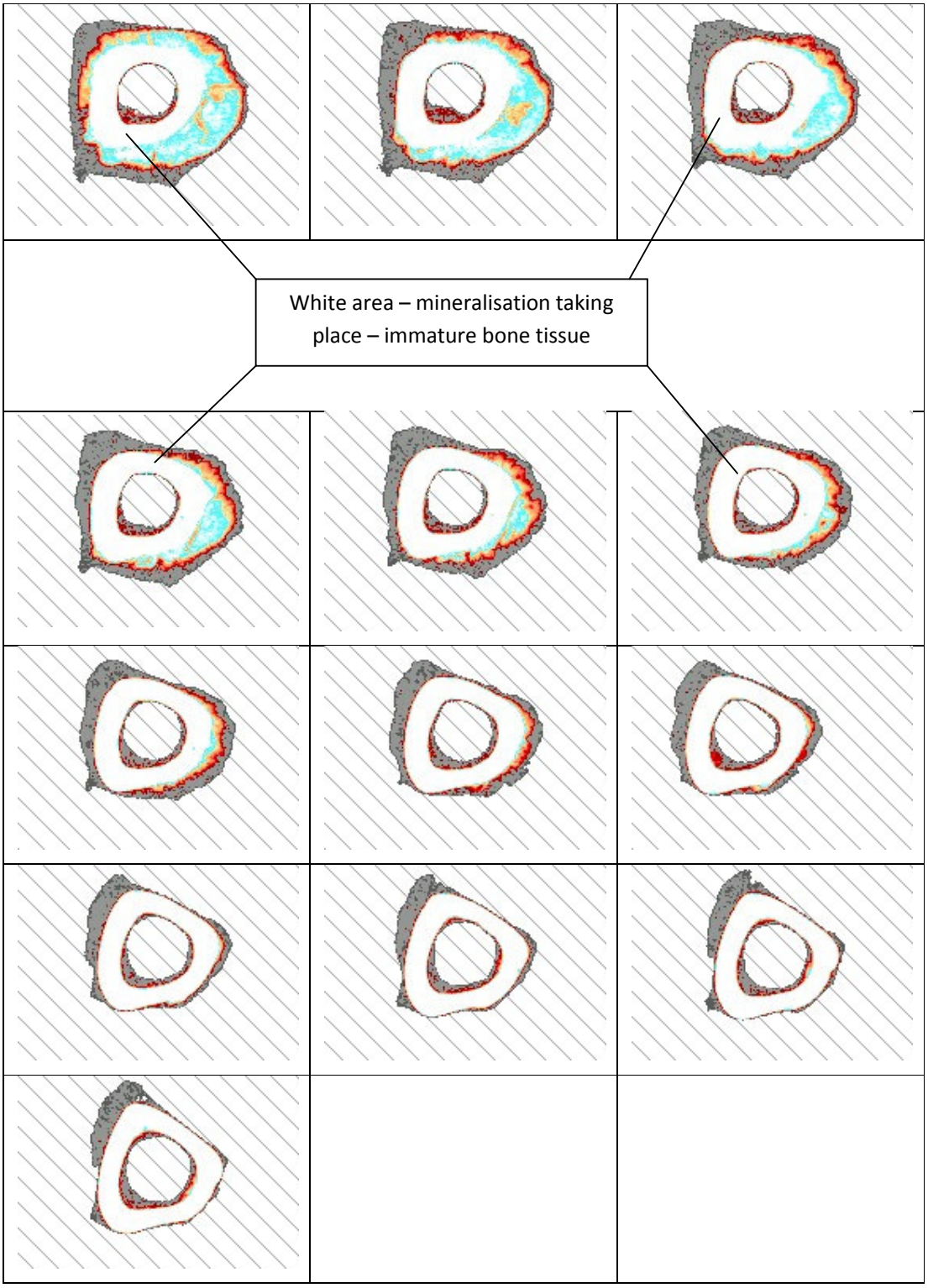

Figure 127: CT images of the bone density of the 5wk old healed callus tissue over 50mm

X-ray CT is a way to look at the density of bone. The different colours show the region of interest with grey being the soft tissue and white the mineralised tissue. The observations that can be noted are that at 31 days mineralization is quite widespread. The callus is fully bridged and after the dynamic testing, it can be assumed that without the ligament damage encountered by this animal, healing would have been successful in the time scale expected.

A transverse cut was made using a saw at the original fracture site as shown on Figure 128. The bone was held back together using the nail re-implanted and was placed back on the Zwick compression machine. Figure 127 is a series of photographs illustrating the above.

Figure 128: Pictures illustrating the excised bone before and after sectioning along the original fracture line

The excised, re-fractured instrumented bone was placed back in the Zwick and the nail was subjected to compressive biomechanical loads of up to 1000N. The strains measured from all the 6 channels with the callus intact and re-fractured are shown in Figure 129 and 130.

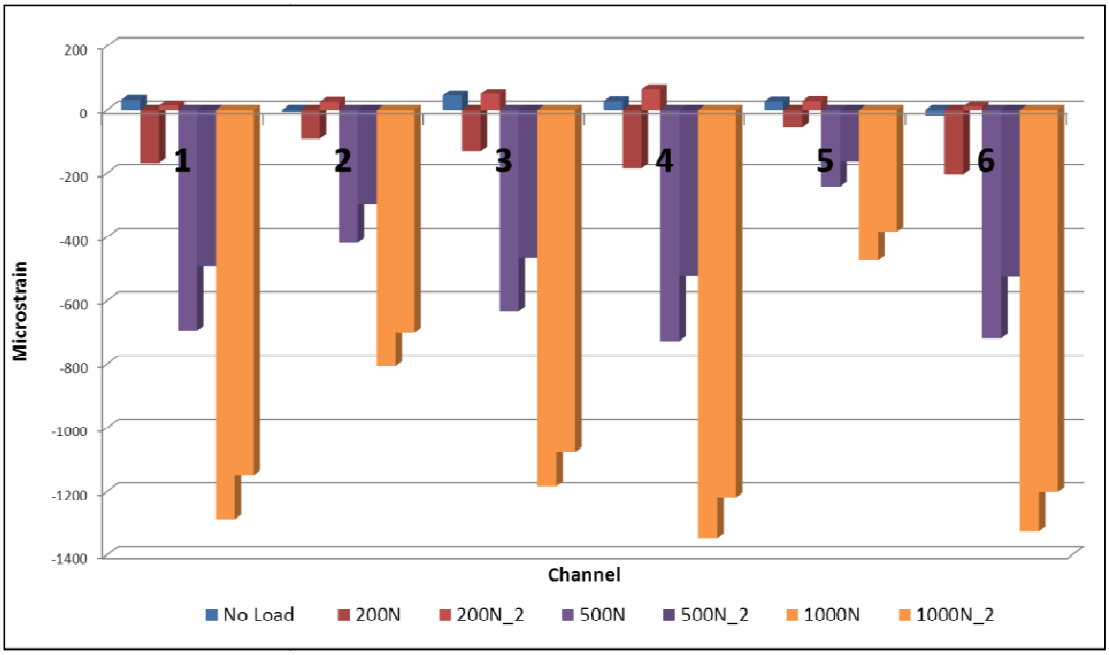

Figure 129 Microstrains measured from strain gauge channels 1-6 for nail implanted in the excised tibia at 4 weeks transverse cut through callus

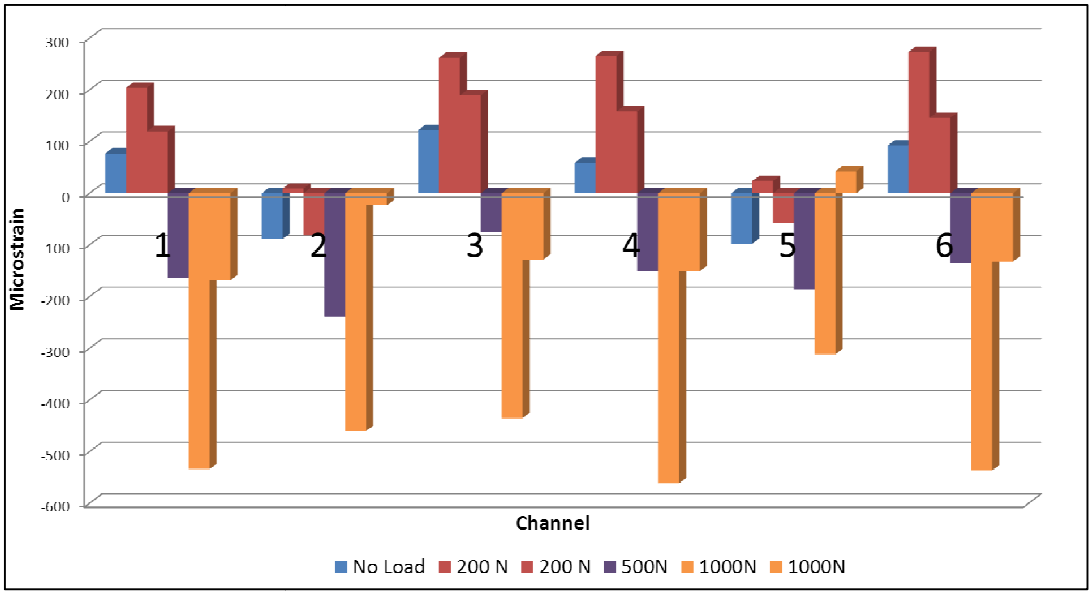

Figure 130 Microstrain measured from strain gauge channels 1-6 for nail 14 implanted in the excised tibia intact callus at 4 weeks

Ultimately, after continual loading the nail (nail 14) would not fail when repeatedly cyclically loaded to 1500N, and the strains returned to similar baseline values each time. Undoubtedly, the wire bonds on this nail were all intact still. It is likely that the encapsulation process was not to the same degree which produced some variation in adhesion of the rubber to the flexi. Given this nail survived both immersion and mechanical stress, it shows that the basic principle can be made to work however there is a variation occurring in the process somewhere rendering the system unreliable.

5.9 Discussion

The insightful experience of being part of a team doing live testing of a medical device was very rewarding. However, this comes with a few pointers. Live testing requires precise planning in order to ensure the welfare of the animals as well as the positive outcome of the task. The pilot study was successful in ensuring that all the animals were trained and that the information gathering for further design and planning of the live phase was conducted successfully.

This led to the design of the loading rig. From CAD design to manufacturing, at every step of the process, there was ample opportunity to trial the rig on the animal before the live phase. This opportunity allowed the team to assess the advantages and disadvantages of the assembly for use on the sheep. The reason the loading rig designed and modelled in Figure 110 was not the right choice for this study is because of the major difference between ovine and human leg anatomy. The ovine leg is much shorter but also the bulk of the muscles were harder to bypass to apply torque to the bone underneath. The orthotic SLA shoe was less bulky however the challenge

of applying torque to the bone was nonetheless still present. A series of Velcro straps was the solution to ensure the bone is fully engaged in the torque test applied and measured using a calibrated torque wrench.

The cadaveric trials of GEN IIIa nails was successful however it should be noted that for any study that require live animal testing, a more in depth *in-vitro* biomechanical test using excised bones should be conducted. A more detailed study testing fully functioning wireless telemetered nail in a bone with fluids, as present in a live model would have given more insight in the potential capability of the nail in hostile biological environment. The nail should have been tested over a period of time in order to ensure functional capability that it is expected to last for in live models during cyclic loading.

The live phase study itself was unfortunately cut short due to the nail failing prematurely once implanted. However, the study could have benefitted from updated plan when the developments of the prototyped IM GEN IIIa nails were delayed. Since the sheep that were selected for the study underwent a selection process as per their weight and width of medullary canal, the delay in the development of the nail meant that with more time between selection and testing, the tibial bone underwent physiological changes. The likelihood of a decrease in density of the tibia which would increase brittleness is high. Implantation of the IM nails despite its fragility at that stage still require some force to fully insert the latter in the medullary canal. With brittle bones, a little too much force on either the nail or screws can produce another fracture once the midshaft fracture induced.

However, the failure of the nails prematurely was unfortunate but can be overcome by changing the wire bonds to a different bonding system all together. The nail from the excised bone showed that when the nail is fully functioning, extremely useful information can be extracted from the models. The nails should be tested with the telemetered parts fully inclusive in saline over many months in order to fully assess its functionality and reliability. GEN III nail has been undergoing major changes in the aspects where failure occurred and another live animal study is set to begin once the nail has passed all the necessary tests.

On this note, the *in-vivo* study showed that an intramedullary nail with a wireless telemetered system is a powerful tool in the monitoring forces *in-vivo*. The system requires some reinforcing before the pre-clinical trials are repeated for validation purposes. However, the *in-vitro* biomechanical testing of the different generations of nail showed monitoring of fracture healing can be successful during the most crucial time scale for bone healing. This can be a unique opportunity to further validate and implement the use of a telemetered nail for successful monitoring bone physiological functions during fracture healing.

5.10 References

[1] http://www.homeoffice.gov.uk/science-research/animal-research/ (last accessed: 21/09/2011 16:56)

[2] Al Pearce, RG Richards, S Milz, E Schneiderm and SG Pearce. Animal models for implant biomaterial research in bone: A review. European Cells and Materials, 2007, 13, ISSN 1473-2262.

[3] WE Huffer, JJ Benedict, AS Turner, A Briest, R Rettenmaier. Repair of sheep long bone cortical defects with Colloss®, Colloss E®, Ossaplast®, Ortho and iliac crest autograft. Proceeding of 52nd Orthopaedic Research Society, Chicago, 2006

[4] E Newman, AS Turner, JD Wark. The potential of sheep for the study of osteopenia: current status and comparison with other animal models. Bone, 1995, 16, 277S-284S.

[5] P Chavassieux, P Pastoureau, G Boivin, S Charhon, M Chapuy, P Delmas, P Meunier. Effects of sodium fluoride on bone remodelling in ewes. Journal of Bone Mineral Research, 1987, 2 Suppl1, Abstract 359

[6] FC den Boer, P Patka, FC Bakker, BW Wippermann, A van LIngen, GQ Vink, K Boshuizen, HJ Haarman. New segmental long bone defect model in sheep: quantitative analysis of healing with dual energy x-ray absorptiometry. Journal of Orthopaedic Research, 1999, 17, 654-660.

[7] P Pastoureau, M Arlot, F Caulin, J Barlet, P Meunier, P Delmas. Effect of oophorectomy on biochemical and histological indices of bone turnover in ewes Journal of Bone Mineral Research, 1999, 4, S237, abstract 477.

[8] Smith & Nephew Trigen Meta-Nail Tibial Nail System Surgical Technique Manual downloadable from http://global.smith-nephew.com/cps/rde/xbcr/smithnephewls/7118-1112_Metanail-Tibial_ST.pdf (last accessed: 22/09/2011 16:42)

[9] William E.Nordt, Paymaun Lotfi, Eric Plotkin, Brian Williamson. The *in-vivo* assessment of tibial motion in the transverse plane in anterior cruciate ligament-reconstructed knees. The American Journal of Sports Medicine, 1999, 27, 5.

[10] A.L.Wallace, E.R.Draper, R.K. Strachan, I.D.McCarthy, S.P.F.Hughes. The effect of devascularisation upon early bone healing in dynamic external fixation. Journal of Bone and Joint Surgery (Br), 1991, 73, 819-25.

[11] P. Seebeck, M.S. Thompson, A. Parwani, W.R. Taylor, H. Schell, G.N. Duda. Gait evaluation: a tool to monitor bone healing? Clinical Biomechanics, 2005, 20, 883-891.

[12] Erich Schneider, Markus C.Michel, Martin Genge, Kurt Zuber, Reinhold Ganz & Stephan M.Perren. Loads acting in an intramedullary nail during fracture healing in the human femur. Journal of Biomechanics, 2001, 34, 849-857.

[13]Seide K, Faschingbauer M, Weinrich N, Wurm M, Mehrtens G, Erhard H, Jürgens Ch, Müller J. “An intelligent internal fixator system for long bones.” 52nd Annual Meeting of the Orthopaedic Research Society, 2006, Paper No. 1698.

[14]Claes L, Cunningham J. Monitoring the mechanical properties of healing bone. Clinical Orthopaedic & Related Research, 2009, 467, 1974-1981.

6 Conclusion and recommendations for future work

Three different generations of instrumented nail have been designed and developed. GEN I was a wired system with an energizer and reader. It had the spiral configuration of 27 gauges in total with 3 gauges per site at +45°, 0° and -45° to the nail axis. GEN I was biomechanically tested *in-vitro* while simulating fracture healing. It was tested in 4th Generation Sawbone® model replicating a tibial model with a 42-A2 fracture 14cm from the distal end of the bone. The instrumented GEN I was implanted in the tibial Sawbone® with screws at the proximal and distal end. The nail was tested biomechanically following a set loading protocol simulating axial compression, torque and 4pt bend test.

In order to simulate fracture healing, an experiment was designed to create composite materials to mimic the physical properties of bone callus tissues. Four different composite mixtures were achieved simulating granulation, fibrous, cartilaginous and immature bone tissue in their compressive modulus properties. These synthetic callus materials were used on the fractured Sawbone®-nail construct in different callus morphology to simulate healing. Using the composite materials two specific callus geometries was tested, segmental and circumferential. GEN I was subjected to the biomechanical tests mentioned above with the fracture healing simulations. The strain readings were measured, processed and analysed. The results show that for both callus morphologies the most distal gauges proved sensitive enough to monitor strain with the callus mimic of 0.2MPa. It also satisfied the hypothesis that as bone heals successfully, the load shifts from the nail to the bone thus reducing strain measurements.

GEN II was instrumented in an extended pocket on the anterior side with 5 slave stations, 4 gauges per slave site, therefore with 20 gauges in total. At each slave site, 3 were positioned at 0° to the nail axis and one at 45° to the nail axis. The system was wired with an energizer and reader however the graphical user interface was more user-friendly. The nail was biomechanically tested using the same protocol as GEN I. However, with two nails available more fractures and callus morphology could be simulated. One bone and nail construct was used to measure the strain in an unfractured bone. The results are discussed at length in Chapter 4. However, at the end of the analysis it was found that GEN II was not reliable at this stage in the development and should have been more robustly tested before being subjected to any mechanical testing. The nail construct was also subjected to callus healing simulation in an attempt to compare the data gathered to GEN I. However, the data was too unreliable for comparison. The unreliability of GEN II should have been a predictor for the fate of GEN III; however, the pre-clinical nail was already developed. The production of GEN II was 1 year over the scheduled date and this led to a high cost.

GEN III was the wireless pre-clinical nail with 2 slave stations and 3 gauges per slave site. 2 of the gauges were at 0° and 1 gauge at 45° to the nail axis. It had a microcontroller which converts the output voltage from the strain gauge. It was a fully wireless system. The nail was tested in a pre-implantation testing on a cadaveric limb. This test was conducted successfully however the loads applied were for a very short period of time and it was done on only one nail. This was more of a test to see if the system is functioning and should have been further tested biomechanically in an *in-vitro* set up simulating the body with all the fluids required. With only one set of data gathered successfully using GEN III, the pre-clinical nail was implanted in 12 animals. The outcome of this animal study was not without losses. Out of the 12 implanted animals, 3 animals were euthanized during surgery due to further complications.

The time taken to develop GEN II & III delayed the pre-clinical trials and hence the animals selected for the study was no longer the best choice necessarily. Over time the density of the animal bone was more brittle. With reaming and other mechanical force used for implantation of the nail, the tight fit nature of the system against the medullary canal meant that one push too much led to further fracturing the bone of the animal. This is the cause that led to the early euthanizing of 3 animals. Once GEN III systems that were successfully implanted were monitored closely and two weeks as planned after the first surgery, the nails were not emitting any signal. Failure of the GEN III nails was consistent in the remaining animals. The intermittent signal received was good only to record 5 seconds of live data from the nails which was only temperature data and not strain readings.

So far GEN I has been tested successfully however in order to get a reliable set of significant data, the tests have to be repeated for statistical significance. GEN II has yet to produce a complete set of data successfully. The results showed that there is potential however, the unreliable nature of the instrumentation meant that it is not valid and useful unless repeated with a fully functioning reliable nail. Currently, GEN I and GEN II have been tested biomechanically with distal fractures *in-vitro* during simulated fracture healing. They have shown that the nail is sensitive enough to monitor strain even with callus growth of Young's modulus 0.2MPa simulating granulation tissue during different biomechanical tests. GEN IIIa has been tested in cadaveric bone models *in-vitro* and has shown that strain measurements can be monitored using telemetry. However, the current pre-clinical nail is yet to be tested *in-vivo* successfully. Despite the malfunctioning that occurred with the pre-clinical nail, experimental results have gone a long way in validating the essential system. Biomechanical tests in saline should be conducted to ensure there is no leakage or drift over several months to simulate the time taken for bone fracture healing. Prior to any further live animal testing, GEN III nail should be tested and have a 100% certainty that the

system functions as required in cadaveric models before any unnecessary surgery using live models.

The synthetic bone composite material has been tried and tested. However, there are a number of factors that require further work. The curing of the composite mixture needs to be addressed as the particulates have the tendency to settle to the bottom if not stirred continuously until it is less viscous. The size of the particulates used so far has been chosen empirically as they were easily available materials. However a closer monitoring of the selection of materials will ensure that the desirable final modulus of the composite can be achieved. Additionally, the distribution of the particulates in the matrix leads to some inconsistency in the composite hence being able to set the distribution of the material effectively will allow the variation in properties. The composites need to be tested visco-elastically by either conducting a creep or stress relaxation test to understand the mechanics of the properties over time. The experimental models can be validated mathematically using Maxwell's Model to derive visco-elastic constitutive models. However, this is a much specialised area which requires a lot of work in order to validate the theory.

Additionally, there are two more layers of callus composite that still require more work as they are the high end modulus, simulating mature and cortical bone. Combined with the variations mentioned above, if successful, the 6 layers of the callus composites can be used in very early testing of medical implants to simulate healing when implanted in other artificial bone models. This opens the door for a completely new set of research proposals on its own. Currently Sawbone® models that are used to test implants mechanically simulate healthy adult bones however, when implants are designed for paediatric orthopaedic areas, those implants are not tested on artificial bones simulating that of young children. There is a potential for whole bone structures to be modelled simulating bones that are more apt to replicate paediatric bones for instance. This means that further research is required regarding new manufacturing techniques to make a whole bone using the callus composite layers. This may be potentially beneficial for the orthopaedic implants industry as well as for other areas of the body.

The project has achieved its aims: it has demonstrated novel methods to conduct pre-clinical testing, with improved precision for bone fracture healing simulation experimentally and shown evidence that the data is transferable to the clinical environment. The telemetered system in an implant to monitor forces *in-vivo* reinforces the statement by Schneider *et al.* [1]. His study proved that an implant equipped with a multi-channel telemetry system is a very powerful tool for investigating the implant loading *in-vivo*. An instrumented nail (GEN IIIa) for pre-clinical use with 6 strain gauges has been provided with the sensitivity to monitor strain measurements in

clinical environments. The nail is able to collect sufficient data to predict fracture healing. Ideally the whole system should be straightforward enough to be used to monitor healing across a whole range of different long bone fractures and further work is warranted to be able to develop a fully functional, wireless telemetered instrumented intramedullary nail.

6.1 References

[1]. Erich Schneider, Markus C.Michel, Martin Genge, Kurt Zuber, Reinhold Ganz & Stephan M.Perren; Loads acting in an intramedullary nail during fracture healing in the human femur. Journal of Biomechanics, 2001, 34 **,** 849-857.

Appendices

A. Project plan
B. Specification of epoxies
C. Curing & repeatability
D. GEN I and GEN II Data Disk
E. X-Ray of Ovine Models OR366, OR451 & OR380
F. Animal Authorisation
G. Torsion rig manufacturing drawings
H. GEN III temperature data